Biosynthesis of polyhydroxyalkanoates for cardiac tissue engineering applications

Andrea V. Bagdadi

School of Life Sciences

Biosynthesis of polyhydroxyalkanoates for cardiac tissue engineering applications

Andrea V. Bagdadi

A thesis submitted to the University of Westminster in candidature for the award of the degree of Doctor of Philosophy

June 2013

AUTHOR'S DECLARATION

I declare that the present work was carried out in accordance with the Guidelines and Regulations of the University of Westminster. The work is original except where indicated by special reference in the text.

The submission as a whole or part is not substantially the same as any that I previously or am currently making, whether in published or unpublished form, for a degree, diploma or similar qualification at any university or similar institution.

Until the outcome of the current application to the University of Westminster is known, the work will not be submitted for any such qualification at another university or similar institution.

Any views expressed in this work are those of the author and in no way represent those of the University of Westminster.

Signed: Andrea V. Bagdadi Date: June, 2013

ACKNOWLEDGMENTS

I would like to first say a very big thank you to my supervisor Dr. Ipsita Roy for all the support, encouragement and constant feedback she gave me during this project. I also thanks to Professor Aldo Boccaccini for being such a supportive co-supervisor and Professor Tajalli Keshavarz for his advice.

I would like to thank all of Dr. Roy's collaborators in whose laboratories I have performed some of the experiments described in my thesis.

I am also indebted to the technical staff Neville, Thakor, Vanita, Glen, Luisa, Harry, Dr. Nicola Mordan, Dr. George Gergiou and Dr. Graham Palmer.

I also thank all the members of the lab, both past and present, for their friendship and for the great time we had in our group. Pooja, thank your patience in the hardest moments. Thank you Anu, Ranjana and Lydia for all your guidance and for all your help. Thank you also to Maryam, Ketki, Bijal and Prachi.

My sincerest thanks are extended to Professor Carlos Amorena for his invaluable advice, support, encouragement, and faith he has in me.

Last but not least, I wish to thank my family for supporting me during these four years I was far from home following my dreams. Thank you mum and dad for always taking care of me and for your unconditional love. Thanks to my sister Marcia and my brother Javier for always making sure that I am happy wherever I am.

I would like to dedicate this thesis to Mariano, who has lived every single minute of this project with me. Thank you for always being by my side and for being so supportive with this project I always wanted to carry out. This work would not have been possible without his huge financial generosity.

ABSTRACT

As a result of the enormous clinical need, cardiac tissue engineering has become a prime focus of research within the field of tissue engineering. In this project, Poly(3-hydroxyoctanoate), P(3HO), a medium chain length (mcl-PHAs) biodegradable, biocompatible and elastomeric polyhydroxyalkanoate, was studied as a potential material for cardiac tissue engineering. Mcl-PHAs are an alternative source of polymers produced by *Pseudomonas sp.* As Gram-negative bacteria, *Pseudomonas sp.* contains lipopolysaccharides in the membrane, which are co-purified with PHAs and may cause immunogenic reactions. This limits the biomedical applications of the mcl-PHAs in several cases. In this work, the *Pseudomonas mendocina* PHA synthase gene (*pha*C1) was expressed in the LPS free, GRAS, Gram-positive microorganism, *Bacillus subtilis* so as to produce LPS-free mcl-PHAs. Our results showed that the recombinant *Bacillus subtilis* containing the *pha*C1 gene produced poly(3-hydroxybutirate), P(3HB), with a maximum yield of 32.3 % DCW, an unexpected result. This result thus revealed the unusually broad substrate specificity of the PHA synthase from *P. mendocina*, which is able to catalyse both medium and short chain length PHAs biosynthesis depending on the metabolic pool available in the host organism. Sequence comparison of this PHA synthase with stringent mcl-PHA synthases revealed possible residues influencing the substrate specificity of PHA synthases.

As studies on mcl-PHAs remain limited mainly because of the lack of availability of mcl-PHAs in large quantities, the capacity to scale-up P(3HO) production from 2 L to 20 L and 72 L pilot plant bioreactors, based on constant oxygen transference, was studied.

The interaction of freshly isolated rat cardiomyocytes with the P(3HO) polymer, during contraction, was studied when cells were stimulated at a range of frequencies of electrical pulses or calcium concentrations. These results showed that P(3HO) did not have any deleterious effects on the contraction of adult cardiomyocytes. P(3HO) cardiac patches non-porous, porous or with P(3HO) electrospun fibres deposited on their surface were developed. Our results showed that the mechanical properties of the final constructs were close to that of the cardiac structures, with a Young's modulus value of 0.41±0.03 MPa. Myoblast (C2Cl2) cell proliferation was studied on the different constructs showing an enhanced cell adhesion and proliferation when both porous and fibrous structures were incorporated together.

Finally, for further enhancement of the cardiac patch function, VEGF and RGD peptide were incorporated. Results obtained in this project showed that the P(3HO) multifunctional cardiac patches were potentially promising constructs for efficient cardiac tissue engineering.

TABLE OF CONTENTS

LIST OF FIGURES

LIST OF TABLES

LIST OF ABBREVIATIONS

3HB	3-hydroxybutirate
3HHp	3-hydroxyheptanoate
3HV	3-hydroxyvalerate
µm	micrometer
ACE	angiotensin-converting enzyme
ARB	angiotensin II receptor antagonist
bFGF	basic fibroblast growth factor
BGSC	*Bacillus* Genetic Stock Centre
$CDCl_3$	deuterated chloroform
CIP	calf intestine phosphatase
CVDs	Cardiovascular diseases
DCC	dicyclohexylcarbodiimide
DCW	dry cell weight
DMA	Dynamic mechanical analysis
DMEM	Dulbecco's modified Eagle's medium
DOT	dissolved oxygen tension
DSC	Differential scanning calorimetry
FBS	foetal bovine serum
FDA	Food and Drug administration
FTIR	Fourier transform infrared spectroscopy
GC-MS	Gas chromatography–mass spectrometry
GRAS	Generally Recognized as Safe
hr	hours
k_La	volumetric oxygen transfer coefficient

KV	kilovolt
L	liter
LB	Luria broth
mcl-PHAs	medium chain length polyhydroxyalkanoates
min	minutes
mL	mililiter
mM	milimolar
Mpa	megapascal
NB	nutrient broth
NCIMB	National Collection of Industrial and Marine Bacteria
NMR	Nuclear magnetic resonance
OTR	Oxygen transference rate
PBS	phosphate buffer saline
P(3HB)	Poly(3-hydroxybutirate)
P(3HD)	Poly(3-hydroxydecanoate)
P(3HO)	Poly(3-hydroxyoctanoate)
P(3HD-co-HDD)	Poly(3- hydroxydecanoate-co-dodecanoate)
P(3HO-co-3HHx)	Poly(3-hydroxyoctanote -co-hexanoate)
PCL	poly(caprolactone)
PCR	Polymerase chain reaction
PEO	poly(ethylene oxide)
PGA	poly(glycolicacid)
PGS	poly(glycerol-sebacate)
PHAs	Polyhydroxyalkanoates
PLA	poly(lactic acid)
PLGA	poly(lactic-glycolic acid)
PVA	poly(vinyl alcohol)

RGD peptide	arginine-glycine-aspartic
rpm	revolutions per minute
RyR	ryanodine channels
scl-PHAs	short chain length polyhydroxyalkanoates
SCPL	solvent cast particle leaching
SD	standard deviation
SDS	sodium dodecyl sulfate
sec	seconds
SEM	Scanning electron microscope
SIS	small intestine submucose
SR	sarcoplasmic reticulum
Tc	crystallization temperature
Tg	glass transition temperature
TGF-b	transforming growth factor
Tm	melting temperature
TnC	troponin complex
VEGF	vascular endothelial growth factor
vvm	air volume/liquid volume per minute

CHAPTER 1

INTRODUCTION

1.1.Cardiovascular diseases

Cardiovascular diseases (CVDs) are the leading cause of death throughout the world (Morosco *et al.*, 2002, Perry *et al.*, 2003). According to the World Health Organization, an estimated 17.3 million people died from CVDs in 2008 and it is predicted that by 2030 almost 25 million people will die from CVDs. CVDs, including coronary heart disease, hypertension, peripheral artery disease, rheumatic heart disease and congenital heart disease among others, are caused by disorders in the cardiac tissue and blood vessels. Myocardial infarction is the main cause of death in patients with CVDs. Myocardial infarction is an irreversible necrosis of the cardiac tissue produced by an imbalance in the oxygen and nutrient supply to a portion of the myocardium. The acute loss of myocardium triggers a cascade of cell signals activating a ventricular remodelling process, which can be divided in two phases: early remodelling and late remodelling. The early ventricular remodelling process includes the formation, thinning and elongation of a fibrotic scar that cause elevation of diastolic and systolic wall stresses. An increased wall stress leads to a late remodelling characterized by myocytes hypertrophy and production of interstitial collagen with an increased wall mass and chamber enlargement (Figure 1.1) (Sutton and Sharpe 2000). Myocardial infarction may eventually lead to the deterioration of systolic or diastolic function and to increased predisposition to arrhythmias and other long-term complications.

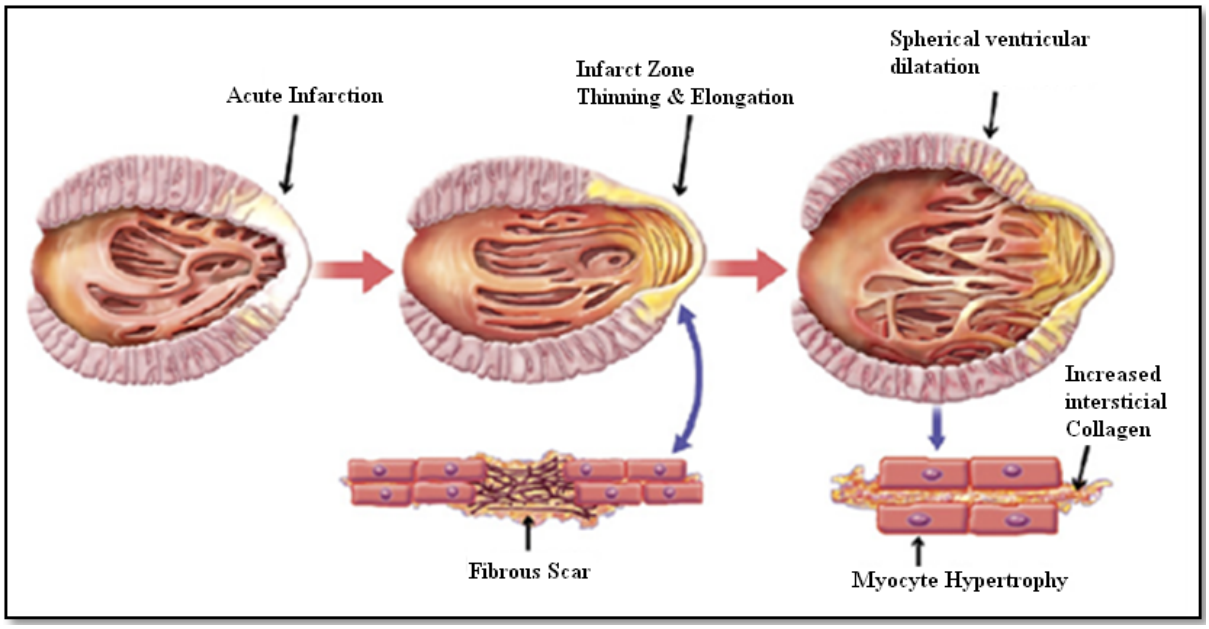

Figure 1.1. Schematic representation of post-myocardial infarction remodelling. The infarction of a specific part of the tissue leads to the formation, thinning and elongation of a

fibrous scar followed by myocytes' hypertrophy and production of interstitial collagen with an increased wall mass and chamber enlargement (Konstam *et al.,* 2011).

1.2. Anatomy of the heart

The heart is the organ responsible for blood supply by repeated rhythmic contractions to all parts of the body. The heart cavity is divided into a right and a left heart, which are further subdivided into two chambers. The upper chambers are called right and left atrium and they receive the blood entering the heart. The lower chambers are called right and left ventricle and they pump the blood out of the heart. The right and left heart are considered as two separate pumps as they are in charge of the pulmonary and peripheral circulation, respectively. As each chamber contracts, blood is forced into the ventricles and out of the heart for re-circulation. In particular, the right atrium receives blood from the different organs via the vena cava and blood passes through the tricuspid valve to the right ventricle where it is pumped out through the pulmonary artery to the lungs. Blood is oxygenated in the lungs and returned via the pulmonary veins to the left atrium. Oxygenated blood is passed to the left ventricle responsible for pumping blood around the whole body (Laizzo *et al.,* 2009). Figure 1.2 illustrates the anatomy of the heart.

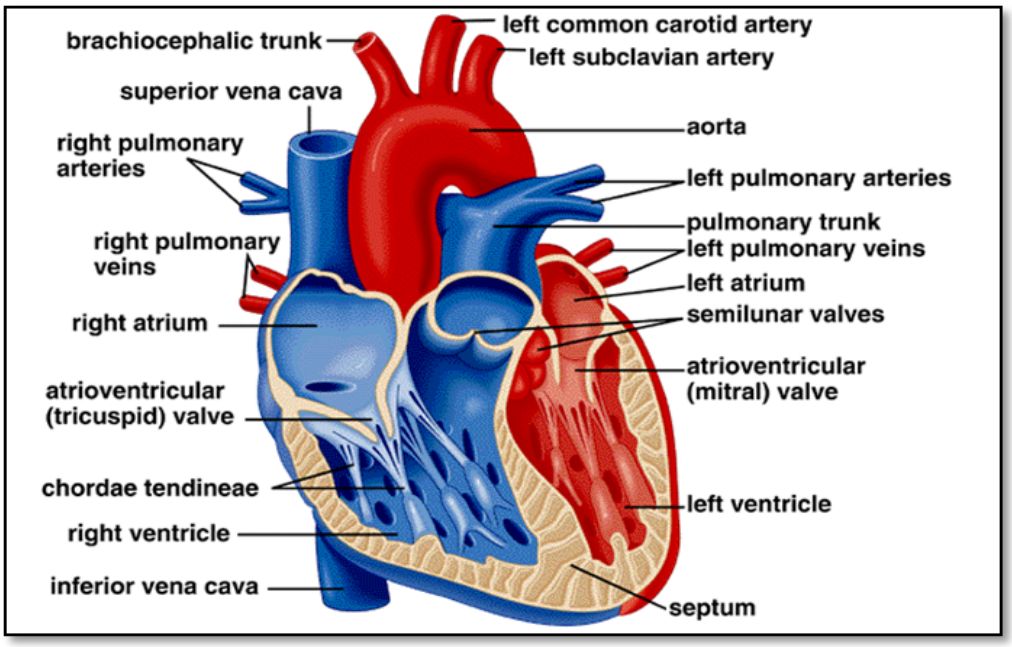

Figure 1.2. Schematic representation of the heart anatomy (Taken from Mader 1999).

The heart wall is composed of the endocardium, myocardium, and epicardium layers (Kierszenbaum *et al.,* 2002). The myocardium is the tissue responsible for the alternating contractions and relaxations cycles induced by electrical impulses, allowing pumping of blood. The myocardium consists of cardiomyocytes, extracellular matrix and blood vessels. The cardiomyocytes are terminally differentiated cells responsible for the contraction and relaxation cycles. On the other hand, the extracellular matrix, mainly composed of type I and type III collagen, provides a framework that couples and aligns adjacent myocytes to optimize and distribute force development in the ventricular walls and avoids deformation (Sutton and Sharpe 2000). The epicardium, also known as the visceral pericardium, is mainly composed of connective tissue and it provides an outer protective layer to the heart. The endocardium is a thin layer of endothelium and connective tissue that lines the chambers of the heart (Kierszenbaum *et al.,* 2002).

1.3. Cardiac contraction

Cardiac excitation–contraction cycle is initiated by an action potential. Here, the cadiomyocytes' membrane is depolarized when ions enter through connexin channels from an adjacent cadiomyocyte inducing the entry of Na^+ through voltage gated-sodium channels. After a rapid depolarization of the membrane, inactivation of Na^+ channels and activation of Ca^{2+} and K^+ channels occur. Ca^{2+} influx triggers Ca^{2+} release from the sarcoplasmic reticulum (SR) through the ryanodine channels (RyR). Both Ca^{2+} influx and Ca^{2+} released from the sarcoplasmic reticulum raises cytosolic free Ca^{2+}, which binds to the troponin complex (TnC) that switches on the myofilaments in a cooperative manner, activating the contraction. Cardiomyocyte relaxation occurs when Ca^{2+} dissociates from troponin after Ca^{2+} is removed from the cytosol by calcium uptake pumps in the sarcoplasmic reticulum and by Na^+/Ca^{2+} exchange pumps present in the cell membrane (Knollmann *et al.*, 2008). Figure 1.3 illustrates the mechanisms involved in cardiac contraction and relaxation cycles.

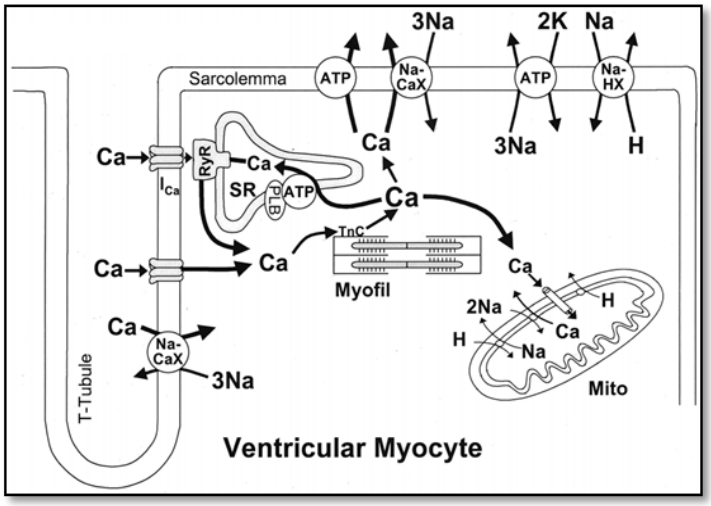

Figure 1.3. Schematic representation of cardiac contraction and relaxation mechanisms (Bers, 2000).

1.4. Cardiac therapies

As cardiac tissue lacks significant regenerative capacity to replace lost cells, the cardiac tissue injury is permanent. Different pharmacological or interventional therapies are currently applied to patients with cardiac failure. Pharmacological therapies aim to reduce the load of the cardiac tissue or to increase the strength of the heart muscle contraction. Among the most common drugs utilized are: angiotensin-converting enzyme (ACE) inhibitors, β-blockers, aldosterone antagonists and angiotensin II receptor antagonist (ARB). Interventional therapies include the implantation of pacemaker/defibrillator devices to synchronize the electrical and mechanical pulses of the heart or surgery to replace the infarcted tissue with a "cardiac patch" that reinforce the organ. Although in some patients these therapies have served to achieve a significant prolongation of life, additional improvement is needed to adequately control the progression of the disease to the end stage, in majority of the patients (Krumholz *et al.*, 2000). Cardiac transplantation has become the last viable treatment option for patients with end stage cardiac disease. However, due to the lack of organ donors and the post-operative complications including infection, sepsis, organ rejection and side effects of the immunosuppressive medication, new strategies need to be developed to treat infarcted hearts (Bishay, 2011).

1.4.1. Cardiac tissue engineering

Recently, cardiac tissue engineering has provided a promising alternative method to treat heart disease. Much research has been carried out in the development of engineered tissues that can replace the infarcted myocardium. In a first approach, studies involving the injection of several cell sources directly into damaged areas or intravenously were carried out. To this end, several cells types were explored including cardiomyocytes, embryonic stem cells and bone marrow-derived mesenchymal stem cells (Ye *et al.,* 2011). Although some studies reported significant improvement in myocardial function, this improvement was not clinically relevant and only transient (D'Alessandro *et al.,* 2010). Investigations to date have shown that the main limitations of this technique include poor cell integration, cell loss and cell death. Additionally, some cell sources showed a negative effect by inappropriate electrical integration leading to occurrences of arrhythmia (Prabhakaran *et al.,* 2011). Fernandes *et al.,* (2010) studied the effect of intramyocardial injection of embryonic stem cell-derived cardiomyocytes after chronic infarction in rats for three months. Results showed that implanted cells were insufficient to restore heart function or alter adverse remodelling. Additionally, different groups have focused on the integration between host and injected cells by studying cell junctional expression molecules, including connexin 43 and cadherin. Results showed no significant cell integration after injection (Nunes *et al.*, 2011).

In a second approach several naturally derived and synthetic polymers were proposed to replace the non-contractile infarcted tissue. Among the natural derived biomaterials were collagen, fibrin, chitosan, gelatine and decellularized extracellular matrix (Pok *et al.*, 2011). One of the major advantages of many naturally occurring polymers is the non-immunogenic nature as they mimic the native extracellular matrix well, facilitating cell adhesion, growth and proliferation. However, most of these materials fail as cardiac patches due to their poor mechanical properties or high degradation rates. One example is collagen, the most abundant constituent of the extracellular matrix, which as expected, showed good cell adhesion properties but poor mechanical support (Atala *et al.,* 2001). Among the decellularized extracellular matrix are porcine small intestine submucosa (SIS) and bovine pericardium. Badylak *et al.,* (2002) showed promising results with good myocardial cell infiltration and spontaneous contraction after SIS membrane implantation in pigs and dogs. However, other studies showed difficulty in finding large portions of SIS with homogeneous properties and *in vivo* xenogenic rejection after implantation (Keith *et al.,* 2005, Tottey *et al.,* 2011). On the other hand, although bovine pericardium showed reliable consistency, durability, easy

handling, good cell migration and proliferation, xenogenic rejection was observed due to the transplantation of bovine proteins/DNA along with the membrane into the host (Li *et al.,* 2011). In contrast, several synthetic biomaterials were developed. Among the most used are: poly(lactic acid) (PLA), poly(glycolicacid) (PGA), polycaprolactone (PCL), poly(lactic-glycolic acid) (PLGA) and poly(glycerol-sebacate) (PGS). The main advantages of synthetic polymers are the capacity to produce them in large quantities and the ability to regulate the microstructure, mechanical properties and degradation rate. However, many of these materials present acidic degradation products and showed reduced cell adhesion properties in contrast to naturally derived materials (Pok *et al.,* 2011). For instance, the intermediate degradation products of PLGA are lactic and glycolic acid, which reduce the local pH, causing not only an inflammatory reaction but also accelerating the polymer´s degradation rate (Liu *et al.*, 2006).

The combination of a natural or synthetic biomaterial with relevant cells and growth factors *ex vivo* is currently receiving much attention as an alternative for cardiac tissue engineering treatments (Giraud *et al.,* 2007) (Figure 1.4). The final goal will be the selection of an appropriate cell type and the development of a biocompatible flexible material that stimulates cell growth and guides and supports tissue regeneration in order to replace formed scar tissue with functioning cardiac muscle tissue. The material's physical and mechanical characteristics should be similar enough to those of the natural myocardium in order to support the organ during the regeneration process, and its composition should allow it to degrade as the new tissue takes over its function (Jawad *et al.,* 2008). Bioabsorbable polymeric materials provide an extracellular matrix where growing cells can localize and interact to form new tissue. An ideal biomaterial should possess five special characteristics. First, the material should be biocompatible. Second, the material mechanical properties should be similar to the host tissue to provide mechanical support to the cells until new extracellular matrix is synthesized by the cells. As previously described, myocardial infarction normally results in wall thinning and ventricular dilatation that cause a significant stress in the heart wall. Overstressed wall leads to a progressive ventricular remodelling with an end stage of heart failure (Sutton and Sharpe 2000). In order to prevent an overstressed wall with a negative ventricular remodelling, the material's mechanical properties should allow reducing the heart wall stress (Chen *et al.,* 2007). Third, the material should possess an appropriate shape and size to guide and organize the cells and to repair at the implant site. Fourth, the chemistry of the material's surface should allow cell attachment, differentiation

and proliferation. Fifth, the composition of the material should allow biodegradation *in vivo* at rates appropriates for tissue regeneration (Williams *et al.,* 1999).

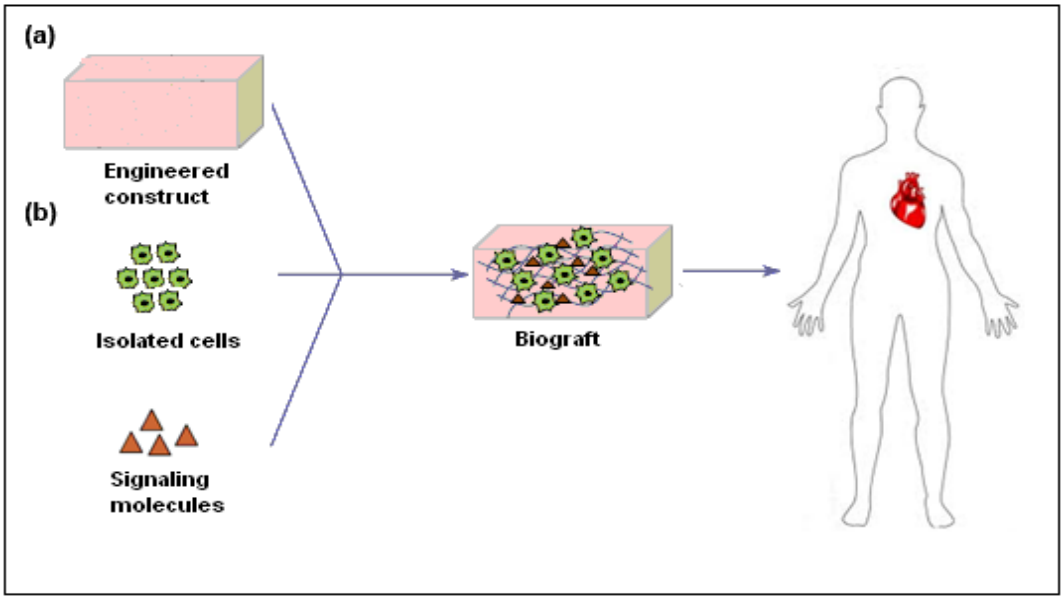

Figure 1.4. A schematic diagram illustrating the principle of myocardial tissue engineering

1.4.1.1. Biomaterials used in myocardial tissue engineering

Several synthetic and naturally occurring materials combined with different cell sources have been explored for myocardial tissue engineering applications. Among the natural polymers, collagen, gelatine and alginate have been under intensive investigation. Kofidis *et al.,* (2002a) seeded neonatal rat cardiomyocytes *in vivo* in a commercially available collagen matrix. Results showed good cell attachment and continuous rhythmic contractions for up to two weeks. However, insufficient size, inadequate geometry, low viability, weak physical properties such as elasticity, integrity and plasticity, low biocompatibility and high production costs were reported. Li *et al.,* (1999) also observed good cell proliferation and spontaneous and regular contraction of the grafts after subcutaneous implantation of a gelatine mesh seeded with cells derived from foetal rat ventricular muscle. However, grafts underwent significant degradation and showed high thrombogenicity. Leor *et al*., (2000) isolated and grew foetal cardiac cells within 3D porous alginate scaffolds for the implantation in rat myocardial scar tissue *in vivo.* Although results showed that the grafts attenuated left ventricular dilatation and heart function deterioration, presence of macrophages, lymphocytes infiltration and low myocardial mass in the graft was observed. In addition to natural

polymers, among the most investigated synthetic polymers were PGA, PCL, PLA and PLGA. Xing *et al.,* (2012) developed myocardial grafts by seeding bone marrow mesenchymal stem cells on scaffolds consisting of 50% polylactic acid (PLA) and 50% polyglycolic acid (PGA). Results showed that PLGA scaffolds implanted in rat peritoneal pocket could form engineered myocardial tissue with structural and functional features resembling those of native tissue. However, the function of the engineered graft in the ischemic heart model should be studied to determine the construct capacity to regenerate and support the organ during regeneration. Shinoka *et al.,* (2005) seeded bone marrow cells in PCL/PLLA scaffolds and resulting constructs were implanted as patches to repair congenital heart defects in 19 patients, ages from 1 to 24 years. No complications such as thrombosis, stenosis, or obstruction of tissue engineered autografts were observed. However, long term analysis is needed to determine the capacity of the graft to support the organ in the long term. Several studies on creating beating engineered synthetic constructs have been reported recently showing that the stiffness of the scaffold impeded the contractions (Shin *et al.,* 2004). Additionally, due to the myocardial tissue cyclic and constant beating, a plastic deformation and failure is expected when thermoplastic polymers such as PGA, PLA and PCL and their copolymers are exposed to long term cyclic strain. Table 1.1 shows the most important mechanical properties of some materials explored for myocardial tissue engineering. These data show that most natural materials are weaker than myocardial structures in contrast to synthetic materials, which are much stiffer than the human myocardium.

Table 1.1. Mechanical properties of materials proposed for myocardial tissue engineering

Polymer	Young's modulus	Tensile strength	References
Collagen	2-22 KPa	1-9 KPa	Roeder *et al.*, 2002
Alginate	10-50 KPa	10-40 KPa	Drury *et al.*, 2004
PGA	7-10 GPa	70 MPa	Webb *et al.*, 2004
PCL	343.9-364.3 MPa	10.5-16.1MPa	Eshraghi *et al.*, 2010
PLA	1-4 GPa	30-80 MPa	Garlotta *et al.*, 2001
PLGA	67 MPa	4 MPa	Lin *et al.*, 2011
Myocardium (human)	0.2-0.5 MPa	3-15 KPa	Watanabe *et al.*, 2006 Nagueh *et al.,* 2004

1.4.1.2. Cells applied in myocardial tissue engineering

As the type and source of cells will have an enormous influence on the success of the tissue engineered constructs, much research has been carried out to determine the most suitable cells to use in myocardial tissue engineering applications. Based on the cell source, cells can be classified into autologous (patient origin), allogeneic (human origin, not patient) and xenogeneic (animal origin). Autologous cells are preferred since no immunosuppressive therapy is required compared to allogeneic and xenogeneic cells. However, difficulty in harvesting a sufficient amount of cells, mainly from aged or diseased patients leads to the use of allogeneic or xenogeneic cell sources (Ikada *et al.,* 2006). Additionally, cells can be classified according to the extent of differentiation (Figure 1.5). Fertilized ovum creates a totipotent cell, zygote, which is capable of developing into all the specialized cells that make up the body. As cells proliferate, they differentiate into two lineages, the pluripotent inner cell mass and the trophoectoderm. Pluripotent cells can be isolated and propagated *in vitro* in an undifferentiated state as embryonic stem cells. Pluripotent cells proliferate into the three major germ layers: endoderm, mesoderm or ectoderm. These three multipotent layers proliferate and differentiate to progenitor cells, which form the organs (Shoukhrat *et al.,* 2009). Adult stem cells, which reside in organs, are defined as multipotent as they have the capacity to differentiate into restricted number of cell lineages.

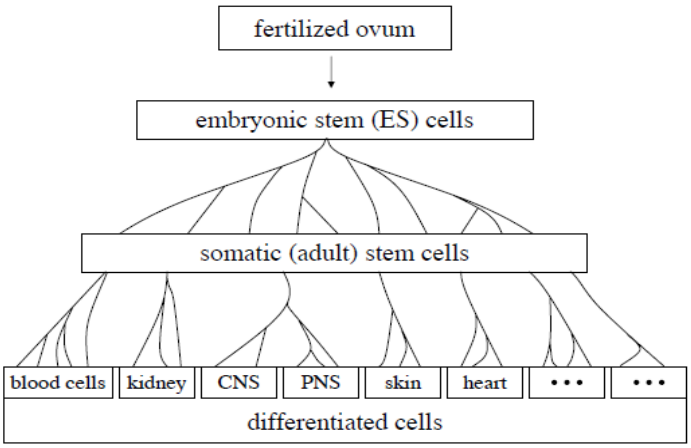

Figure 1.5. A schematic diagram illustrating the different stages of cells differentiation (Taken from Ikada *et al.,* 2006).

The optimal cell source to create a myocardial patch should be non-immunogenic, easy to isolate, proliferative, and with the capacity to differentiate into functional cardiomyocytes (Leor *et al.,* 2005). Different cells were proposed for myocardial tissue engineering including foetal cardiomyocytes, skeletal myoblasts, mesenchymal stem cells, smooth muscle cells, endothelial progenitor cells, bone marrow cells, fibroblasts and human embryonic stem cells (Li *et al.,* 1999, Kamelger *et al.*, 2004, Krupnichk *et al.*, 2001, Matsubayashi *et al.,* 2003, Ryu *et al.,* 2005, Kadner *et al.,* 2004, Levenberg *et al.*, 2003). It is expected that the most suitable cells for myocardial tissue regeneration are cardiomyocytes, due to their natural electrophysiological, structural, and contractile properties. However, healthy cardiomyocytes capable of contracting at high pacing rates are difficult to obtain, to expand, and can be maintained in culture for only up to 36–48 hr (Pinz *et al.,* 2011). The alternatives to cardiomyocytes are cardiac adult stem cells or embryonic stem cells, which are able to differentiate to cardiomyocytes *in vitro* under appropriate conditions. One of the problems associated with adult stem cells is the difficulty in harvesting a sufficient amount of cells, especially when the patient is aged or diseased. On the other hand, it was demonstrated that embryonic stem cells could generate spontaneously contracting engineered heart tissue (Eschenhagen *et al.,* 2005). For this reason, embryonic stem cells are one of the best alternatives for myocardial tissue engineering applications. Table 1.2 shows some advantages and disadvantages of different cell types used in myocardial tissue engineering.

Table 1.2. Advantages and disadvantages of different cell types proposed for myocardial tissue engineering applications (adapted from Chen *et al*., 2010, Galvez-Monton *et al.*, 2013 and Leor *et al.*, 2005).

Cell type	*Advantages*	*Disadvantages*
Fetal cardiomyocytes	Cardiomyocytes phenotype	Limited availability Low survival Host immune response Ethical problems
Embryonic stem cells	Multipotent	Limited availability Ethical problems
Adult stem cells	Autologous Easily isolated Multipotent Low immune response	Low survival Limited availability
Mesenchimal stem cells	Autologous Easy isolated Multipotent	Non authentic cardiomyocytes lineages
Skeletal myoblasts	Easily isolated High rate of proliferation Hypoxia-resistant Autologous	High incidennce of arrhythmias
Fibroblasts	Easily isolated High rate of proliferation Autologous	No cardiac myogenesis No clinical experience
Smooth muscle cells	Easily isolated High rate of proliferation Autologous	No cardiac myogenesis No clinical experience

1.4.1.3. Active molecules used in myocardial tissue engineering

There are a range a proteins produced by the cells in the body that play key role in cell adhesion, proliferation, migration and differentiation. Several reports have shown an enhanced response of the engineered construct by the addition of these bioactive agents (Epstein *et al.,* 2001, Richardson *et al.,* 2001, Yamoto *et al.,* 2003). Among the most frequently used growth factors are basic fibroblast growth factor (bFGF), vascular endothelial growth factor (VEGF) and transforming growth factor-b (TGF-b) (Ikada *et al.,* 2006). These growth factors assist cellular proliferation, differentiation, migration and vascularization (Jakowlew *et al.,* 2006, Neufeld *et al.,* 1999). As the contractile nature of the cardiac tissue demands readily available high oxygen and nutrient concentrations, delivery of angiogenic growth factors from the engineered graft is a key factor to encourage the rapid development

of the vascular network. Several studies have confirmed the capacity of these angiogenic factors to facilitate blood vessel growth when they are incorporated into bioengineered tissues. Perets *et al.,* (2003) proved that the local release of bFGF incorporated into alginate scaffolds enhanced the rate and extent of vascularization, when implanted into rat peritoneum. Singh *et al.,* (2012) showed that VEGF simulated angiogenesis, after encapsulation in PCL scaffolds, when implanted subcutaneously in mouse.

One critical aspect in the application of these angiogenic growth factors in tissue engineering, due to their short biological half-life and high tumorigenic potential, is the delivery of these factors to the site of action in a sustained and controlled manner (Faranesh *et al.,* 2004). Shankha *et al.,* (2004) investigated the effect of intramyocardial and intracoronary administration of bFGF in chronically ischemic porcine myocardium. Results showed that direct intramyocardial injection results in significant improvement in regional myocardial blood flow, in contrast to intracoronary perfusion. In order to allow direct release at the site, several groups have been working towards the incorporation of growth factors in biodegradable polymers to provide localized and sustained release. The incorporation of these growth factors in biodegradable polymers not only allows a localized release but also allows adjusting the magnitude of the release by altering the polymer degradation rates. Growth factors can be incorporated into engineered constructs by two main approaches. The first approach involves the mixing of the factor before processing the polymer into the final construct. The second approach involves pre-encapsulation of a factor in microspheres and the incorporation of these microspheres in the final construct. Richardson *et al*., (2001) showed a much-controlled release when VEGF was incorporated into PLGA microspheres than direct incorporation into the engineered PLGA constructs.

One important problem in the application of different biomaterials in tissue engineering is the inadequate interaction of the construct with the cells, leading to foreign body reactions, infections, implant encapsulation, thrombosis and embolization (Thull *et al.,* 2001). In order to address this issue much research is been carried out in the immobilization of cell recognition motifs to obtain controlled interaction between the cells and the material (Hubbell, 1999). Among the most explored proteins that allow efficient host cell recruitment and adhesion are fibronectin and arginine-glycine-aspartic tripeptide sequence (RGD peptide) (Hersel *et al.*, 2003, Ota *et al.,* 2005, Yoon *et al*., 2003). Matsuzaka *et al.,* (2004) showed that the number of rat bone marrow cells adhering to a fibronectin immobilized polystyrene disk increased after 1 or 2 hr incubation compared with non-immobilized surfaces. Shachar *et al.,*

(2011) investigated the effect of neonatal rat cardiac cells on RGD-immobilized or unmodified alginate scaffolds. Results showed that RGD immobilized surfaces promoted cell adherence to the matrix accelerating cardiac tissue regeneration and that within 6 days myofibres composed of multiple cardiomyocytes in a typical myofibre bundle were formed.

1.4.1.4. Techniques for the fabrication of engineered constructs

The main goal in tissue engineering is the fabrication of a matrix that restores and maintains the lost biological function of the host tissue (Langer *et al*., 1993). Much research is carried out to design engineered structures that can mimic the natural extracellular matrix of the tissue to support the native tissue until host cells can repopulate and resynthesize a new natural extracellular matrix. A number of fabrication technologies were developed for the production of engineered structures including: (I) Porogen leaching such as solvent cast particle leaching (SCPL), compression moulding (Wu *et al*., 2005) and gas foaming (Leatrese *et al*., 1998); (II) Phase transitions, including solvent evaporation (Park *et al.,* 2011), phase separation (Tu *et al.,* 2003) and gel casting (Chopra *et al.,* 2012); (III) Rapid prototyping such as stereolithography (Dhariwala *et al.,* 2004) and fused deposition modelling (Zein *et al.,* 2002) and (IV) fibre deposition, including electrospinning (Zong *et al.,* 2005) and bonded fibre meshes (Mikos *et al*., 1993). Figure 1.6 shows an example of some of the structures obtained with the most used methods from the four mentioned processing techniques.

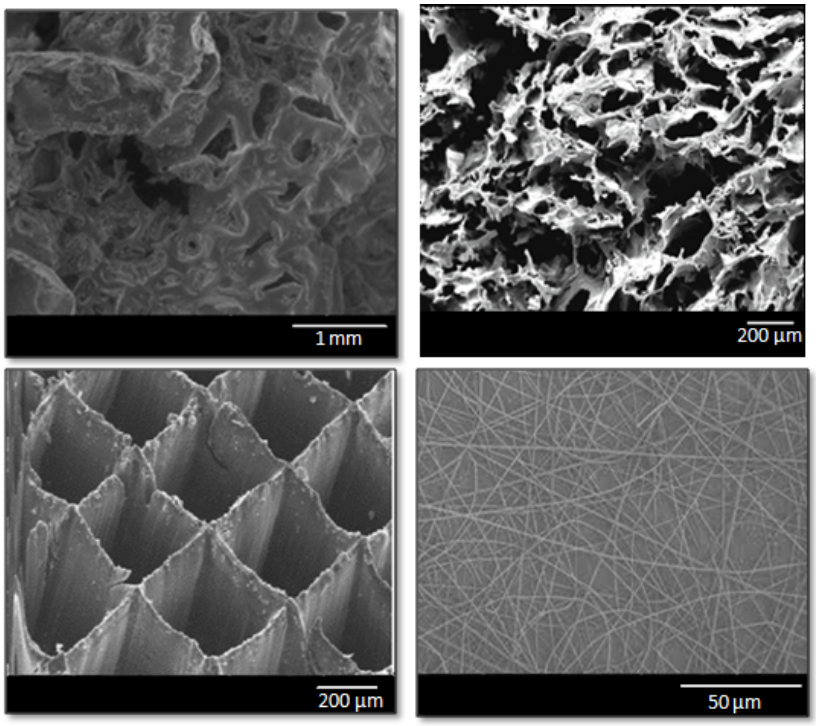

Figure 1.6. SEM images of the different structures obtained by SCPL, freeze drying emulsions, stereolithography and electrospinning (Flaibani *et al.*, 2012, Lu *et al.*, 2004, Sultana *et al.*, 2012).

1.4.1.4.1. Solvent cast particle leaching

The SCPL method is a technique widely used in the design of constructs for tissue engineering to incorporate porous structures due to its easy operation and capacity to precisely control number and size of pores. The particle leaching technique involves the addition of water-soluble particles to a polymer solution follow by casting of the films and porogen removal (Ikada *et al.*, 2011). This technique is simple, low cost and can be used for many soluble polymers. The size of porous structures can vary from 30-300 µm and the porosity that can be obtained is 20-50% (Chen *et al.*, 2007). Figure 1.7 illustrates the different steps involved in the solvent cast particle leaching technique.

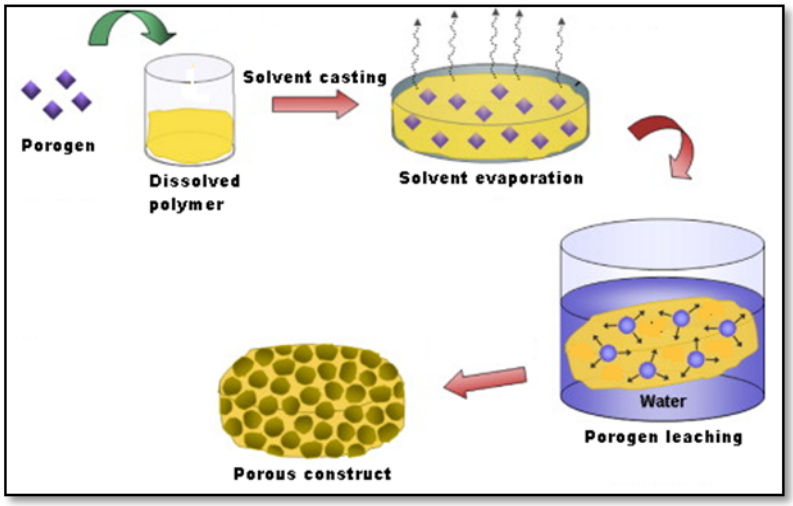

Figure 1.7. Schematic diagram of the solvent cast particle leaching technique (adapted from Chung *et al.*, 2007)

1.4.1.4.2. Freeze-drying emulsions

In the freeze-drying emulsions method water is emulsified in a polymer solution until homogeneity is achieved (Figure 1.8). The obtained emulsion is immediately poured into a metal mould, frozen and freeze-dried, creating porous structures. This technique was developed by Whang *et al.,* (1995) for the fabrication of porous biodegradable scaffolds with PLGA. The resulting scaffolds porosities obtained were greater than 90% with median pore diameters ranging from 15-35 µm and larger pores greater than 200 µm.

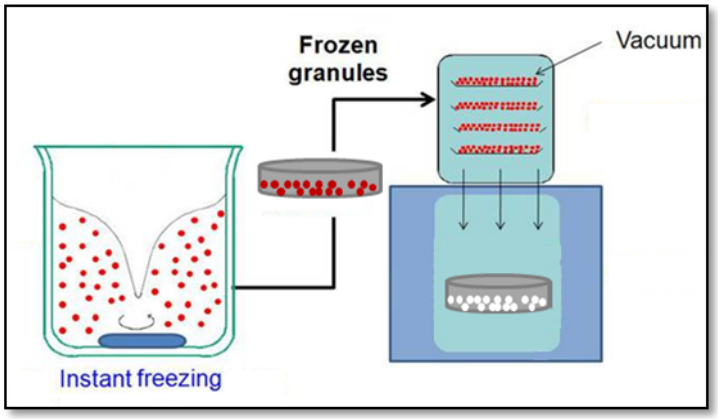

Figure 1.8. A schematic diagram of the freeze-drying emulsions method (adapted from www.powderpro.se).

1.4.1.4.3. Stereolithography

The stereolithography method requires a computer model of the desired scaffold architecture for the production of an accurate structure (Figure 1.9). In this technique an ultraviolet laser bean guided by a computer is focused on the surface of a liquid photopolymer tank drawing a slice of the structure and converting the thin layer of liquid plastic to a solid piece. The layer is immersed in the tank and covered with liquid photopolymer and in the following step the laser beam draws a layer over the previous one (Lanza *et al.,* 2011). This technique allows the production of 100% interconnected porous structures ranging from 45-150 µm pore sizes (Chen *et al.,* 2007).

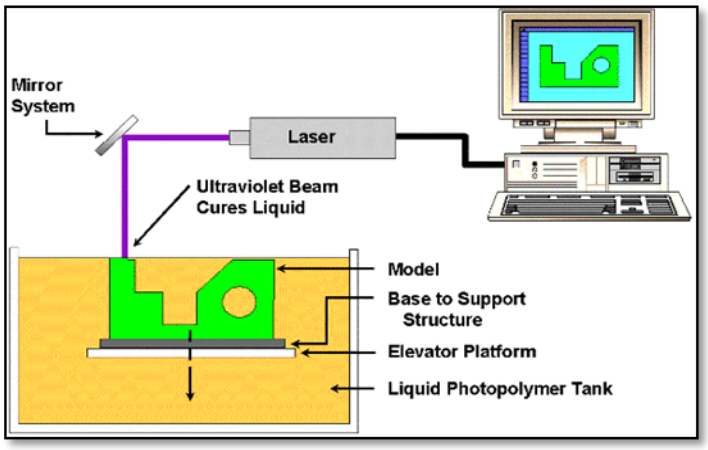

Figure 1.9. Schematic diagram of the stereolithography setup (adapted from www.rpc.msoe.edu).

1.4.1.4.4. Electrospinning

Electrospinning allows the fabrication of micro- and nano- structures that recreate the natural three-dimensional environment of the tissue for better cell organization, survival and function (Zong *et al.,* 2005). Micro- or nano- fibres based matrix are fabricated for multiple biomedical applications, including production of scaffolds in tissue engineering, drug delivery and medical implants (Boland *et al.*, 2001, Min *et al.,* 2004, Khil *et al.*, 2003). In this technique, a polymer solution is loaded and pumped through a syringe fitted with a nozzle connected to a voltage source. The suspended droplet created by gravity and mechanical pumping at the tip of the nozzle, is electrically charged creating a repulsion force directly

opposite to the surface tension. As the intensity of the electric field is increased, the surface of the droplet elongates to form a conical shape called Taylor cone (Taylor 1969). When the electric charges overcome the surface tension of the droplet a charged jet is ejected from the tip of the Taylor cone. As the jet is ejected from the droplet and travel through the air, the solvent evaporates and fibre is deposited on a grounded collector. Figure 1.10 shows the experimental setup for the electrospinning technique.

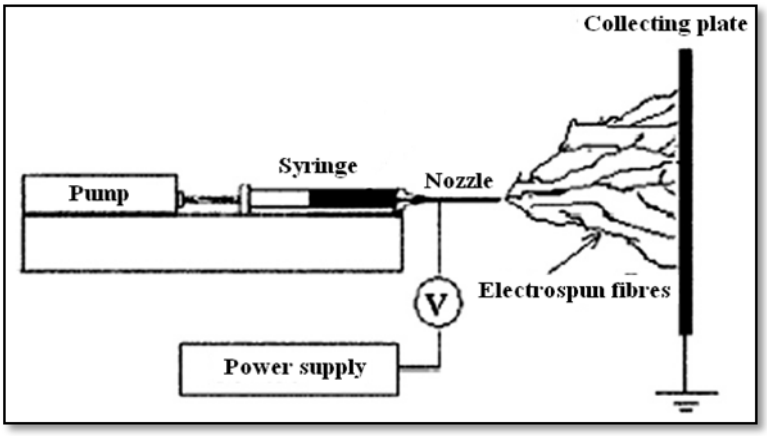

Figure 1.10. Schematic diagram of the electrospinning technique (adapted from Khan *et al.*, 2008)

Electrospinning is a simple, low cost technique, suitable for many soluble polymers. Fibrous structures are obtained with pores ranging from 20-100 μm and porosity higher than 95% (Chen *et al.,* 2007). Different parameters were described to have an effect in the size and shape of the produced fibres including the solution properties, the controlled variables and the ambient parameters. Among the solution properties are viscosity, conductivity and surface tension. On the other hand, the controlled variables include pump flux, electric potential and the distance between the nozzle tip and the collector. Finally, the ambient parameters are temperature, humidity and air velocity (Doshi *et al.,* 1995). By appropriately varying one or more of the above parameters different non-woven, porous and nano/micro-scale fibre based matrix were obtained with different synthetic and natural materials. Among the most used materials are PLGA, PLLA, poly(vinyl alcohol) (PVA), poly(ethylene oxide) (PEO), poly(caprolactone) (PCL), collagen, silk protein and fibrinogen (Smith *et al.,* 2009). Duan *et al.,* (2007) observed good cell attachment of fibroblast cells to a 275 ± 175 nm PLGA–chitosan/PVA composite fibers. Chen *et al.,* (2007) found that cell adhesion and growth are significantly affected as a function of fibre diameter and that in the range of 428-1051 nm fibres, cell adhesion and growth decreased with increasing fibre diameter. On the other hand,

Lu *et al.,* (2012) studied the effect of Poly(3-hydroxybutyrate-co-3-hydroxyvalerate), P(3HB-co-3HV), fibre orientation on the growth behaviour of bone-marrow-derived mesenchymal stem cells, showing that random-oriented nanofibrous scaffold are most favourable for cell growth, compared to aligned fibre scaffold.

1.5. Polyhydroxyalkanoates

In this project we proposed Poly-3-hydroxyoctanoate, P(3HO), a medium chain length biodegradable and biocompatible polyhydroxyalkanoate, as the biomaterial to deliver cells to the injured tissue and to support the organ during its regeneration process. PHAs are polyesters composed of several units of hydroxyalkanoate monomers linked to each other through ester linkages. Figure 1.11 represents the PHA's general formula where 'n' is the number of monomer units in each polymer chain, which varies between 100 and 30000, 'R_1' and 'R_2' the side chain that includes alkyl groups with 1 to 13 carbons and 'x' in the main chain which ranges from 1 to 4.

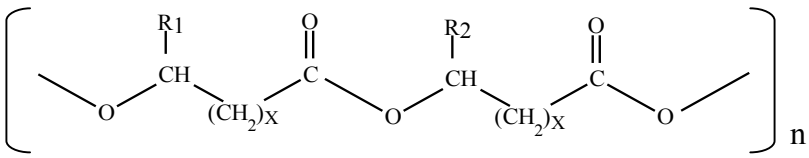

Figure 1.11. General formula for PHAs. R_1/R_2: Alkyl groups C_1-C_{13}, x: 1-4, n: 100-30000.

Numerous microorganisms synthesize PHAs by the fermentation of a carbon source and then accumulate them as intracellular carbon reserve inclusion bodies. In order to accumulate PHAs in most bacteria an excess supply of carbon and limitation of nitrogen, phosphorus, oxygen or magnesium is required. These elements are essential for the cell growth i.e. nitrogen is one of the main constituents of aminoacids, nucleic acid, nucleotides and coenzymes, phosphorous constitutes nucleic acids, nucleotides and phospholipids and magnesium is cofactor for certain enzymes reactions. These unfavorable growth conditions result in a decrease in cell growth and division, and a redirection of their metabolism towards the biosynthesis of the PHAs (Jurasek *et al.,* 2004). The stored PHA can be degraded by intracellular depolymerases and metabolized as carbon and energy source when needed (Byrom *et al.,* 1994).

The properties of PHAs vary depending on the distance between ester groups in the molecule, the structure of the side groups and the number of monomer units in the polymer chain. For example, the length of the side chain and its functional group has a direct effect on the polymers physical properties such as flexibility, crystallinity, melting point and glass transition temperature (Volvoa *et al.*, 2004). The nature and proportion of the PHA monomers are influenced by the type and relative quantity of carbon sources supplied to the growth media, the organism used and the culture conditions provided (Ojumu *et al.*, 2004). For instance, based on growth conditions and the used microorganism, the molecular weight of the polymers can vary from 2×10^5 to 3×10^6 Daltons (Byrom *et al.,* 1994).

PHAs can be either thermoplastic or elastomeric materials with variable mechanical, thermal stability and durability properties. They are water insoluble and impermeable to oxygen (Chen *et al.,* 2010). Due to the stereospecificity of the PHA synthase, all the hydroxyalkanoate monomers incorporated in the polymer are in the R(-) configuration, resulting in an optically pure polymer (Zinn *et al.,* 2005). Additionally, they are biodegradable; hence, they can be degraded and metabolized by microbes and by enzymes within the human body; biocompatible, they do not generate toxic by-products and some of them are piezoelectric, a property known to stimulate cell growth (Philip *et al.*, 2007).

Based on the number of carbon atoms in the monomer units PHAs can be divided in two main different groups: the short chain length polyhydroxyalkanoates (scl-PHAs), which consist of C_3-C_5 atoms, and the medium chain length polyhydroxyalkanoates (mcl-PHAs) consisting of C_6-C_{14} atoms (Ojumu *et al.*, 2004). Also, it has been observed that some organisms produce copolymers including both scl and mcl monomers, these are referred to as scl-mcl PHAs. These groups are a consequence of the PHA synthase substrate specificity, which accepts precursors of a certain range of carbon length (Rehm *et al.*, 2001).

Poly(3-hydroxybutyrate), P(3HB), the simplest and most common example of the scl-PHAs, is a highly crystalline, brittle, stiff and piezoelectric material with a melting temperature of 177 °C, glass transition temperature of 4 °C, tensile strength of 40 MPa and elongation at break of 6 %. Its biological properties include, complete biodegradability, water resistance, high biocompatibility and a suitable substrate for tissue engineering which enhances cell adhesion, migration, proliferation and differentiation functions (Saad *et al.*, 1999). The mcl-PHAs such as poly(3-hydroxyhexanoate), P(3HHx), or P(3HO) are thermoplastic elastomers with melting point, T_m, ranging between 40-60 °C and glass transition temperature, T_g

ranging between -50 to -25 °C. The mcl-PHAs have lower crystallinity with higher flexibility and softness. They are more thermally stable than scl-PHAs, with an elastomeric nature, which increases with the length of the side chain. These are also biodegradable, water resistant and biocompatible, which could be utilized in medical implants, such as scaffolding for the regeneration of arteries and nerve axons (Witholt *et al.,* 1999). Table 1.3 describes the physical properties of P(3HB), a scl-PHA, P(3HO), a mcl-PHA, and polypropylene, a commonly used synthetic polymer. The crystallinity and tensile strength of P(3HB) are similar to those of propylene, however, the elongation to break is significantly lower than that of propylene. On the other hand, the Young's modulus and elongation to break values for, P(3HO) are comparable to those of propylene and dissimilar in terms of crystallinity and tensile strength. The scl-mcl PHA copolymers have properties intermediate between scl and mcl PHAs (Nomura *et al.*, 2004). Nowadays, most of the studies focus in the development of different types of copolymers for the production of tailor made materials to suit different applications. For example, one of the most commonly produced copolymers that is commercially available is P(3HB-co-3HV). This copolymer is more ductile, elastic and flexible than P(3HB), due to the presence of the hydroxyvalerate groups (El-Hadi *et al.*, 2002). Moreover, it has been reported that the increment in hydroxyvalerate units results in a melting temperature, crystallinity and tensile strength reduction, but an increment in flexibility, impact strength and ductility of the material (Conti *et al.*, 1996). These approaches make PHAs suitable for a wider range of applications and a promising class of new emerging biomaterial (Akaraonye *et al.*, 2010).

Table 1.3. Comparison of the physical properties of P(3HB), a scl-PHA, P(3HO), a mcl-PHA and polypropylene (Ojumu *et al.*, 2004, Rai *et al.*, 2010).

Properties	***scl –PHAs (P(3HB))***	***mcl-PHAs (P(3HO))***	***Polypropylene***
Melting point (°C)	175	49	176
Glass-transition temp (°C)	15	-36	-10
Crystalline (%)	81	30	70
Young's modulus (GPa)	3.5	0.01	1.7
Tensile strength (MPa)	40	1.8	34.5
Elongation to Break (%)	6	276	400

1.5.1. Biodegradability of PHAs

One of the most valuables properties of PHAs is their biodegradability in natural environments. PHAs are degraded completely to carbon dioxide and water under aerobic conditions and lead to methane formation under anaerobic conditions (Volvoa *et al.,* 2006). PHAs can be degraded by depolymerases present in microorganisms and enzymes present in the blood and animal tissues (Jendrossek *et al*., 2002). It has been demonstrated that the main factors that influence PHA biodegradation are the stereoconfiguration of the monomers, the crystallinity, the molecular mass and the chemical composition of the polymer. Only ester linkages of monomers in the (R)- configuration are hydrolysed by the depolymerases (Volvoa *et al*., 2004). In terms of the molecular mass, high molecular mass polymers are degraded more slowly than low molecular mass polymers. For instance, Quinteros *et al.,* (1999) studied the relation between alkyl side chain length and biodegradability, showing an increment in the degradation rates with the polymer length. Additionally, Abe *et al.,* (1999) reported that an increment in the polymer crystallinity resulted in a reduction of the degradation rate and that the depolymerases first hydrolyse polymer chains in the amorphous phase, followed by crystalline phases, with a depolymerisation rate 20 times higher in amorphous than the crystalline phase. Volvoa *et al.,* (2004) described PHA biodegradation based on data obtained from different PHAs as follows: In the first week, the amorphous phase of the polymer is eroded. Then, a disruption of the polymer chain results in the formation of tetramers, dimers and monomers with a decrease in the molecular mass. Finally, the polymer loses it mass and this process can take from months up to 2-3 years, depending to the polymer properties and environmental conditions. Weng *et al.,* (2011) studied the influence of chemical structure on the biodegradability of P(3HB-co-3HV). Results showed that an increment in the hydroxyvalerate subunits resulted in an increment in the biodegradation and that the biodegradation occurred by enzyme catalysed erosion from the surface to the interior. Rai *et al.,* (2011a) studied the degradation behaviour of the P(3HO) homopolymer films. In contrast to other amorphous polymers such as PLGA, which showed bulk degradation, P(3HO) films showed only around 15% of degradation on DMEM media after 3 months and this could be due to the semicrystalline structure of the polymer .

1.5.2. Biocompatibility of PHAs

One of the fundamental requirements for a material to be suitable for medical applications is that it should display adequate biocompatibility. In response to the material composition and degradation products, the host body can release either pro- or anti-inflammatory mediators, which can eventually cause initial acute inflammation, followed by chronic inflammation and possible ultimate rejection of the biomaterial. In addition to the chemical and molecular structure, different parameters were reported to have an influence on the biocompatibility of the material such as the size, porosity, shape and surface topography of the material (Zhao *et al.*, 2003). Among the different parameters, the haemocompatibility of the material is one of the main aspects that will determine the suitability of the material for medical applications. The material should not cause thrombosis, embolisms, antigenic response and destruction of plasma proteins. The haemocompatibility of a material can be evaluated by the haemostasis system, which can be studied by different parameters such as the morphology of the attached platelets and complement activation. Sevastianov *et al.,* (2001) studied the haemocompatibility of P(3HB) and P(3HB-co-3HV) films produced from *R. eutropha* through the determination of relative number and morphology of adherent platelets, complement activation and coagulation system activation. PHA films in contact with blood did not activate the haemostasis system at the level of cell response, but they did activate the coagulation system and the complement reaction. Further experiments, which included purification of the produced polymers showed that resulting P(3HB) and P(3HB-co-3HV) were suitable to be used in contact with blood and that the presence of lipopolysaccharides from the producer bacteria was the factor activating the haemostasis systems ((Sevastianov *et al.,* 2003). One of the main reasons of PHA biocompatibility is the presence of some PHA monomer units in human blood and tissues. It has been demonstrated that the monomer present in the P(3HB) polymer, (R)-3-hydroxybutanoic acid, is present at concentrations of 3-10 mg in 100 ml of blood in healthy humans. Additionally, the presence of low molecular weight forms of P(3HB) have also been detected in lipoprotein fractions of human tissues (Hocking *et al*., 1994, Nelson *et al.,* 1981). However, although a material can be biocompatible, the presence of impurities derived from the method of production and extraction can affect the final biocompatibility of the material, as previously described by Williams *et al*., (1996). Several reports have shown that cell adhesion and proliferation are highly affected by the surface structure of the polymers. Bellino *et al.,* (2013) demonstrated that it is possible to modify cell adhesion and proliferation of a human osteoblastic cell line

by modifying the nanopore size of titania and silica film coating. Rebollar *et al.,* (2008) showed that surface laser modification of polystyrene films resulted in a significant enhancement of human embryonic kidney cell adhesion and proliferation compared to unmodified structures.

1.5.3. Biosynthesis of PHAs

PHA biosynthesis has been intensively studied over the years. Different metabolic pathways were described and the particular pathway used for PHA production was found to depend on the particular metabolic pathways that are operating in a particular microorganism and the carbon source provided. PHA biosynthesis can be divided in two main steps. The first step involves the synthesis of hydroxyacyl-CoA, the PHAs activated monomer units for PHAs. The second step involves a reaction catalysed by the PHA synthase, which use the hydroxyacyl-CoA units as substrates and catalyse their polymerization into PHAs with the concomitant release of CoA (Rehm *et al*., 2001). The synthesis of the 3-hydroxyacyl CoA units can occur mainly by three different pathways (Figure 1.12) (Kim *et al.,* 2007, Doi *et al.*, 1990, Poirier *et al.*, 1995, Steinbüchel *et al.*, 1991). Two of the pathways involve the production of PHAs using carbohydrates as a carbon source and a third using fatty acids.

In the first pathway, PHA biosynthesis occurs from carbohydrates unrelated in structure to the final PHA monomer unit (Kazunori *et al.*, 2001). Three key enzymes are implicated: β-ketothiolase, NADPH-dependent acetoacetyl-CoA reductase, and PHA synthase. The β-ketothiolasecatalyses the condensation of two acetyl-CoA molecules from the tricarboxylic acid cycle. The resulting acetoacetyl-CoA subunits are then converted to 3-hydroxybutyryl-CoA and the PHA synthase catalyzes the esterification of these subunits leading to the formation of P(3HB) (Philip *et al.*, 2007). This pathway can also be utilised for the synthesis of P(3HB-co-3HV).

The second pathway involves the production of PHAs via the fatty acid degradation pathway. In this case, the resulting monomers in the polymer chain were similar in structure to the carbon source or shortened by 2, 4 or 6 carbon atoms (Huisman *et al.*, 1989). In this pathway the fatty acids are first converted to the corresponding acyl-CoA which are then oxidised by the ß-oxidation pathway via enoyl-CoA, (*S*)-3-hydroxyacyl-CoA and 3-ketoacyl-CoA precursors. Finally, enzymes like the enoyl-CoA hydratase, hydroxyacyl-CoA epimerase, and

β-ketoacyl-CoA reductase connect the β-oxidation pathway to the medium-chain length PHA biosynthesis through the PHA synthase (Rehm *et al.*, 2009).

The third pathway involves mcl-PHA production via the fatty acid *de novo* biosynthesis metabolic pathway. This pathway is of significant interest due to the ability of producing mcl-PHAs from carbohydrates that are structurally unrelated to the carbon source and are inexpensive (Kazunori *et al.*, 2001). In this pathway, the carbohydrates are first oxidized to acetyl-CoA molecules that enter into the fatty acid *de novo* biosynthesis. The fatty acid *de novo* biosynthesis leads to the formation of R-3-Hydroxyacyl-ACP precursor, which is then linked to the PHA synthase for the mcl-PHA biosynthesis via the (R)-3-hydroxyacyl-ACP-CoA transacylase (Chen, 2010).

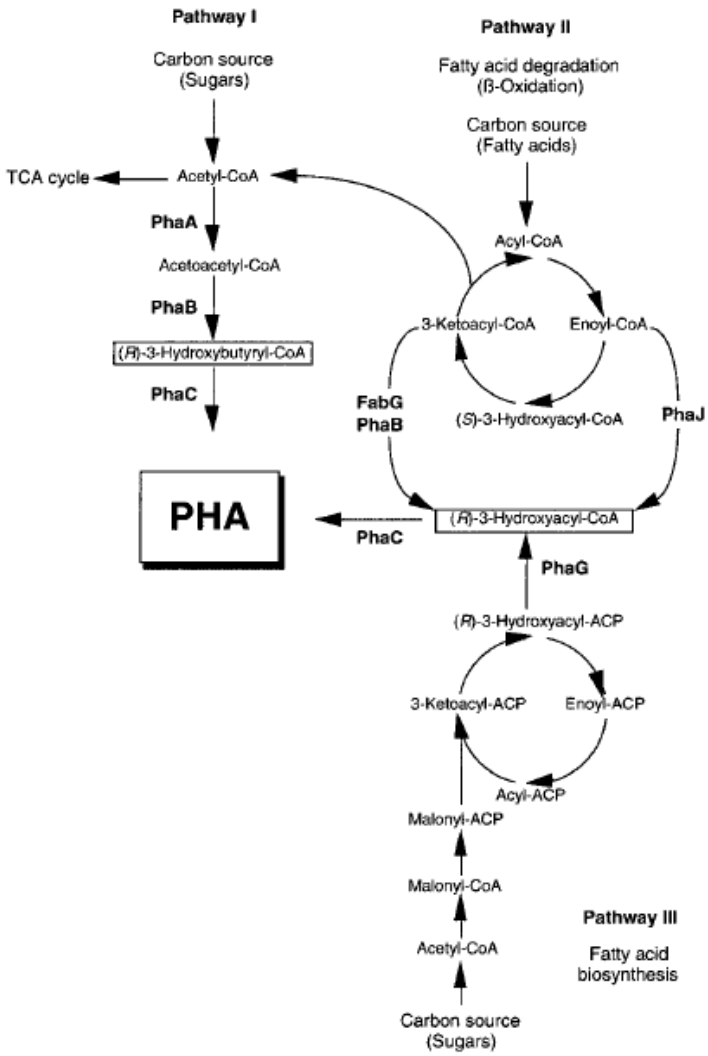

Figure 1.12. Metabolic pathways involved in the biosynthesis of PHAs from related and unrelated carbon sources (adapted from Kazunori *et al.*, 2001).

1.5.4. PHA biosynthetic genes

The PHA synthase gene and the genes encoding other proteins related to the metabolism of PHAs have been studied in a variety of microorganisms. In particular, PHA synthases are the key enzymes of PHA biosynthesis. They are encoded by the *pha*C gene and use coenzyme A (CoA) thioesters of HA as substrates to catalyse the polymerization of HAs into PHAs with the release of CoA (Rehm *et al*., 2002). According to their primary structure, substrate specificities of the enzymes and subunit composition, PHA synthases can be divided into four major classes. Class I and class II PHA synthase enzymes consisting of only one type of subunit (*pha*C), and class III and class IV PHA synthases include two subunits, *pha*C, similar to class I and II PHA synthases, and one subunit with no similarity (*pha*E and *pha*R, respectively). *In vivo* substrate specificity studies showed that class I PHA synthases (e.g. present in *C. necator*) preferably utilize coenzyme A thioesters of scl-3-hydroxyalkanoate subunits (containing from 3 to 5 carbon atoms in the alkyl side chain). On the other hand, class II PHA synthases (e.g. present in *P. aeruginosa*) preferentially utilize coenzyme A thioesters of mcl-3-hydroxyalkanoate subunits (containing more than 5 carbon atoms in the alkyl side chain). Finally, class III (e.g. present in *Aeromonascaviae*) and class IV PHA synthases (present in *Bacillus megaterium*) include enzymes consisting of two subunits. Both subunits preferably utilize coenzyme A thioesters of scl-3-hydroxyalkanoate subunits (containing from 3 to 5 carbon atoms in the alkyl side chain) (Rehm *et al.,* 2003). Table 1.4 illustrates the four different classes of polyester synthases.

Table 1.4. The four classes of PHA synthases (Rehm *et al.*, 2003).

Class	*Subunits*	*Size*	*Substrate*	*Species*
I	PhaC	(60-73 KDa)	$3HA_{SCL}$	*C. necator*
II	PhaC	(60-65 KDa)	$3HA_{MCL}$	*P. aeruginosa*
III	PhaC PhaE	(40 KDa)-(40KDa)	$3HA_{SCL}$	*A. caviae*
IV	PhaC PhaR	(40 KDa)-(22KDa)	$3HA_{SCL}$	*B. cereus SPV*

The PHA genes that encode for the biosynthetic proteins, and genes related to the PHA metabolism are often clustered together in the bacterial genomes. For instance, Steinbuchel *et al.,* (1991) showed that *C. necator* contains PHA synthase gene (*pha*C), β-ketothiolase (*pha*A) gene and NADPH-dependent acetoacetylo-CoA reductase (*pha*B) gene, which comprise the three individual steps in the P(3HB) biosynthetic pathway, organized in a single operon. Rehm *et al.,* (1999) reported that *Pseudomonas sp.* possess two different PHA synthase genes (*pha*C), separated by another gene, *pha*Z, that encodes an intracellular PHA depolymerase. Downstream of the second *pha*C gene are the *pha*D, *pha*I and *pha*F genes. *Pha*D plays a role in the regulation of the size and number of PHA granules formed, *pha*F codes for a regulatory protein which is associated with PHA granules and controls the expression of the *pha*C and *pha*I genes and *pha*I codes for a newly identified granule-associated protein (Prieto *et al.,* 1999). Hein *et al.,* (2002) compared both PHA synthases (*pha*C1 and *pha*C2) from *Pseudomonas mendocina* by creating knock-out mutants. Results provide evidence that *pha*C1 is the major enzyme for PHA synthesis, whereas *pha*C2 contributes to the accumulation of PHAs to only a minor extent. Levergiesell *et al.,* (1992) showed that *C. vinosum* and all bacteria that possess two component PHA synthases (*pha*C and *pha*E) contain both enzymes and all PHA metabolism genes in the same operon.

1.5.5. PHA producing microorganisms

1.5.5.1. Wild type producing microorganisms

More than 250 strains were described as PHAs producers, however, only a few of them are usually employed for PHA production. Among the most used are *Cupriavidus necator, Alcaligenes latus, Bacillus megaterium, Pseudomonas oleovorans* and *Pseudomonas putida* due to their capacity to grow in a range of substrates and their ability to synthesize a wide range of PHAs depending on the carbon source and the cultivation condition utilized (Chen *et al.,* 2010). P(3HB) is the most common and widely studied PHA (Lemoigne *et al*., 1926). Since then, various bacterial strains among Gram positive and Gram negative bacteria have been identified to accumulate P(3HB) both aerobically and anaerobically. Awareness of the cost of production of PHAs and the need of industrialization encouraged several groups to work intensively in reducing production costs. In 1990, Hangii reported *A.latus* as the main candidate for P(3HB) production due to the fast growth and the ability to use cheap carbon sources. However, since then, many different strains and strategies were developed for the

P(3HB) production. Yu *et al.,* (2008) achieved a 57% P(3HB) dry cell weight (DCW) yield under appropriate C/N ratios in *C. Necator.* Omar *et al.,* (2001) reported P(3HB) content of cells of up to 50% when *B. megaterium* was fed with date syrup and beet molasses. Akaraonye *et al.,* (2011) obtained 67% DCW yield of P(3HB) using *Bacillus cereus* SPV in the presence of sugarcane molasses.

Among the mcl-PHA producer microorganisms *P. oleovorans* was the first bacteria reported to produce a mcl-PHA copolymer containing P(3HO) when grown on *n*-octane as the sole carbon source (De Smet *et al.,* 1983). After this finding, Haywood *et al.,* (1989) examined various *Pseudomonas* species for grow and polymer accumulation with different alkanes, alcohols and alkanoic acids as the sole carbon source and proved that mcl-PHA production were not only restricted to *P. oleovorans* but also to *P. aeruginosa, P. putida, P. fluorescens,* and *P. testosterone*. Later, it was found that mcl-PHAs are accumulated mainly by *Pseudomonas* belonging to rRNA-DNA homology group I and that a number of strains in this group were able to produce scl- and mcl-PHA copolymer (Kabilan *et al.*, 2012). Mcl-PHAs and copolymers attracted a lot of attention due to their flexible and elastomeric properties for industrial and particularly biomedical applications, where flexible biocompatible biomaterials are required. Liu *et al.,* (2011) produced Poly(3-hydroxydecanoate-co-dodecanoate), P(3HD-co-HDD), copolymer when *P. putida* was grown on dodecanoic acid as a single carbon source. Mechanical characterization of the polymer properties showed the flexible nature of the material. Rai *et al.*, (2011a) reported the production of an absolute homopolymer of P(3HO) when *P. mendocina* was grown in octanoate, in contrast to other well studied organisms such as *P. putida, P. oleovorans, P. aeruginosa, P. resinovorans* and *P. stutzari,* which accumulate copolymers. Mechanical, thermal, and chemical analysis carried out on the P(3HO) produced homopolymer revealed the flexible, elastomeric and semicrystalline structure of the material (Rai *et al*., 2011a).

1.5.5.2. Recombinant PHA producer microorganisms

One of the most popular strategies for enhancing the type, quality or quantity of the produced PHAs consists in the homologous or heterologous expression of the PHA biosynthetic enzymes in different microorganisms including PHA or non-PHA producers. Several used strategies aim to reduce the cost of the polymers by developing recombinant strains able to utilize cheap carbon sources and free of PHA degradative pathways to accumulate high

amounts of PHAs. For example, Park *et al.,* (1997) over expressed the PHA biosynthetic genes from a plasmid on *C. necator* showing increased levels of P(3HB) and reduced fermentation times. Povolo *et al.,* (2010) converted *C. necator*, a strain unable to grow on lactose, into an organism capable of growing on lactose contained in waste material, by cloning the *Escherichia coli lac* genes into the PHA depolymerase gene. Higher PHA yield was obtained compared to the wild type strain.

Other strategies have focused on the development of novel PHAs by introducing new PHA biosynthetic pathways or genes into different strains. Li *et al*., (2011) cloned PHA biosynthetic genes from *Aeromonas caviae* into *P. putida* allowing the recombinant bacteria to produce a scl-mcl-PHA copolymer consisting of 3HB, 3-hydroxyvalerate, 3HV, and 3-hydroxyheptanoate, 3HHp. The resulting copolymer, P(3HB-co-HV-co-3HHP), was shown to have highest tensile strength and stiffness compared with other commercially available PHAs. Ma *et al.,* (2009) showed that when the 3-hydroxyacyl-CoA dehydrogenase gene was partially or completely deleted in *P. putida*, the produced copolymer composed of P(3HD-co-3HDD) showed the highest melting temperature and Young's modulus among all the studied PHAs.

Escherichia coli is one of the most widely used hosts for the production of heterologous PHAs as it has shown outstanding results in standard recombinant expression applications and a capacity for large scale production, to meet commercial demands (Sorensen *et al*., 2005). Zheng *et al.,* (2011) worked on the development of an *E.coli* capable of synthesising PHAs and succinate from a mixture of glycerol, glucose and fatty acids (by-products of the biodiesel production process) by overexpressing the *pha*C1 gene from *P. aeruginosa*. The resulting strain was able to synthesize succinate and a copolymer composed of P(3HO) and P(3HD). However, the presence of toxic lipopolysaccharides present in all Gram-negative stains, which are co-purified with PHAs, limited the use of these polymers in medical applications.

Singh *et al.,* (2009) described *Bacillus subtilis* as a potential host for the production of PHAs. Gram-positive bacteria lack LPS and hence they are preferred hosts for the production of PHAs for biomedical applications (Valappil *et al*., 2007). In particular, *B. subtilis* is generally recognized as a safe (GRAS) organism by Food and Drug administration (FDA) and is among the most studied and widely used microbes for large-scale production of recombinant proteins, amino acids and chemicals. In addition, *B. subtilis* subsp. s*ubtilis* was described as a

non-PHA producer like *E.coli*, and hence it can also be used for the expression and study of PHA biosynthetic genes (Singh *et al.,* 2009). Wang *et al.,* (2006) have worked on the expression of the *pha*C1 gene from *Pseudomonas aeruginosa* in *B. subtilis* DB104, in the presence of glucose as a carbon source. Results showed that recombinant bacteria were able to produce P(3HD-co-3HDD). Furthermore, the incorporation of the *pha*A gene, encoding the β-ketothiolase and the *pha*B gene encoding the acetoacetyl-CoA-reductase from *R. eutropha* resulted in the production of a Poly(3-hydroxybutyrate-co-3-hydroxydecanoate-co-3-hydroxydodecanoate, P(3HB-co-3HD-co-3HDD), when malt waste was used as carbon source.

1.5.6. Production of PHAs by fermentation

PHA production in bioreactors was carried out in batch, fed-batch and continuous processes (Jung *et al*., 2001, Sun *et al*., 2007, Suwannasing *et al.,* 2011). In a batch process, the bioreactor is supplied with fresh media and inoculum. At the end of the fermentation process, the content of the bioreactor is harvested and the polymer is extracted. In fed-batch processes, fresh nutrient is continuously supplied in the bioreactor during the fermentation process. In this case, cells are allowed to grow exponentially until stationary phase. At this point, specific substrates were added to promote the production of specific PHAs. In some cases, when cells grow exponentially and nutrients start to be consumed, specific carbon sources are supplied to allow an increment in the cell concentration, the production phase and the final product. Continuous processes are based on a continuous feed and withdrawal of nutrients and culture from the system. In this case, a high cell concentration is achieved by a continuous circulation of media, allowing to maintain a substrate concentration at one desirable level, followed by a product formation phase with nutrient depletion (Rehm *et al*., 2009).

Based on the culture conditions required for PHA synthesis, bacteria can be divided into two major groups. One group requires an excess supply of carbon and limitation of nitrogen, phosphorus, oxygen or magnesium such as C. *necator* and *P. oleovorans*, while the second group do not require nutrient limitation for PHA accumulation such as *A. latus*, *A. vinelandii* and recombinant *E. coli.* These characteristics are important to be considered for deciding the fermentation strategy for PHA production. The fermentation condition should be designed to allow cells to grow to a high density for high productivity and then to stop growing or dividing and redirect their metabolism to the accumulation of PHAs (Jurasek *et al*., 2004).

Generally, when processes involve a complete depletion of a nutrient, fed-batch fermentations were utilized with PHA accumulation occurring during the nutrient depletion stage (Kim *et al*., 1997; Lee *et al*., 2000; Diniz *et al*., 2004).

As different strains require different growth conditions, the fermentation strategy used for PHA accumulation varies with the organism used. Additionally, physiological conditions used have a direct effect in PHA subunit composition, cellular PHA content, specific PHA synthesis rate and overall volumetric productivity (Sun *et al*., 2007). Page *et al.,* (1989) reported that when *A. vinelandii* was grown in batch culture, under an oxygen limiting condition, a reduction in the activity of the tricarboxylic acid cycle, and the redirection of acetyl-CoA molecules resulted in P(3HB) production. Later, Chen *et al.,* (1997) reported higher yield of PHAs when *A. vinelandii* was growth in fed-batch cultures, with high aeration during the first stage and low aeration in the second stage, prompting P(3HB) formation. Presuting *et al.,* (1991) studied the mcl-PHA production with *P. oleovorans* showing that the specific mcl-PHA accumulation rate is strongly dependent on the specific growth rate of the strain and is highest when it grows at 0.2 h^{-1}, which is less than half of the maximum specific growth rate. Jung *et al.,* (2001) worked on the production of mcl-PHAs in two-stage continuous cultivation with a dilution rate of 0.2 and 0.16 h^{-1} in the first and second stage, respectively. Under these conditions, *P. oleovorans* cells contained 63% DCW PHAs, which was one of the highest PHA yield obtained in *P. oleovorans*. Hence, as optimal conditions for PHA production are not the same in all the cases, it is necessary to assess the optimal condition for different bacteria, carbon source or media composition employed.

One of the main limitations in the PHA production is the production cost. For example, it has been reported that PHA production is 10 times more expensive than polyethylene production (Kasemsap *et al*., 2007). The most important limitation factors in the production of PHAs are the special growth conditions required, the media utilized, the fermentation process and the PHA recovery. Hence, several groups have focused in developing systems that allow a high volumetric productivity. This parameter will define the size of a product needed to meet market demands. Currently, one of the main PHA produced at industrial scale, is the copolymer P(3HB-co-3HV) by *C. necator,* due to the cost effectiveness of the process (Verlinden, 2007).

It is well known that trying to reproduce results obtained in shaken flask, in bioreactors is a difficult task and in many cases the variables involved are not very well understood. For this

reason, there is a need to find the optimal growth conditions when bioreactors are used (Peña *et al.*, 2011). Once the optimal growth condition for a specific strain and media composition is achieved, PHA production can be scaled-up. Scale-up studies based on the constant power input or constant oxygen transfer parameters have been carried out. The constant power input scaling-up criteria is based on a constant amount of energy required to maintain fluid motion within a vessel, in a given period of time. Power input is often referred to as volumetric power consumption and is representative of the turbulence degree and media circulation in vessels, and influences heat and mass transfer, mixing and circulation times (Marques *et al.,* 2010). On the other hand, the constant oxygen transfer technique is based on keeping the same oxygen transfer rate (OTR) at different scales. The dissolved oxygen concentration in a suspension depends on the rate of the oxygen transfer from the gas phase to the liquid phase, the rate at which oxygen is transported into the cells and on the microorganism oxygen uptake rate. In stirred tank bioreactors, different variables affect the mass transfer, however, the main ones are the stirrer speed, type and number of stirrers and gas flow rate used. The correct measurement of the OTR is a crucial step for the prediction of the conditions for larger scales (Garcia-Ochoa *et al.,* 2009).

1.5.7. Applications of PHAs

As discussed earlier, PHAs are a family of biodegradable polyesters produced by the bacterial fermentation of a carbon source. According to the monomer content, PHAs properties can range from rigid and stiff to flexible and elastomeric material. Several bacterial strains, carbon sources and growth conditions have been explored and more than 150 PHA monomer subunits have been incorporated into PHA polymers allowing the development of a range of PHAs (Chen 2010). As a result, tailor made materials have been developed for different applications ranging from packaging material to biomedical applications.

1.5.7.1. Bulk applications

PHAs have attracted a lot of attention as materials for various applications for substitution of oil-derived polymers, due to their capacity to be produced from a renewable source, their biodegradable characteristics which allow them to degrade without generation of toxic by-products and the ample range of monomer compositions appropriate for different kinds of applications. Initially, PHAs were used in packaging films such as bags, containers, paper

coatings and disposable items including razors, utensils, diapers, feminine hygiene products and cosmetics. The first consumer product made from PHAs was shampoo bottles launched by Wella® (Germany) in 1990 (Chen 2010). However, they have not had a wide application mainly because of their production costs. For this reason, currently, only a few PHAs are available in the market. Although, at present, petrochemical plastics are a more economically feasible choice than biodegradable ones, future lack in oil supply will result in a drastic increase in the petrochemical plastic production costs. On the other hand, further research on microbial strains, inexpensive substrate sources, diverse fermentations strategies, polymer recovery and purification can substantially reduce the production cost and make PHAs commercially relevant.

1.5.7.2. Medical applications

PHAs are attractive materials for biomedical applications because of their natural origin, enhanced biocompatibility, biodegradability, and their ability to support cell growth and proliferation (Valappil *et al.,* 2006). The biological response of a biomaterial *in vivo* is the main property that will determine the material use in the medical field. For example, Shishatskaya *et al.,* (2002) tested the toxicity of P(3HB) and P(3HB-co-HV) threads implanted in Wistar rats during a period of six months. Results showed no adverse changes in physiological and biochemical parameters. Williams *et al.,* (1999) reported the effect of a subcutaneous poly(3-hydroxyoctanoate-co-3-hydroxyhexanoate),P(3HO-co-HHx), implant for 40 days in mice with no infiltration of macrophages and a minimal reaction to the implants, which were encapsulated, with a thin layer of fibroblasts during the 40 days experiment. From all the produced PHAs, only some of them are currently in sufficient quantities to be evaluated as potential material for different applications, including P(3HB), P(3HB-co-3HV), poly-4-hydroxybutyrate, P(4HB), poly(3-hydroxybutyrate-co-3-hydroxyhexanoate), P(3HB)-co-HHx, and P(3HO) (Byrom, 1992, Chen *et al.,* 2001, Hrabak, 1992). These PHAs have been utilized to develop devices for different biomedical applications such as wound dressing, orthopaedic pins, slings, adhesion barriers, stents, articular cartilage, bone marrow scaffolds, nerve guides, tendon repair devices and cardiovascular patches (Chen *et al.,* 2005). In addition to this, the potential use of PHAs in drug delivery has been evaluated in a number of studies as subcutaneous implants,

compressed tablets for oral administrations and microparticulate carriers for intravenous use (Williams *et al*., 1996).

1.5.7.2.1. Cardiovascular applications

As many synthetic materials were unable to repair and regenerate cardiac tissue and some of them show high risks of immune responses, several groups have been focused on finding alternative materials for cardiac tissue engineering applications (Smaill *et al.,* 2000). Malm *et al.,* (1992) studied the effect of P(3HB) as a pericardial patch after the pericardium was excised and replaced with the polymer in 18 sheep. Patches were removed between 2 and 30 months after operation and examined for adhesions, infection and inflammatory responses. No adhesion was observed between the heart and the sternum in 14 of the treated animals. After 24 months post-operation, polymer remnants were still present on the animals. Although some macrophages were still found at 30 months, no platelet aggregates were detected. Duvernoy *et al.,* (2007) evaluated the effect of P(3HB) patches in 50 human patients admitted for bypass surgery or valvular replacement. Results showed a low incidence of postoperative adhesions between the patch and the cardiac surface in patients treated with the patches. Malm *et al.,* (1994) worked on the implantation of P(3HB) transannular patches into the right ventricular outflow tract and pulmonary artery of 13 sheep. Dacron patches were implanted in the control groups. Implanted patches were analyzed 3 to 24 months later showing no aneurysm formation. Comparable amounts of native arterial tissue of neointima and neomedia were obtained with the test group but not with the control group. Dacron implants presented a collagen layer and dense lymphocytes infiltration due to the inflammatory reaction of the material. In contrast, P(3HB) patches were phagocytated by macrophages and no platelet aggregates were observed. Furthermore, the P(3HB) regenerated vessel showed structural and biochemical qualities in common with the native pulmonary artery. Shum-Tim *et al.,* (1999) evaluated the elastomeric polymer P(3HO-co-3HHx) as a copolymer with PGA for the production of tissue engineered vascular grafts seeded with autologous cells. Resulting constructs were placed in lambs aortic segments. Results showed no aneurysms formation and an insignificant inflammatory response, with increased cell density, collagen formation and mechanical properties that resemble those of the native aorta. Stock *et al.,* (2000) showed good vascular cell growth, no thrombus formation and good mechanical properties when P(3HO-co-3HHx) films were blended with PGA and used to

replace pulmonary valve leaflet in lambs, in contrast to results obtained with PGA-PLA blends implants which show high stiffness and rigidity.

AIMS AND OBJECTIVES

The aim of this project was to synthesise P(3HO), a unique mcl-PHA homopolymer and its use in the production of cardiac patches.

The specific objectives to be met in order to fulfil the above overall aim include:

1- *An attempt towards the development of a Gram-positive recombinant strain for the production of LPS-free P(3HO).* At present, Gram-negative bacteria are the only industrial source of mcl-PHAs. However, the membrane of Gram-negative bacteria species contain lipopolysaccharides (LPS), which are co-purified with PHAs and cause immunogenic reactions. Consequently, part of this study was aimed to express the *Pseudomonas mendocina* PHA synthase gene (*pha*C1) in the LPS-free Gram-positive microorganism *Bacillus subtilis.* The produced polymer was characterized in terms of mechanical, thermal, wettability and surface topography properties.

2- *Production and characterization of P(3HO) using Pseudomonas mendocina.* P(3HO) homopolymer was produced from *P. mendocina* in 2 L bioreactors. The obtained polymer was fully characterized in terms of mechanical, thermal, wettability and surface topography properties. Its effect on contraction and viability of fresh rat isolated cardiomyocytes was assessed.

3- *Large scale production of P(3HO).* Optimization of P(3HO) production was carried out in 2 L bioreactors. Optimized conditions were scaled-up for the production of P(3HO) in the 20 L bioreactor and the 72 L pilot plant bioreactor.

4- *Construction of P(3HO) cardiac patches*. P(3HO) cardiac patches were designed using the solvent casting, particle leaching technique and electrospinning. Resulting constructs were characterized in terms of mechanical, thermal, wettability and surface topography properties. Biocompatibility of the P(3HO) cardiac patches was assessed using C2C12 myoblast cell line.

5- *Functionalisation of the cardiac patches*. The arginine-glycine-aspartic acid (RGD) tripeptide sequence was immobilized on the surface of the P(3HO) films to allow efficient host cell recruitment and adhesion. Vascular endothelial growth factor (VEGF) was incorporated in the films to assist cellular proliferation, differentiation, migration and vascularisation. Additionally, VEGF was incorporated in P(3HB) microspheres produced

using the recombinant *B. subtilis* created in the first part of the project. The VEGF release profile was assessed. *In vitro* cell culture work was carried out with C2C12 myoblast cell line to assess the biocompatibility of the final functionalised cardiac patches.

CHAPTER 2

Materials and Methods

2.1. MATERIALS

2.1.1. Bacterial strains

Pseudomonas mendocina was obtained from the National Collection of Industrial and Marine Bacteria (NCIMB) and the *Bacillus subtilis 1604* was bought from *Bacillus* Genetic Stock Centre (BGSC). All the *Escherichia coli* strains were obtained from the culture collection of University of Westminster, London, UK.

2.1.2. Cell line and cell culture materials

C2C12 myoblast cell line was purchased from Sigma-Aldrich, Dorset UK.

2.1.3. Plasmid vector used for cloning and expression

The pHCMC04 vector, extracted from *Escherichia coli* ECE 189, is 8089 base pairs in size. It is a *B. subtilis*-*E. coli* shuttle vector that replicates as theta circles and it contains a PxylA promoter, which is functional in the presence of xylose in the media (Nguyen *et al*., 2005). The genes that compose the pHCMC04 are described in Table 2.1.

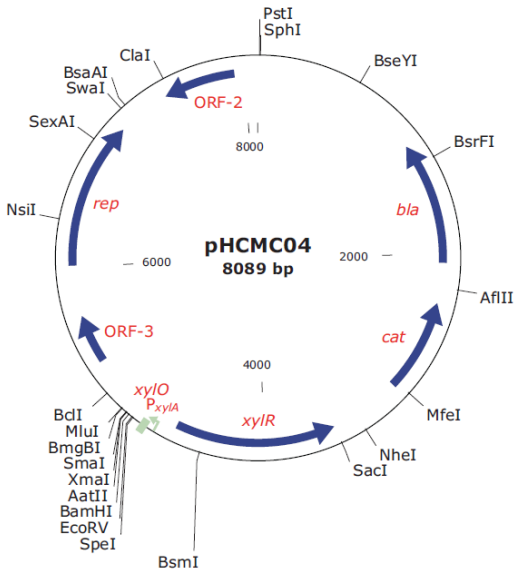

Figure 2.1. Genetic and restriction map of the pHCMC04 expression vector (taken from *Bacillus* Genetic Stock Centre manual).

Table 2.1. pHCMC04 genetic map description

GENE	***FUNCTION***
Rep	replication initiation protein from theta replication plasmid pBS72.
Cat	encodes chloramphenicol acetyl transferase; selectable in either *E. coli* or *B. subtilis* (chloramphenicol 5 µg/ml)
Bla	encodes β-lactamase; selectable in *E. coli* only (ampicillin 100 µg/ml)
ORF	unknown function
xylR	represses transcription from the P_{xylA} promoter; xylose relieves repression

2.1.4. Chemicals proteins and kits

The chemicals used in this study were purchased from Sigma-Aldrich (Dorset, England) and VWR (Poole, UK). The Wizard Genomic DNA Purification Kit, the 1-Kb step ladder, the *Pfu* DNA polymerase master mix and all the primers were purchased from Promega (Southampton, UK). The gel extraction and miniprep kits were obtained from QIAGEN (Sussex, UK). The restriction enzymes were acquired from New England Biolabs (Hertfordshire, UK). The VEGF ELISA kit was purchased from Invitrogen (Paisley, UK).

2.1.5. Reagents

2.1.5.1. Agarose gel

- Tris-borate-EDTA buffer (g/L) (5X): 54 g of Tris-Base, 27.5 g of Boric acid and 20 ml of 0.5 M EDTA (pH=8).
- Loading dye (6X): 30 % Glycerol, 0.25 % Bromophenol blue and 0.25 % Xylene Cyanol FF.

2.1.5.2. Miniprep plasmid extraction

- Solution I: 50 mM Glucose, 25 mMTris-HCl pH 8 and 100 mM EDTA
- Solution II: 0.2 N NaOH and 1% SDS

- Solution III: 60 % of 5 M Potassium acetate and 11.5 % Acetic acid glacial.

2.1.5.3. SDS-PAGE

- *Resolving gel (12%):* 4.9 ml of 1.5 M Trizma base pH 8.8, 100 µl 10 % SDS, 3 ml of 40 % Acrylamide, 100 µl of 10 % Ammonium persulfate, 20 µl of TEMED and 4.9 ml water.
- *Stacking gel (4%):* 625 µl of 0.5 M Trizma base pH 6.8, 50 µl 10 % SDS, 500 µl of 40 % Acrylamide, 50 µl of 10 % Ammonium persulfate, 10 µl of TEMED and 3.6 ml water.
- *Sample buffer (4x):* 6 ml of Trizma base 0.5 M pH 6.8, 9.6 ml of 10 % SDS, 2.4 ml of β-mercaptoethanol, 2.4 ml of 10 % Bromophenol blue, 4.8 ml of Glycerol and 4.8 ml of water.
- *Running buffer (10x):* 25 mM of Trizma base, 192 mM of Glycine and 0.1 % of SDS.
- *Staining solution*: 0.25 g/L of Brilliant Blue R and 10 % of Acetic acid glacial.
- *Destaining solution:* 10 % Acetic acid.

2.1.5.4. *Krebs-Henseleit* solution (mmol/L): NaCl 119, KCl 4.7, $MgSO_4$ 0.94, KH_2PO_4 1.2, $NaHCO_3$ 25 and glucose 11.5.

2.1.6. Bacterial growth media composition

2.1.6.1. *Pseudomonas mendocina* growth media

- Mineral salt medium production media (MSM_{PM}) (g/L): $(NH_4)_2SO_4$ 0.50, $MgSO_4$ 0.40, Na_2HPO_4 3.80, KH_2PO_4 2.65 and trace elements (PM) solution 1 mL/L.
- Mineral salt medium production media ($MSM_{2nd\ seed}$) (g/L): $(NH_4)_2SO_4$ 0.50, $MgSO_4$ 0.40, Na_2HPO_4 3.80, KH_2PO_4 2.65 and trace elements (PM) solution 1 mL/L.
- Trace elements (PM) (g/L): $CoCl_2$ 0.22, $FeCl_3$ 9.70, $CaCl_2$ 7.80, $NiCl_3$ 0.12, $CrCl_6.H_2O$ 0.11, $CuSO_4.5H_2O$ 0.16.

2.1.6.2. *Bacillus subtilis* growth media

- Ramsay media (g/L): $Na_2HPO_4.7H_2O$3.7, $KH_2PO_4$0.83, $(NH_4)_2SO_4$ 2.0, $MgSO_4.7H_2O$ 0.2, ferrous ammonium citrate 60, $CaCl_2$.$2H_2O$ 10 and trace elements (BS) solution 1 mL/L.
- Trace elements (BS) (g/L): 0.3 g/L H_3BO_3, 0.2 g/L $CoCl_2.6H_2O$, 0.1 g/l $ZnSO_4.7H_2O$,

- 30 mg/L $MnCl_2.4H_20$, 30 mg/L $NaMoO_4.2H_2O$, 20 mg/L $NiCl_2.6H_20$, and 10 mg/L $CuSO_4.5H_20$).
- Kannan and Rehacek media (g/L): Yeast extract 2.5, Potassium chloride 3, Ammonium sulphate 5 and Soybean dialysate 100 mL/L
- Soybean dialysate: Dialysis of 10 g of defatted soybean flour in 1L of distilled water for 24 hr at 4°C.

2.1.7. Bioreactors

2.1.7.1. 2 L Bioreactor

The 2 L bioreactor used in this study was a stirred tank with 2 Rushton turbine impellers and buffers. The vessel was a 200 series Fer mac® (Electrolab) and total volume was 2 L. The ratio of impeller to vessel was 2. The vessel temperature was controlled with a wrap-around heating belt and the pH and dissolved oxygen tension (DOT) were controlled with Bradley James® electrodes. The bioreactor sterilization was carried out in an autoclave at 132 ºC for 30 minutes.

Figure 2.2. The 2 L stirred tank bioreactor used in this study

2.1.7.2. 20 L Bioreactor

The 20 L bioreactor was a stirred tank with 2 Rushton turbine impellers and buffers. The vessel was a 2000 series LH® and total volume was 20 L. The ratio of impeller to vessel was 3.28. The vessel temperature was controlled with a heat exchanger and the pH and dissolved oxygen tension (DOT) were controlled with Mettler Toledo® electrodes. The bioreactor sterilization was carried out in place with live steam at 132 ºC for 30 minutes.

Figure 2.3. 20 L stirred tank bioreactor used in this study

2.1.7.3. 72 L Bioreactor

The 72 L bioreactor was a stirred tank with 2 Rushton turbine impellers and buffers. The vessel was a 1075 series LH® and total volume was 72 L. The ratio of impeller to vessel was 3.09. The vessel temperature was controlled with a heating jacket and the pH and dissolved oxygen tension (DOT) were controlled with Mettler Toledo® electrodes. The bioreactor sterilization was carried out in place with live steam at 132 ºC for 30 minutes.

Figure 2.4. 72 L stirred tank bioreactor used in this study

2.2. EXPERIMENTAL METHODS

2.2.1. Construction of recombinant *Bacillus subtilis* strain

For the construction of the recombinant *Bacillus subtilis* strain containing the *pha*C1 gene, *P. medocina* genomic DNA was extracted and the *pha*C1 gene was amplified by PCR. The *pha*C1 gene was ligated to the pHCMC04 *B. subtilis-E. coli* shuttle vector and *E. coli* XL1 blue competent cells were transformed with ligation products for plasmid amplification. The *pha*C1-pHCMC04 plasmid was isolated and the *pha*C1 sequence integrity was confirmed by sequencing. *B. subtilis 1604* was transformed with the *pha*C1-pHCMC04 plasmid. Figure 2.5 shows a schematic representation of the steps followed for the cloning of the *pha*C1 gene into *B. subtilis* 1604.

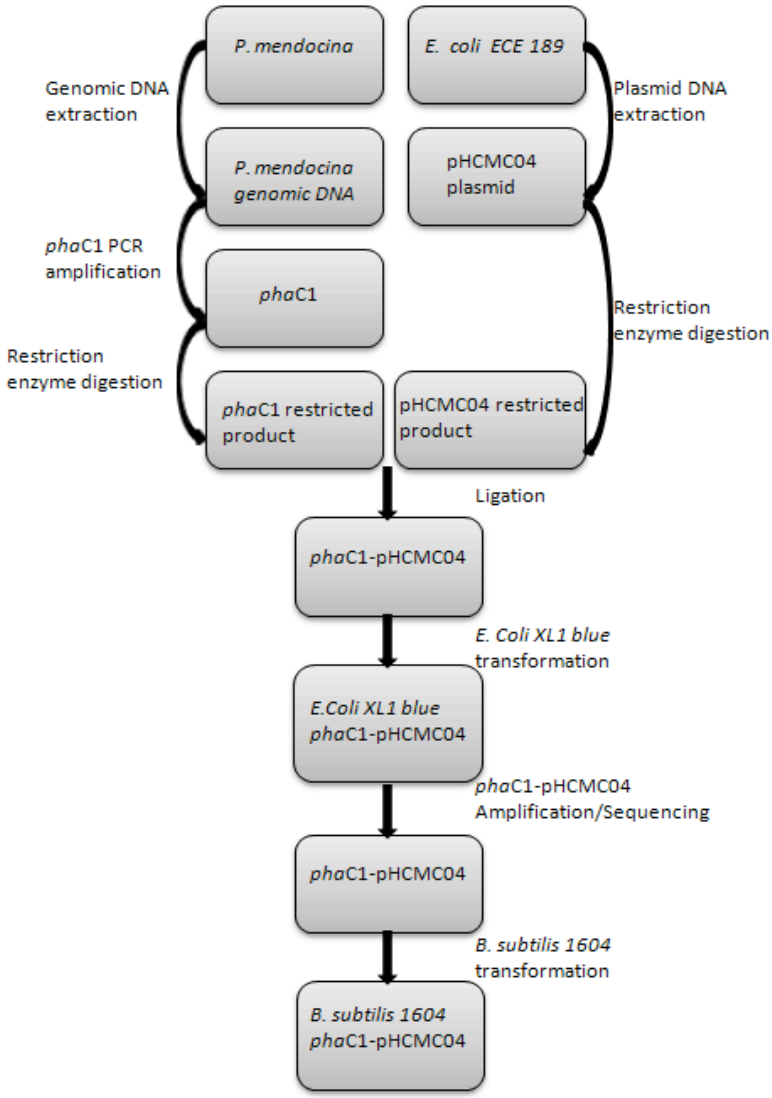

Figure 2.5. Schematic representation of the strategy used for the cloning of *pha*C1 into *B. subtilis 1604*.

2.2.1.1. *P. mendocina pha*C1 amplification

A *Pseudomonas mendocina* single colony was used to inoculate 10ml of nutrient broth and the culture was grown at 30 ºC and 200 rpm overnight. After the centrifugation at 2500 g for 10 minutes, the bacterial genomic DNA was extracted from the pellet using the Wizard Genomic DNA Purification Kit. The *pha*C1 gene from *P. mendocina* was amplified in an Eppendorf® Mastercycler PCR using the *P. mendocina* genomic DNA as template and 04F and 04R primers (Table 2.2). The product size was 1.68 Kbp.

Table 2.2. Primers designed for the cloning of *pha*C1 into pHCMC04 vector

Addition 5'	Forward primer sequence	Addition 3'	Reverse primer sequence
EcoRV **GATATC**	*O4F*: **5'ATGAGTGACAAGAATAACG AAGACC3'**	*BamH1* **GGATCC**	*O4R*: **5'TCAGCGTTCGTGTAC ATAGG3'**

The primers were designed using the known sequence of *P. mendocina* to include *EcoR*V and *BamH*I restriction sites and to facilitate the cloning of the PCR product. PCR was carried out with the Phusion Flash high-Fidelity PCR master mix and the mix consisting of primers, template and master mix was made up to 100µl with MiliQ water. The PCR program used is shown in Table 2.3.

Table 2.3. PCR program used for the amplification of the *pha*C1 gene

	Temperature (ºC)	Time (min)	
Initial denaturation	95ºC	2	
Denaturation	95ºC	1	30 cycles
Annealing	60ºC	1.4	
Extension	72ºC	1	
Final extension	72ºC	1	

2.2.1.2. *pha*C1 purification

The *pha*C1 gene was isolated by electrophoresis and purified from the agarose gel. For electrophoresis, the *pha*C1 PCR product was loaded onto a 0.8 % agarose gel and run in *Tris-borate-EDTA* buffer (2.1.5.1.) at 100V for 1 hour. The resulting band was excised from the gel and purified using a QIAGEN gel extraction kit.

2.2.1.3. pHCMC04 purification

An *E. coli ECE 189* single colony was used to inoculate 10 ml of Luria Broth (LB) media and the culture was grown at 37 ºC and 200 rpm, overnight. The resulting culture was centrifuged at 2500 g for 10 minutes and the plasmid DNA was extracted from the pellet by the miniprep plasmid extraction protocol. For this, the cells were lysed with 350 µl of *Solution I* (2.1.5.2), following by the addition of 5 µl of RNase and 300 µl of *Solution II* (2.1.5.2). After incubating the sample on ice for 5 minutes, 300 µl of *Solution III* (2.1.5.2) were added and the sample was centrifuged for 5 min at 7000 g. The supernatant was isolated and the same amount of Phenol-Chloroform was added. After vortexing, the sample was centrifuged at 7000 g for 12 min and the upper phase was kept. For the DNA precipitation, 600 µl of isopropanol was added followed by centrifugation at 7000 g for 20 minutes at 4 ºC. The resulting pellet was washed twice with 500 µl 70 % ethanol and dissolved in 30 µl of MiliQ water.

2.2.1.4. *pha*C1 and pHCMC04 restriction enzyme treatment

Restriction enzyme digests were carried out to prepare the purified vector pHCMC04 and PCR amplified *pha*C1 insert for the ligation. For this, 25 µl of each product were double digested with *Bam*H1 and *Eco*RV enzymes in NEB restriction buffer 3, containing BSA, for 2.5 hours at 37 ºC. The final volume of the reaction was 70 µl. In order to avoid self-ligation the vector was treated with 0.5 µl of Calf intestine phosphatase (CIP), 20 minutes prior to the end of the reaction.

2.2.1.5. *pha*C1 and pHCMC04 ligation

For the *pha*C1 and pHCMC04 ligation reaction, one part of restricted *pha*C1 product and seven parts of the restricted pHCMC04 vector were ligated together using T4 DNA ligase in ligase buffer for 4 hours at room temperature.

2.2.1.6. Transformation of the *Escherichia coli XL1 blue* competent cells

The *pha*C1-pHCMC04 construct was used for *E.coli XL1 blue* heat shock transformation. Competent *Escherichia coli XL1 blue* cells were designed for high efficiency transformation. For this, *E. coli XL1 blue* was grown at 37 ºC and when the OD_{600} reached 0.3-0.4, 10 ml of the culture were centrifuged at 2500 g for 10 minutes. The resulting cell pellet was resuspended in 0.1 M ice-cold $MgCl_2$ solution and centrifuged at 2500 g for 10 min at 4 ºC. Then, the obtained pellet was resuspended in 0.1 M ice-cold $CaCl_2$ solution and again centrifuged at 2500 g for 10 min at 4ºC. The cell pellet was dissolved in 6 ml of a 50 % glycerol solution in 0.1 M $CaCl_2$ and stored at -80 ºC.

The *E.coli XL1 blue* heat shock transformation was carried out by mixing 7 µl of the *pha*C1-pHCMC04 ligation product with 50 µl of competent *Escherichia coli XL1 blue* cells. After the reaction was incubated on ice for 5 minutes, 750 µl of LB broth were added. The cells in LB broth were incubated at 37 ºC for 1 hour with shaking and the transformed colonies were selected in LB agar containing 100 µg/ml of ampicillin.

2.2.1.7. *pha*C1-pHCMC04 plasmid purification and sequencing

Ampicillin resistant colonies were grown in LB broth containing 100 µg/ml of ampicillin at 37 ºC and 200 rpm. The overnight culture was centrifuged and plasmid DNA was extracted using the QIAGEN miniprep kit. Digests were carried out using *EcoR*V and *BamH*I enzymes and *pha*C1 gene presence was confirmed by running the resulting product in a 0.8 % agarose gel. In order to confirm the lack of sequence changes in the *pha*C1 insert due to PCR, the pHCMC04-*pha*C1 product was sequenced using the automated DNA sequencer at the Wolfson Institute, University College London, UK.

2.2.1.8. Transformation of *Bacillus subtilis* 1604

Bacillus subtilis 1604 was transformed with pHCMC04-*pha*C1 plasmid by electroporation. *B. subtilis 1604* was grown in 10 ml of LB broth at 30 ºC and when the OD_{600} reached 0.8, the culture was incubated on ice for 20 minutes and centrifuged at 2500 g for 15 minutes. Following centrifugation, the cell pellet was resuspended in 10 ml of chilled water and centrifuged for 5 minutes at 2500 g at 4ºC. Then, the cell pellet was resuspended in 10 ml of 10% glycerol and again centrifuged for 5 minutes at 2500 g at 4 ºC. This procedure was repeated thrice. The cell pellet was incubated on ice for 15 minutes and 200 µl were transferred into a cold eppendorf. After the addition of 1 µl of the *pha*C1-pHCMC04 plasmid, the reaction was transferred into a cold 2 mm Bio-rad® Gene-pulser cuvette and the cells were transformed in a Bio-rad® Micro Pulser electroporator with a pulse of 2.5 KV. Following the transformation, 500 µl of LB broth were added and the cells were incubated at 37 ºC for 1 hour. Transformed colonies were selected in LB agar containing 5µg/ml of chloroamphenicol. The plasmid was extracted and the presence of the *pha*C1 insert was confirmed by PCR with primers flanking the *pha*C1 sequence.

2.2.2. Expression of *pha*C1 in *B. subtilis pha*C1-pHCMC04

2.2.2.1. Determination of early mid-log phase, mid-log phase and late mid-log phase for xylose induction in LB broth media

Transformed *Bacillus* strains were grown in LB media containing 5 µg/mL of chloramphenicol at 30 °C and 200 rpm and the early mid-log phase, mid-log phase and late mid-log phase were determined by measuring the absorbance at 600 nm in a standard Novaspec II® visible spectrophotometer at different time points. At these time points, cultures were induced with different xylose solutions, i.e. 0.2%, 0.5%, 0.8% and 1.1%. Samples were taken at 15, 30, 60, 120 and 180 minutes after induction and centrifuged at 2500 g for 15 min. The obtained pellets were prepared for SDS-PAGE.

2.2.2.2. SDS-PAGE

The *pha*C1 protein expression profile was analysed using SDS-PAGE. The cell pellet was disrupted in 4x *Sample buffer* (2.1.5.3.), boiled for 10 minutes and allowed to cool down. Samples were loaded on a 12%/4 % *resolving/stacking* acrylamide gel (2.1.5.3.) and

electrophoresis was carried out at a constant voltage of 200 V in *Running buffer* (2.1.5.3.) using a Bio-Rad®Mini-Protean II electrophoresis system. For protein size estimation, a Bio-Rad® reference protein ladder was used. In order to add a reference band closer to the sample size, to facilitate the size estimation, Bovine serum albumin (BSA) was added to the marker. The gels were stained with *Staining solution* (2.1.5.3) to fix and stain proteins, destained and stored in *destaining solution* (2.1.5.3).

2.2.3. PHA production from *B. subtilis pha*C1-pHCMC04

The PHAs production in recombinant *B. subtilis* was carried out using a two stage seed culture preparation. Briefly, the first culture was inoculated with a single colony of the recombinat strain. The culture in mid-log phase was then used for inoculating the PHAs production media. PHAs production was induced with a xylose solution when the culture in PHAs production media reached mid-log phase. After 30 hr cells were harvested and cells pellet was dried by freeze-drying. PHAs were extracted from lyophilised cells. Figure 2.6 shows a schematic representation of the steps followed for PHAs production in recombinant *B. subtilis* strain.

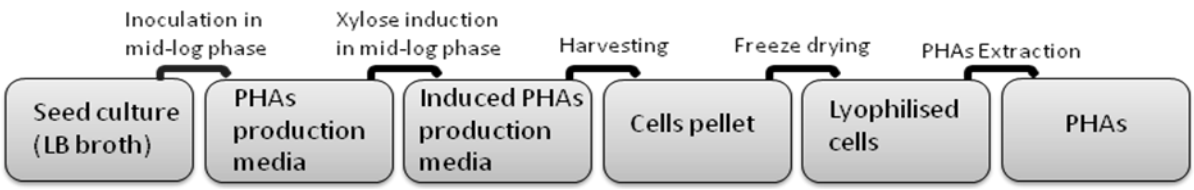

Figure 2.6. Schematic representation for the PHA production in *B. subtilis pha*C1-pHCMC04.

2.2.3.1. Production of PHAs in *B. subtilis 1604 pha*C1-pHCMC04 from carbohydrates

The PHA polymer production was carried out in *Ramsay* media (2.1.6.2.) in two stages using sucrose as a sole carbon source. To this end, a *B. subtilis 1604 pha*C1-pHCMC04 single colony was used to inoculate LB broth and the culture was grown at 30 ºC and 200 rpm until mid-log phase was reached. This culture was then used to inoculate the PHA production media with 20 g/l of sucrose. The growth of the organism was monitored by measuring the OD at 600 nm and a solution of 0.5 % xylose was used to induce the culture when mid-log phase was reached. The culture was grown for 30 hr at 30 ºC and 200 rpm.

2.2.3.2. Production of PHAs in *B. subtilis 1604 pha*C1-pHCMC04 from fatty acids

The PHA production was also carried out with a range of oils (groundnut oil, corn oil and coconut oil) and fatty acids (from 3 to 12 carbons) in *Ramsay* media and *Kannan and Rehacek* media (2.1.6.2.). The fatty acid concentration used in this study was always 20 mM. The procedure used was the same as described in section 2.2.3.1.

2.2.3.3. Extraction of PHAs in *B. subtilis 1604 pha*C1-pHCMC04

The PHA extraction was carried out using the dispersion of chloroform and sodium hypoclorite method (Rai *et al*., 2011). For this, the cells were harvested and the cell pellet lyophylised. Dried cell were incubated at 30 ºC and 150 rpm with a solution of 80 % sodium hypochlorite and chloroform (1:4). After 2 hours of incubation, the solution was centrifuged for 18 min at 3680 g and the lower layer containing the polymer and chloroform was concentrated in a Bűchi®rota vapour (R-114) and precipitated in cold methanol.

2.2.4. Structural characterization of PHAs from *B. subtilis 1604 pha*C1-pHCMC04

The structural characterization of the polymer obtained from *B. subtilis pha*C1-pHCMC04 was carried out by FTIR, GC-MS and NMR.

2.2.4.1. Fourier transform infrared spectroscopy (FTIR)

FTIR analysis was carried out to determine the presence of the PHA functional groups in the sample. A Perkin Elmer series 2000 FTIR spectrometer with a spectral range 4000 to 400 cm^{-1} was used at the Department of Biomaterials and Tissue engineering, Eastman Dental Institute, University College London, UK. For both, the whole cell analysis and extracted PHA polymer, 2 mg of lyophilised cells or polymer were used.

2.2.4.2. Gas Chromatography-Mass spectroscopy (GC-MS)

The monomer content of the extracted PHA was identified by GC-MS. Before the analysis, the polymer was methanolysed as described by Wang *et al*., (2006). For this, 15 mg of polymer were added to 1 ml of the esterification solution containing 3 ml of 95–98% H_2SO_4, 0.29 g of benzoate, and 97 ml of methanol. Then, 1 ml of chloroform was added and the

mixture was heated at 100 °C for 4 hr. After the 4 hours, the mixture was cooled and 1 ml of MiliQ water was added and vortexed for phase separation. The lower phase was extracted, dried over anhydrous Na_2SO_4, neutralized by Na_2CO_3, filtered and sent to the School of Chemistry, University of Southampton, UK, for the GC-MS analysis.

2.2.4.3. Nuclear magnetic resonance (NMR)

The extracted PHA monomer structure was confirmed by NMR. The analysis was carried out on 30 mg of polymer dissolved in 1 mL of the deuterated chloroform ($CDCl_3$). The ^{1}H and ^{13}C spectra were obtained in a Bruker® AV400 (400 MHz) spectrometer at the Chemistry Department, University College London, UK.

2.2.5. Sequence analysis

Protein sequences for *pha*C1 from *P. mendocina* (*pha*C1$_{P.mendocina}$) and 9 other *Pseudomonas* sp. were retrieved from NCBI or UniProt database.

2.2.5.1. Sequences alignment

Multiple sequence alignment of the protein sequences were performed using Clustal Omega (Goujon *et al.,* 2010) and pair wise alignments were performed on Jalview (Waterhouse *et al*., 2009), a fast Java based multiple alignment editor and analysis tool.

2.2.5.2. Phylogenetic analysis

A phylogenetic tree based on the multiple sequence alignment of the 10 *pha*C1 amino acid sequences was constructed using ClustalW Phylogeny from the ClustalW2 package at the EBI using the neighbour joining clustering method.

2.2.6. Production of mcl-PHAs from *Pseudomonas mendocina*

2.2.6.1. Cell growth

P. mendocina was used for the production of poly-3-hydroxyoctanoate, a mcl-PHA. The polymer production was carried out in three steps according to Rai *et al*., 2011. For the seed culture production, a *P. mendocina* single colony was grown in nutrient broth at 30 ºC at

200 rpm for 24 hr. The second seed was produced by inoculating the *Mineral salt medium production media* ($MSM_{2nd\ seed}$) (2.1.6.1) containing 20 mM of sodium octanoate as a carbon source with the seed culture and grown at 30 ºC at 200 rpm until the OD_{450} was 1.6. The resulting culture was used to inoculate the PHA *Mineral salt medium production media* (MSM_{PM}) (2.1.6.1) containing 20mM of sodium octanoate. The volume of the inoculums used in all the cases was 10 % of the final production media working volume.

2.2.6.2. P(3HO) extraction

The P(3HO) polymer extraction was carried out as described in section 2.2.3.3.

2.2.6.3. P(3HO) purification

The P(3HO) polymer purification was carried out by dissolving and precipitating the polymer in a series of solvents (Rai *et al.,* 2011). In the first step, the polymer was dissolved in chloroform and precipitated in an ice-cold methanol: ethanol solution (50:50). In the second step the polymer was dissolved in acetone and precipitated in ice-cold methanol. For the last step, the polymer was again dissolved in chloroform and precipitated in ice-cold methanol.

2.2.7. Production of mcl-PHAs in Bioreactors

The P(3HO) production was optimized in 2 L bioreactors and scaled-up to 20 L and 72 L. In all cases the MSM_{PM} (without magnesium) was sterilized with the bioreactors and the sterilized magnesium, trace elements and sodium octanoate solution were added to the bioreactor before the inoculation. The bioreactor was inoculated with 10 % of second seed inoculum.

2.2.7.1. Optimisation in a 2 L Bioreactor

The P(3HO) polymer production was optimised by varying the carbon:nitrogen ratio and pH in the production media. The working volume in the 2 L bioreactor was 1.4 L. The pH of the medium was maintained using 2 M NaOH and 2 M H_2SO_4. Table 2.5. shows the four conditions tested in this study.

Table 2.5. Fermentation conditions tested for the optimisation studies

	C:N	pH	Stirrer speed (rpm)
Condition 1	20:1	7.15	200
Condition 2	15:1	7.5	200
Condition 3	15:1	6.8	200
Condition 4	10:1	7.15	200

2.2.7.2. Scaling-up

The P(3HO) production was scaled-up from the 2 L to the 20 L and 72 L bioreactors. The scaling up was based on a constant oxygen transfer coefficient, k_La. By employing the gassing out method, the k_La values were calculated at different sets of impeller speeds and airflow rates. Briefly, the bioreactor was filled with distilled water and the concentration of O_2 in the water was lowered by gassing the liquid out with nitrogen gas. Aeration was then initiated at a constant airflow rate and the increase in dissolved oxygen tension (DOT) was recorded at different time points. The rate of oxygen transfer from the air bubble to the liquid phase can be described by the equation 2.1:

$$dC/dt = k_La\ (C^*-C) \qquad (2.1)$$

where C* is the saturated dissolved oxygen concentration, C is the recorded concentration of dissolved oxygen in the bioreactor and dC/dt is the change of the oxygen concentration over a period of time. The k_La of each bioreactor at each stirrer speed and airflow rate was determined from the slot of the plot of ln (C*-C) vs. time.

In a stirrer tank reactor, the efficiency of oxygen absorption in a liquid is expressed in terms of k_La and it is a measure of the aeration capacity of a reactor. In this case, the k_La is dependent on the airflow rate and stirrer speed, and the relation is described by the equation 2.2:

$$k_La = F^xN^y \qquad (2.2)$$

Where F is the airflow rate, N is the stirrer speed and x and y are constants.

The k_La of the 2 L bioreactor at the optimized C:N condition, pH and stirrer speed was determined. As it was not possible to keep the pH constant in both 20 L and 72 L bioreactors, the optimised pH was used to initiate the fermentations in the scaling-up study. To determine the k_La, the 2 L bioreactor was filled with 1.4 L of distilled water and the oxygen was lowered with nitrogen supply. When the DOT reached 10, the air supply was switched on and the DOT was recorded every 30 seconds until 90 seconds. The obtained k_La was the chosen parameter to be kept constant as the scale increases. The k_La of the 20 L and 72 L bioreactor was determined in a similar way at a range of stirrer speeds and airflow rates. The total volume vs. working volume ratio used in the 2 L bioreactor was kept constant in the 20 L and 72 L bioreactors (for the 20 L and 72 L bioreactor the working volume used was 14 L and 50. 4 L, respectively). Due to the fact that the stirrer speed can be regulated with more precision, the aeration rate was kept constant and the estimation of the stirrer speed for a constant oxygen transfer in the 20 L and 72 L bioreactors was obtained from the extrapolation of the Log k_La vs. Log rpm.

2.2.8. P(3HO) characterization

2.2.8.1. Fourier transform infrared spectroscopy (FTIR)

The sample preparation and analysis was carried out as described in section 2.2.4.1.

2.2.8.2. Gas Chromatography-Mass spectroscopy (GC-MS)

The sample preparation and analysis was carried out as described in section 2.2.4.2.

2.2.8.3. Nuclear magnetic resonance (NMR)

The sample preparation and analysis was carried out as described in section 2.2.4.3.

2.2.9. P(3HO) cardiac patches

2.2.9.1. Plain and porous film fabrication

The plain and porous films fabrication was carried out by dissolving 0.5 g of P(3HO) in 10 ml of chloroform and casting the solution on 60 mm diameter glass petridishes. For the

porous film, 50 mg of sucrose particles between 250 and 300 μm of size were added to the dissolved polymer. The polymer was dried at room temperature for 7 days and then freeze dried for 10 days.

2.2.9.1.1. Porosity measurements

The porosity of the films was determined using equation 2.3.

$$\text{Porosity (\%)} = \frac{Vm - Vp}{Vm} \times 100 = \frac{Vm - (W\rho/\rho)}{Vm} \times 100 \qquad (2.3)$$

where Vm is the volume of the plain films (cm^3), Vρ is the volume of the porous film (cm^3), and Wρ and ρ is the mass and density of the porous film, respectively. Porosity measurements were taken in quadruplicates.

2.2.9.2. Electrospinning

The electrospinning technique was used for the fabrication of P(3HO) microfibres. For this, the following P(3HO) solutions were produced in acetone: 0.2 wt%, 0.5 wt%, 0.6 wt%, 0.7 wt%, 1 wt% and 1.2 wt%. A syringe was loaded with the polymer solution and pumped by a Harvard® syringe pump through silicone tubing connected to a 330 μm inner diameter nozzle. The conductive steel nozzle was connected to a positive terminal of a Glassman Europe® high voltage supply source. The electric potential and the pump speed were adjusted for each concentration until a stable cone-jet was obtained. A distance of 15 cm between the needle and collector was used in all the conditions tested. A range of collection times were assessed in each condition (from 1 second to 10 minutes) and one collection time was selected in each case. The fibre collection was carried out on plain and porous P(3HO) films and glass slides.

2.2.9.2.1. Fibre measurements

The size and shape of the fibres obtained by electrospinning was assessed by optical microscopy. Image tool® software was used to measure the size of the fibres. An average of the fibres size was calculated in each condition from the measurement of 30 fibres.

2.2.9.3. Human vascular endothelial growth factor (VEGF) incorporation within the P(3HO) film

The VEGF film fabrication was carried out by dissolving 0.5 g of the P(3HO) polymer in 10 ml of chloroform. Then, 2 µl of a 1 µg/µl human VEGF solution in MiliQ water were added into the polymer solution. The resulting solution was vortexed for 5 minutes and cast in 60 mm petridishes. Films were dried at 4 ºC for 21 days.

2.2.9.4. Arg-Gly-Asp (RGD) peptide film immobilization

The RGD peptide immobilization protocol used in this project was adapted from Yoon *et al.,* (2003). The immobilization was carried out in two stages. First, the P(3HO) material was aminated and films were cast. Then, the surface immobilization of the RGD peptide was carried out on one side of the aminated solvent cast films. Figure 2.7 shows the synthetic scheme for the RGD peptide immobilization in PHAs.

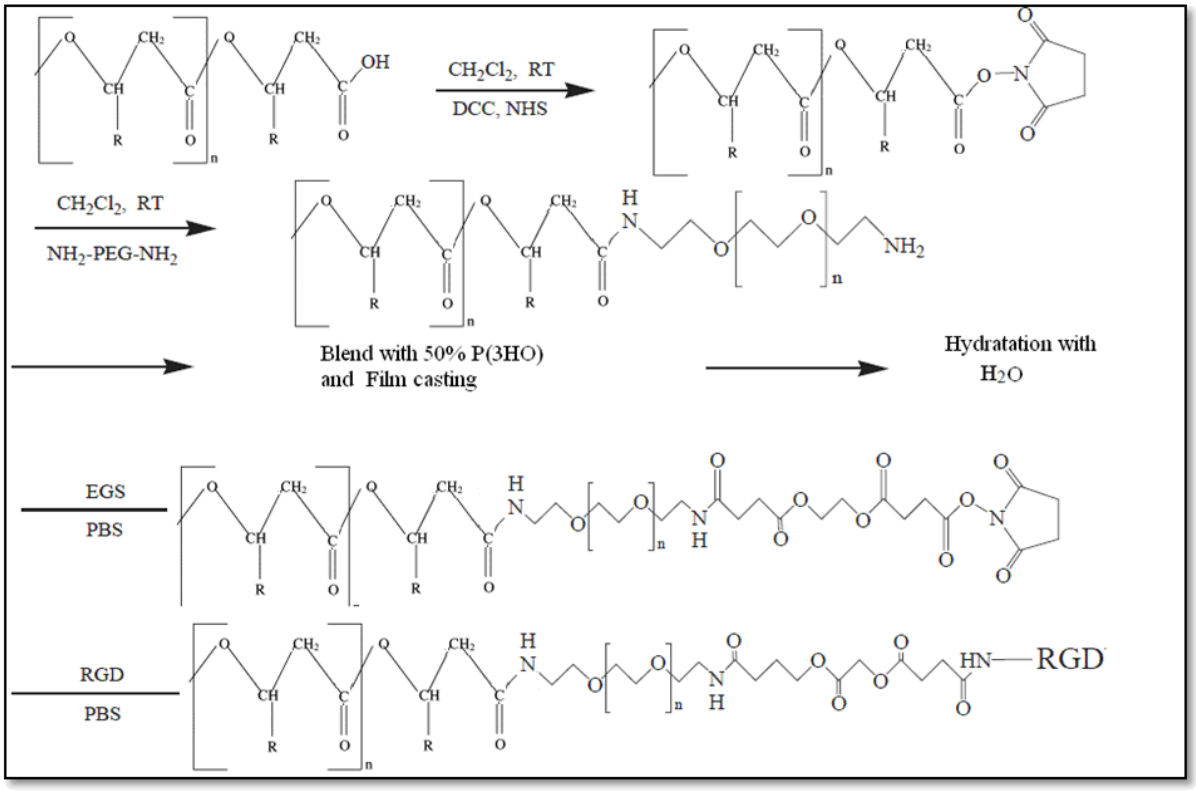

Figure 2.7. Synthetic scheme of the RGD peptide immobilization.

2.2.9.4.1. Preparation of aminated P(3HO)

In order to attach a terminal amine group to the P(3HO), the carboxylic acid terminal group was activated and reacted with hexaethyleneglycol-diamine. For this, 1 g of P(3HO) was dissolved in 10 ml of methylene chloride. 0.22 mmol of dicyclohexylcarbodiimide (DCC) and 0.22 mmol of N-hydroxysuccinimide was added into the polymer solution with stirring. The reaction was stirred for 12 hr at room temperature. Insoluble dicyclohexylurea was removed by filtration, and the carboxylic group activated polymer was isolated by precipitation in DMSO and dried for two days at room temperature. The activated P(3HO) was reacted with an excess of hexaethyleneglycol-diamine (75 mg) in 10 ml of methylene chloride for 12 hr at room temperature with stirring. The aminated P(3HO) was precipitated into cold ethanol.

2.2.9.4.2. Surface immobilization of RGD peptide on aminated P(3HO) films

The film casting was carried out by dissolving 0.25 g of aminated P(3HO) with 0.25 g of non-aminated P(3HO) (50:50) in 10 ml of methylene chloride. After 5 minutes of vortexing, the solution was cast in a glass petridish and dried for 4 days at room temperature. Dried films were pre-wetted in 70 % ethanol and washed in distilled water. Resulting films were hydrated in PBS for 4 hr. In order to introduce amine reactive groups onto the film surface, films were soaked in 20 ml of PBS containing 100 nM ethyleneglycol-bis-succinimidylsuccinate (EGS) and agitated for 4 hr at room temperature. Films were washed with PBS three times and soaked into 20 ml of PBS containing 30 nmoles of the RGD peptide. The solution was stirred for 12 hr at 4 ºC. The peptide immobilized films were washed with PBS and distilled water and then freeze-dried.

2.2.9.4.3. Confirmation of the RGD peptide immobilization on P(3HO) films

The presence of the RGD peptide on the constructs surface was confirmed by FTIR (2.2.4.1.), and contact angle analysis (2.2.5.4.).

2.2.10. P(3HO) films characterization

2.2.10.1. Dynamic mechanical analysis (DMA)

The mechanical properties of the polymer were analysed using a Perkin–Elmer®dynamic mechanical analyser at the Department of Biomaterials and Tissue engineering, Eastman Dental Institute, University College London, UK. The analysis was carried out under static conditions on polymer strips of 10 mm length and 4 mm width. The initial load was set to 1 mN and then increased to 6000 mN at the rate of 200 mN min^{-1} and the stress and strain were measured. The Young's modulus, tensile strength and elongation at break were calculated from the stress vs. strain plot.

2.2.10.2. Differential scanning calorimetry (DSC)

The thermal properties of the polymer were determined using a Perkin Elmer®Pyris Diamond DSC at the Department of Biomaterials and Tissue Engineering, Eastman Dental Institute, University College London, UK. For the analysis, approximately 8 mg of sample were placed in aluminium pans and the samples were cooled down to -57 ºC. Then, samples were heated, cooled and heated again at a heating rate of 20 ºC min^{-1} from -57 ºC to 175 ºC, and the glass transition temperature (T_g), melting temperature (T_m) and crystallization temperature (T_c) were determined.

2.2.10.3. Contact angle analysis

The water contact angle of the fabricated films was analysed on a KSV Cam 200® optical contact angle meter at the Department of Biomaterials and Tissue Engineering, Eastman Dental Institute, University College London, UK. For this, a Hamilton® syringe was loaded with MiliQ water and a drop of water was dispensed on the film. A series of photos were taken every second to record the shape of the drop over 20 seconds. The water contact angle was measured using a KSVCam® software.

2.2.10.4. Scanning electron microscopy (SEM)

The surface of the films was examined under a JEOL 5410LV Scanning electron microscope (Hertfordshire, UK) at the Department of Biomaterials and Tissue Engineering, Eastman

Dental Institute, University College London, UK. The samples were placed on Agar Scientific® Carbon conducting tabs and then coated with gold-palladium using a Quorum Technologies® Polaron E5000 Sputter Coater (East Sussex, UK) for 2 minutes. The SEM images were taken with an acceleration voltage of 10 kV at 15 cm working distance.

2.2.10.5. Surface roughness analysis

Surface roughness studies were carried out on a UBM laser scanning profilometer at the Department of Material Science and Engineering, University of Erlangen-Nuremberg. An area of 2 mm x 2 mm (± 500 µm) was scanned by the machine in two directions. Graphic representation of the scans and average roughness values were recorded.

2.2.10.6. Protein adsorption study

The protein adsorption study was carried out by measuring the protein concentration after soaking the P(3HO) films in Foetal Bovine Serum (FBS). To this end, 1 cm^2 films were incubated with 400 µl of FBS at 37 ºC for 24 hr. For a negative control, films were incubated only in PBS. For the collection of the adsorbed proteins, films were washed three times with PBS and incubated in 1 ml of 2 % SDS in PBS for 24 hr, at room temperature, with shaking. The amount of protein in the solution were quantified using a ThermoScientific® bicinchoninic acid (BCA) reagent kit. The experiment was carried out in triplicates of each sample.

2.2.11. *In vitro* cell culture studies

2.2.11.1. Cardiomyocytes viability

In vitro biocompatibility studies were performed using adult fresh rat isolated cardiomyocyte cells. The cell viability on the P(3HO) UV sterilized films were studied over a period of 0, 1, 2, 3, 24, 25 and 26 hours. The number of live vs. dead cells was determined by counting the cells with rod shape (live cells) vs. cells with round shape (dead cells) under the optical microscope. The viability studies were also carried out on standard tissue culture plastic as a control. The study was carried out in triplicates for each sample.

2.2.11.2. Cardiomyocyte contraction experiments

Fresh adult rat beating cardiomyocytes were seeded on a P(3HO) coated cover slip. The cardiomyocytes were superfused at 37 ˚C in a *Krebs-Henseleit* solution (2.1.5.4) containing 1 mM $CaCl_2$ and bubbled with a mixture of 95 % O_2 5 % CO_2. For the study, rod shaped cardiomyocytes with regular and no spontaneous contraction without stimulation were selected. Cells were stimulated with pulses of 50 V for 2 ms with 2 second intervals. Contraction amplitude (% shortening), 'time to peak 90 %' and 'time to relaxation 50 %' were recorded with a IonOptix® video based system. Figure 2.8. shows an illustration of the time to peak and time to relaxation parameters analysed for each peak during the cardiomyocyte contraction.

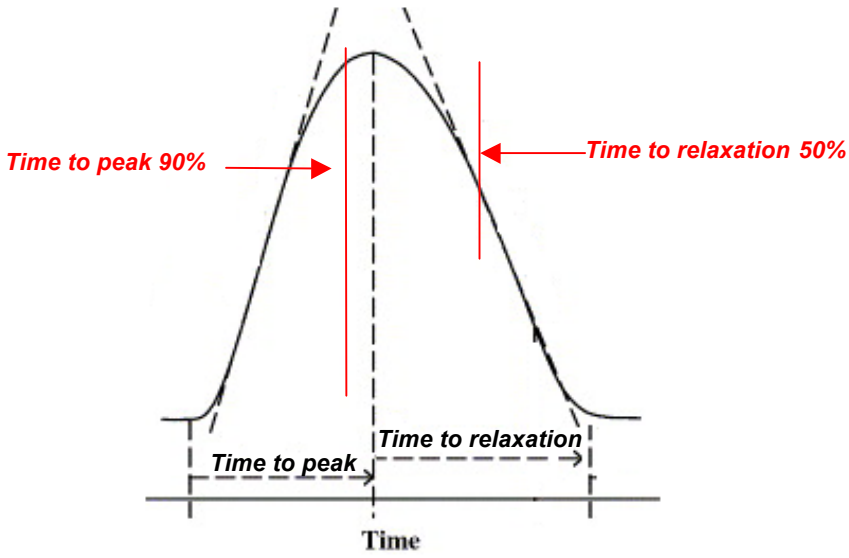

Figure 2.8. An illustration of the time to peak and time to relaxation of a cardiomyocyte. Arrows in red show the time to peak 90% and time to relaxation 50% assessed during the contraction measurements.

The myocyte contraction was studied at a range of frequencies of electrical pulses of 50 V for a period of 2 ms. Starting from 2 second interval pulses, the intervals were increased to 5 seconds, and then decreased to 2 seconds, 1 second and 0.5 seconds. Following this, the effect of the calcium increment was studied. With a 2 second interval pulse of 2 ms at 50 V, the $CaCl_2$ concentration of the solution was increased from 1 mM to 2 mM, and then 3 mM and 4 mM. A stabilization period was allowed in each condition. The contraction studies

were also carried out on uncoated cover slips as controls. The contraction experiments were carried out in quadruplicates.

2.2.11.3. C2C12 myoblast proliferation

The C2C12 myoblast cell line was used to assess cell proliferation in the P(3HO) constructs by the MTT (3-(4,5-Dimethylthiazol-2-yl)-2,5-diphenyltetrazolium bromide) colorimetric assay and SEM.

2.2.11.3.1. C2C12 cell growth

C2C12 myoblast cells were grown in DMEM supplemented with 10 % of foetal calf serum, 1% w/v penicillin and 1 % w/v streptomycin solution and grown at 37 ºC with 5 % of CO_2. Media was pre-warmed at 37 ºC and filter sterilized prior to use. Cell passages were carried out before confluence, every one or two days. For the passages, cells were detached from the flask using a 5 % trypsin at 37 ºC for 2.5 minutes and the reaction was stopped by adding equal volume of supplemented DMEM. Samples were centrifuged at 400 g for 10 min and the resulting pellet was dissolved in freshly supplemented DMEM. Cells were seeded in sterile 75 cm^2 tissue culture flasks.

2.2.11.3.2. Sample preparation

P(3HO) film constructs were cut in to 1 cm^2 squares and sterilized under the UV light for 30 minutes each side. P(3HO) films were soaked in supplemented DMEM for 12 hr prior to cell seeding. Cell culture studies were performed in triplicates.

2.2.11.3.3. C2C12 cell seeding

C2C12 myoblast cells in 70 % confluence were used for the cell seeding. Scaffdex® cell crowns were used to hold the cells on the well's surface. Around 20,000 cells were seeded on the pre-wetted constructs in a 24 well plate. As a positive control, cells were seeded in the wells without films. For the negative control, films were incubated in supplemented DMEM without cells. Plates were incubated at 37 ºC with 5 % of CO_2 and media was changed every 2 days. Cell proliferation was assessed at 24 hr.

2.2.11.3.4. C2C12 MTT assay

The MTT assay was performed on the constructs containing the cells at 24 hr. For this, 100 µl of a 5 mg/ml MTT solution in distilled water were added to each well at 24 hr and the plates were incubated for two hours at 37 ºC with 5 % of CO_2. After this, films were transferred to new 24 well tissue culture plates and 500 µl of DMSO were added. After a 5 minute incubation, 100 µl of the resulting solution were transferred to 96 well plates and the absorbance at 540 nm was measured on a Thermomax®microtitre plate reader. The absorbance of the samples were normalised with respect to the positive control. The difference in the surface areas of the tissue culture plate wells and the films were considered for the calculation of the % cell viability on the films.

2.2.11.4. C2C12 myoblast SEM

At 24 hr constructs containing the cells were visualized using SEM. To this end, cells were fixed in 0.1 M cacodylate buffer containing 3 % glutaraldehyde for 12 hr at 4 ºC and dehydrated in a series of ethanol solutions (50 %, 70 %, 90 % and 100 %) for four times, incubating 10 minutes in each solution. Samples were air dried, coated and examined under the SEM, as described in section 2.2.5.5.

2.2.12. P(3HB) microspheres

2.2.12.1. P(3HB) microsphere production

The microspheres were produced using the P(3HB) polymer obtained from *B. subtilis pha*C1-pHCMC04 as described by Francis *et al*., 2011. Briefly, 1 g of polymer was dissolved in 8 ml of chloroform. The polymer solution was slowly added in the form of drops into 40 ml of 1 % polyvinylalcohol (PVA) water solution, stirred at 1000 rpm for 3 minutes. The solution was then poured into a second 0.5 % PVA solution stirred at 800 rpm for 4 hours. The resulting microspheres were isolated by centrifugation at 3680 g for 5 minutes, washed with distilled water three times and air dried.

2.2.12.2. Microspheres porosity

The porosity of the microspheres was measured using the liquid displacement method (Chen *et al*., 2005). For this, 5ml of ethanol were weighed in a measuring cylinder. Then, the microspheres were immersed in the ethanol and sonicated to ensure the ethanol penetration through the pores. The sample porosity was calculated according to equation (2.4).

$$\text{Porosity} = \frac{V_f}{V_s+V_f} = \frac{W_2 - W_3 - W_s}{(W_1 - W_3)} \times 100 \qquad (2.4)$$

$$V_f = \frac{W_2 - W_3 - W_s}{\rho_e}$$

$$V_s = \frac{W_1 - W_2 + W_s}{\rho_e}$$

where W_1 is the weight of the cylinder + ethanol, W_2 is the weight of the cylinder+ethanol+sample after removing the excess of ethanol above 5 ml, W_3 is the weight of ethanol+ cylinder after removing the microspheres sample saturated with ethanol and W_s is the weight of the microsphere sample used in the experiment.

2.2.12.3. Encapsulation of VEGF in P(3HB) microspheres

VEGF was encapsulated within P(3HB) microspheres. For this, 5 µl of a 1 µg/µl VEGF solution in water were added to 1 g of polymer dissolved in 8 ml of chloroform. The solution

was vortexed for 5 minutes and the microsphere production was carried out as described in section 2.2.13.1.

2.2.12.3.1. Determination of VEGF encapsulation efficiency

The encapsulation efficiency (EE%) of the protein encapsulation was determined using equation (2.5).

$$EE\% = \frac{\text{actual amount of VEGF}}{\text{experimental amount of VEGF loaded}} \times 100 \qquad (2.5)$$

The actual amount of VEGF loaded into the microspheres was determined by dissolving 5 mg of VEGF loaded microspheres in 1 ml of chloroform and 5 ml of water and the water phase was then analysed for the VEGF content by the the invitrogen®VEGF human ELISA kit (R&D Systems, Minneapolis, USA).

2.2.12.4. P(3HB) microsphere characterization

Microspheres were characterized by FTIR (described in section 2.2.4.1.), DSC (described in section 2.2.5.3.) and SEM (described in section 2.2.5.5.).

2.2.12.5. VEGF release kinetics from P(3HB) microspheres and P(3HO) films

The *in vitro* VEGF release from the microspheres and films was studied for 30 days (Sipahigil *et al*., 2012). In this experiment, 10 mg of microspheres or 10 mg of films were incubated in Eppendorf tubes containing 1 ml of PBS at 37 ºC with constant agitation at 100 rpm. 500 µl of PBS were periodically withdrawn from the tubes and replaced with fresh PBS at the following time points (days): 1, 3, 5, 7, 10, 13, 17, 21, 25 and 30. The amount of VEGF released in the medium was measured using the Invitrogen®VEGF human ELISA kit (R&D Systems, Minneapolis, USA).

2.3. DATA ANALYSIS

Data are reported as mean ± STDEV. Statistical significance was assessed using ANOVA with the Newman-Keuls' test. Differences were considered statistically significant when $*p<0.05$, very significant $**p<0.01$ and highly significant when $***p<0.001$.

CHAPTER 3

Production of PHAs in recombinant Gram-positive bacteria

3.1. INTRODUCTION

Polyhydroxyalkanoates (PHAs) are an alternative source of polymers produced by bacterial fermentation of sugar or lipids. Due to their outstanding properties, including biocompatibility, biodegradability, and their adjustable mechanical properties, PHAs are gaining importance as potential candidates for medical applications. In particular, medium chain length-PHAs (mcl-PHAs) have flexible and elastomeric properties that make the material unique for soft tissue engineering applications (Rai *et al*., 2011a).

Mcl PHAs are commonly produced by *Pseudomonas* belonging to rRNA homology group I (Lageveen *et al.*, 1988). The *Pseudomonas sp.* PHA synthesis gene cluster consists of two different *pha*C genes encoding class II PHA synthases separated by another gene, *pha*Z, that encodes an intracellular PHA depolymerase. Downstream of the second *pha*C gene are the *pha*D, *pha*I and *pha*F genes, which encode structural and regulatory proteins (Figure 3.1). Knock-out mutants in *Pseudomonas mendocina* studied previously provided evidence that *pha*C1 is the major enzyme for PHA synthesis (Hein *et al*., 2002).

Figure 3.1. The PHA-related gene cluster of *Pseudomonas sp*., which encodes the proteins involved in PHA metabolism.

The *Pseudomonas sp*. has been widely studied due their capacity to grow on different carbon sources, and their ability to produce mcl-PHAs using a related or an unrelated carbon source. *P. mendocina* has been recently found to be a source of the homopolymer P(3HO), an unusual observation (Rai *et al.*, 2011a). The P(3HO) homopolymer is flexible and elastomeric in nature. In addition, it has the capacity to support cell attachment, differentiation, and maturation, making the material a promising candidate for soft tissue engineering (Rai *et al.*, 2011b). However, Gram-negative bacteria have LPS, which are co-purified with the PHAs. The presence of this endotoxin is responsible not only for the pyrogenicity, but also for complement activation, which stimulates an undesirable immune response. This limits the biomedical applications of the PHAs in several cases.

Gram positive bacteria, which lack LPS, are the focus for polymer production for medical and pharmaceutical applications (Valappil *et al*., 2007). Among Gram-positive bacteria,

Bacillus subtilis is one of the most well studied organisms for heterologous expression due to its versatility in the acceptance of varied growth conditions, capacity of growth at a very high cell density and their non-pathogenic nature, essential for medical applications (Zweers *et al*., 2008). Thus, *B. subtilis* is an ideal microorganism for the expression of heterologous genes (Singh *et al.,* 2009). In this work, the *P. mendocina* PHA synthase gene (*pha*C1) was expressed in the LPS free Gram-positive microorganism, *B. subtilis,* so as to produce LPS-free mcl-PHAs. *B. subtilis* is a GRAS organism widely used in industry that has not yet been explored as a PHA producer at a commercial scale. To this end, *P. mendocina pha*C1 gene was amplified and cloned in *B. subtilis* 1604 through the pHCMC04 expression vector. Sequence analysis of the cloned *pha*C1 gene was carried out to confirm the integrity of the gene. The *pha*C1 expression was induced and analysed with SDS-PAGE. *B. subtilis* was grown in PHA production media with sucrose as the sole carbon source and the produced polymer was quantified and analysed by FTIR, GC-MS and NMR.

PHA biosynthesis can be divided in to two main steps. The first step involves the synthesis of hydroxyacyl-CoA, the PHA monomer units. The second step involves a reaction catalysed by the PHA synthase which use the hydroxyacyl-CoA units as substrates and catalyses their polymerization into PHAs with the concomitant release of CoA (Rehm *et al.,* 2002). The synthesis of the 3-hydroxacyl-CoA units can occur mainly by three different pathways and the particular pathway used for PHA production depends on the specific metabolic pathways operating in a particular microorganism and the carbon source provided (Steinbüchel *et al.*, 1991; Doi *et al*., 1990, Poirier *et al*., 1995). In the first pathway, P(3HB) or P(3HB-co-3HV) are produced from carbohydrates through a precursor from the tricarboxylic acid cycle. The second pathway involves the production of mcl-PHAs via the fatty acid oxidation pathway from fatty acids related to the final polymer structure. The third pathway involves mcl-PHA production via the fatty acid *de novo* biosynthesis using carbohydrates structurally unrelated to the final polymer structure. To assess the capacity of the recombinant *B. subtilis* to produce mcl-PHAs through the fatty acid biosynthesis and degradation pathways, production of PHAs was carried out in a range of carbohydrates, fatty acids and oils.

3.2. RESULTS

3.2.1. Construction of recombinant *Bacillus subtilis*

P. mendocina was grown in nutrient agar and a single colony was used to inoculate nutrient broth. The *P. mendocina* genomic DNA was isolated from an overnight bacterial culture by using the Wizard Genomic DNA Purification Kit. The integrity of the isolated DNA was confirmed by electrophoresis (Figure 3.2).

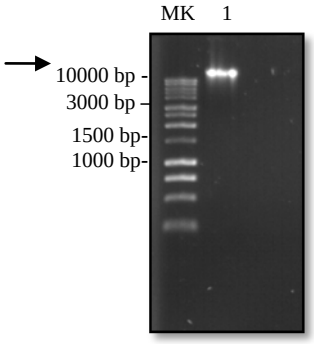

Figure 3.2. *P. mendocina* genomic DNA. Lane MK represents the 1Kb ladder. The arrow in the figure shows the integrity of *P. mendocina* genomic DNA obtained in Lane 1.

The PHA synthase gene (*pha*C1) was amplified by PCR as described in section 2.2.1.1 using specific primers flanking the complete *pha*C1 sequence and including *Bam*H1 and *Eco*RV restriction enzyme sites present in the plasmids, to be used later for cloning. The resulting product was run using a 0.8% agarose gel after gel purification (Figure 3.3).

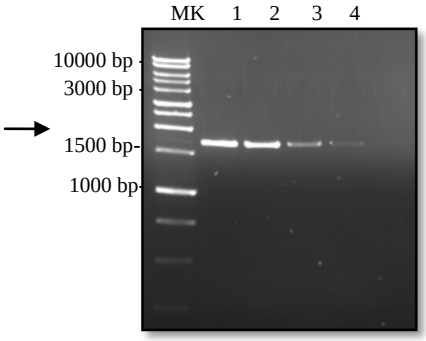

Figure 3.3. The *P. mendocina* synthase gene *pha*C1 containing the *Bam*H1 and *Eco*RV sites (1692bp). Lane MK represents the 1Kb ladder and lanes 1-4 correspond to elutions 1-4 obtained from the column used to purify the product from the gel. The arrow in the figure indicates the *pha*C1 amplified sequence.

Escherichia coli ECE 189 was grown overnight and pHCMC04 plasmid (a *Bacillus-E. coli* shuttle vector, described in section 2.1.3) was isolated by miniprep as described in section

2.2.1.3. Digests were carried out to prepare the vector and inserts for ligation (section 2.2.1.4). The pHCMC04 plasmid and PCR insert were digested using *Eco*RV and *Bam*HI enzymes. Figure 3 shows a 0.8% agarose gel with both digested insert and vector (Figure 3.4).

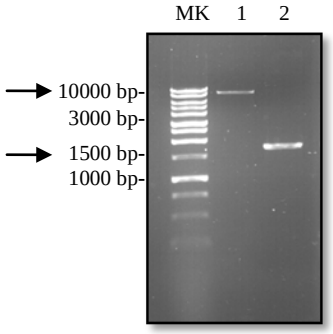

Figure 3.4. Digested insert and pHCMC04 vector with *Bam*H1 and *Eco*RV enzymes. MK represents the 1Kb ladder. Lane 1: digested pHCMC04 (8089bp); Lane 2: The digested *pha*C1 PCR product (1692bp). The arrows in the figure indicate the digested insert and vector.

The pHCMC04 vector was ligated with the *pha*C1 fragment and transformed into *Escherichia coli XL1 blue* cells using heat shock (section 2.2.1.6). The transformed cells were grown and selected in 100 µg/mL ampicillin LB agar plates. Restriction digestion of plasmids, isolated from randomly chosen ampicillin-resistant colonies was carried out (Figure 3.5). Note that both plasmids contained an upper band representing the vector, pHCMC04 and a lower band representing the insert, which confirmed the successful cloning of the *pha*C1 insert into pHCMC04. This plasmid was named pHCMC04-*pha*C1.

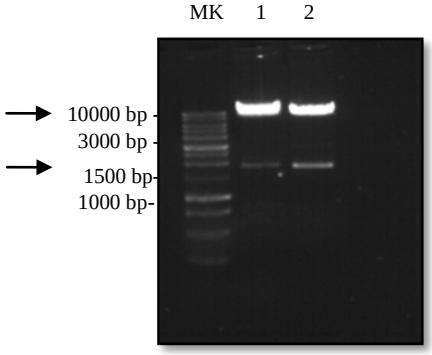

Figure 3.5. Restriction Digestion of the pHCMC04-*pha*C1 clones. MK represents the 1Kb ladder. Lane 1 and Lane 2: Double digestion of pHCMC04-*pha*C1 plasmid obtained from ampicillin resistant colony 1 and 2, respectively, using *BamH1* and *EcoRV*. The arrows in the

figure show the upper bands corresponding to the vector pHCMC04 (8089bp kb) and the smaller bands corresponding to the *pha*C1 insert (1692bp kb).

E.coli XL1 blue containing pHCMC04-*pha*C1 plasmid was grown overnight and the plasmids were extracted using the Qiagen Kit (Sussex, UK). The resulting constructs were sequenced to confirm that no undesirable mutations were introduced by the PCR reaction (section 2.2.1.7). The sequence obtained is shown in Figure 3.6. The sequence of *pha*C1 cloned into pHCMC04 vector shows only one mistake at the highlighted position, which results in a thymine instead of a cytosine.

```
atgagtgacaagaataacgaagacctgaaacgccaggcctcggaaaacacgctgggcctc
 M  S  D  K  N  N  E  D  L  K  R  Q  A  S  E  N  T  L  G  L
aacccggtgattggcatccgcggcaaggatcttttgacctctgcccgcatggtgctcgcc
 N  P  V  I  G  I  R  G  K  D  L  L  T  S  A  R  M  V  L  A
caggcactcaaacaatccttccacagcgccaagcatgtcgcccatttcggcctcgaactg
 Q  A  L  K  Q  S  F  H  S  A  K  H  V  A  H  F  G  L  E  L
aagaacgtcatgctcggccagtccgcgctaaagcccgaagacggtgaccgccgctttgcc
 K  N  V  M  L  G  Q  S  A  L  K  P  E  D  G  D  R  R  F  A
gatccggcctggagccagaacccgctgtaccgccgctacctgcagacttacctggcctgg
 D  P  A  W  S  Q  N  P  L  Y  R  R  Y  L  Q  T  Y  L  A  W
cgcaaggagctgcacgactgggtcgagcacagctcgctgtccgagcaggacgccagccgc
 R  K  E  L  H  D  W  V  E  H  S  S  L  S  E  Q  D  A  S  R
ggcaccttcgtgatcaacctgatgaccgaagacatggcaccctccaacagcatggccaac
 G  T  F  V  I  N  L  M  T  E  D  M  A  P  S  N  S  M  A  N
ccggcagcggtcaaacgcttcttcgaaaccggcggcaagagcctgctcgacggcctgtcg
 P  A  A  V  K  R  F  F  E  T  G  G  K  S  L  L  D  G  L  S
cacctggccaaggacatggtgcacaacggcggcatgccgagtcaggtgaatatggaggcc
 H  L  A  K  D  M  V  H  N  G  G  M  P  S  Q  V  N  M  E  A
ttcgaggtcggcaagaacctggccaccaccgacggcgccgtggtgtttcgcaacgatgtg
 F  E  V  G  K  N  L  A  T  T  D  G  A  V  V  F  R  N  D  V
ctggagctgatccagtacaagccgatcaccgagagcgtgcatgagcgcccgttgctagtg
 L  E  L  I  Q  Y  K  P  I  T  E  S  V  H  E  R  P  L  L  V
gtgccgccgcagatcaacaagttctatgtcttcgacctgtcgccggacaagagcctggcg
 V  P  P  Q  I  N  K  F  Y  V  F  D  L  S  P  D  K  S  L  A
cgcttcctcctgcgcagccaggtgcagaccttcgtggtcagctggcgcaacccgaccaag
 R  F  L  L  R  S  Q  V  Q  T  F  V  V  S  W  R  N  P  T  K
gcgcagcgcgagtggggcctgtccacctacatcgaggcgctcaaggaagccatcgacgtc
 A  Q  R  E  W  G  L  S  T  Y  I  E  A  L  K  E  A  I  D  V
atctgcgccatcaccggcagcaaagacgtgaacatgctcggcgcctgctccggtggcctg
 I  C  A  I  T  G  S  K  D  V  N  M  L  G  A  C  S  G  G  L
accactgcttcgctgctcggccactacgccgcgctcggccaacctaaagtcaatgccctg
 T  T  A  S  L  L  G  H  Y  A  A  L  G  Q  P  K  V  N  A  L
```

Continues on the following page

```
accttgctggtcagcgtgctcgacacccagctcgacacccaggtagcgctgttcgccgac
 T  L  L  V  S  V  L  D  T  Q  L  D  T  Q  V  A  L  F  A  D
gagaagaccctggaacgcggccaacgccgctcctaccaggccggagtgctggaaggcagc
 E  K  T  L  E  R  G  Q  R  R  S  Y  Q  A  G  V  L  E  G  S
gacatggccaaggttttcgcctggatgcgccccaacgacctgatctggaactactgggtc
 D  M  A  K  V  F  A  W  M  R  P  N  D  L  I  W  N  Y  W  V
aacaactacctgctcggcaacgagccgccggtgttcgacattctctactggaacaacgac
 N  N  Y  L  L  G  N  E  P  P  V  F  D  I  L  Y  W  N  N  D
accacacgcctgccggctgcgctgcacggcgagttcatcgaaatgttccagaccaacccg
 T  T  R  L  P  A  A  L  H  G  E  F  I  E  M  F  Q  T  N  P
ttgacccgtcccggcgcgctggaagtgtgcggtacgccgatcgacctcaaacaggtcacc
 L  T  R  P  G  A  L  E  V  C  G  T  P  I  D  L  K  Q  V  T
tgcgacttcttcgtcgtcgccggcaccaccgaccacatcacgccatgggattcctgctac
 C  D  F  F  V  V  A  G  T  T  D  H  I  T  P  W  D  S  C  Y
aaatcggctcatctgttcggcggcaaatgcgagttcgtgctctccaacagcggccatatc
 K  S  A  H  L  F  G  G  K  C  E  F  V  L  S  N  S  G  H  I
cagagcattctcaacccgccgggcaaccccaaggcgcgctacatgaccaatagcgagatg
 Q  S  I  L  N  P  P  G  N  P  K  A  R  Y  M  T  N  S  E  M
ccgctggacccgaaagcctggcaggaaagctcgaccaagcatgccgactcctggtggctg
 P  L  D  P  K  A  W  Q  E  S  S  T  K  H  A  D  S  W  W  L
cattggcaaagctggctggccgagcgctcgggcgaaaccaagaatgctccacgggcgctg
 H  W  Q  S  W  L  A  E  R  S  G  E  T  K  N  A  P  R  A  L
ggcaacaagaaattcccggccggcgaagccgcaccgggcacctatgtacacgaacgctga
 G  N  K  K  F  P  A  G  E  A  A  P  G  T  Y  V  H  E  R  -
```

Figure 3.6. Sequencing results obtained from *pha*C1 gene cloned into pHCMC04 shuttle vector. The highlighted position shows the mutation observed.

Further, *B. subtilis 1604* was transformed with the pHCMC04-*pha*C1 construct by electroporation as described in section 2.2.1.8. Transformed colonies were selected in 5 µg/mL chloroamphenicol. In addition, *B.subtilis1604* strain was transformed with pHCMC04 without insert, to be used as control in further experiments. *B. subtilis* containing the pHCMC04-*pha*C1 construct and *B. subtilis* containing the vector without insert were named *B. subtilis-pha*C1 and *B.subtilis*-vector, respectively. In order to confirm the presence of *pha*C1 in the chloroamphenicol-resistant *B. subtilis-pha*C1, the isolated plasmid was amplified by PCR using specific primers flanking the last 301 bp of the *pha*C1 gene. Figure 3.7 shows the results obtained. The first and the last lanes show the PCR product of negative controls where no template or the plasmid extracted from *B.subtilis*-vector, respectively, were used. The second lane shows the PCR product obtained when the plasmid extracted from *B.subtilis-pha*C1 was used as template.

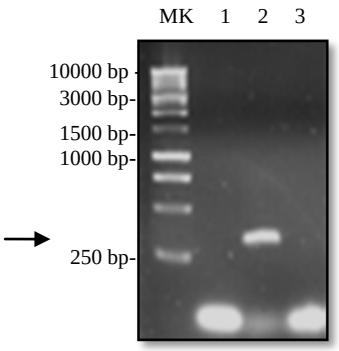

Figure 3.7. Confirmation of transformation of *B. subtilis 1604* with pHCMC04-*pha*C1. MK represents the 1Kb ladder. The picture shows results from PCR reactions using primers flanking the last 301 bp of *pha*C1 sequence. Lane 1: PCR without template; Lane 2: PCR with *B.subtilis-pha*C1 extracted plasmid as template; Lane 3: PCR with *B.subtilis*-vector extracted plasmid as template. The arrow in the figure indicates the PCR amplification product obtained.

3.2.2. Expression of the *pha*C1 gene in the recombinant *Bacillus subtilis* 1604

Recombinant *B. subtilis* was tested for *pha*C1 gene expression (section 2.2.2). The plasmid construct contained the *xylA* constitutive promoter, inducible by xylose. It was important to identify the various growth phases during xylose induction for the recombinant *B. subtilis 1604* in order to determine the correct induction time using xylose. Hence, the recombinant strain was grown in LB broth at 30 °C in the presence of chloramphenicol. The OD_{600nm} was measured every 30 minutes. Figure 3.8 shows the resulting growth profile and the chosen OD_{600nm} values for the xylose induction.

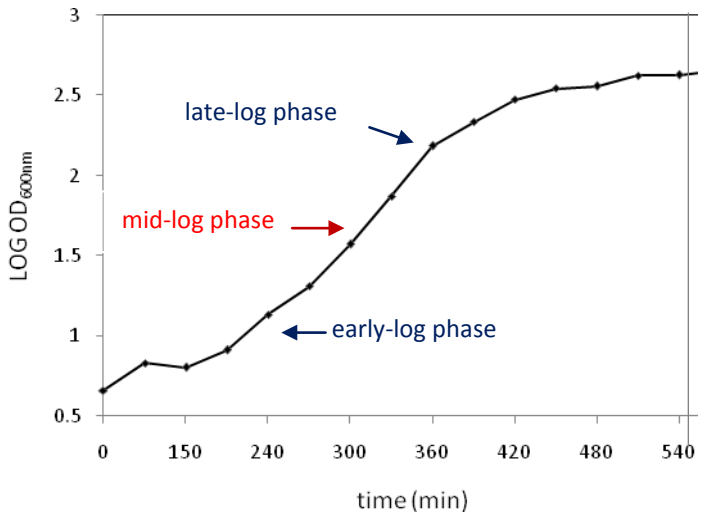

Figure 3.8. *B. subtilis* recombinant growth curve. LogOD_{600nm} of 1.5 (mid-log phase) was chosen for induction using xylose.

B. subtilis 1604 recombinant bacteria were grown in duplicate in LB media at 30 °C and one of the duplicates was induced with a solution of 0.5 % xylose as described in literature at Log OD_{600nm} 1.5 (Nguyen *et al.*, 2005). Aliquots of the growth cultures were taken at different time points after induction (min.): 0, 15, 30, 60, 90 and 120. The same procedure was carried out for *B. subtilis* wild type. Whole cell extracts were prepared for SDS-PAGE and run in 12% SDS-PAGE gel at 140 V. Figure 3.9 shows the resulting gels. The *pha*C1 protein is 62.4 KDa in size. Results show that no distinct band of this size was found in either the induced or uninduced samples. However, there was appearance of a band at around 66 KDa when compared with the wild type bacteria at the different time points, which might indicate *pha*C1 expression. In this case, the fact that the bands appear in both induced and uninduced conditions, may indicate the "leaky" characteristics of the plasmids. In order to enhance the levels of protein expression, this protocol was repeated using xylose solutions of various concentrations (0.2%, 0.8% and 1,1%) at mid-log phase (Log OD_{600nm} 1.5), early-log phase (Log OD_{600nm} 1.1) and late-log phase (Log OD_{600nm} 2.2), but no differences were observed compared with the 0.5% xylose induction (results not shown). A Western blot could have been carried out to determine the presence of *pha*C1, however, due to the lack of availability of a suitable antibody against *pha*C1, this was not possible.

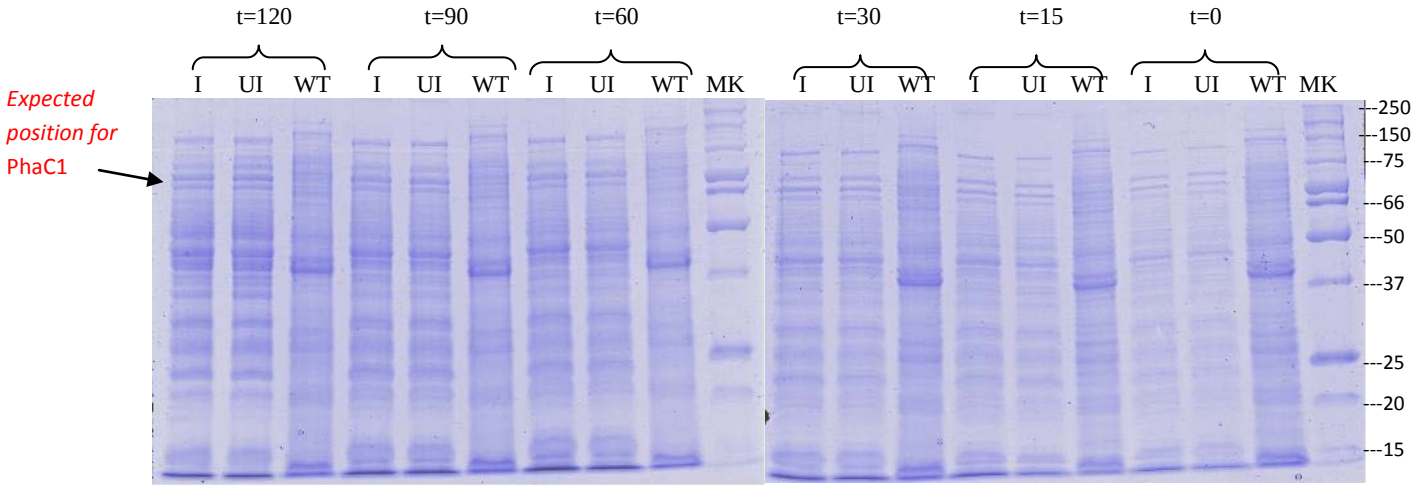

Figure 3.9. SDS-PAGE of *B.subtilis 1604* recombinant and wild type at different time points after induction with xylose 0.5%.WT: wild type *B.subtilis 1604*, UI: uninduced recombinant *B.subtilis*, I: xylose induced recombinant *B.subtilis.*

Hence, for the purpose of confirming that the recombinant *B. subtilis* expresses the *pha*C1 gene, both *B. subtilis-pha*C1 and *B. subtilis*-vector were grown in PHA production media. A single colony was grown in nutrient broth until mid-log phase and used as inoculum for the PHA production media. Figure 3.10 shows the growth curve for the recombinant *B. subtilis-pha*C1 strain at 30 °C, in PHA production media indicating the mid-log phase for the xylose induction.

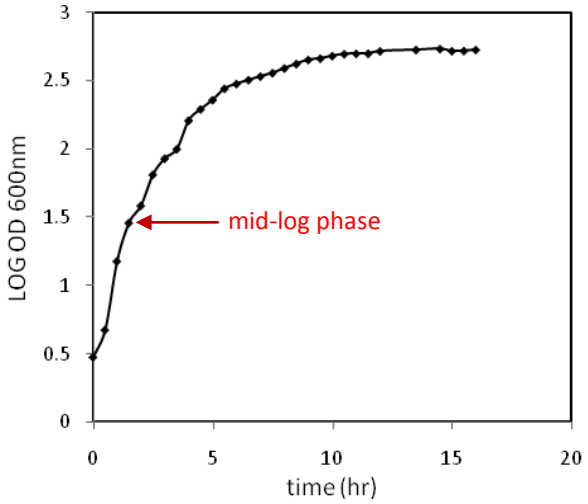

Figure 3.10. Growth curve for *B. subtilis* recombinant strain harbouring pHCMC04-*pha*C1 in PHAs production media. Note that the mid-log phase for *B. subtilis* 1604 is at $LogOD_{600}$ 1.5.

3.2.3. Production of PHAs from recombinant *B. subtilis* from carbohydrates

The recombinant *B. subtilis* harbouring pHCMC04-*pha*C1 was grown in LB broth and the resulting culture in mid-log phase was used as a 10% inoculum for PHA production using the PHA production media described by Ramsay *et al.*, (1990) with sucrose as a carbon source. The culture was grown at 30 °C in the PHA production media and induced with a 0.5 % xylose solution at an OD_{600nm} of 0.385. After 30-hours of growth in the PHA production media, the cells were harvested and dried in a freeze-dryer for two days. As controls this protocol was repeated with *B. subtilis* wild type and *B. subtilis*-vector.

Figure 3.11 shows a Gram-staining of the recombinant *B. subtilis* grown in LB broth after induction. The recombinant bacteria were seen to consistently form aggregates in contrast to the *B. subtilis* wild type. Such aggregates were previously observed by Babic *et al.*, (2011) who showed that recombinant *B. subtilis* grow in chains in order to accelerate the spread of DNA within microbial communities and that DNA transference appeared to occur at a cell pole or along the lateral cell surface by conjugation (Figure 3.8).

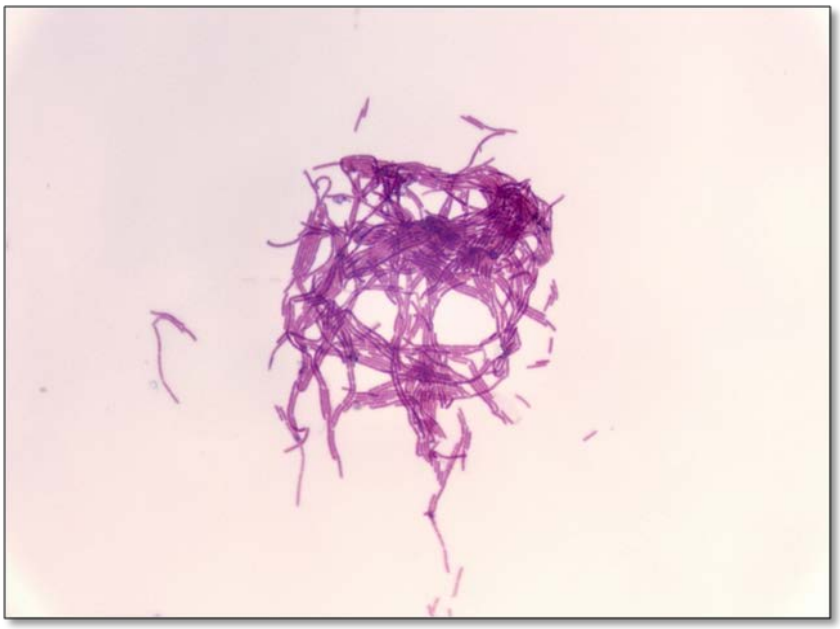

Figure 3.11. Gram-staining of recombinant *B. subtilis* grown in LB broth showing the aggregates formed.

The cells obtained from these cultures were freeze dried and analysed by Fourier Transform Infrared Spectroscopy (FTIR) as described in section 2.2.4.1. Figure 3.12 shows the FTIR spectral analysis confirming the presence of a strong, distinct ester carbonyl band at

1733 cm^{-1} in the case of the recombinant *B.subtilis-pha*C1 strain which was absent in *B. subtilis*-vector and *B. subtilis* wild type. These results indicated the successful production of PHAs by the recombinant *B. subtilis* harbouring pHCMC04-*pha*C1.

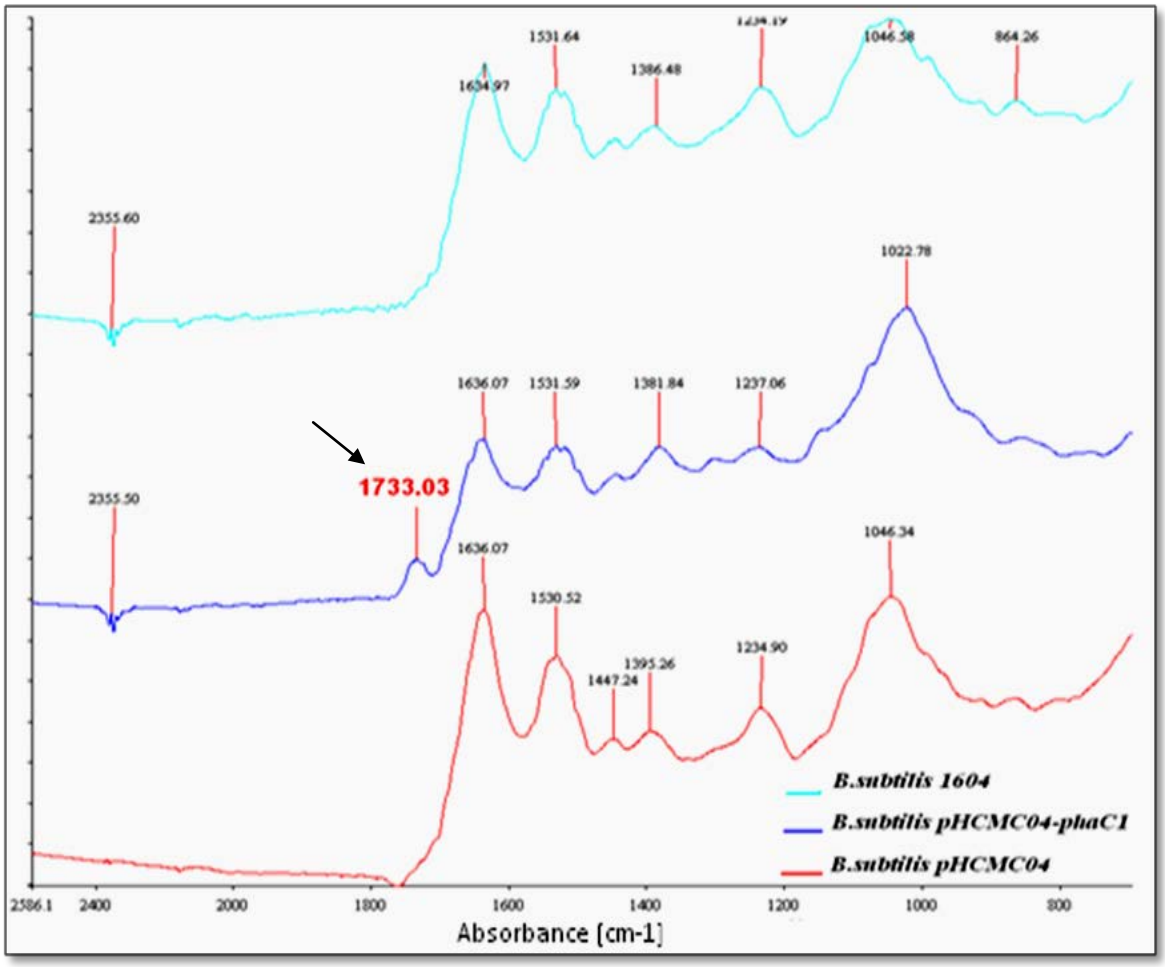

Figure 3.12. FTIR spectra for *B. subtilis* wild type (—) *B. subtilis-pha*C1 (—) and *B. subtilis*-vector (—). The arrow in the figure indicates the presence of a distinct ester carbonyl band at 1733 cm^{-1} for *B.subtilis-pha*C1.

In order to analyse the polymer produced by the recombinant *B. subtilis-pha*C1, the growth and induction conditions were repeated in large scale. The cells were harvested immediately, dried in a freeze-dryer for two days and the polymer was extracted and analysed by FTIR and GC. The resulting polymer is shown in Figure 3.13.

Figure 3.13. Polymer produced by recombinant *B. subtilis-pha*C1.

In order to determine the nature and amount of polymer, *B. subtilis* wild type, *B. subtilis-pha*C1 and *B. subtilis*-vector were subjected to fermentation in 2 L PHA production media in quadruplicates. Polymer was extracted from the resulting cells, quantified and characterized by GC-MS (described in section 2.2.4.2) and NMR (described in section 2.2.4.3). Figure 3.14(A) and 3.14(B) shows the GC-MS and NMR results, respectively, of the obtained polymer. These results showed the presence of the P(3HB) homopolymer.

3.14 (A)

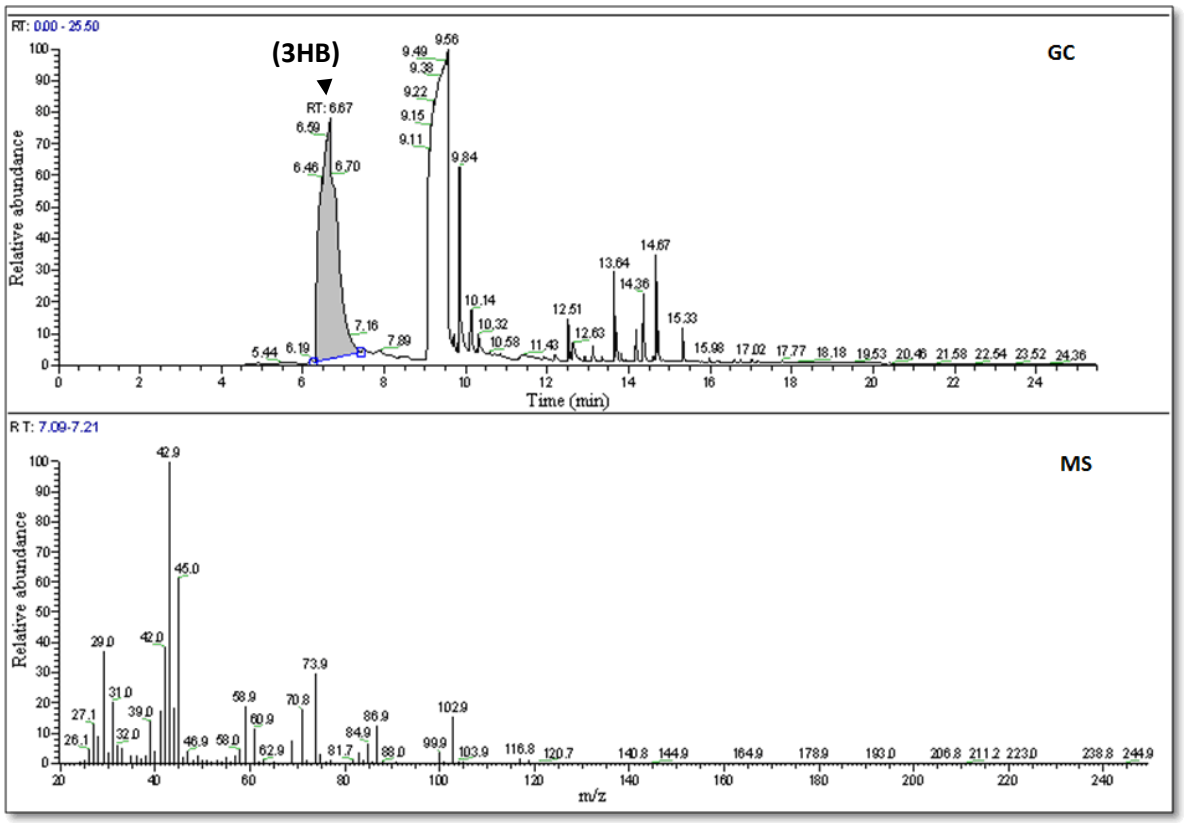

Continues on the following page

(B)

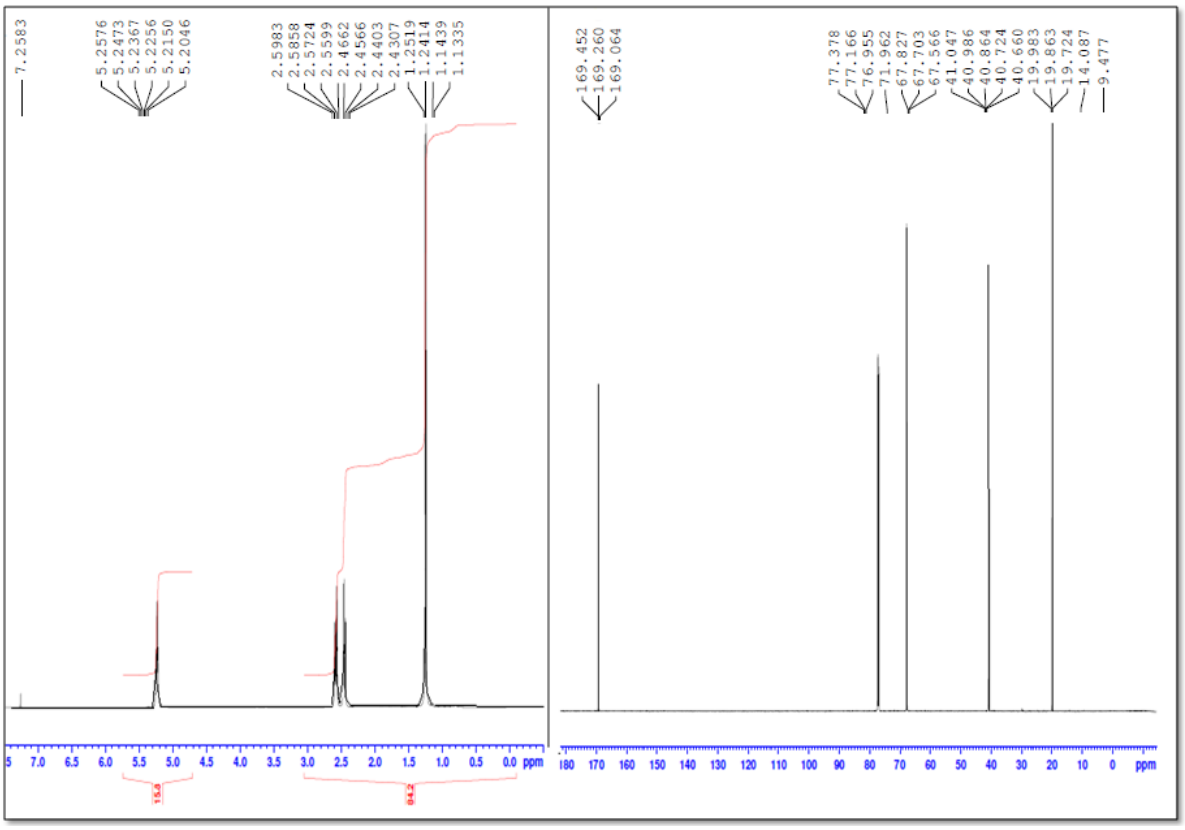

Figure 3.14. (A) GC-MS spectra of the extracted polymer produced from *B. subtilis-pha*C1. Note the presence of a peak at RT: 6.67 and the corresponding mass spectra for P(3HB) (the peak obtained at RT: 9.56 corresponded to methyl benzoate used as the internal control) and (B) ^{1}H NMR on the left, ^{13}C NMR on the right. This spectrum is characteristic of the P(3HB) homopolymer.

Figure 3.15 shows the dry cells weight (A), PHA content (B) and amount of polymer normalized per gram of dry cells (C) of *B. subtilis* wild type (wt), *B. subtilis* wild type, *B. subtilis*-vector and *B. subtilis-pha*C1 after fermentation. According to these results *B. subtilis-pha*C1 shows a significant higher dry cell weight, PHA production and polymer content compared to *B. subtilis*-vector and *B. subtilis* wild type.

3.15 (A)

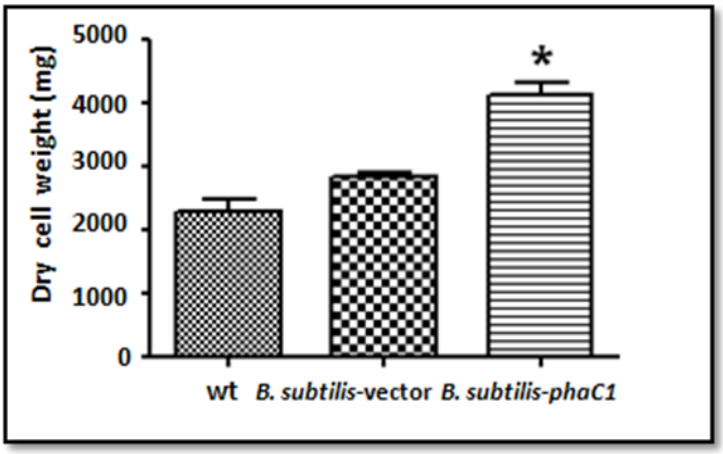

(B)

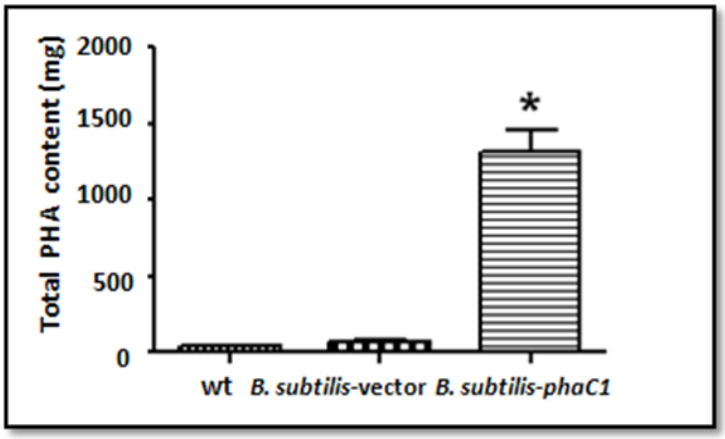

(C)

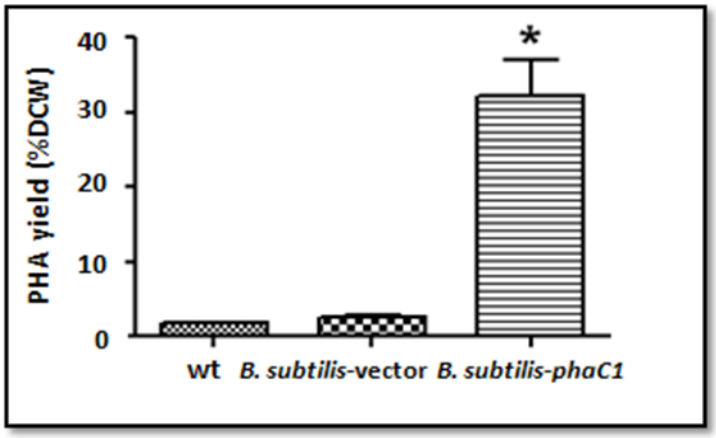

Figure 3.15. PHA production by *B. subtilis* wild type (wt), *B. subtilis*-vector and *B. subtilis*-*pha*C1. (A) Dry cell weight (B) Total PHA content and (C) PHA yield in % dry cell weight.

3.2.4. Production of PHAs from the recombinant *B. subtilis* in fatty acids

In order to test the capability of the recombinant *B. subtilis-pha*C1 to produce mcl-PHAs via the fatty acid degradation pathway, a range of carbon sources including oils (groundnut oil, corn oil and coconut oil) and a series of alkanoic acids (monomer length from five to twelve carbons) were used. Presence of PHAs was detected only when pentanoic, hexanoic and heptanoic acids were used. The produced polymers were characterized by GC-MS and results show the production of Poly(3-hydroxyvaleric acid), P(3HV), with small amounts of P(3HB) in all the three cases (Figure 3.16).

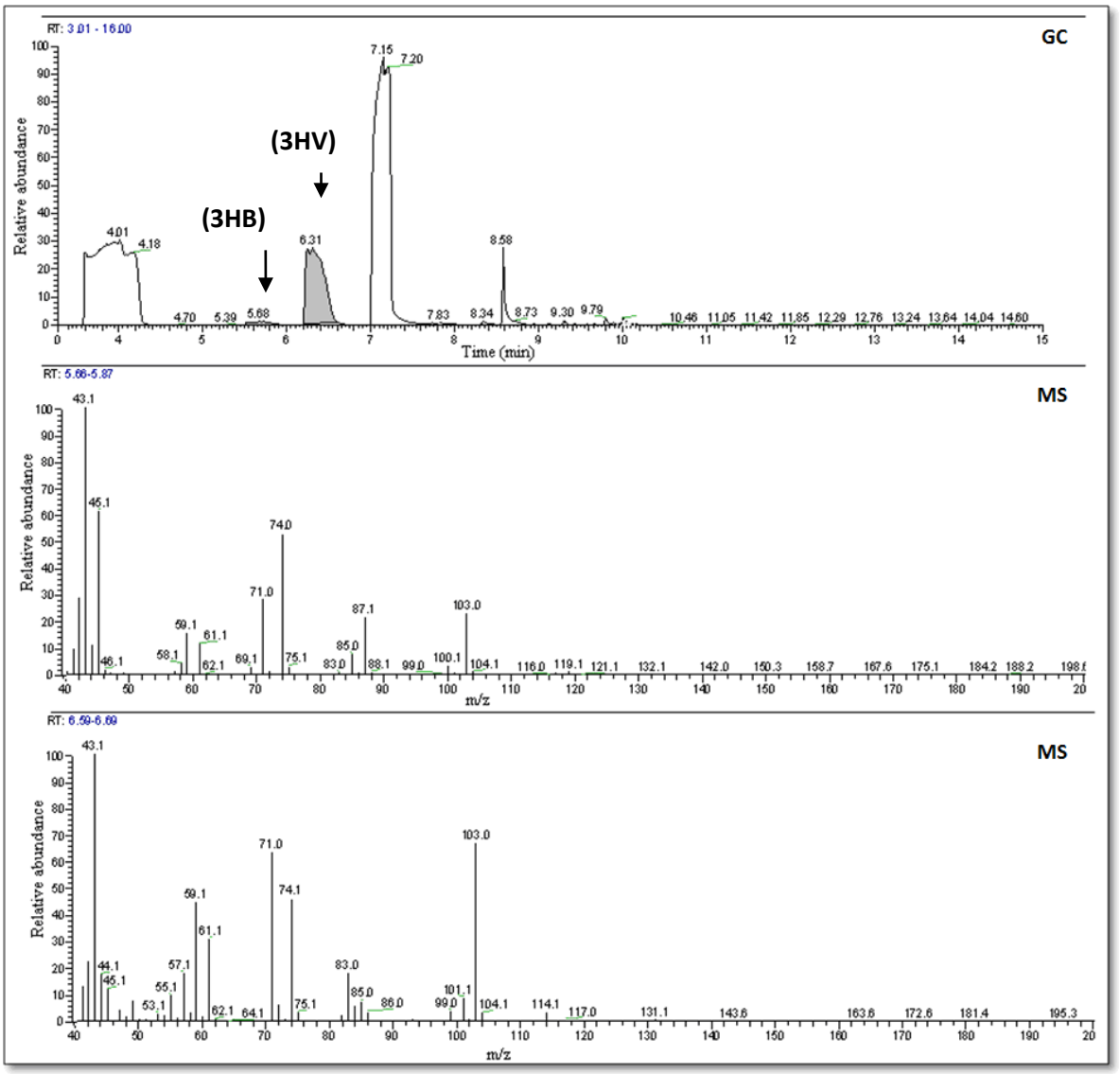

Figure 3.16. GC-MS spectra of the extracted polymer produced from *B. subtilis-pha*C1 when heptanoic acid was used as a sole carbon source. Note the presence of a peak at RT: 5.68 and

6.31 and the corresponding mass spectra for (3HB) and (3HV), respectively (the peak obtained at RT: 7.15 correspond to methyl benzoate used as the internal control).

3.2.5. Sequence analysis

Results obtained in section 2.4 indicate that the *pha*C1 enzyme from *P. mendocina* has the capacity to catalyse the production of both scl-PHAs and mcl-PHAs. In order to understand the broad substrate specificity sequence comparison was carried out with *pha*C1 protein sequences from other *Pseudomonas sp*. including known mcl-PHA producers such as *Pseudomonas aeruginosa*, *Pseudomonas putida* and *Pseudomonas oleovorans*. From the multiple sequence alignment (Figure 8), the residues in the catalytic triad (Cys296, Asp451, His479) and residue Ser297, which plays an important role in the formation of an oxyanion hole during catalysis (indicated by a red asterisk, Wahab *et al*., 2006), were found to be conserved in *pha*C1$_{P.mendocina}$ and also in all other sequences, suggesting that they share a similar catalytic mechanism. Another conserved feature, the lipase-box like consensus motif (GACSG,) located at residues 294 – 298, was found in all the sequences used in this study (underlined in red, Figure 3.17).

A closer look at the stretch of residues from position 267 to position 484 revealed some interesting differences in the protein sequence of *pha*C1$_{P.mendocina}$ which could potentially explain its broad substrate specificity. This region contained the conserved catalytic residues is referred to as the core region by Wahab *et al.*, (2006) in their threaded 3D model of *pha*C1$_{Pseudomonas\ sp.\ \mathrm{USM4\text{-}55}}$.

It is interesting to note that all *pha*C1 homologues used in this study have a conserved Ala-Ala-Lys motif at positions 346-348 except in *pha*C1$_{P.mendocina}$ where it is substituted with Arg-Gly-Gln. Similarly Gln314, a neutral amino acid residue, conserved in *pha*C1$_{P.mendocina}$, *pha*C1$_{Pseudomonas\ sp.\ \mathrm{USM4\text{-}55}}$ and *pha*C1$_{P.nitroreducens}$ was substituted with a negatively charged Glu314 in all other sequences. Another charge alteration was observed at Gln417, a neutral amino acid residue, conserved in *pha*C1$_{P.mendocina}$, *pha*C1$_{Pseudomonas\ sp.\ \mathrm{USM4\text{-}55}}$, *pha*C1$_{P.nitroreducens}$, *pha*C1$_{P.stutzeri}$ and *pha*C1$_{P.fulva}$ were substituted with a positively charged Lys417 in all other sequences. The above mentioned substitutions are indicated by a blue star in Figure 3.17.

```
                                                  10        20        30        40        50        60        70        80        90       100       110
gi|20086523|P.mendocina/1-559   1 MSDKNNEDLKRQASENTLGLNPVIGIRGKDLLTSARMVLAQALKQPFHSAKHVAHFGLELKNVMLGQSALKPEDGDRRFADPAWSQNPLYRRYLQTYLAWRKELHDWVEHSSLSE 115
gi|161344526|P.sp_USM4-55/1-559 1 MSDKNNEDLKRQASENTLGLNPVIGIRGKDLLTSARMVLAQALKQPFHSAKHVAHFGLELKNVMLGQSALKPEDGDRRFADPAWSQNPLYRRYLQTYLAWRKELHDWIEHSSLSD 115
tr|Q8RPZ6|P.nitroreducens/1-559  1 MSDKNDEDLKRQASENTLGLNPVIGIRGKDLLTSARMVLAQALKQPFHSAKHVAHFGLEXKNVMLGQSALKPEDGDRRFADPAWSQNPLYRRYLQTYLAWRKELHDWIEHSSLSD 115
gi|28916412|P.stutzeri/1-559    1 MSDKNNEDLKRQASENTLGLNPVIGIRGKDLLTSARMVLAQALKQPFHSAKHVAHFGLELKNVVFGQSELKPEDGDRRFADPAWSQNPLYRRYLQTYLAWRKELHDWIEHSSLSE 115
gi|10835919|P.resinovorans/1-559 1 MSNKNNEDLQRQASDNTLNLNPVIGIRGKDLLSSARMVLLQAIKQPFHSAKHVAHFGLELKNVLLGQSGLQPEADDRRFNDPAWSQNPLYKRYLQTYLAWRKELHSWIDESNLSS 115
gi|333898614|P.fulva_12-X/1-559 1 MSEKQNDDLKYKPTKSTMGINPVIGIRGRDLLTSARLVLTQAMRQPLHSARHAAHFGLELKNVLLGQSKLQPDENDRRFNDPAWSQNPLYRRYLQTYLAWRQELHDWVEHSSLSE 115
gi|62637857|P.mediterranea/1-559 1 MSNKNNDDLKYQASENTLGLNPVVGLRRKDLLASARMVLTQTLKQPLHSARHVAHFGAELKNVLFGRSALQPAADDRRFNDPAWSQNPLYKRYMQTYLAWRKELHAWIDDSNLPP 115
gi|375300666|P.aeruginosa/1-559 1 MSQKNNNELPKQAAENTLNLNPVIGIRGKDLLTSARMVLLQAVRQPLHSARHVAHFSLELKNVLLGQSELRPGDDDRRFSDPAWSQNPLYKRYMQTYLAWRKELHSWISHSDLSP 115
gi|151442|P.oleovorans/1-559    1 MSNKNNDELQRQASENTLGLNPVIGIRRKDLLSSARTVLRQAVRQPLHSAKHVAHFGLELKNVLLGKSSLAPESDDRRFNDPAWSNNPLYRRYLQTYLAWRKELQDWIGNSDLSP 115
gi|21689573|P.putida/1-559      1 MSNKNNDELQRQASENTMGLNPVIGIRRKDLLSSARTVLRQAVRQPLHSAKHVAHFGLELKNVLLGKSSLAPDSDDRRFNDPAWSNNPLYRRYLQTYLAWRKELQDWVSSSDLSP 115

                                                 120       130       140       150       160       170       180       190       200       210       220
gi|20086523|P.mendocina/1-559 116 QDASRGTFVINLMTEDMAPSNSMANPAAVKRFFETGGKSLLDGLSHLAKDMVHNGGMPSQVNMEAFEVGKNLATTDGAVVFRNDVLELIQYKPITESVHERPLLVVPPQINKFYV 230
gi|161344526|P.sp_USM4-55/1-559 116 QDASRGHFVINLMTEAMAPSNSMANPAAVKRFFETGGKSLLDGLSHLAKDMVHNGGMPSQVNMEAFEVGKNLATTEGAVVFRNDVLELIQYKPITESVHERPLLVVPPQINKFYV 230
tr|Q8RPZ6|P.nitroreducens/1-559 116 QDASRGHFVINLMTEAMAPSNSMANPAAVKRFFETGGKSLLDGLSHLAKDMVHNGGMPSQVNMEAFEVGKNLATTEGAVVFRNDVLELIQYKPITESVHERPLLVVPPQINKFYV 230
gi|28916412|P.stutzeri/1-559   116 QDASRGHFVINLMTEAMAPSNSMANPAAVKRFFETGGKSLLDGMSHLAKDMINNGGMPSQVNMAAFEVGKNLATTEGAVVFRNDVLELIQYKPITESVHERPLLVVPPQINKFYV 230
gi|10835919|P.resinovorans/1-559 116 QDASRGHFVINLMTEAMAPTNSMANPAAVKRFFETGGKSLLDGLSHLAKDMVNNGGMPSQVNMDAFEVGQNLATTEGAVVFRNDVLELIQYKPITESVYERPLLVVPPQINKFYV 230
gi|333898614|P.fulva_12-X/1-559 116 QDVSRGHFIINLLTEAMAPSNSLANPAALKRIFDTGGKSLLDGLSHMAKDLLNNGGMPSQVDMKAFEVGRNLATTEGAVVFRNEVLELIQYTPVTEQVYKRPLLVVPPQINKYYV 230
gi|62637857|P.mediterranea/1-559 116 QDISRGHFVINLMTEAMSPTNSANPAAVKRFFETGGKSLLDGLSHLAKDLVHNGGMPSQVDMGAFEVGKSLGVTEGAVVFRNDVLELIQYRPITEQVHERPLLVVPPQINKFYV 230
gi|375300666|P.aeruginosa/1-559 116 QDISRGQFVINLLTEAMSPTNSLSNPAAVKRFFETGGKSLLDGLGHLAKDLVNNGGMPSQVDMDAFEVGKNLATTEGAVVFRNDVLELIQYRPITESVHERPLLVMPPQINKFYV 230
gi|151442|P.oleovorans/1-559   116 QDISRGQFVINLMTEAMAPTNTLSNPAAVKRFFETGGKSLLDGLSNLAKDLVNNGGMPSQVNMDAFEVGKNLGTSEGAVVYRNDVLELIQYKPITEQVHARPLLVVPPQINKFYV 230
gi|21689573|P.putida/1-559     116 QDISRGQFVINLMTEAMAPTNTLSNPAAVKRFFETGGKSLLDGLSNLAKDMVNNGGMPSQVNMDAFEVGKNLGTSEGAVVYRNDVLELIQYSPITEQVHARPLLVVPPQINKFYV 230

                                                 240       250       260       270       280       290  **   300       310  *    320       330       340
gi|20086523|P.mendocina/1-559 231 FDLSPDKSLARFLLRSQVQTFVVSWRNPTKAQREWGLSTYIEALKEAIDVICAITGSKDVNMLGACSGGLTTASLLGHYAALGQPKVNALTLLVSVLDTQLDTQVALFADEKTLE 345
gi|161344526|P.sp_USM4-55/1-559 231 FDLSPDKSLARFLLRSQVQTFVVSWRNPTKAQREWGLSTYIEALKEAIDVICAITGSKDINMLGACSGGLTTASLLGHYAALGQPKVNALTLLVSVLDTQLDTQVALFADEKTLE 345
tr|Q8RPZ6|P.nitroreducens/1-559 231 FDLSPDKSLARFLLRSQVQTFVVSWRNPTKAQREWGLSTYIEALKEAIDVICAITGSKDINMLGACSGGLTTASLLGHYAALGQPKVNALTLLVSVLDTQLDTQVALFADEKTLE 345
gi|28916412|P.stutzeri/1-559   231 FDLSPDKSLARFLLRSQVQTFVVSWRNPTKAQREWGLSTYIAALKEAIEVICAITGSKDVNMLGACSGGLTTASLLGHYAALGEQKVHALTLLVSVLDTQLDTQVALFADEKTLE 345
gi|10835919|P.resinovorans/1-559 231 FDLSPEKSLARFCLRSNLQTFIVSWRNPTKAQREWGLSTYIEALKEAIDVILKITGAKDLNILGACSGGITTVALLGHYQAIGETKVNAFTQMVSVLDFNLDSQVALFADEQTLE 345
gi|333898614|P.fulva_12-X/1-559 231 FDLSPEKSLARFLLRSQVQTFIVSWRNPTKAQREWGLSTYIEALKKAVEVVCAITGSADVNVLGACSGGATTASLLGHYAAIGEQKVHAQTLLVSVLDTQLDSQYALFADEQTLE 345
gi|62637857|P.mediterranea/1-559 231 FDLSPDKSLARFCLRSNVQTFIISWRNPTKEQREWGLSTYIEALKEAVDVVTAITGSKDVNMLGACSGGITCTALLGHYAALGEKKVNALTLLVSVLDTTLDTDVALFVDEQTLE 345
gi|375300666|P.aeruginosa/1-559 231 FDLSPDKNLARFCLRNGVQTFIVSWRNPTKSQREWGLTTYIEALKEAIEVVLSITGSKDLNLLGACSGGITTATLVGHYVASGEKKVNAFTQLVSVLDFELNTQVALFADEKTLE 345
gi|151442|P.oleovorans/1-559   231 FDLSPEKSLARYCLRSQQQTFIISWRNPTKAQREWGLSTYIDALKEAVDAVLAITGSKDLNMLGACSGGITCTALVGHYAALGENKVNALTLLVSVLDTTMDNQVALFVDEQTLE 345
gi|21689573|P.putida/1-559     231 FDLSPEKSLARFCLRSQQQTFIISWRNPTKAQREWGLSTYIDALKEAVDAVLSITGSKDLNMLGACSGGITCTALVGHYAALGENKVNALTVLVSVLDTTMDNQVALFVDEQTLE 345

                                  ***  350       360       370       380       390       400       410  *    420       430       440       450 *
gi|20086523|P.mendocina/1-559 346 RGQRRSYQAGVLEGSDMAKVFAWMRPNDLIWNYWVNNYLLGNEPPVFDILYWNNDTTRLPAALHGEFIEMFQTNPLTRPGALEVCGTPIDLKQVTCDFFVVAGTTDHITPWDSCY 460
gi|161344526|P.sp_USM4-55/1-559 346 AAKRRSYQAGVLEGSDMAKVFAWMRPNDLIWNYWVNNYLLGNEPPVFDILYWNNDTTRLPAALHGEFIEMFQTNPLTRPGALEVCGTPIDLKQVTCDFFVVAGTTDHITPWDSCY 460
tr|Q8RPZ6|P.nitroreducens/1-559 346 AAKRRSYQAGVLEGSDMAKVFAWMRPNDLIWNYWVNNYLLGNEPPVFDILYWNNDTTRLPAALHGEFIEMFQTNPLTRPGALEVCGTPIDLKQVTCDFFVVAGTTDHITPWDSCY 460
gi|28916412|P.stutzeri/1-559   346 AAKRRSYQAGVLEGSDMAKVFAWMRPNDLIWNYWVNNYLLGNEPPVFDILYWNNDTTRLPAALHGEFIEMFQTNPLTRPGALEVCGTPIDLKQVTCDFFCVAGTTDHITPWDSCY 460
gi|10835919|P.resinovorans/1-559 346 AAKRRSYQAGVLEGKDMAKVFAWMRPNDLIWNYWVNNYLLGNEPPAFDILYWNNDTTRLPAAFHGELVEMFKTNALTRPNALEVCGTPIDLKQVTSDFFCLAGTTDHITPWEACY 460
gi|333898614|P.fulva_12-X/1-559 346 AAKRRSYQAGVLEGSDMAKVFAWMRPNDLIWNYWVNNYLLGNEPPVFDILYWNNDTTRLPAALHGEFIEMFQTNPLTRAGALEVCGTPIDLSQVTCDYYVVAGSNDHITPWTSCY 460
gi|62637857|P.mediterranea/1-559 346 AAKRHSYQAGVLEGRDMAKVFAWMRPNDLIWNYWVNNYLLGNEPPVFDILFWNNDTTRLPAAFHGDLIEMFKTNPLTRPNALEVCGTPIDLKQVTADIFALAGTNDHITPWKSCY 460
gi|375300666|P.aeruginosa/1-559 346 AAKRRSYQSGVLEGKDMAKVFAWMRPNDLIWNYWVNNYLLGNQPPAFDILYWNNDTTRLPAALHGEFVELFKSNPLNRPGALEVSGTPIDLKQVTCDFYCVAGLNDHITPWESCY 460
gi|151442|P.oleovorans/1-559   346 AAKRHSYQAGVLEGSEMAKVFAWMRPNDLIWNYWVNNYLLGNEPPVFDILFWNNDTTRLPAAFHGDLIEMFKSNPLTRPDALEVCGTPIDLKQVKCDIYSLAGTNDHITPWQSCY 460
gi|21689573|P.putida/1-559     346 AAKRHSYQAGVLEGSEMAKVFAWMRPNDLIWNYWVNNYLLGNEPPVFDILFWNNDTTRLPAAFHGDLIEMFKSNPLTRPDALKVCGTAIDLKQVKCDIYSLAGTNDHITPWPSCY 460

                                                 470  *480      490       500       510       520       530       540       550
gi|20086523|P.mendocina/1-559 461 KSAHLFGGKCEFVLSNSGHIQSILNPPGNPKARYMTNSEMPLDPKAWQESSTKHADSWWLHWQSWLAERSGETKNAPRALGNKKFPAGEAAPGTYVHER 559
gi|161344526|P.sp_USM4-55/1-559 461 KSAHLFGGKCEFVLSNSGHIQSILNPPGNPKARYMTNSEMPLDPKAWQESSTKHADSWWLHWQSWLAERSGETKNAPRALGNKKFPAGEAAPGTYVHER 559
tr|Q8RPZ6|P.nitroreducens/1-559 461 KSAHLFGGKCEFVLSNSGHIQSILNPPGNPKARYMSNSEMPLDPKAWQESSTKHADSWWLHWQSWLAERSGETKNAPRALGNKKFPAGEAAPGTYVHER 559
gi|28916412|P.stutzeri/1-559   461 KSAHLFGGKCEFVLSNSGHIQSILNPPGNPKARYMTNSEMPADPKAWQESSTKHADSWWLHWQSWLAERSGKTKNAPTALGNKKFPAGEAAPGTYVHER 559
gi|10835919|P.resinovorans/1-559 461 RSALLLGGKCEFVLSNSGHIQSILNPPGNPKARFSTGSEMPKDPKAWLENATKHADSWWLHWQQWIGERSGKTKKASFTLGNKAFPAGEASPGTYVHER 559
gi|333898614|P.fulva_12-X/1-559 461 KSARLFGGQCEFVLSSSGHIQSILNPPGNPKARYMTNPEMPADPKAWQEDATKHADSWWLHWQKWLTTRSGESKKAPAKLGNKRYPAAEAAPGTYVHER 559
gi|62637857|P.mediterranea/1-559 461 KSAQLFGGKVDFVLSSSGHIQSILNPPGNPKSRYMTSEDMPAKAEDWQENSTKHTDSWWLHWQAWQAERSGKLKKAPTVLGNKTYLAGEAAPGTYVHER 559
gi|375300666|P.aeruginosa/1-559 461 KSARLLGGKCEFILSNSGHIQSILNPPGNPKARFMTNPELPAEPKAWLEQAGKHADSWWLHWQQWLAERSGKTRKAPASLGNKTYPAGEAAPGTYVHER 559
gi|151442|P.oleovorans/1-559   461 RSAHLFGGKIEFVLSNSGHIQSILNPPGNPKARFMTGADRPGDPVAWQENATKHADSWWLHWQSWLGERAGELEKAPTRLGNRAYAAGEASPGTYVHER 559
gi|21689573|P.putida/1-559     461 RSAHLFGGKIEFVLSNSGHIQSILNPPGNPKARFMTGADRPGDPVAWQENAIKHADSWWLHWQSWLGERAGALKKAPTRLGNRTYAAGEASPGTYVHER 559
```

Continues on the following page

Figure 3.17. Multiple sequence alignment of *pha*C1 protein sequences from 10 different *Pseudomonas sp*. The catalytic triad and Ser297 are highlighted by a * and the lipase-box like consensus motif (GACSG) is underlined in red. Sequence variations between *P. mendocina* and the most common PHAs producers including *P. oleovorans, P. aeruginosa* and *P. putida* are indicated by a *.

From the pairwise sequence alignment, the percentage identity between the *pha*C1$_{P.mendocina}$ protein sequence and *pha*C1 protein sequence from other *Pseudomonas sp.* was sequentially calculated (Table 3.1). Interestingly, *pha*C1$_{P.mendocina}$ shared a higher percentage identity to *pha*C1$_{Pseudomonas\ sp.\ \text{USM4-55}}$ (98.39 %) and *pha*C1$_{P.nitroreducens}$ (97.85%) than the other known mcl-PHA producers such as *pha*C1$_{P.aeruginosa}$ (81.22%), *pha*C1$_{P.putida}$ (79.79 %) and *pha*C1$_{P.oleovorans}$ (80.68 %). Phylogenetic analysis further illustrates this divergence (Figure 3.18).

Table 3.1. List of sequences used in this study and their percentage identity with respect to *pha*C1$_{P.mendocina}$

Species name	Sequence identifier	Pairwise percentage identity (%)
P. mendocina	AAM10544.1	100
P. nitroreducens	Q8RPZ6	97.85
P. resinovorans	AAD26365.2	84.26
P. putida	AAM63407.1	79.79
P. stutzeri	AAO59383.1	95.89
P. mediterranea	AAX92633.1	81.40
P. sp_USM4-55	ABX64434.1	98.39
P. fulva_12-X	YP_004472487.1	83.01
P. oleovorans	AAA25932.1	80.68
P. aeruginosa	AFA46810.1	81.22

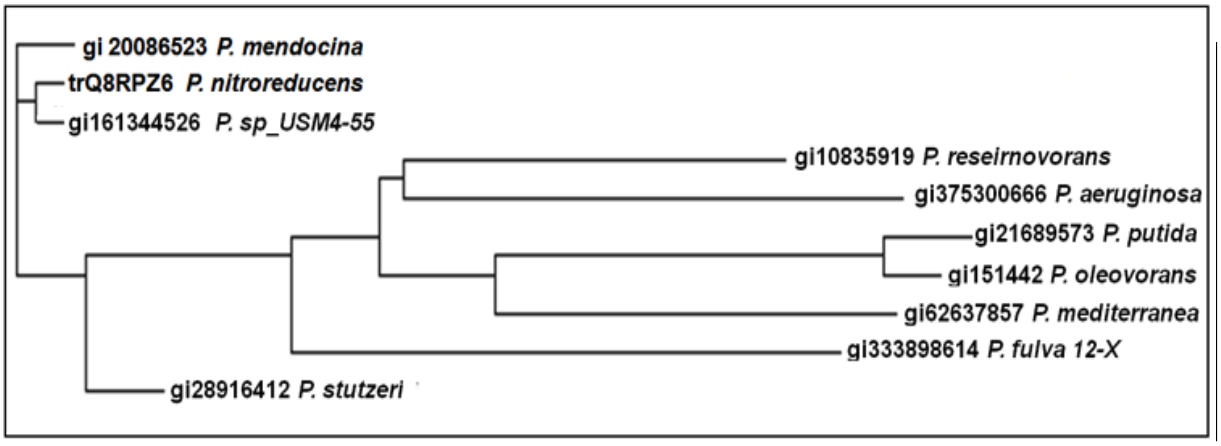

Figure 3.18. Phylogenetic relationship of the analysed *Pseudomonas sp.* based *pha*C1 protein sequence. The tree was constructed using the neighbour joining algorithm using the ClustalW Phylogeny from the ClustalW2 package at the EBI.

A 3D model for *pha*C1$_{P.mendocina}$ was generated (Figure 3.19A) using the structure of the human gastric lipase (PDB code 1hlg) as template and PHYRE2, an automatic fold recognition server for structure prediction (Kelley and Sternberg 2009). The active site residues of the catalytic triad (Cys296, Asp451, and His479) are shown in Figure 3.19B. Also, the amino acid differences observed in *pha*C1$_{P.mendocina}$, ArgGlyGln346-348, Gln315 and Gln417, as compared to the most used *Pseudomonas* strains have been highlighted in the structure (Figure 3.19(C)). However in the absence of X-ray crystallographic data for type II PHA synthases, with and without the substrates, it would be difficult to evaluate the significance of the sequence divergence observed in *pha*C1$_{P.mendocina}$ with respect to the other known mcl-producing strains.

3.19 (A)

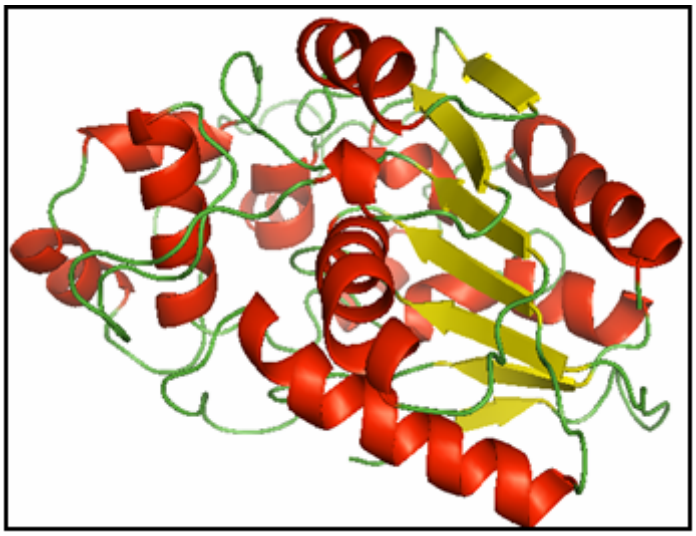

Continues on the following page

(B)

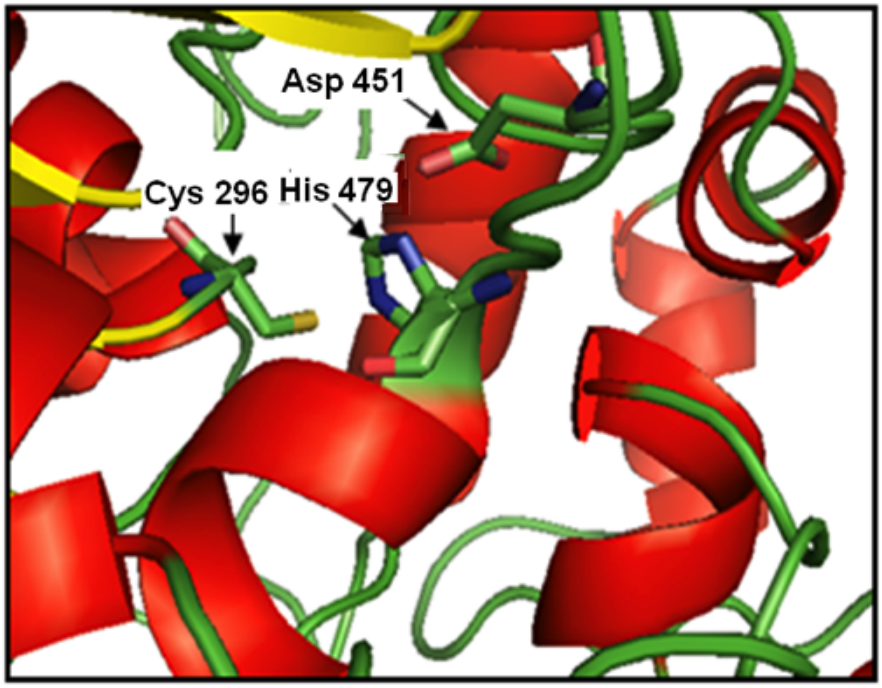

(C)

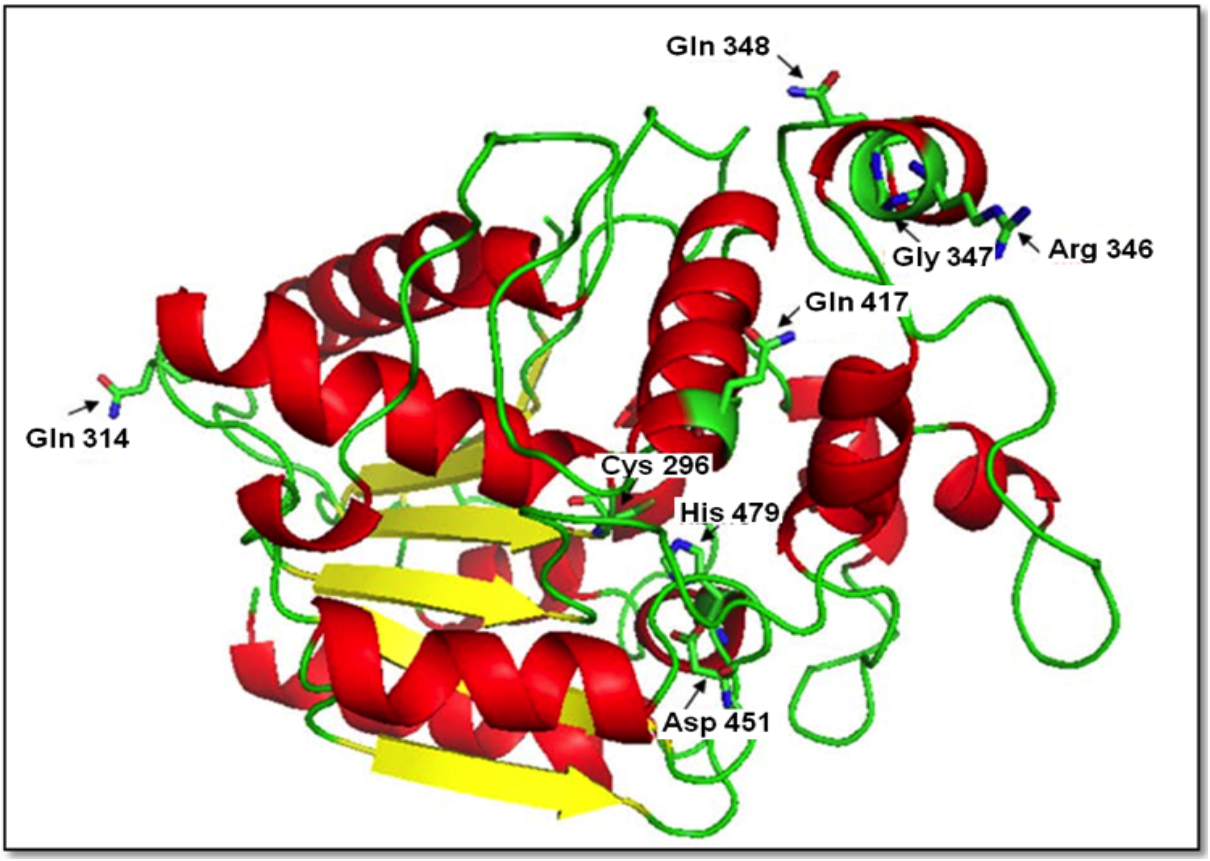

Figure 3.19. (A) The predicted 3D model for *pha*C1$_{P.mendocina}$ generated using the structure of the human gastric lipase (PDB code 1hlg) as template on the PHYRE2 server (B) The active site residues of the catalytic triad (Cys296, Asp451, and His479) are highlighted (C) Amino

acid differences identified in *pha*C1$_{P.mendocina}$ protein sequence as compared to the most used *Pseudomonas* strains during sequence analysis and catalytic triad is highlighted on the model.

3.3. DISCUSSION

In this chapter, we investigated the *pha*C1 gene expression from *P. mendocina* in *B. subtilis 1604*. The *B. subtilis 1604-pha*C1 recombinant strain was subjected to fermentation and showed PHA accumulation. The incorporation of the *pha*C1 gene in *B. subtilis* confirmed the potential of the host bacteria to produce significant levels of PHAs. In contrast to what was expected, GC-MS and NMR studies confirmed the presence of an scl-PHA homopolymer, P(3HB), when the *B. subtilis 1604-pha*C1 recombinant strain was grown in PHA production media with sucrose as the sole carbon source. This is a very unusual result and has not been reported before. *P. mendocina pha*C1 gene was expected to encode an enzyme that would polymerise mcl-PHA monomers units leading to the production of mcl-PHAs.

Wang *et al.,* (2006) have cloned and expressed the *pha*C1 gene from *Pseudomonas aeruginosa* in *B. subtilis*. The gas chromatography results showed that the expression of the *pha*C1 gene into *B. subtilis* DB104, in the presence of glucose as a carbon source, resulted in the production of Poly(3-hydroxydecanoate-co-3-hydroxydodecanoate), P(3HD-co-3HDD), a mcl-PHA copolymer. Furthermore, the inclusion of the *pha*A gene, encoding the β-ketothiolase and the *pha*B gene encoding the acetoacetyl-CoA-reductase from *Ralstonia eutropha* resulted in the production of a Poly(3-hydroxybutyrate-co-3-hydroxydecanoate-co-3-hydroxydodecanoate P(3HB-co-3HD-co-3HDD), a scl-mcl copolymer.

In contrast to Wang *et al.,* (2006) our results showed that only the incorporation of the *pha*C1 synthase gene from *P. mendocina* in *B. subtilis 1604* resulted in the production of a scl-PHA, P(3HB), and no mcl-PHAs were observed. The fact that *pha*C1$_{P.aeruginosa}$ and *pha*C1$_{P.mendocina}$ showed only 81.22% of identity (table 3.1) can explain differences in *Pha*C1 substrate specificity. However, further experiments should be carried out by Wang *et al.* to confirm the nature of the produced PHAs.

B. subtilis containing the *pha*C1 gene showed a higher amount of dry cells weight and a significant PHA production compared to *B. subtilis* containing the vector without the insert

and the wild type. The amount of PHA produced, normalized per gram of cells (g of PHA/g dry cell weight) was 1.7%±0.43, 2.7%±0.45 and 32.3%±9.6 for *B. subtilis* wild type, *B. subtilis*-vector and *B. subtilis-pha*C1 gene, respectively. These results confirmed the role of the *PhaC1* synthase in PHA accumulation in the recombinant *B. subtilis*.

P. mendocina wild type produces a copolymer composed of short chain length and medium chain length PHAs when sucrose is used as the carbon source. In contrast to our results, previous reports showed production of only mcl-PHAs by *P. putida, P. aeruginosa, P. resinovorans* and *P. mediterranea* in the presence of carbohydrates confirming the different substrate specificity of *P. mendocina Pha*C1 enzyme (Ashby *et al.,* 2001, Huijberts *et al*., 1992, Palmeri *et al.,* 2012, Rosas *et al*., 2007).

As described previously, mcl-PHAs can be produced via the fatty acid *de novo* biosynthesis pathway and the fatty acid β-oxidation pathway. When sucrose was used as a carbon source the mcl-PHA polymer production was expected to occur via the fatty acid *de novo* biosynthetic metabolic pathway. However, contrary to our expectations, a scl-homopolymer was obtained. In order to test the capability of the recombinant *B. subtilis* to produce mcl-PHAs via the fatty acids degradation pathway, a range of fatty acids were screened. Only when pentanoic, hexanoic and heptanoic acids were used as carbon sources, PHAs were obtained. The resulting polymer was a scl-copolymer composed of Poly-(3-hydroxybutanoate) and Poly-(3-hydroxypentanoate), (P3HB-co-HV). As previously reported by Valappil *et al*., (2007) within the Gram-positive genera, only *Corynebacterium*, *Nocardia* and *Rhodococcus* can naturally synthesize the commercially important co-polymer P(3HB-co-3HV) from simple carbon sources such as glucose (Alvarez *et al*., 2000, Haywood *et al*., 1991). In this case, the addition of the *pha*C1 gene from *P. mendocina* to *B. subtilis* allowed the strain to synthesize LPS-free P(3HB-co-3HV) copolymer. However, no mcl-PHAs production was observed. One of the main enzymes that play a pivotal role in the mcl-PHAs synthesis is the (R)-3-hydroxyacyl-ACP-CoA transacylase, which converts the (R)-3-Hydroxyacyl-ACP precursor from the fatty acid *de novo* biosynthetic pathway to (R)-3-hydroxyacyl-CoA, the substrate required by the PHA synthase for mcl-PHA production. As BLAST results revealed the presence of a hypothetical protein predicted to be a hydrolase/acyltransferase in *B. subtilis* 1604, it is not possible to attribute the incapability of the *pha*C1 synthase from *P. mendocina* to support mcl-PHA production in *B. subtilis* to the absence of (R)-3-hydroxyacyl-ACP-CoA transacylase. However, as this protein was not studied previously, further studies should be carried out to confirm the nature of the protein.

No structural information for the class II PHA synthases is available. Threading models generated for *pha*C1 from *Pseudomonas aeruginosa* (Amara and Rehm, 2003) and *Pseudomonas sp. USM 4–55* (Wahab *et al*., 2006) have provided insights into the residues critical for catalysis in these enzymes. Therefore, in order to understand the exceptionally broad substrate specificity of the *pha*C1 enzyme in *P. mendocina,* sequence analysis and 3D structure prediction was undertaken. Multiple sequence analysis and phylogenetic analysis was carried out with *pha*C1 protein sequences from other *Pseudomonas sp*. containing class II PHA synthases. Of the 9 sequences compared, *pha*C1$_{P.mendocina}$ shared the lowest sequence identity with other well established mcl-PHA producers such as the *P. aeruginosa*, *P. putida* and *P. oleovorans*. The phylogenetic analysis further emphasised this sequence divergence, as *pha*C1$_{P.mendocina}$ was placed in a distinctly different cluster along with *pha*C1 $_{Pseudomonas\ sp.\ \mathrm{USM4\text{-}55}}$ and *pha*C1$_{P.nitroreducens}$. Previous reports has shown that surprisingly, *Pseudomonas nitroreducens*, that shares 97.85% of identity with *P. mendocina* in the *pha*C1 sequence (Table 3.1), produced P(3HB) homopolymer when hexanoate was used as a sole carbon source and Poly(3-hydroxyoctanoate-co-hydroxydecanoate) copolymer in the presence of butyrate, decanoate, lauric acid and tetradecanoic acid (Yao *et al*., 1999). These results confirm the broad substrate specificity of the PHA synthase in *P. nitroreducens*, very similar to that found in *P. mendocina*.

Although the important residues such as the catalytic triad (Cys296, Asp451, His479), Ser297 and the lipase-box like consensus motif are conserved in all the sequences used in this study, certain amino acid substitutions were observed in the core region (residue 267- 484) of the *pha*C1protein sequence from *P. mendocina*, which were otherwise conserved in other mcl-PHA producers such as the *P. aeruginosa*, *P. putida* and *P. oleovorans*. As described previously, some of these amino acid changes result in charge alterations, for example the change from neutral amino acid Gln314 in *pha*C1$_{P.mendocina}$, *pha*C1$_{Pseudomonas\ sp.\ \mathrm{USM4\text{-}55}}$ and *pha*C1$_{P.nitroreducens}$ to a negatively charged Glu at the same position in all other *Pseudomonas* species. There is no information on the functional significance of these amino acid differences. A 3D model was generated for *pha*C1$_{P.mendocina}$ using human gastric lipase as the template. From the predicted model, the catalytic residues and structural position of the observed amino acid differences in *pha*C1$_{P.mendocina}$ could be mapped. However without a crystal structure it is difficult to exactly predict the structural effect of these amino acid changes on the active site of the enzyme and their role in the catalytic mechanism of the *pha*C1. It is possible that the catalytic core of *pha*C1$_{P.mendocina}$ is different from the other mcl-

PHA producers in its charge distribution and side chain composition and therefore exhibits broader substrate specificity.

Hence, in conclusion, this work confirms the capability of a Gram-positive GRAS organism to express a Gram-negative gene from *P. mendocina*. Additionally, our results demonstrate the unusually broad substrate specificity of the PHA synthase from *P. mendocina*, which was found to be able to catalyse production of both mcl-PHA and scl-PHA production depending on the metabolic pool available in the host organism. Such a PHA synthase can therefore be used for the production of the entire range of PHAs (both scl and mcl-PHAs) by simply varying the available substrate pool, a great advantage.

CHAPTER 4

Production of P(3HO) using *Pseudomonas mendocina* and scaling up of the process

4.1. INTRODUCTION

Medium chain length PHAs are gaining importance due to their adjustable flexible material properties that are suitable for a range of biomedical applications. The type of mcl-PHA produced and hence their properties can be varied with the type and relative quantity of carbon sources supplied to the growth media, the organism used and the culture conditions provided (Ojumu *et al*., 2004). In addition to the different properties obtained with different mcl-PHAs, the production of co-polymers, blends and composites further increase the range of applications allowing the fabrication of tailor made materials. However, despite the varied applicability of these polymers, widespread use of the mcl-PHAs remain limited, mainly because of the lack of availability of these materials in large quantities (Rai *et al*., 2011b). Awareness of the need of industrialization of these polymers has reinforced the interest in scientists to develop different strategies for their production in large scale.

Although there are many microorganisms that are able to produce PHAs, mcl-PHA production has been restricted to different strains of *Pseudomonas* (Prieto *et al.,* 2007). In order to achieve a high productivity and high yield of mcl-PHAs, fermentation processes using these strains need to be optimized. To this end, in the first part of this chapter, P(3HO) polymer production in *P. mendocina* was optimized in 2 L bioreactors and the effect of different parameters such as pH, and carbon/nitrogen ratio was analyzed.

As no work has been carried out in the scaling-up of P(3HO) production using *P. mendocina*, in the second part of the chapter we have studied the capacity to scale-up the polymer production from 2 L to 20 L and 72 L bioreactors using the constant oxygen transfer coefficient technique. In aerobic bioprocesses, the oxygen transfer rate (OTR) in the media is a key factor that will influence a culture performance. Therefore, it is important to ensure an adequate delivery of oxygen to the media. In a stirred tank bioreactor, the OTR is mainly affected by the stirrer speed, the type and number of stirrers and the gas flow rate used. Accurate estimation of the OTR in bioreactors is essential in order to establish aeration efficiency at different scales under different stirrer speeds and airflow rates. In stirred tank bioreactors, the stirrer is the main gas dispersing tool and stirrer speed and airflow rate are the main factor that will determine the k_La values. In this project, the P(3HO) polymer production was scaled up from the 2 L to the 20 L and 72 L bioreactors based on the constant oxygen transfer coefficient, k_La. The oxygen transfer from air to liquid phase is controlled by the liquid phase mass transfer resistance, described by the following equation:

$$[dC_L/dt] = k_La \times (C^*-C_L) \qquad (4.\ 1)$$

where C* is the saturation concentration of oxygen in liquid, C_L is the dissolved oxygen concentration in liquid, t is time and dC_L/dt is the volumetric rate of mass transfer. The $-k_La$ value can be obtained from the slope of $\ln(C^*-C_L)$ against time.

In this project, k_La values were determined by the dynamic method. The dynamic method involves the elimination of oxygen in the liquid, followed by the supply of air. The variation in oxygen concentration in the water is measured through time. Firstly, the k_La value of the 2 L bioreactor was determined under the condition that produced maximum polymer in the optimization work. Then, in order to keep the same oxygen transference in the 20 L and 72 L bioreactors, the k_La values of both bioreactors were calculated at different sets of impeller speeds and airflow rates. *P. mendocina* was grown under the obtained condition for a constant k_La in the 20 L and 72 L bioreactors and P(3HO) was extracted at different scales. The evaluation of the scaling-up process was carried out by the comparison of the amounts of polymer produced at different scales.

4. 2. RESULTS

4. 2. 1. Production of P(3HO) in *P. mendocina*

The P(3HO) production from *P. mendocina* with sodium octanoate as a sole carbon source was optimized in 2 L bioreactors as described in section 2. 2.7.1 Four conditions were tested where the pH and carbon/nitrogen ratio were varied (Table 2.5). To enhance P(3HO) production, the C/N ratios of 20:1, 15:1 and 10:1 and pH of 6.8, 7.15 and 7.5 in mineral salt medium production media were compared in order to determine the optimal conditions.

Figure 4. 1 shows the fermentation profile obtained for condition 1 (pH 7.15, carbon/nitrogen 20:1 and stirrer speed 200 rpm). Under this condition the organism reaches exponential phase after 3 hours of growth. At this point, the DOT reaches zero, as a consequence of the oxygen consumption of the growing bacteria in the media. At 29 hours, stationary phase is achieved and as a result of the cell death, the DOT starts to increase. The maximum OD_{450nm} achieved during the fermentation was 4.7. PHAs were extracted at 24 hr, 36 hr and 48 hr and these time points were at the exponential phase, stationary phase and death phase, respectively. The maximum PHA yield of 20.6 % DCW was obtained during the stationary phase, at 36 hr.

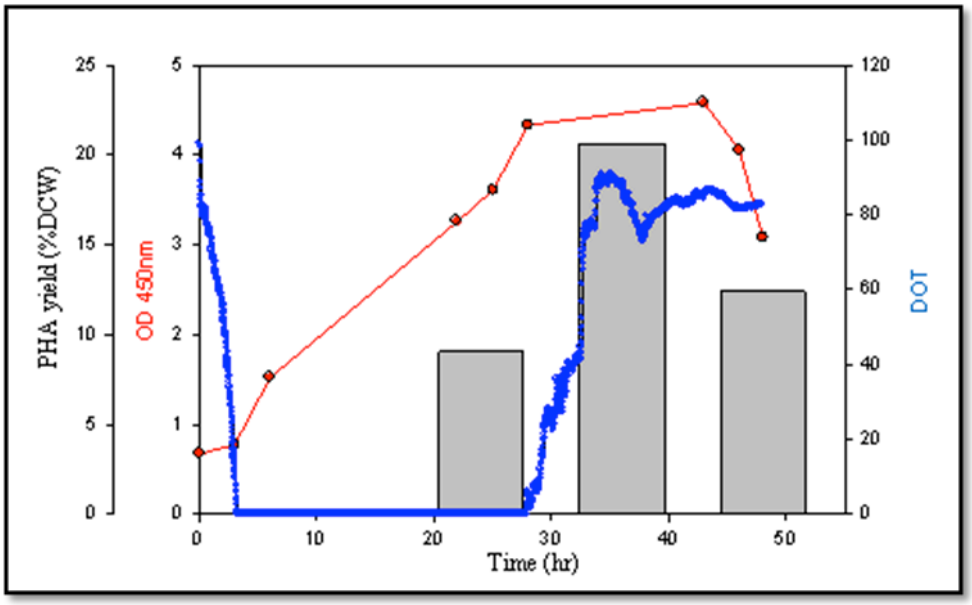

Figure 4. 1. Fermentation profile of *P. mendocina* and P(3HO) accumulation obtained under condition 1 (pH 7. 15, carbon/nitrogen 20:1 and stirrer speed 200 rpm). OD_{450nm} (—) , DOT (—) and PHA yield (grey bars).

Figure 4.2 shows the fermentation profile obtained under condition 2 (pH 7. 5, carbon/nitrogen 15:1 and stirrer speed 200 rpm). In this condition the organism reached exponential phase before 3 hours of growth. As a consequence, the oxygen consumption by the organism decreased to zero in 1.2 hr. The stationary phase was achieved at 23 hr, when the DOT increased drastically. The maximum OD_{450nm} achieved during the fermentation was 4.5. PHAs were extracted at 24 hr, 36 hr and 48 hr with the first two values at the stationary phase and the last one at the death phase. The maximum PHA yield of 12.3 % DCW was obtained during early stationary phase, at 24 hr.

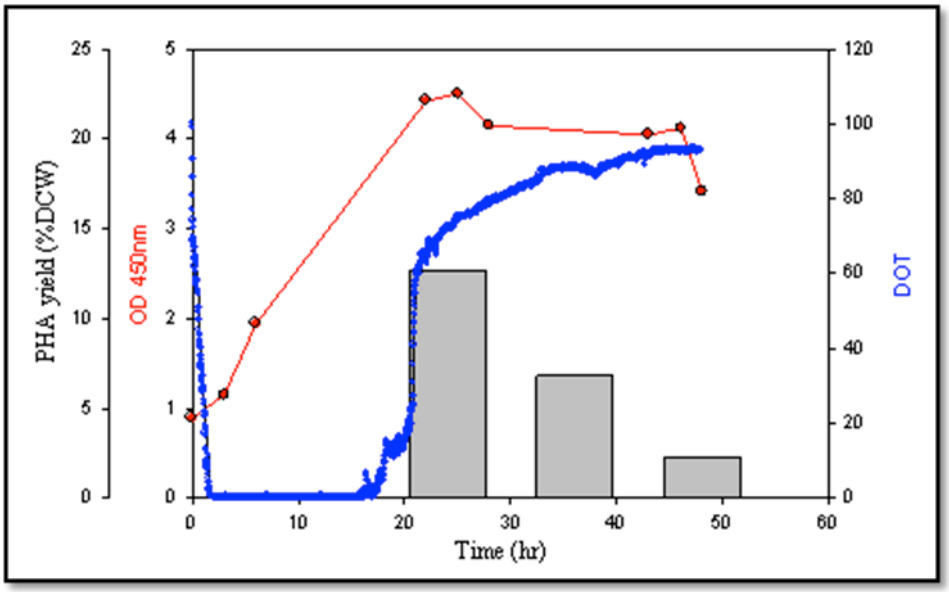

Figure 4. 2. Fermentation profile of *P. mendocina* and P(3HO) accumulation obtained under condition 2 (pH 7.5, carbon/nitrogen 15:1 and stirrer speed 200 rpm). OD_{450nm} (—) , DOT (—) and PHA yield (grey bars).

Figure 4. 3 shows the fermentation profile obtained for condition 3 (pH 6. 8, carbon/nitrogen 15:1 and stirrer speed 200 rpm). Under this condition the organism achieved exponential phase after 3 hours of growth with a slower growth than condition 1, represented by the smaller slope of the OD_{450nm} and DOT graph. At 23 hr, the stationary phase was achieved and as a result of the cell death, the DOT started to increase. The maximum OD_{450nm} achieved during the fermentation was 4.2. PHAs were extracted at 24 hr, 36 hr and 48 hr at the stationary phase. The maximum PHA yield of 10.5 % DCW was obtained during early stationary phase, at 24 hr.

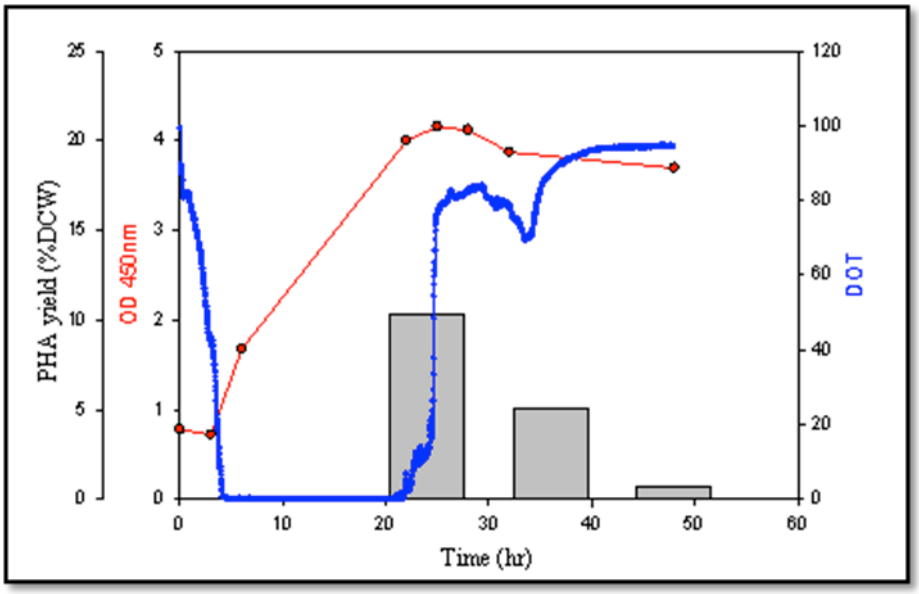

Figure 4. 3. Fermentation profile of *P. mendocina* and P(3HO) accumulation obtained under condition 3 (pH 6. 8, carbon/nitrogen 15:1 and stirrer speed 200 rpm). OD_{450nm}(—) , DOT (—) and PHA yield (grey bars)

Figure 4.4 shows the fermentation profile obtained under condition 4 (pH 7.15, carbon/nitrogen 10:1 and stirrer speed 200 rpm). In this condition the exponential phase is achieved before conditions 1, 2 and 3. As a consequence, the organism's oxygen consumption in the media decreased to zero within 1 hr. The stationary phase was achieved between 9 hr and 23 hr and as a result, the DOT increased drastically at 15 hr. The maximum OD_{450nm} achieved during the fermentation was 3.3. PHAs were extracted at 24 hr, 36 hr and 48 hr, at the stationary phase. The maximum PHA yield of 2.3 % DCW was obtained at 24 hrs.

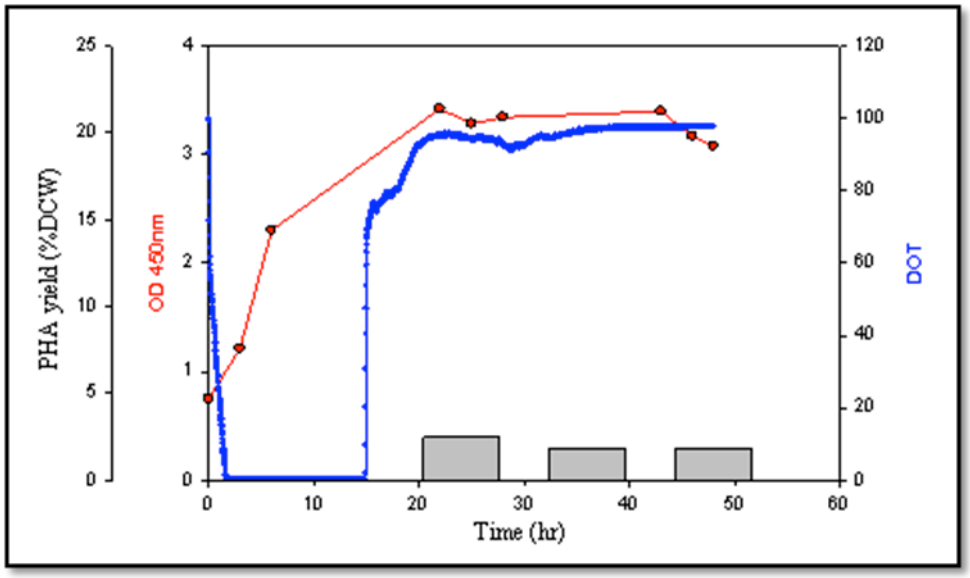

Figure 4. 4. Fermentation profile of *P. mendocina* and P(3HO) accumulation obtained under condition 4 (pH 7. 15, carbon/nitrogen 10:1 and stirrer speed 200 rpm). OD_{450nm}(—) , DOT (—) and PHA yield (grey bars)

4. 2. 2. Scaling-up production of P(3HO) from *Pseudomonas mendocina*

4. 2. 2. 1. Determination of k_La and scaling-up conditions

The condition in which the highest PHA yield was obtained was scaled-up to 20 L and 72 L bioreactors as described in section 2.2.7.2. For this, condition 1, when pH is 7.15, carbon/nitrogen 20:1 and stirrer speed 200 rpm was used. In a first step, the k_La of the 2 L bioreactor, at an airflow rate of 1 vvm and stirrer speed 200 rpm was determined by the gassing out method. For this, the bioreactor was filled with 1.4 L of distilled water and the oxygen of the liquid was removed with nitrogen. Then, air was supplied to the bioreactor and the increment in DOT with time was measured. Equation 4.1 shows that k_La can be obtained from the inverse of the slope of ln(C*-C) vs. time and the obtained value was 0.256 (Figure 4.12).

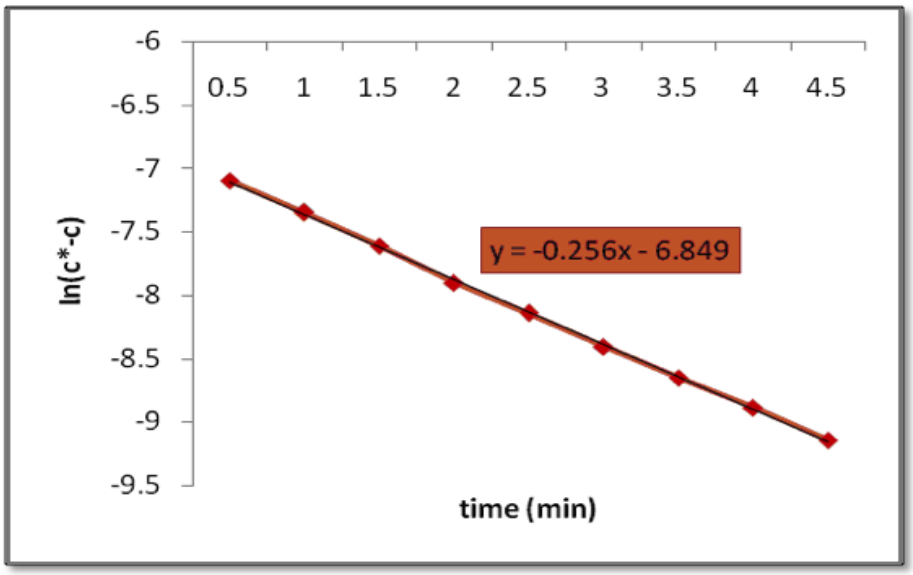

Figure 4. 5. Ln (C*-C) vs. time for the 2 L bioreactor at 1vvm and 200 rpm. Note that the inverse of the slope is the k_La.

In the second part, in order to determine the condition to be used in the 20 L bioreactor for constant oxygen transfer, the k_La values were determined at a range of air flow rates (from 0.5 vvm to 1. 25 vvm) and stirrer speed (from 100 rpm to 250 rpm), in the 20 L bioreactor. Figure 4. 6 shows the plot of the ln(C*-C) vs. time at different stirrer speeds of 100, 150, 200 and 250 rpm and A) 0.5 vvm B) 0.75 vvm C) 1 vvm D) 1.25 vvm constant air flow rates.

A)

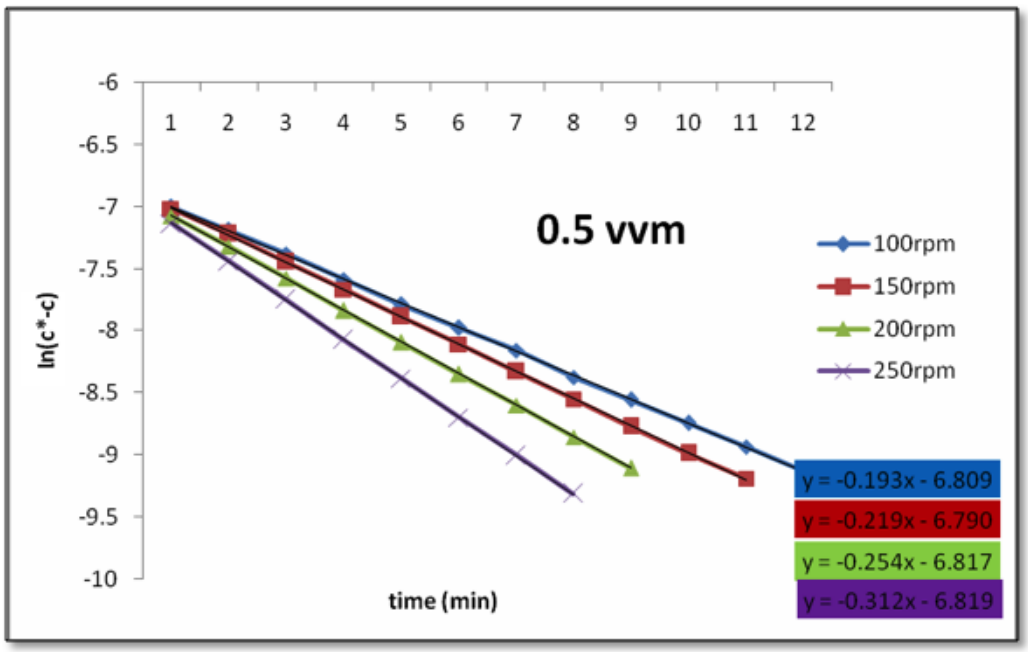

Continues on the following page

B)

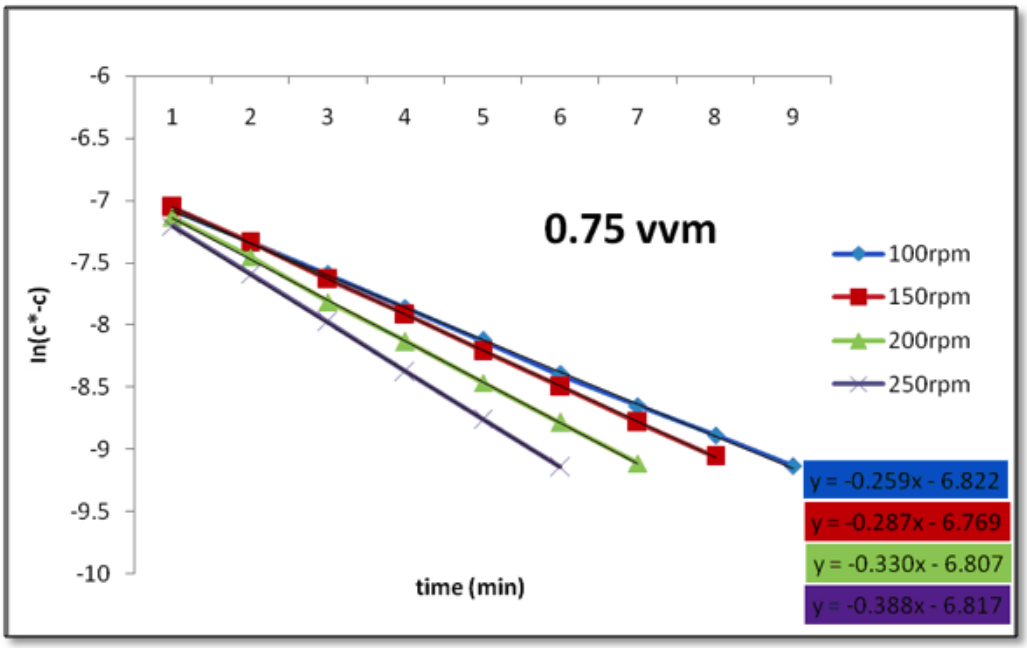

C)

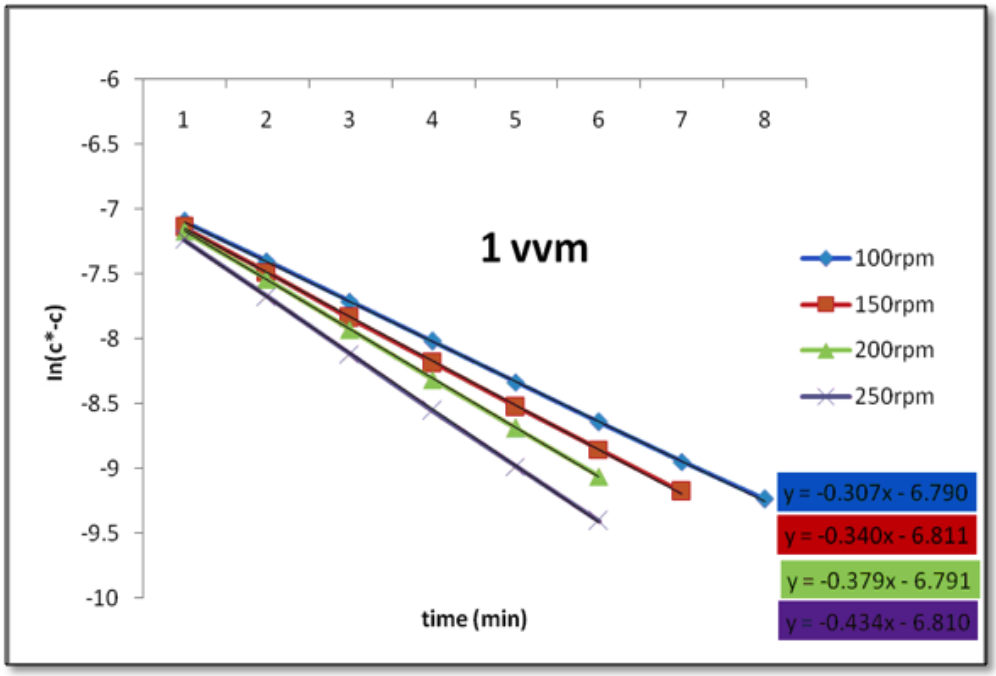

Continues on the following page

D)

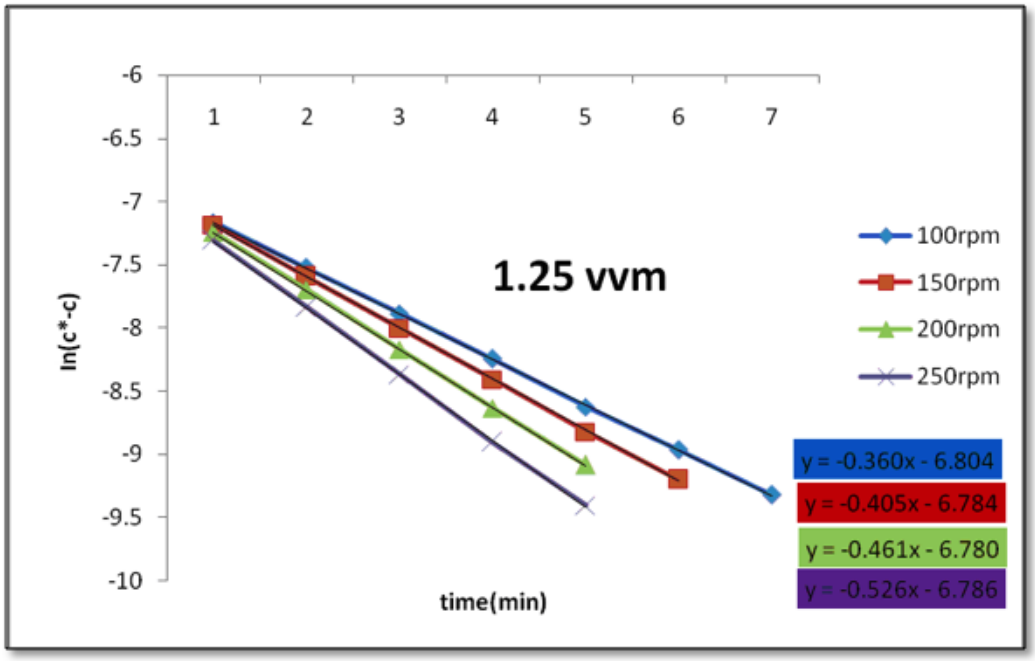

Figure 4. 6. Ln (C*-C) vs. time for the 20 L bioreactor at 100, 150, 200 and 250 rpm at A) 0.5 vvm B) 0.75 vvm C) 1 vvm and D) 1. 25 vvm. Note that the inverse of the slope for each condition is the k_La.

The k_La obtained at 200 rpm and 1 vvm in the 2 L bioreactor was 0.256. Table 4.1 summarizes the k_La values obtained at the different air flow rates and stirrer speeds in the 20 L bioreactor. The results obtained show that the k_La value obtained with the 2 L bioreactor is within the range of the k_La values obtained at 0.5 vvm in the 20 L bioreactor (Table 4.1). Hence, in order to determine the stirrer speed to be used in the 20 L bioreactor for a k_La of 0.256, a plot of the k_La vs. stirrer speed at 0.5 vvm was carried out and the stirrer speed was calculated from the obtained linear regression (Figure 4.7). The obtained stirrer speed was 186 rpm.

Table 4. 1. k_La values obtained in the 20 L bioreactor at different air flow rates and stirrer speeds

	0.5 vvm	0.75 vvm	1 vvm	1. 25 vvm
100 rpm	0.193	0.259	0.307	0.360
150 rpm	0.219	0.287	0.340	0.405
200 rpm	0.254	0.330	0.379	0.461
250 rpm	0.312	0.388	0.434	0.526

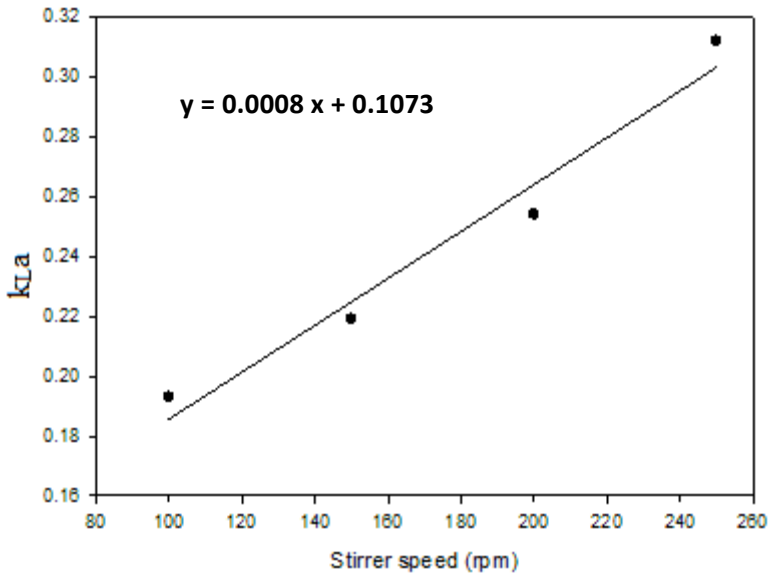

Figure 4.7. k_La vs. stirrer speed at 0.5 vvm and linear regression for the 20 L bioreactor.

The same procedure was repeated to determine the condition to be used in the 72 L bioreactor in order to maintain constant the oxygen transference. Figure 4.8 shows the plot of the ln(C*-C) vs. time at different stirrer speeds of 100, 150, 200 and 250 rpm and A) 0.5 vvm B) 0.75 vvm C) 1 vvm D) 1.25 vvm constant air flow rates.

A)

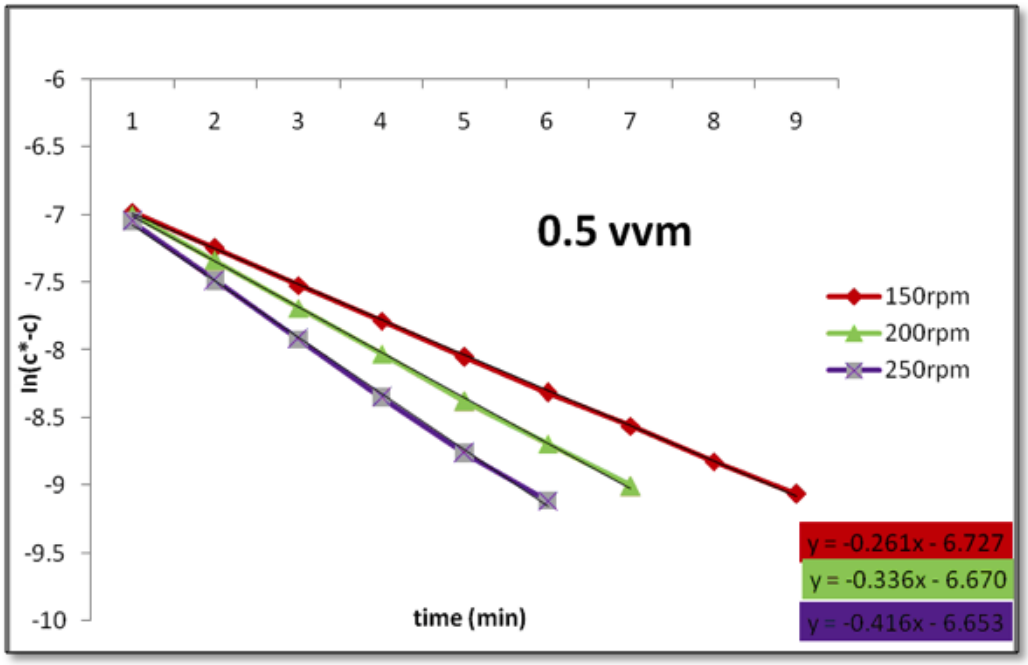

B)

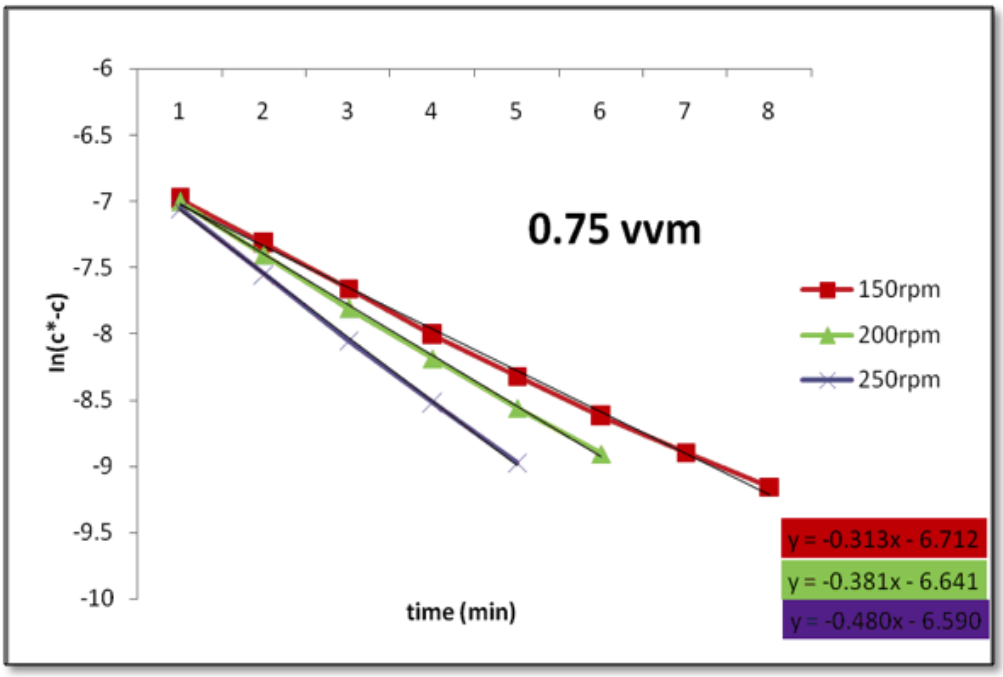

Continues on the following page

C)

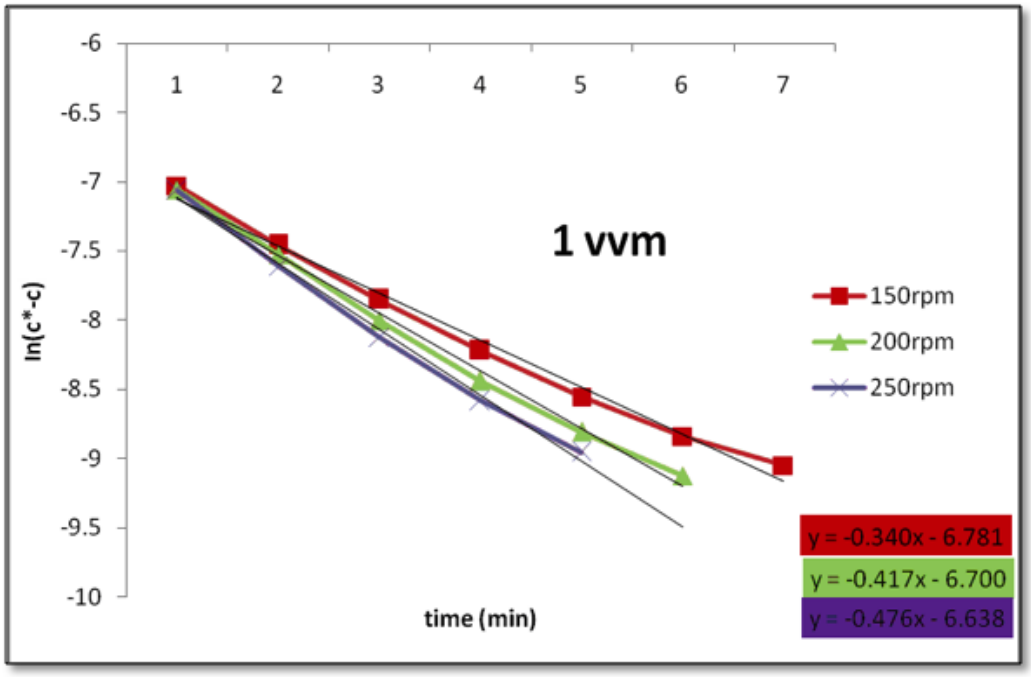

D)

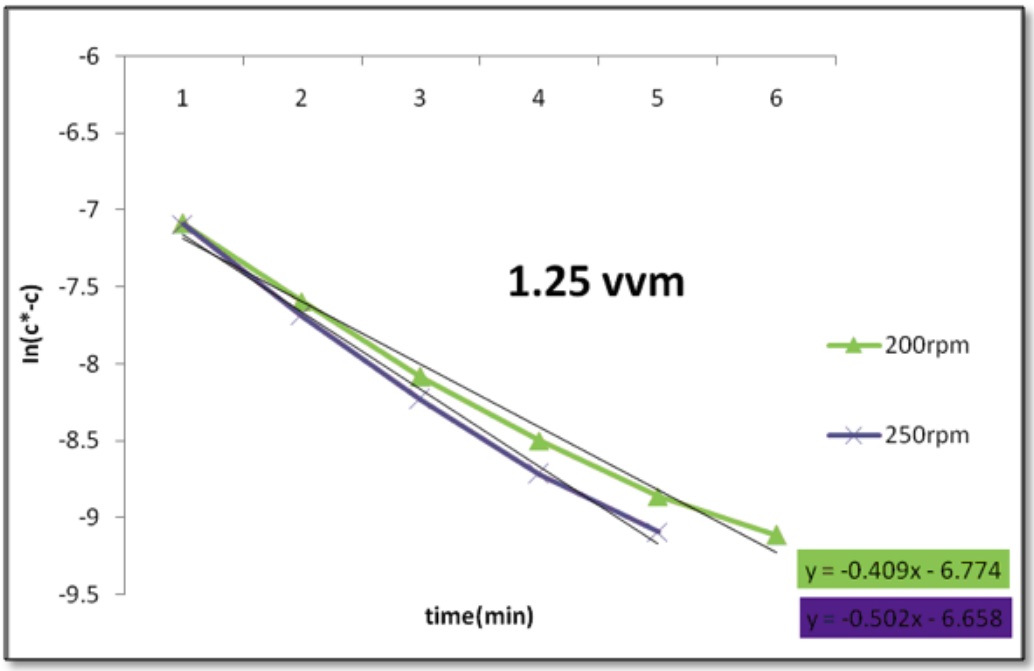

Figure 4. 8. ln (C*-C) vs. time for the 72 L bioreactor at 100, 150, 200 and 250 rpm at A) 0.5 vvm B) 0.75 vvm C) 1 vvm and D) 1. 25 vvm. Note that the inverse of the slope for each condition is the k_La.

Table 4. 2 summarizes the k_La values obtained at the different air flow rates and stirrer speeds in the 72 L bioreactor. Results showed that the k_La value obtained with the 2 L bioreactor is closer to the k_La values obtained at 0.5 vvm in the 72 L bioreactor. Hence, in order to determine the stirrer speed to be used in the 72 L bioreactor for a k_La of 0.256, a plot of the k_La vs. stirrer speed at 0.5 vvm was carried out and the stirrer speed was calculated from the obtained linear regression by interpolation (Figure 4.9). The obtained stirrer speed was 143 rpm.

Table 4. 2. k_La values obtained in the 72 L bioreactor at different air flow rates and stirrer speeds

	0.5 vvm	**0.75 vvm**	**1 vvm**	**1. 25 vvm**
150 rpm	0.261	0.313	0.340	_
200 rpm	0.336	0.318	0.417	0.409
250 rpm	0.416	0.480	0.476	0.502

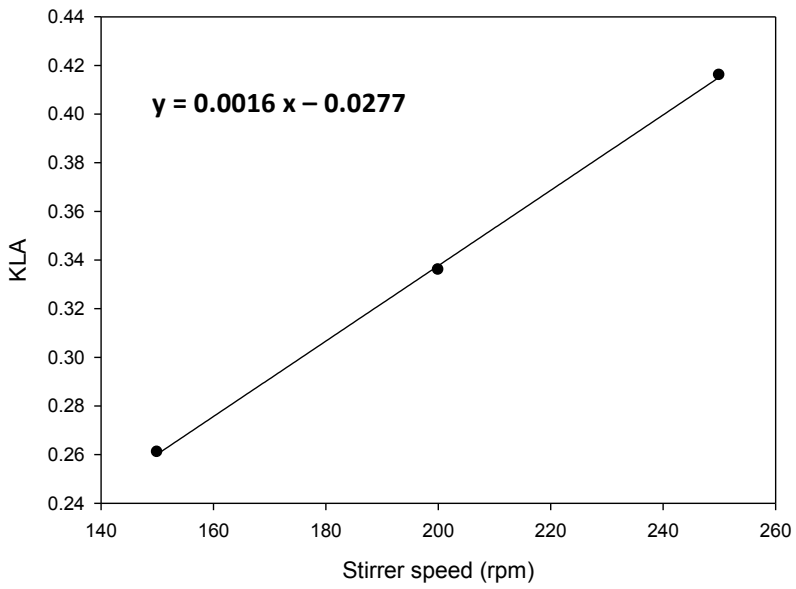

Figure 4. 9. k_La vs. stirrer speed at 0.5 vvm and linear regression for the 72 L bioreactor.

4. 2. 2. 2 Scaling-up

The scale-up studies based on a constant oxygen transfer coefficient, k_La from 2 L to 20 L and 72 L of aerated and agitated bioreactors were performed. Table 4.3 summarizes the conditions obtained for a constant k_La of 0.256. All the fermentations were carried out with an initial carbon/nitrogen ratio 20:1 and pH 7. 15.

Table 4. 3. Scaling-up conditions for the 2 L, 20 L and 72 L bioreactor for a constant k_La of 0.256

Bioreactor scale	Stirrer speed (rpm)	Air flow rate (vvm)
2 L	200	1
20 L	186	0.5
72 L	143	0.5

P. mendocina was grown in the 2 L bioreactor at 200 rpm and 1 vvm. Figure 4.10 shows the fermentation profile obtained. Under this condition, within 7 hr of fermentation, a decrease in the dissolved oxygen tension, from 100% to zero was observed. After 27 hr the oxygen concentration in the media started to increase. The maximum OD_{450nm} achieved during the fermentation was 5. 9. PHAs were extracted at 36 hr and 48 hr, during the stationary phase. The maximum PHA yield was 26.84±0.35 %DCW, obtained during early stationary phase, at 36 hrs.

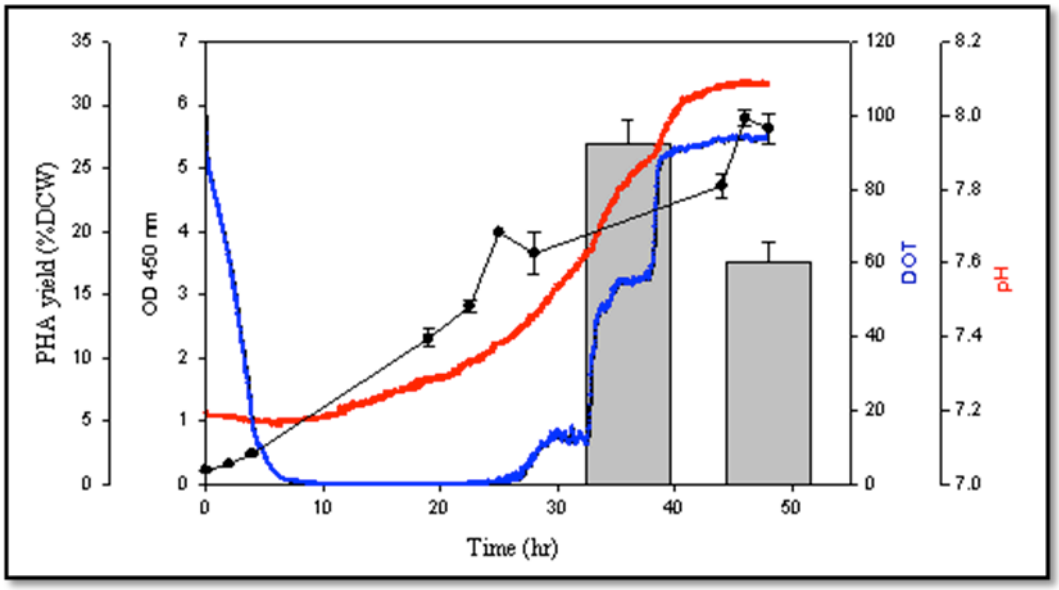

Figure 4. 10. Fermentation profile of *P. mendocina* and P(3HO) accumulation obtained in the 2 L bioreactor with an initial carbon/nitrogen ratio of 20:1 and pH of 7.15, stirrer speed 200 rpm and air flow rate 1 vvm. OD_{450nm}(—) , pH (—), DOT (—) and PHA yield (grey bars).

P. mendocina was grown in the 20 L bioreactor at 187 rpm and 0.5 vvm. Figure 4.11 shows the fermentation profile obtained. Under this condition the amount of oxygen in the media were zero between 4 hrs and 64 hrs of fermentation. The maximum OD_{450nm} achieved during the fermentation was 6. PHAs were extracted at 66 hr and 78 hr during the stationary phase. The maximum PHAs yield was 23.17±1.47 %DCW, obtained during the late stationary phase at 36 hr.

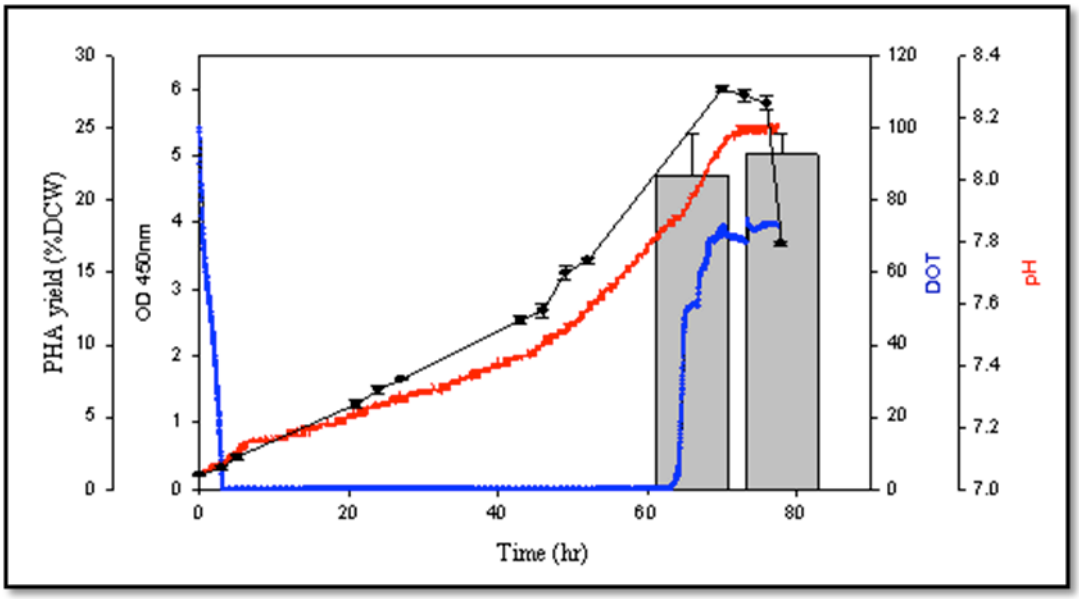

Figure 4. 11. Fermentation profile of *P. mendocina* and P(3HO) accumulation obtained in the 20 L bioreactor with an initial carbon/nitrogen ratio of 20:1 and pH of 7. 15, stirrer speed 186 rpm and air flow rate 0.5 vvm. OD_{450nm} (—) , pH (—), DOT (—) and PHA yield (grey bars).

P. mendocina was grown in the 72 L at 143 rpm and 0.5 vvm. Figure 4.12 shows the fermentation profile obtained. In this condition, within 8 hr of fermentation, a decrease in the amounts of oxygen from 100% to zero was observed. After 46 hr, the oxygen concentration in the media started to increase. The maximum OD_{450nm} achieved during the fermentation was 5.6. PHAs were extracted at 48 hr and 65 hr during the stationary phase. The maximum PHA yield of 13.80 ± 2.82 %DCW was obtained during the early stationary phase at 48 hr.

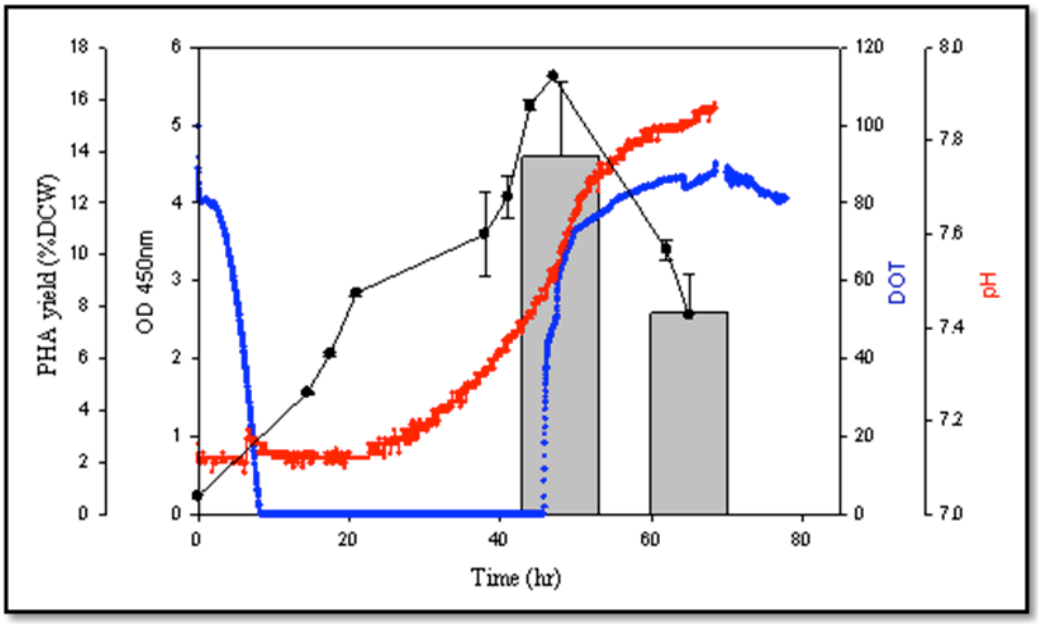

Figure 4. 12. Fermentation profile of *P. mendocina* and P(3HO) accumulation obtained in the 72 L bioreactor with an initial carbon/nitrogen ratio of 20:1 and pH of 7. 15, stirrer speed 143 rpm and air flow rate 0.5 vvm. OD_{450nm}(—) , pH (—), DOT (—) and PHA yield (grey bars).

4. 3. DISCUSSION

4. 3. 1. Optimization of P(3HO) production in *P. mendocina*

Studies were carried out to assess the effect of pH and carbon:nitrogen (C:N) ratio on the P(3HO) yield. Four conditions were studied (Table 2. 5): pH 7.15 and C:N 20:1 (condition 1), pH 7.5 and C:N 15:1 (condition 2), pH 6.8 and C:N 15:1 (condition 3) and pH 7.15 and C:N 10:1 (condition 4). From the comparison of the four conditions it was observed that the smallest lag phase and consequently a faster achievement of exponential phase occurred under condition 4, at pH 7.15 and C:N 10:1. It has been assumed that lag phase allows the adaptation required for bacterial cells to begin to grow under new environmental conditions (Madigan *et al*., 2000). The main reason for this observation might be that long chain fatty acids have been proven to have a toxic effect on bacterial growth and condition 4 represents the lowest amount of sodium octanoate (10mM), used as a carbon source (Dubos 1946). Additionally, we have observed that lower concentrations of sodium octanoate results in shorter exponential phases. For example, condition 4, containing the lowest amounts of sodium octanoate has the shortest exponential growth phase and condition 1, containing the highest amounts of sodium octanoate, the longest one. It is expected that the lower concentration of carbon source leads to shorter times of bacterial growth. By comparing conditions 2 and 3, we observed that pH values of 7.5 resulted in a smaller lag phase and consequently a quicker adaptation of the bacteria to the media than pH values of 6.8. However, similar durations of the exponential phase were obtained in both cases. Upon nutrient starvation or entry into the stationary phase, some bacteria develop different mechanisms that allow stress tolerance and starvation survival, including PHAs production (Ruiz *et al.,* 2001). PHAs were extracted in the four conditions at 24, 36 and 48 hr. As expected, our results show that the highest PHA accumulation occurred during the early stationary phase. By comparing condition 1 and 4, where only the C:N ratio differed, we observed that when the ratio C:N is increased from 10:1 to 20:1 the PHA yield (%DCW) increased from 2.3 to 20.6 %DCW. Also, by comparing condition 2 and 3, where only the pH differs, we can conclude that no significant differences in terms of PHA accumulation occurred when the pH varied from 6. 8 to 7. 5, suggesting that within this pH range there is no significant effect of pH on PHA production. The highest PHA accumulation of 20.6% DCW was observed under condition 1 at 36 hr, during the early stationary phase.

4. 3. 2. Scaling-up production of P(3HO) from *Pseudomonas mendocina*

With a product development there is a need to achieve successful scale-up strategies in order to convert laboratory results to industrial scale. Despite much research that has been carried out for the development of strategies to allow an efficient scale-up, no common strategies were described and hence, for each individual product, process and facility a suitable scale-up strategy has to be elaborated (Schmidt *et al.,* 2005). It is not possible to maintain all the parameters constant between scales and hence, different characteristics are suggested to be maintained constant during scale-up processes (Ju and Chase 1992). As oxygen transfer is often a limiting factor in aerobic bioprocesses due to the low solubility of this gas in the medium, the oxygen supply in bioreactors is a decisive factor in microorganism growth and plays a pivotal role in the scale-up of aerobic biosynthesis systems (Amaral *et al.* , 2008, Galaction *et al.* , 2004). As a result, one of the most common strategies used for scaling-up aerobic systems is based on maintaining the volumetric oxygen transfer, k_La, constant through the different scales (Puthli *et al*., 2005). The determination of k_La in bioreactors is essential in order to establish the aeration efficiency and to quantify the effects of the operating variables on the oxygen provision. In this project, the production of PHAs from *P. mendicina* was scaled-up from 2 L to 20 L and 72 L bioreactors based on a constant k_La. The k_La value was determined by employing the gassing out technique and the obtained value was kept constant upon scale-up to maintain similar mass-transfer of oxygen at the larger production scale. The chosen volumetric oxygen transfer coefficient was the one obtained with the 2 L bioreactor at 200 rpm stirrer speed and 1 vvm air flow rate. For this, as a first step, the k_La of the 2 L bioreactor, at 200 rpm and 1 vvm of air flow rate was determined from the slope of the ln(C*-C) vs. time. The k_La value obtained under this condition was 0.256. In order to find the condition in the 20 L and 72 L bioreactors that gave the same k_La, the k_La values for the 20 L and 72 L bioreactors were calculated at different set of impeller speeds and air flow rates. Due to the fact that the stirrer speed can be regulated with more precision, the aeration rate was kept constant and the estimation of the stirrer speed for a constant oxygen transfer in the 20 L and 72 L bioreactors was carried out from the extrapolation of the k_La vs. stirrer speed plot. As expected, an increment in the k_La values was observed with an increment in the stirrer speed or air flow supply for both 20 L and 72 L bioreactors. For the 20 L bioreactor, a k_La of 0.256 was among the values obtained at 0.5 vvm air flow rate. The stirrer speed was obtained from the linear regression of k_La vs. stirrer speed at 0.5 vvm. The obtained stirrer speed was 186 rpm. Note that although a k_La of 0.254 was

obtained at 200 rpm (Figure 4.7), a lower stirrer speed of 186 rpm was obtained for a k_La of 0.256 from the linear regression and this is due to the fact that the values did not follow a perfect linear trend. For the 72 L bioreactor, a k_La of 0.256 was close to the values obtained at 0.5 vvm air flow rate. The stirrer speed was obtained from the interpolation of k_La vs. stirrer speed at 0.5 vvm. The obtained stirrer speed was 143 rpm. The conditions obtained for a constant k_La in the 2 L, 20 L and 72 L bioreactors showed that bigger bioreactors supply more oxygen at the same stirrer speeds and air flow rates. The main reason of this observation is that bigger bioreactors require more power input to achieve the same air flow rate and, hence, more oxygen is supplied at a certain air flow rate. In this work, the k_La at different scales was determined experimentally and, hence, differences in the dimensions of the bioreactors, the aspect ratio, the ratio diameter bioreactor and the number of impellers and buffers are contemplated in the final k_La obtained for each bioreactor.

The conditions obtained for the scale-up work in the 2 L, 20 L and 72 L bioreactors were evaluated by the PHA yield obtained at different scales. From the profiles obtained we observed that the stationary phase, in which we expected the highest PHA production, was achieved at different times for the different bioreactors. Surprisingly, the stationary phase was achieved after around 27 hr of fermentation for the 2 L bioreactor, after 64 hr of fermentation for the 20 L bioreactor and after 46 hr of fermentation for the 72 L bioreactor. PHAs were extracted during the stationary phase for each of the different scales; hence, the extraction times were modified accordingly. The highest PHA yield was 26.84±0.35 % DCW for the 2 L bioreactor, 23.17±1.47 % DCW for the 20 L bioreactor and 13.80±2.82 % DCW for the 72 L bioreactor. Our results showed that similar values were obtained in terms of PHA yield with the 2 L and 20 L bioreactors, and hence we can conclude that based on a constant k_La it was possible to scale-up the PHA production from the 2 L to the 20 L bioreactor. However, the PHAs amount obtained for the 72 L bioreactor were considerably lower than the amount obtained with the 2 L and 20 L bioreactors. Our results showed that based on a constant k_La it was not possible to scale-up the PHA production to 72 L bioreactor. The reason of this observation is that by maintaining the k_La constant, other parameters such as the specific power input and the superficial air velocity will change and can thus produce undesired effects on the polymer yield (Ju and Chase 1992). The manipulation of specific power input and superficial air velocity should be also considered to scale-up from 2 L or 20 L to 72 L bioreactors.

CHAPTER 5

Characterization of P(3HO) for cardiac tissue engineering applications

5.1. INTRODUCTION

There is an increasing interest in the development of biomaterials for regenerative medicine and tissue engineering. Certain requisites are crucial for a successful material in cardiac tissue engineering applications. The material's physical and mechanical characteristics should be similar enough to those of the natural tissue in order to support the organ during the regeneration process, and its composition should allow it to degrade as the new tissue takes over its function (Neal *et al*., 2012). Biodegradable materials have attracted significant interest since further surgery is not required to remove the implanted material. Although most of the currently investigated materials are biodegradable, many of these have toxic by-products and poor mechanical properties that are not compatible with the injured tissue.

As a result of the enormous clinical need, myocardial tissue engineering has become a special area of focused research within the field of tissue engineering. In this project, medium chain length polyhydroxyalkanoates, mcl-PHAs, were studied as potential materials for cardiac tissue engineering. These biopolymers are promising materials for various applications due to their mechanical properties, biodegradability and biocompatibility.

In this chapter, P(3HO), a mcl-PHA, produced by *Pseudomonas mendocina,* was fully characterized and assessed for cardiac tissue engineering applications. As discussed previously, the material's mechanical properties are crucial for supporting the organ during the new tissue regeneration. In the first part of this chapter, the mechanical properties of P(3HO) were determined using dynamic mechanical analysis and the values obtained were compared with the values required by the native cardiac structures. The mechanical properties of the myocardium are as follows: Young's modulus 0.02-0.5 MPa, tensile strength 3-15KPa, and elongation at break between 100-300% (Nagueh *et al*., 2004, Watanabe *et al*., 2006). In order to define the processability of the material, the thermal properties of the material were determined by differential scanning calorimetric analysis. Surface roughness and wettability have been known to play a crucial role in cell adhesion and proliferation, hence, P(3HO) films were formed by the solvent casting method and the surface topography, roughness and water contact angle were determined using Scanning Electron Microscopy (SEM), white light interferometry and contact angle analysis, respectively.

An appropriate level of cardiomyocyte contraction is a crucial factor for a highly regulated mechanical system such as the heart, in order to maintain its accurate pumping function.

In vivo, cardiomyocytes' interaction with the extracellular matrix during contraction is the main factor in determining the heart's performance (Tracqui *et al*., 2008). In a preliminary study, the effect of the P(3HO) polymer on contracting cardiomyocytes was studied by seeding freshly isolated cardiomyocytes from rat on P(3HO) films and the viability of the cardiomyocytes was studied over time.

The change in cardiomyocyte contraction in response to a change in electrical stimulation is a general property of the cardiac muscle and in most species the contraction increases with the frequency of the electrical stimulation (Antoos *et al*., 2002). Intracellular Ca^{2+} is the central trigger factor for cardiomyocyte contraction and in most species, larger intracellular Ca^{2+}concentrations result in higher cardiomyocyte contraction (Knollmann *et al.*, 2008). In this project, the contraction of individual fresh adult rat cardiomyocytes on the P(3HO) polymer was studied at different frequencies of electrical pulses and calcium concentrations. For this, cardiomyocytes were seeded on glass cover slips coated with P(3HO) and glass cover slips without coating were used as positive controls.

Finally, in order to understand and compare the properties of P(3HO) with materials available in the market being used as basic cardiac patches, in the last part of the chapter we have characterized two types of biological membranes currently used as patches by surgeons, i.e. bovine pericardium and small intestinal submucosa (Pires *et al.,* 1999, Tan *et al*., 2009).

5.2. RESULTS

5.2.1. Characterization of P(3HO) from *Pseudomonas mendocina*

5.2.1.1. P(3HO) chemical characterization

P. mendocina was grown in shaken flask under nitrogen limiting conditions in MSM growth media. As a carbon source, sodium octanoate was used. The obtained polymer was extracted and the nature of the polymer was determined by FTIR, GC-MS and NMR. Figure 5.1 shows the obtained polymer.

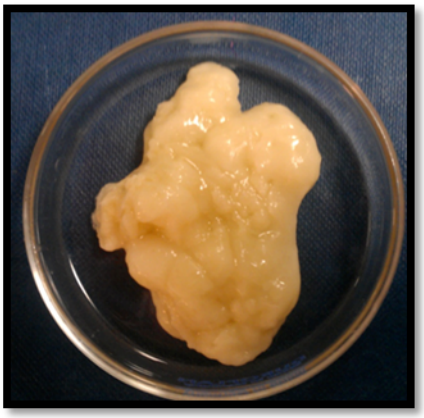

Figure 5.1. Polymer produced by *P. mendocina* with sodium octanoate as a sole carbon source.

FTIR analysis was carried out in order to determine the functional groups present in the obtained polymer, as described in section 2.2.8.1. Figure 5.2 represents the FTIR absorbance spectrum, which shows the presence of the characteristic ester band at 1728 cm^{-1}. The bands corresponding to O-H stretching groups from carboxylic acids and C-H stretching groups from alkyl side chains were observed at 2955 cm^{-1} and 2928 cm^{-1}, respectively. The bands at 1466 cm^{-1} and 1379 cm^{-1} occurred due to CH_3 stretching and the band at 1095 cm^{-1} describes the methylene C-H vibration. According to Ramalingan *et al.*, 2011, four bands are characteristic of mcl-PHAs: 1740, 2859, 2924 and 1069 cm^{-1}. The polymer FTIR spectrum showed the presence of bands in the range of these characteristic bands, suggesting that the PHA produced was indeed a mcl-PHA.

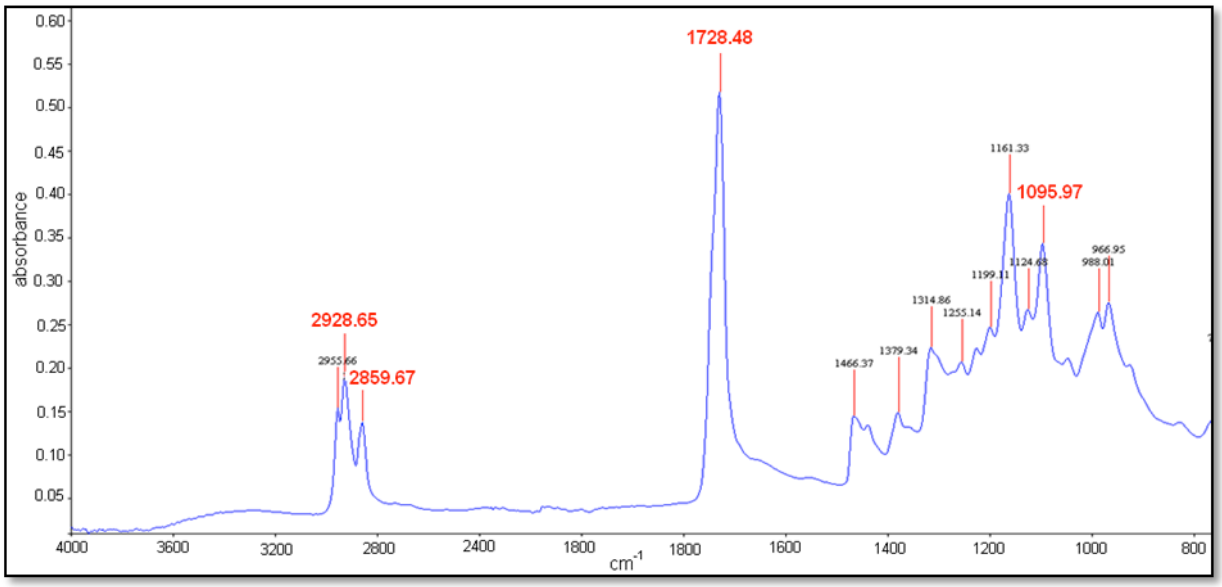

Figure 5.2. FTIR spectra of the polymer produced by *P. mendocina*. Note the four characteristic bands of mcl-PHAs highlighted in red.

In order to confirm the exact chemical nature of the sample, GC-MS and NMR were carried out as described in section 2.2.8.2 and 2.2.8.3, respectively. The GC-MS spectrum of the methanolysed polymer shows the presence of a main band with a retention time of 10.49-10.51 (Figure 5.3). The mass spectrum of the compound obtained at this retention time corresponded to the octanoic acid 3-hydroxy-methyl ester, confirming the presence of poly-(3-hydroxyoctanoate) homopolymer, P(3HO). The band obtained at a retention time of 9-9.8 belonged to the methyl ester of benzoic acid, used as a positive control. Peaks obtained at 9.83 and 15.13 corresponded to other ester forms of the P(3HO) and benzoic acid. Finally, other peaks at retention time 11.87 and 12.11 corresponded to impurities that had co-purified with the polymer.

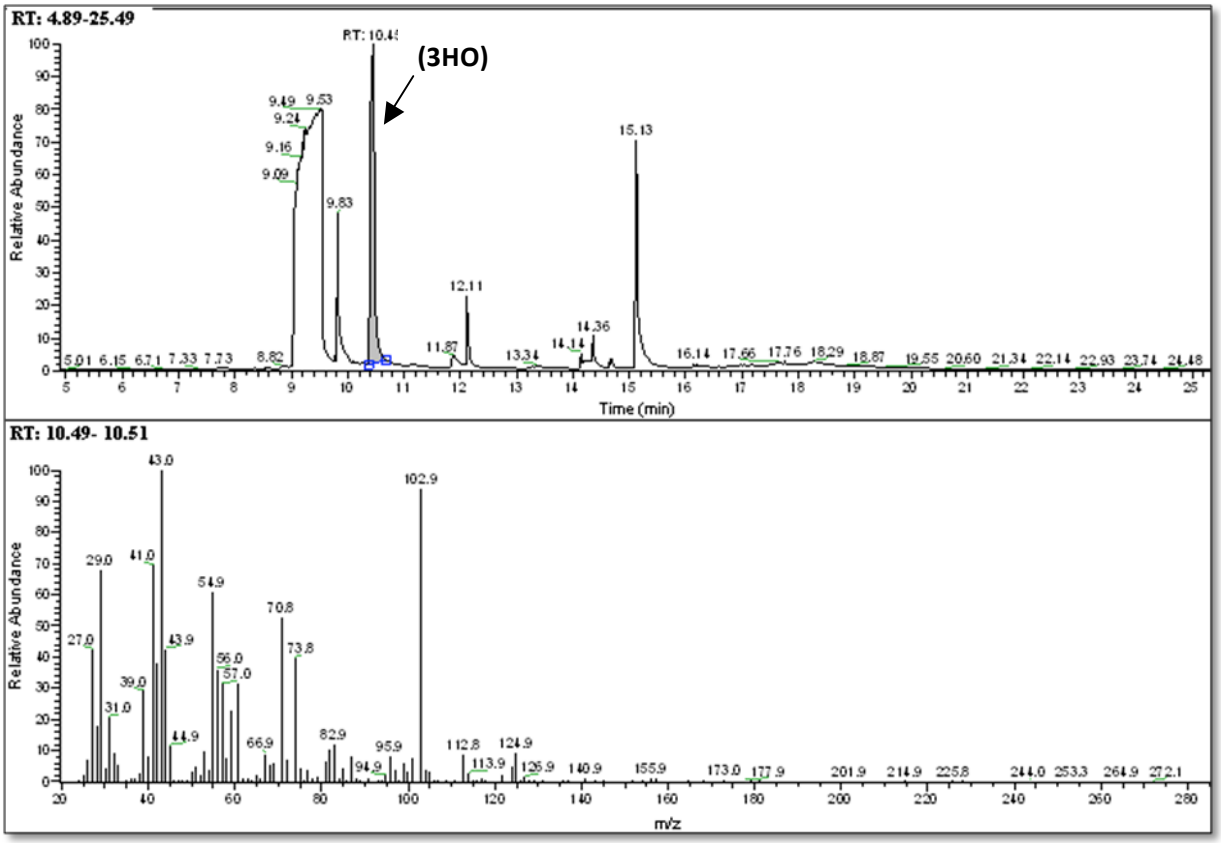

Figure 5.3. GC-MS spectra of the polymer produced from *P. mendocina*. Note the presence of a peak at RT: 10.49-10.51 and the corresponding mass spectra for P(3HO) (the peak obtained at RT: 9-9.8 correspond to methylbenzoate used as the internal control).

Figure 5.4 shows the (A) ^{13}C and (B) ^{1}H NMR spectra. The ^{13}C spectra showed the presence of nine main peaks corresponding to the eight different carbon environments of P(3HO) plus one at 77.15 ppm corresponding to the carbon present in $CDCl_3$ used as solvent. The eight peaks that belong to the P(3HO) molecule are: 169.56, 70.94, 39.17, 33.84, 31.61, 25.17, 22.60 and 13.91. These peaks correspond to the different carbon atoms present from the carboxylic group of the P(3HO) molecule to the last carbon present in the alkyl group of the side chain. The proton spectra showed the presence of five main peaks that correspond to the five different types of protons in the P(3HO) molecule. The five peaks obtained were: 5.17, 2.50, 1.56, 1.27 and 0.82 ppm. The first two peaks correspond to the protons present in the -CH groups and $-CH_2$ groups of the main carbon chain. The last three peaks are from the different types of protons of the alkyl group in the side chain, starting from the first $-CH_2$ group bonded to main carbon chain and following to the $-CH_2$ and $-CH_3$ groups present in the side chain.

(A)

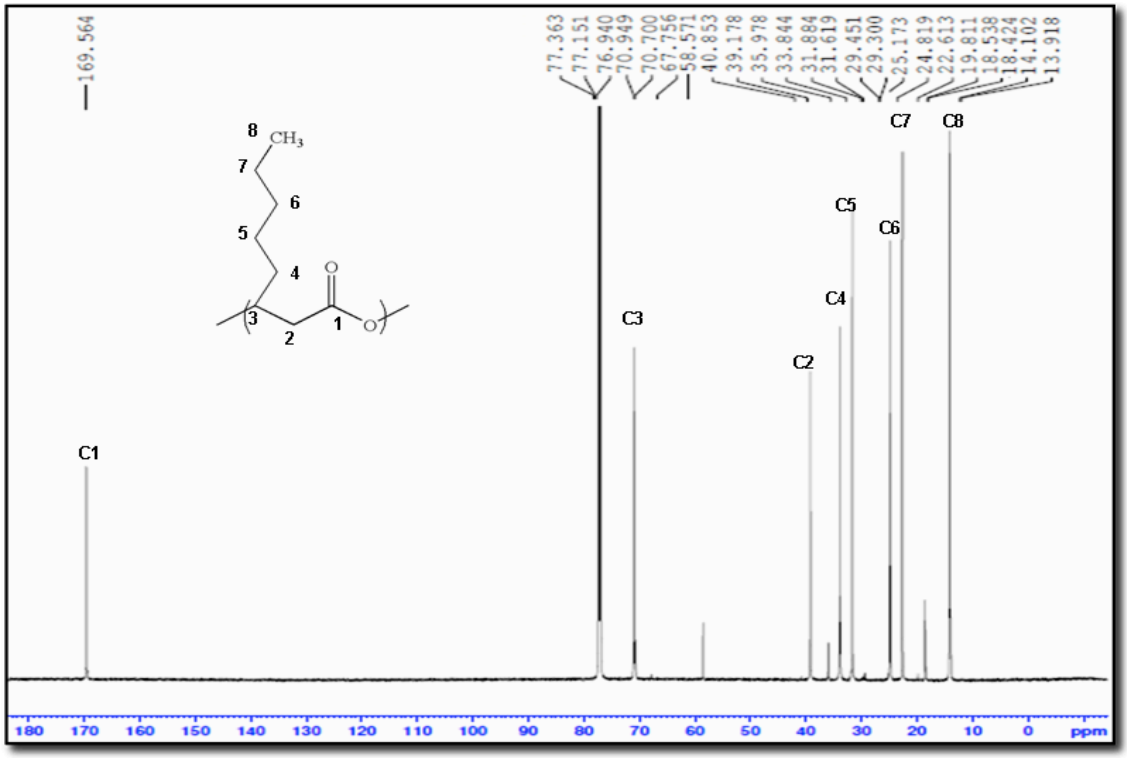

(B)

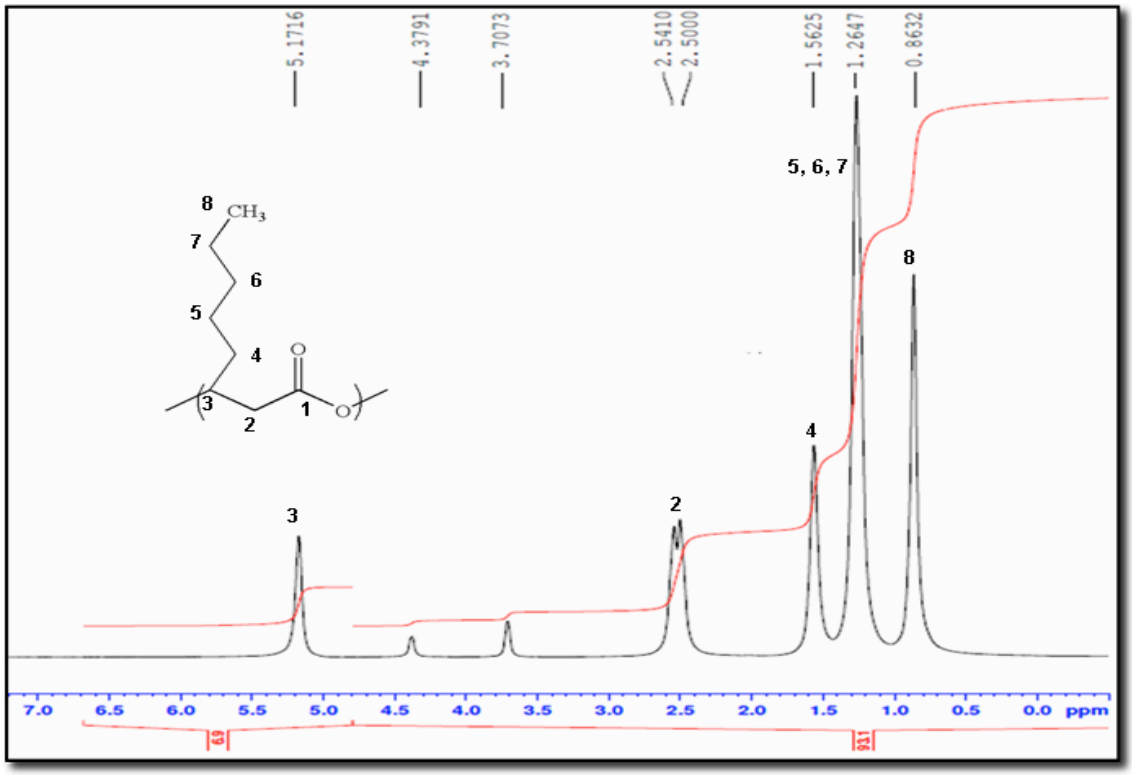

Figure 5.4. (A) ^{13}C and (B) ^{1}H NMR spectra for the polymer produced by *P. mendocina***.** The chemical structure of the P(3HO) molecule indicating the position of the different environments for Carbon or Proton atoms in the molecule is shown in the figures.

5.2.1.2. P(3HO) mechanical and thermal characterization

P(3HO) films were fabricated by solvent casting as described in section 2.2.9.1 and characterized in terms of the mechanical and thermal properties as described in section 2.2.10.1 and 2.2.10.2, respectively. The mechanical properties were determined by dynamic mechanical analysis. Results are represented in a static strain vs. stress plot (Figure 5.5). The initial slope of the plot corresponds to the Young's modulus and the obtained value was 3.7±0.3 MPa. The % elongation at break and the tensile strength, obtained at the maximum elongation before the material is broken was 299±29 % and 3.4±0.2 MPa, respectively.

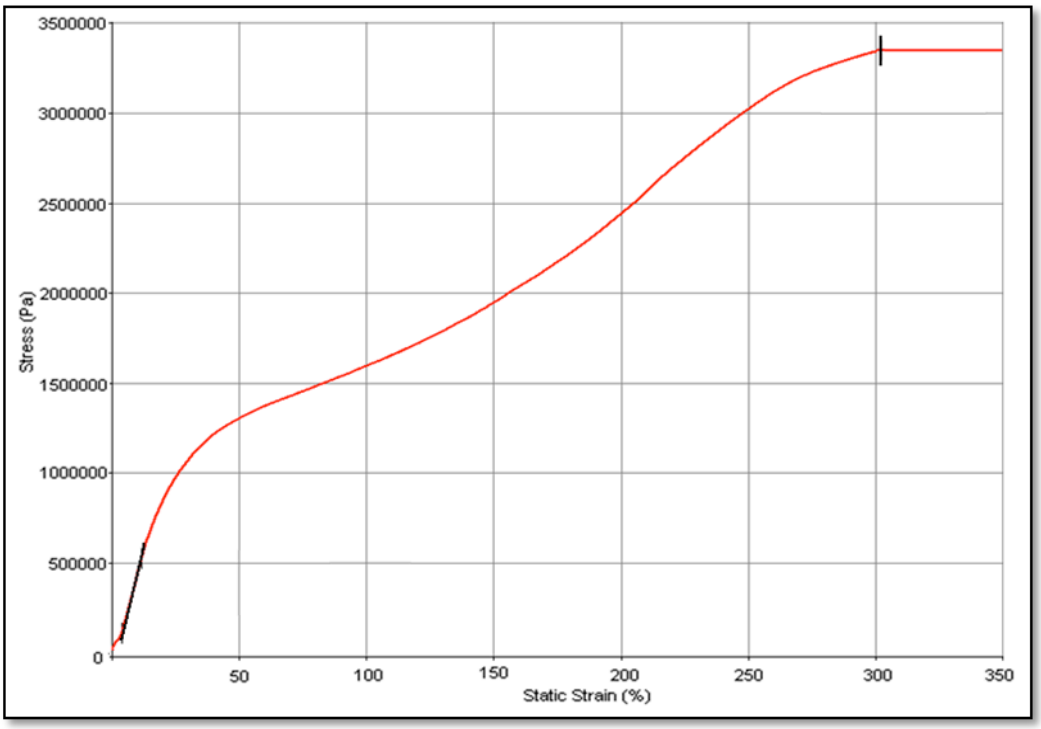

Figure 5.5. Static strain vs. Stress profile of the P(3HO) polymer. The initial slope and the maximum elongation are indicated with a black line.

The thermal properties of the material were determined by the differential scanning calorimetry analysis. The thermograms show the presence of two peaks corresponding to the melting temperature and glass transition temperature (Figure 5.6). The melting temperature obtained was 43.7±4.1 ºC and the glass transition temperature was -32.9±3.8 ºC.

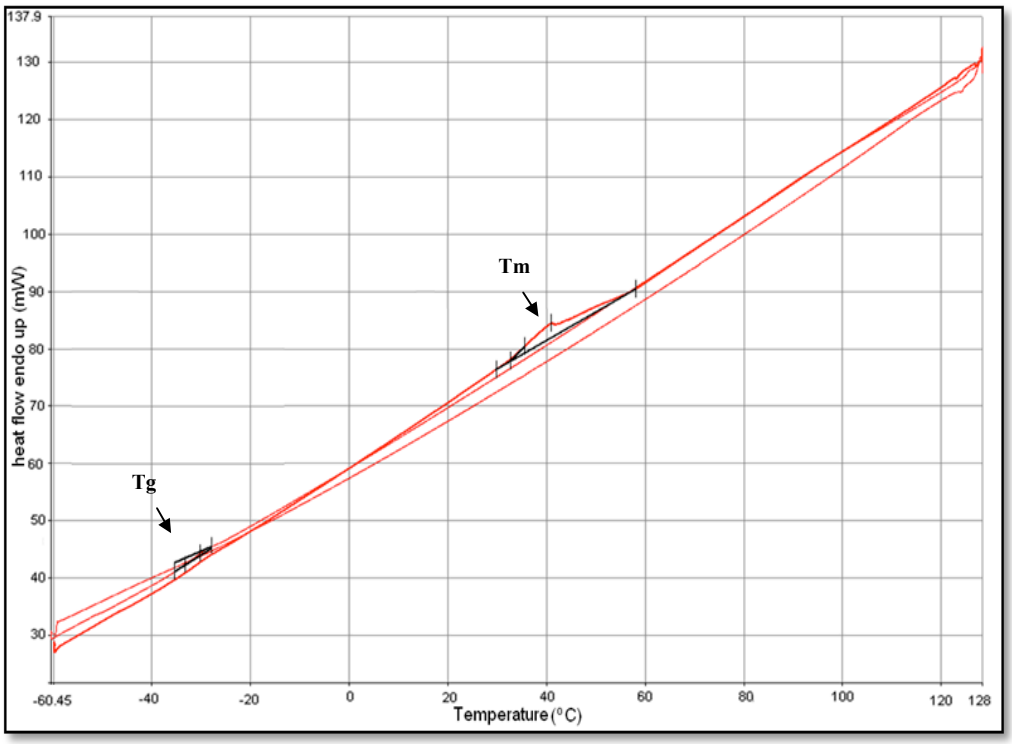

Figure 5.6. Thermal profile of the P(3HO) polymer. The peaks corresponding to the T_g and T_m are indicated with arrows.

5.2.1.3. P(3HO) surface characterization

In order to analyze the surface structure of the P(3HO) polymer, P(3HO) films were created by the solvent casting technology. The surface wettability of the P(3HO) films was studied with a contact angle meter as described in section 2.2.10.3. The water contact angle on the P(3HO) films was 101.1±0.8 º, indicating a hydrophobic surface. The surface roughness of the P(3HO) film was determined using white light interferometry, as described in section 2.2.10.5. Results showed that the average surface roughness of the P(3HO) film was 0.17 µm (Figure 5.7). Finally, the surface morphology and microstructure of the P(3HO) films was studied using scanning electron microscopy, as described in section 2.2.10.4. Figure 5.8 shows the smooth surface properties obtained.

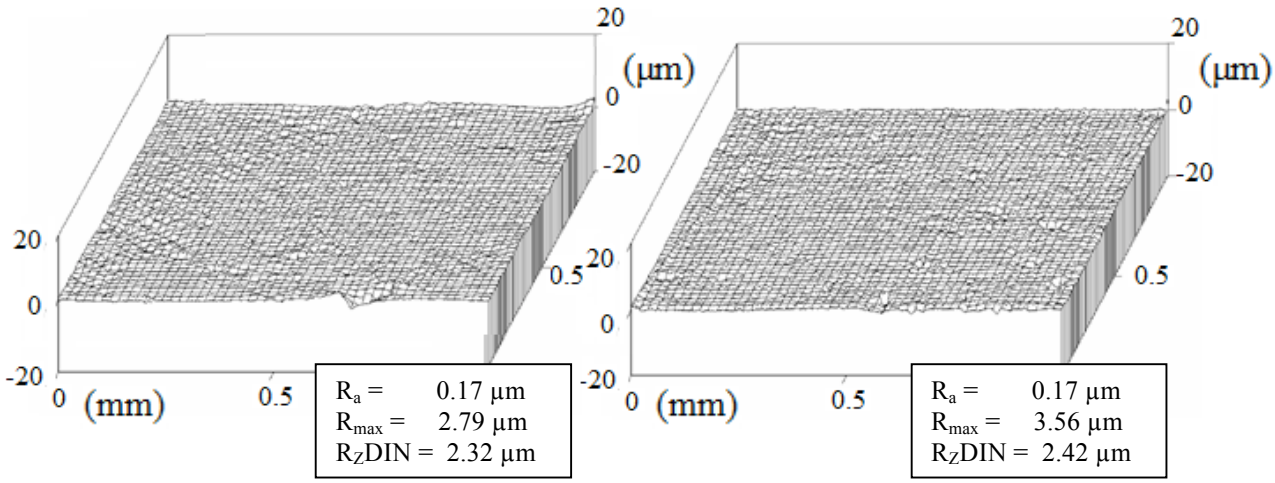

Figure 5.7. Surface roughness analysis of two typical P(3HO) films. R_a describes the average surface roughness, R_{max} the maximum roughness depth, R_ZDIN is the average peak to valley height minus R_{tm} and R_{tm} is the average distance between the highest peak and lowest valley in each sample.

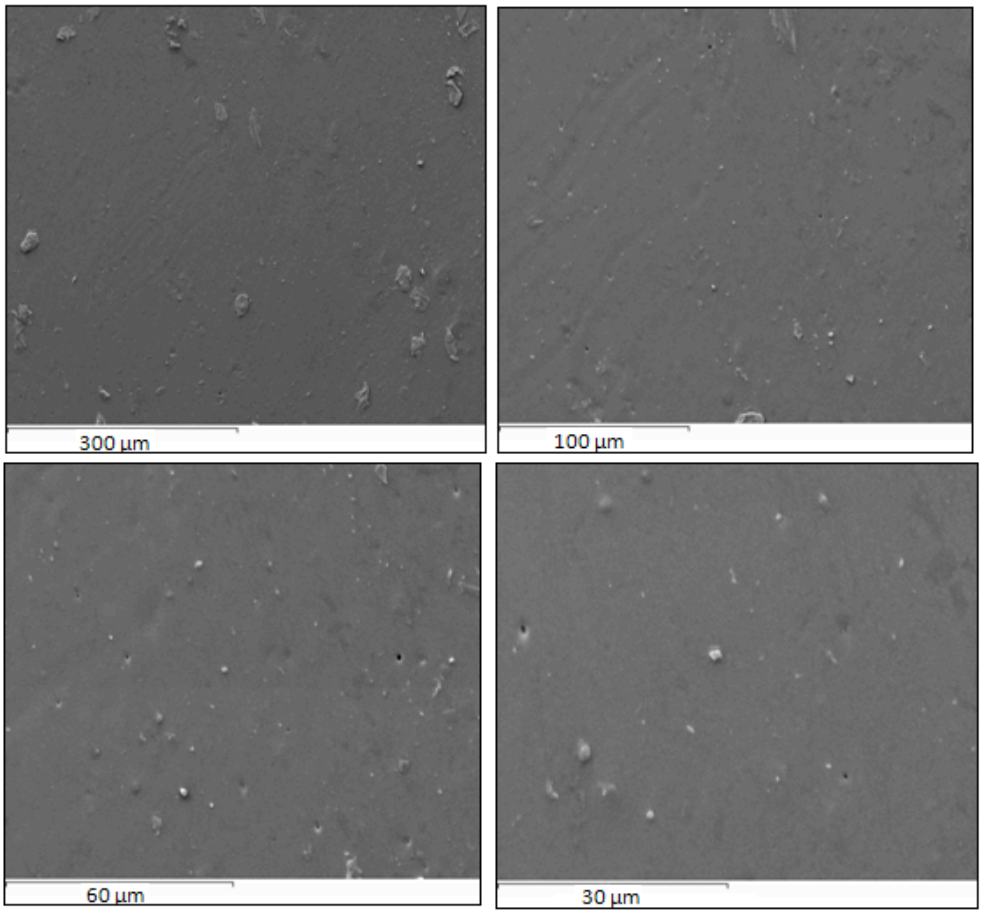

Figure 5.8. SEM images obtained from P(3HO) films showing the smooth surface of the films at different magnifications.

5.2.1.4. *In vitro* cytocompatibility studies

5.2.1.4.1. Cardiomyocyte viability on P(3HO) films

In a preliminary study, the effect of the P(3HO) polymer on cardiomyocyte viability was studied. Fresh isolated adult rat cardiomyocytes were seeded on the P(3HO) films as described in section 2.2.11.1. Based on the shape, the number of live and dead cells were determined with an inverted microscope at the following times after seeding: 0, 1, 2, 24, 25 and 26 hours. Figure 5.9 shows the rod shape of a live cardiomyocyte vs. the round shape of dead cardiomyocytes. As a positive control, cardiomyocytes were seeded on plastic tissue culture plates.

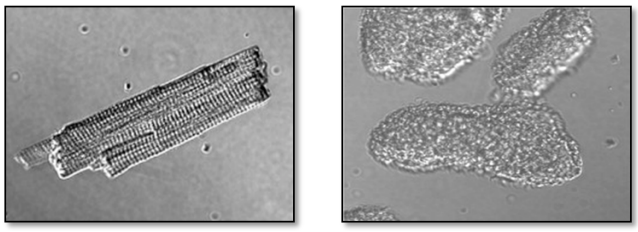

Figure 5.9. Live vs. dead cardiomyocytes. The picture on the left shows a live cardiomyocyte and the picture on the right shows dead cardiomyocytes (Gonzalez-Granillo *et al*., 2012).

The ratios of live/dead cells at the different time points are illustrated in Figure 5.10. These results show a significant slightly higher viability on the polymer than in the control at 0, 2, 25 and 26 hr .

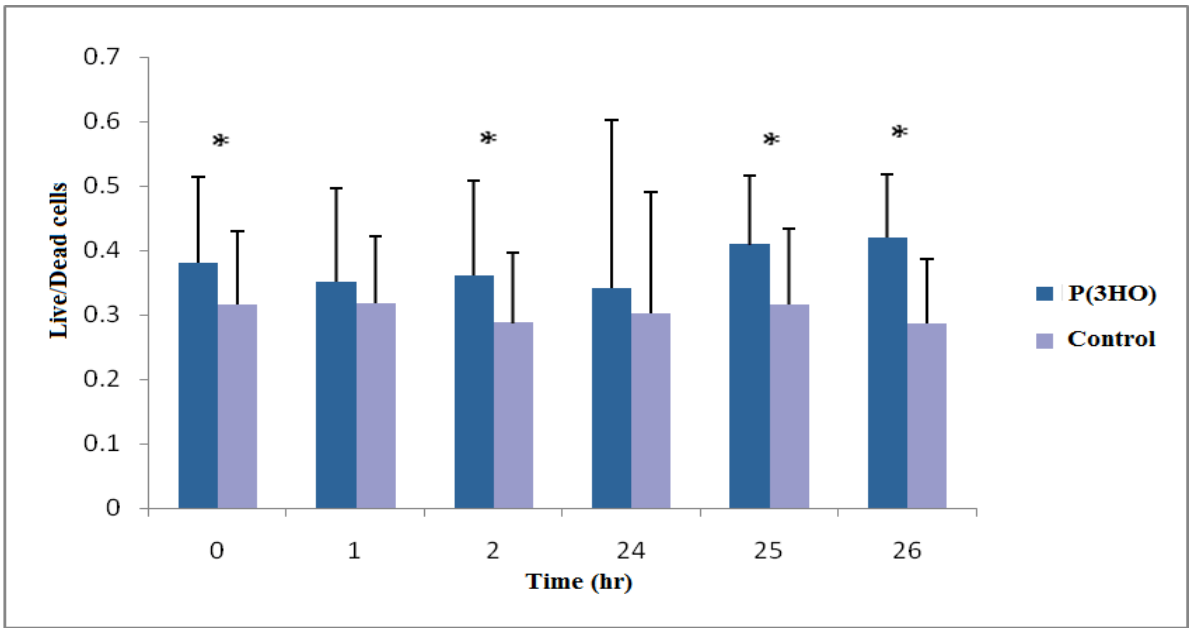

Figure 5.10. Live/dead rat cardiomyocytes seeded on the P(3HO) film vs. control at 0, 1, 2, 24, 25, 26 hours (n=6; error bars=±SD).

5.2.1.4.2. Cardiomyocytes' contraction on P(3HO) films

The effect of the P(3HO) polymer on the contraction of the cardiomyocytes was studied. Fresh isolated adult rat cardiomyocytes were seeded on P(3HO) coated cover slips and superfused in a Krebs-Henseleit solution at 37°C and bubbled with 95% O_2, 5% CO_2 as described in section 2.2.11.2. Cover slips without coating were used as controls. For the study, rod shaped cardiomyocytes with regular and no spontaneous contraction without stimulation were selected. Cells were stimulated with pulses of 50 V for a period of 2ms with 2 seconds intervals. The contraction amplitude (% shortening), 'time to peak 90%' and time to 'relaxation 50%' were recorded with a video and analyzed with the Inoptix program.

5.2.1.4.3. Effect on cardiomyocyte contraction at different intervals of electrical impulses

The effect on cardiomyocyte contraction at a range of electrical impulse frequencies was analyzed. Cells were stimulated with pulses of 50 V for during 2 ms at the following time intervals: 2, 5, 2, 1 and 0.5 seconds. Figure 5.11 shows the profile of one representative experiment obtained.

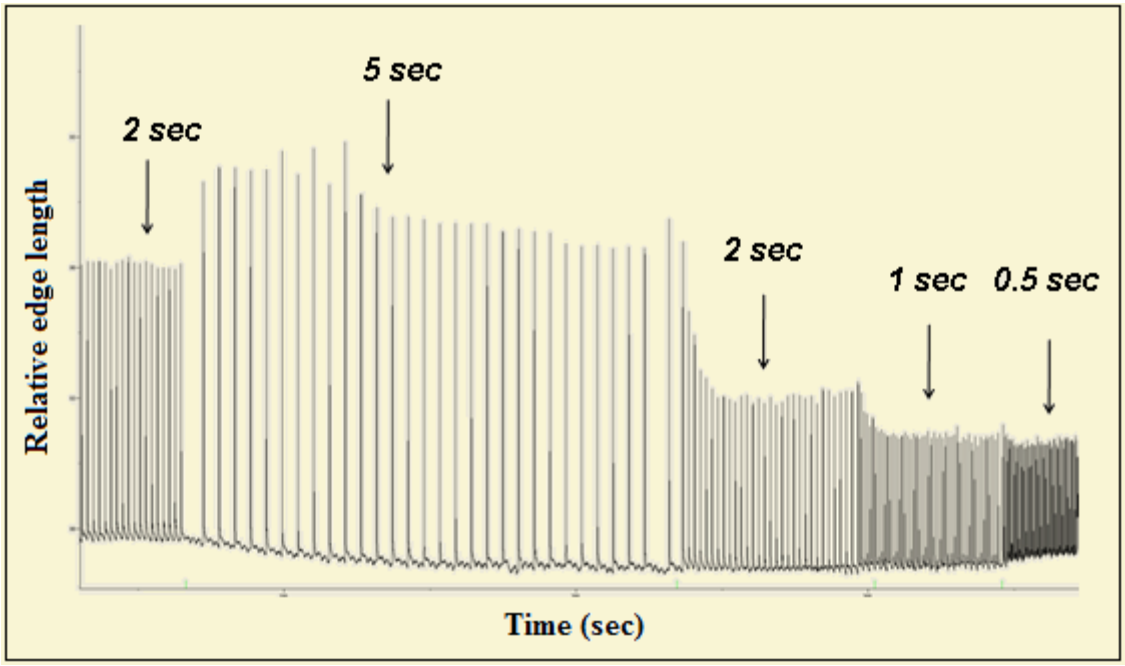

Figure 5.11. Effect of 50 V pulses for 2 ms at 2, 5, 2, 1 and 0.5 seconds intervals on cardiomyocyte contraction.

Figure 5.12 and 5.13 show the effect of 50 V electrical pulses for 2 ms at 2, 5, 2, 1 and 0.5 second intervals on the 'time to peak 90%' and 'time to baseline 50%', on the P(3HO) polymer, respectively. Results show differences when the frequency of electrical pulses increases from 5 to 0.5 seconds, where the time to peak 90% decreases in both polymer and control (Figure 5.12). Additionally, differences were significant only in control when the intervals of electrical pulses decreased from 5 to 2, 1 and 0.5 seconds (Figure 5.13).

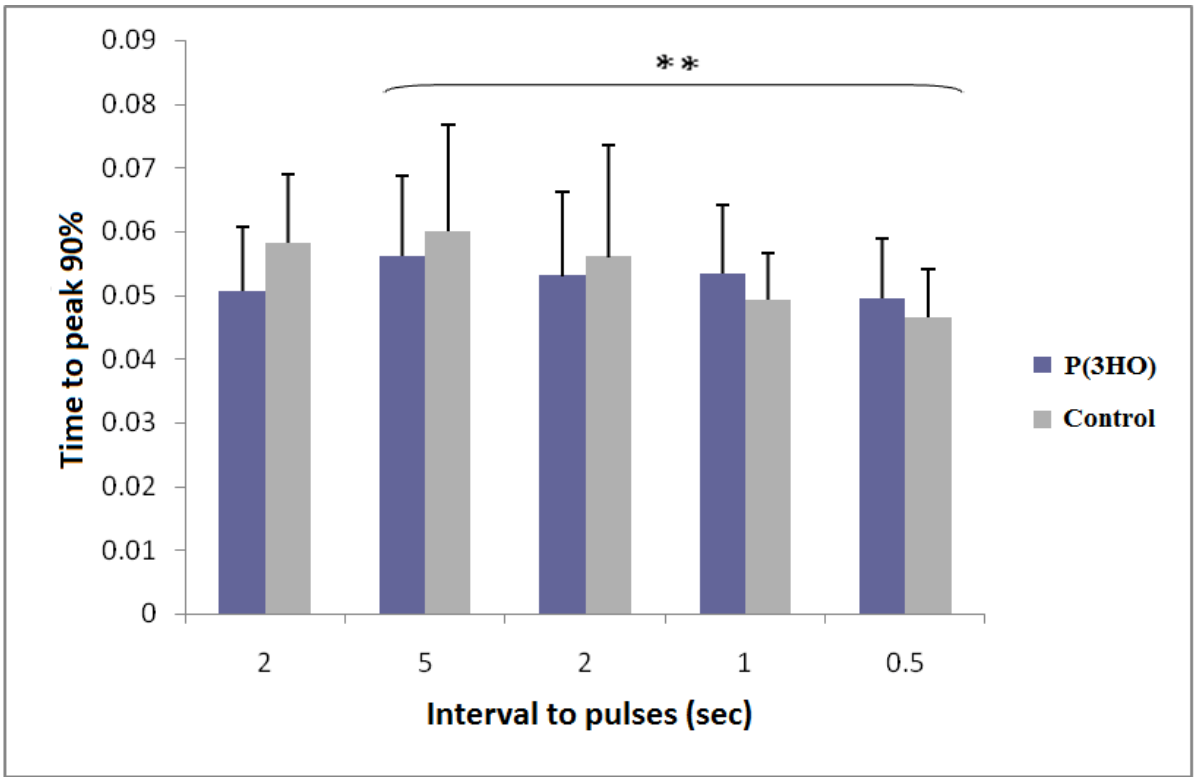

Figure 5.12. Effect of 50 V pulses for 2ms at 2, 5, 2, 1 and 0.5 seconds intervals on the 'time to 90% peak' of rat cardiomyocytes for cardiomyocytes contraction on P(3HO) polymer and control glass slides (n=5; error bars=±SD). The data were compared using the *t*-test and the differences were considered significant when $^{**}p < 0.01$.

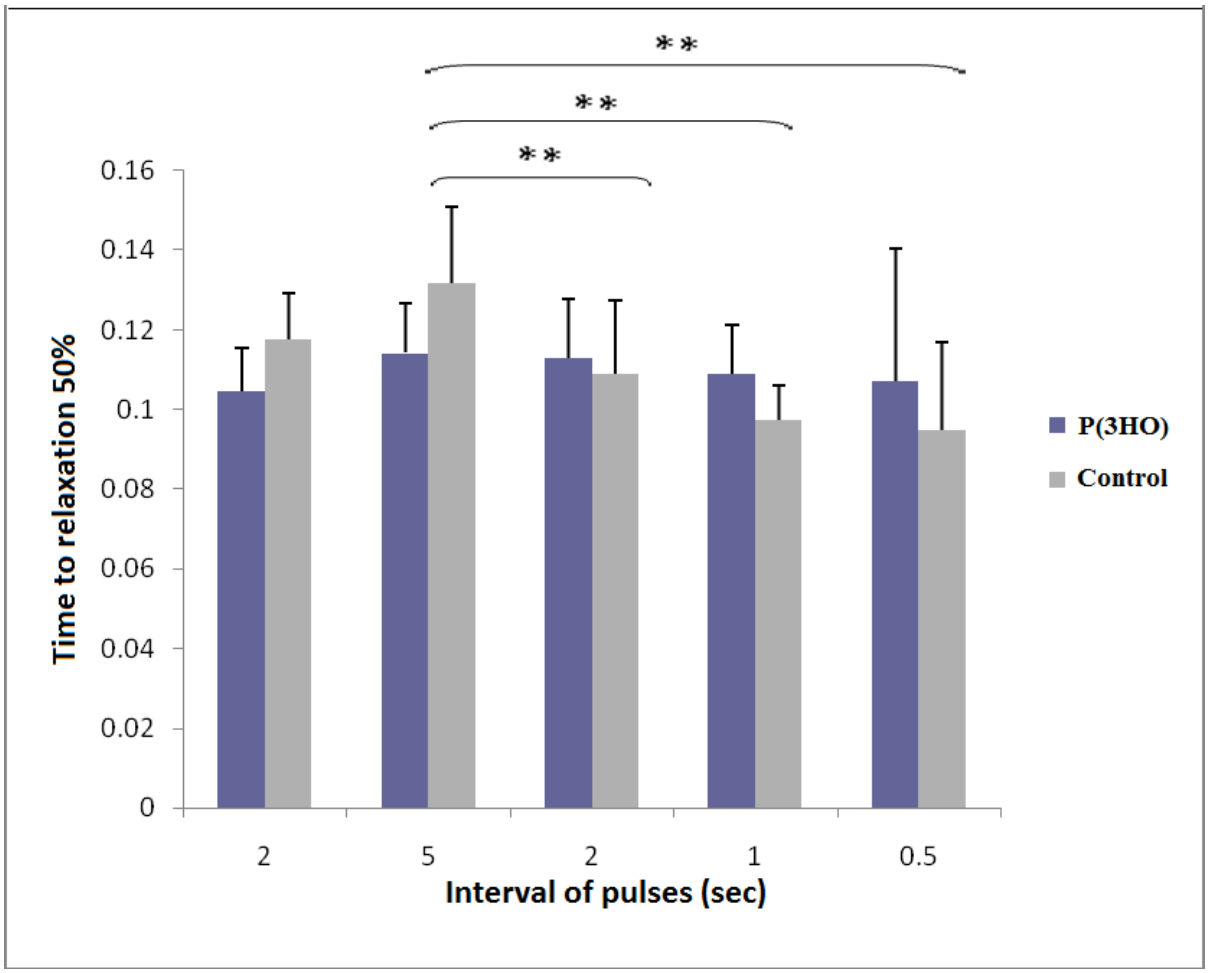

Figure 5.13. Effect of 50 V pulses for 2m at 2, 5, 2, 1 and 0.5 seconds intervals on time from peak to 50% relaxation of rat cardiomyocytes on P(3HO) polymer and control glass slides (n=5; error bars=±SD). The data were compared using the *t*-test and the differences were considered significant when $^{**}p < 0.01$.

Figure 5.14 shows the effect on cardiomyocyte contraction (% shortening) of electrical pulses of 50 V for 2 ms at 2, 5, 2, 1 and 0.5 seconds interval on P(3HO) polymer. The data was normalized against 2 second interval pulses. Results show that no differences were observed between the cardiomyocyte on the control and polymer. Only when the frequency of electrical pulses was increased from 5 to 2, 1 and 0.5 seconds, the percentage of shortening decreased significantly in the control but not in the polymer.

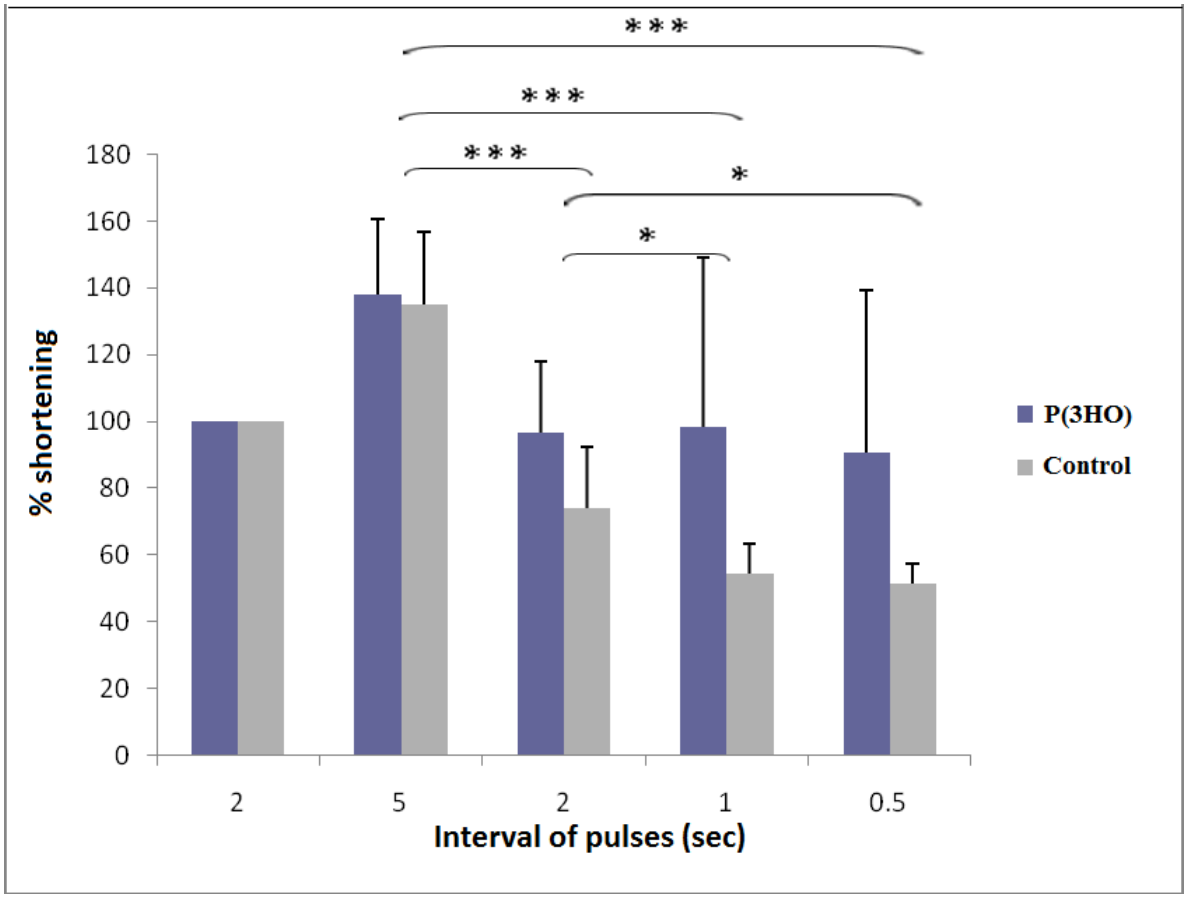

Figure 5.14. Normalized contraction amplitude (% shortening) of rat cardiomyocytes on P(3HO) polymer with electrical pulses of 50 V for 2 ms at 2, 5, 2, 1 and 0.5 seconds intervals (n=5; error bars=±SD).The data was normalized against 2 seconds interval pulses and compared using the *t*-test and the differences were considered significant when $*p < 0.01$, $***p < 0.001$.

5.2.1.4.4. Effect on cardiomyocyte contraction at different calcium concentrations

In this section, the effect of calcium concentration on cardiomyocyte contraction was studied. For this, the calcium concentration in the Krebs-Henseleit solution was increased from 1 to 2, 3 and 4 mM. The experiments were carried out as described in section 2.2.11.2. Figure 5.15 shows the profile of one representative experiment.

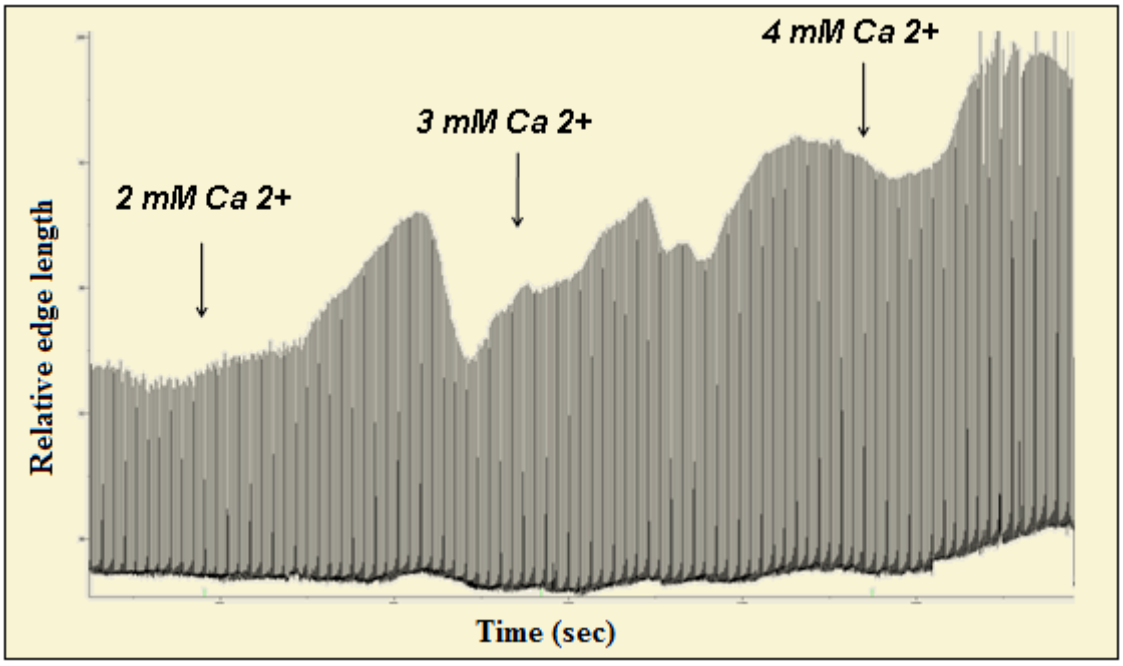

Figure 5.15. Effect of calcium concentration on cardiomyocyte contraction (the calcium concentration of the Krebs-Henseleit solution was increased from 1 to 2, 3 and 4 mM).

Figure 5.16 and 5.17 shows the effect on 'time to peak 90%' and 'time to baseline 50%' of the cardiomyocytes on the P(3HO) polymer, when the calcium concentration in the Krebs-Henseleit solution was increased from 1 to 2, 3 and 4 mM, respectively. Results show that no differences were observed between the data obtained for the polymer and control at different calcium concentrations. An increment in the 'time to baseline 50%' was observed in the control but not in the polymer when the calcium concentration was increased from 2 to 3 and 4 mM.

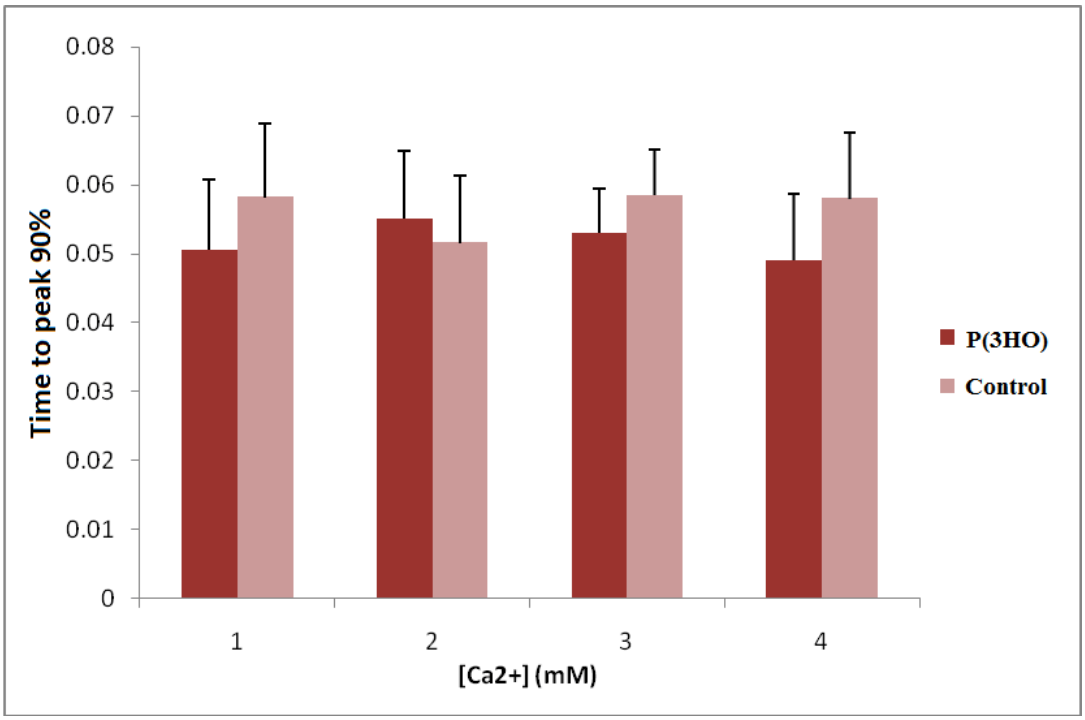

Figure 5.16. Response on cardiomyocyte beat duration, 'time to peak 90%', to an increment in Ca^{2+} concentration from 1 to 2, 3 and 4 mM on P(3HO) films (n=5; error bars=±SD). The data were compared using *t*-test.

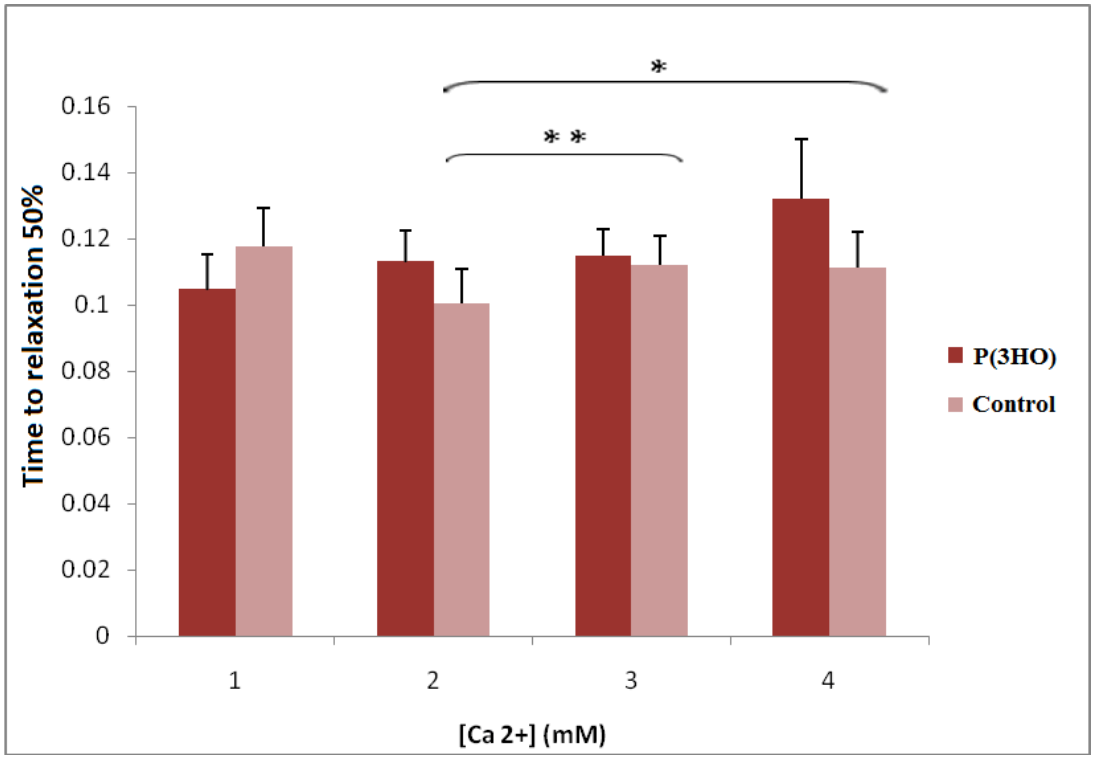

Figure 5.17. Response on cardiomyocyte beat duration 'time from peak to 50% relaxation' to an increment in Ca^{2+} concentration from 1 to 2, 3 and 4 mM on P(3HO) films (n=5; error

bars=±SD). The data were compared using the *t*-test and the differences were considered significant when $*p < 0.05$, $**p < 0.01$.

Figure 5.18 shows the effect on cardiomyocyte contraction (% shortening) at 1, 2, 3 and 4 mM calcium when grown on P(3HO) polymer. Data were normalized against 1 mM calcium. The results showed that no differences were observed between the control and polymer. A slightly higher response in the % of shortening is observed when the calcium concentration is increased from 1 to 2 and 3 mM in the polymer.

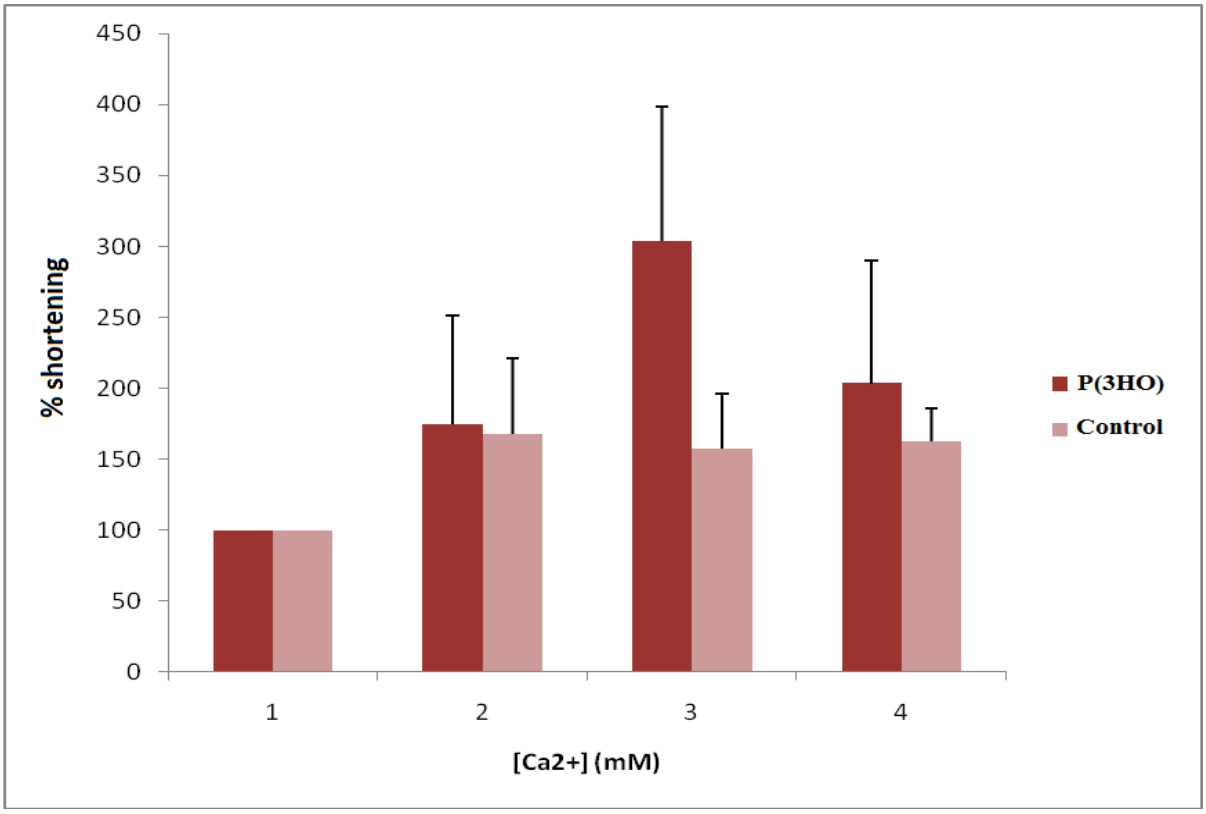

Figure 5.18. Normalized contraction amplitude (% shortening) of rat cardiomyocytes on P(3HO) polymer at different calcium concentrations (n=5; error bars=±SD). The data were normalized against 1 mM calcium and compared using *t*-test.

5.2.2. P(3HO), SIS and pericardium

The SIS and pericardium were characterized in terms of mechanical properties, thermal properties, wettability, protein adsorption and surface roughness. The SIS and pericardium properties were then compared with the properties of P(3HO). Mechanical properties were determined using Dynamic Mechanical Analysis as described in section 2.2.10.1. The pericardium and SIS mechanical profile are represented in a static strain vs. stress plot shown in Figure 5.19 and Figure 5.20, respectively. The initial slope of the plot corresponds to the Young's modulus and the obtained value was 0.4 ±0.1 MPa and 329.9±2.2 MPa for the pericardium and SIS, respectively. Section 5.2.1.2. shows that the P(3HO) Young's modulus was 3.7±0.3 MPa. These results indicate that P(3HO) stiffness is more similar to the pericardium than SIS. In the case of the pericardium the tensile strength was 6.33 MPa and elongation at break 114.5%. For SIS the obtained tensile strength was 10.5 MPa and elongation at break 10%. The tensile strength and elongation at break for P(3HO) was 3.4±0.2 MPa and 299±29 %, respectively. Comparison of the values showed that P(3HO) had the lowest tensile strength and the highest elongation at break and is hence a rather soft and flexible polymer.

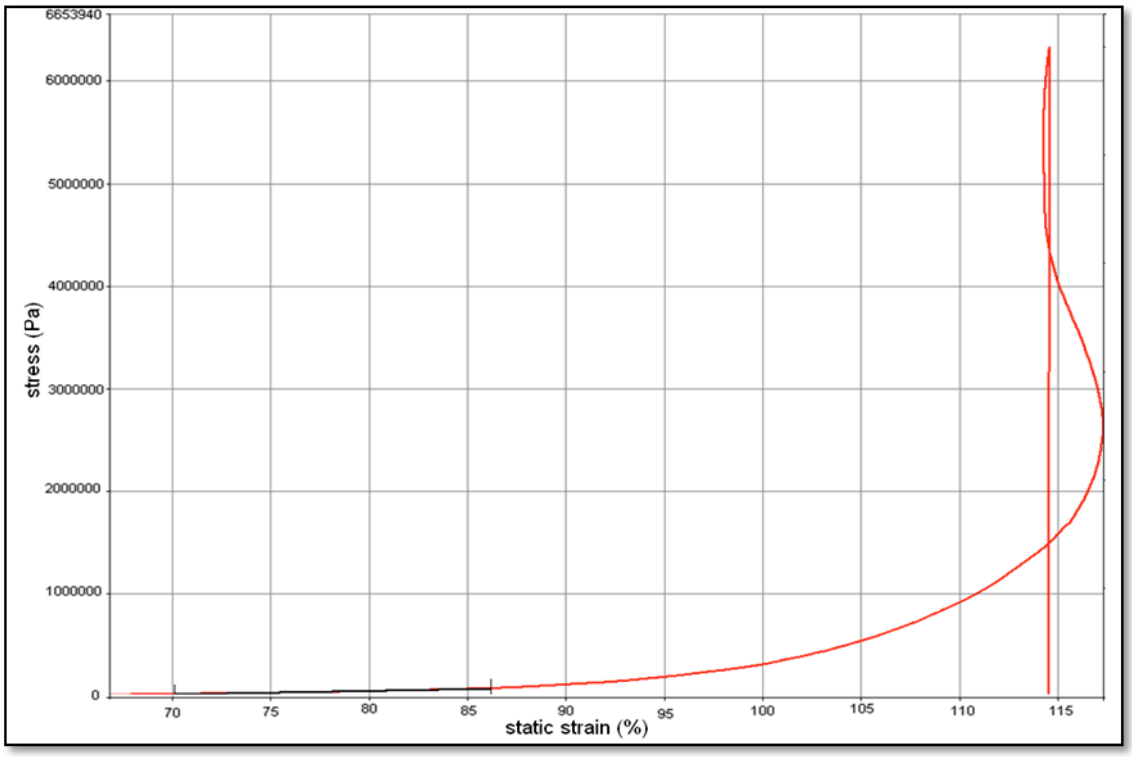

Figure 5.19. Static strain vs. stress profile of pericardium.

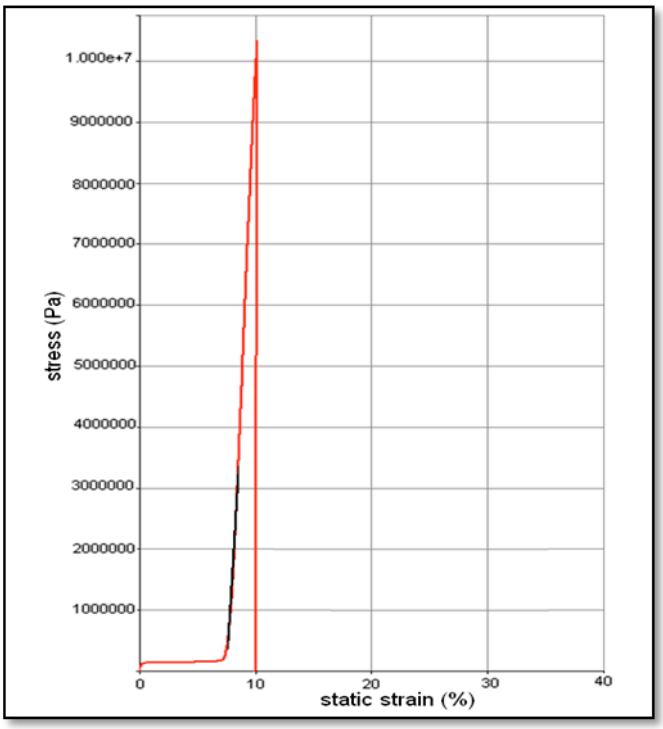

Figure 5.20. Static strain vs. stress profile of SIS

The thermal properties of the two biological membranes were studied by Differential Scanning Calorimetry, as described in section 2.2.10.2. Figure 5.21 and 5.22 show the thermal profiles obtained for the pericardium and SIS, respectively. As collagen is the main constituent of both membranes, the thermograms showed a typical denaturation peak starting at 70 ºC, which corresponds to the collagen denaturation temperature as found in literature (Samouillan *et al.,* 2011). The peak observed at 5 ºC for the pericardium belongs to the solvent in which the tissue was preserved. As described in section 5.2.1.2, P(3HO) showed a melting temperature of 43.7±4.1 ºC, indicating a lower processability of the polymer respect to the two biological tissues.

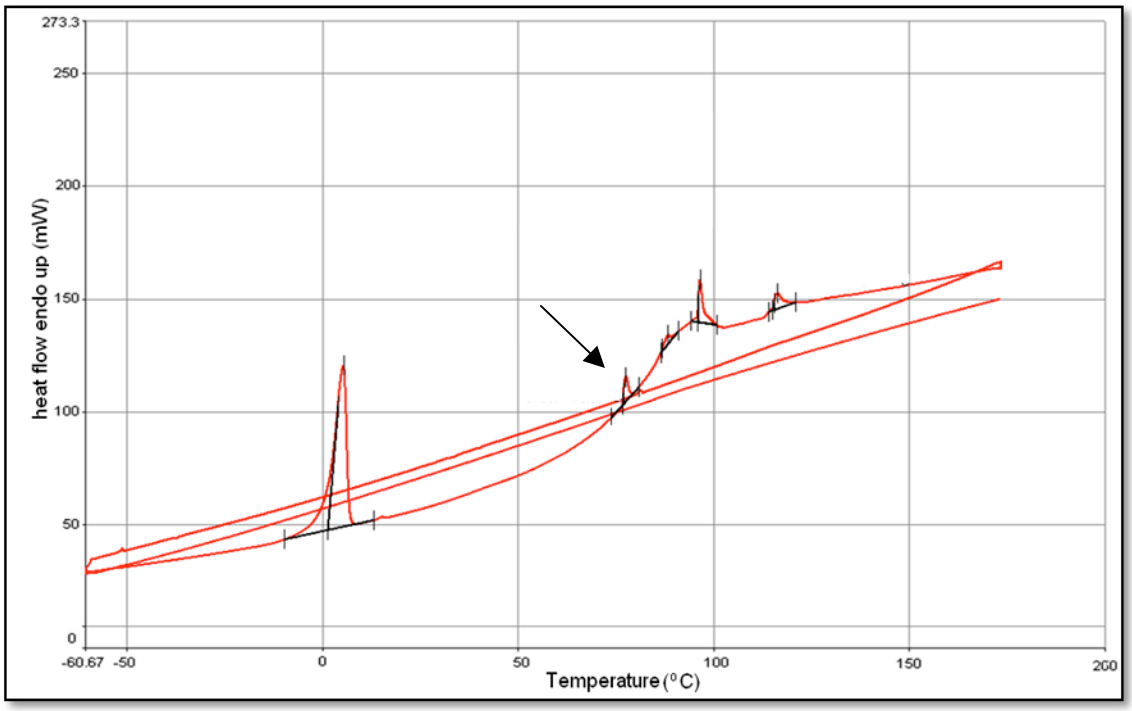

Figure 5.21. Thermal profile of the pericardium. The arrow shows the typical denaturation peak starting at 70 ºC. The first peak observed at 5 ºC corresponds to the solvent used to preserve the tissue.

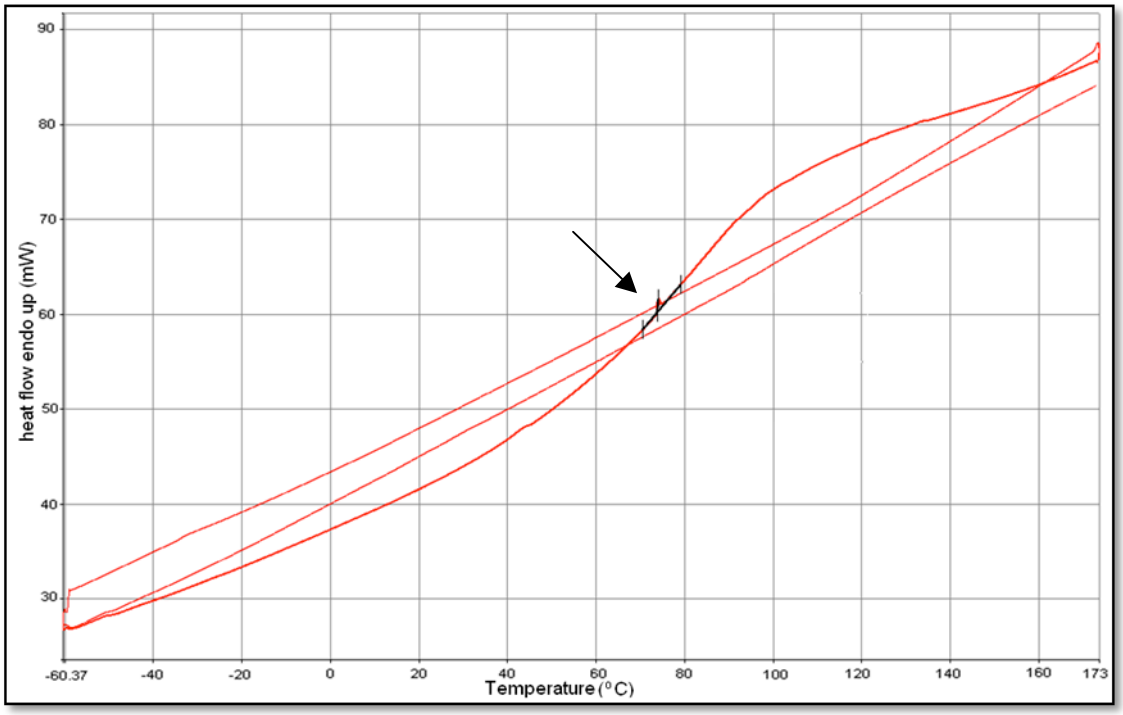

Figure 5.22. Thermal profile of SIS. The arrow shows the presence of one main peak starting at 70 ºC which shows the denaturation of the membrane.

Wettability studies were carried out with a contact angle meter as described in section 2.2.10.3. The contact angle obtained for the pericardium was 41.6±9.6 º and for SIS was 96.2±6.6 º. These results show that the pericardium surface is hydrophilic, while SIS surface is hydrophobic. The P(3HO) water contact angle was 101.1±0.8 º, hence, the P(3HO) wettability is similar to that of SIS. The thicknesses of both biological membranes and the 5 wt% P(3HO) were measured and results were as follows: P(3HO) 0.18 mm, SIS 0.16 mm and pericardium 0.58 mm. Hence, the thickness of the P(3HO) film used in this study was similar to SIS and less than that of the pericardium. Surface roughness analysis was carried out by SEM and white light interferometry as described in section 2.2.10.4 and 2.2.10.5, respectively. Figure 5.23 shows the SEM images for pericardium. These pictures reveal an uneven surface. Figure 5.24 shows the SEM images obtained for SIS. In these pictures it is possible to recognize the presence of some cells and veins that were not removed from the membrane which would increase the roughness of the surface.

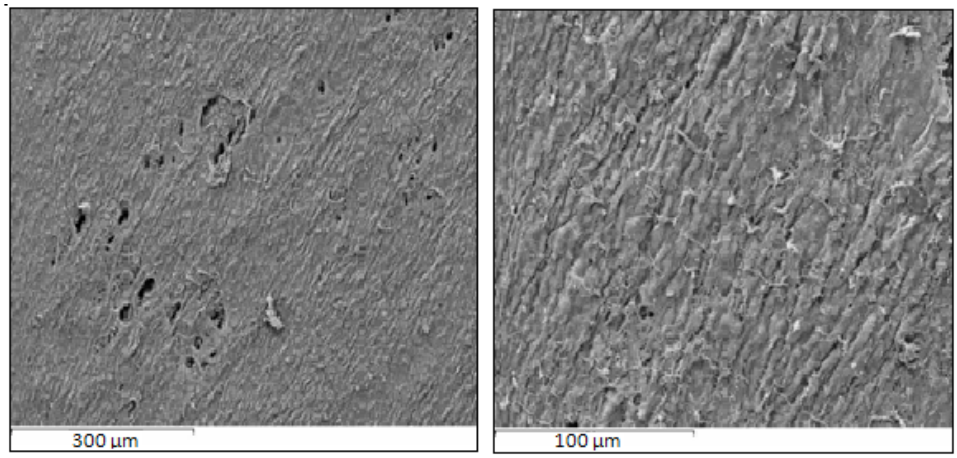

Figure 5.23. SEM images of pericardium at different magnifications.

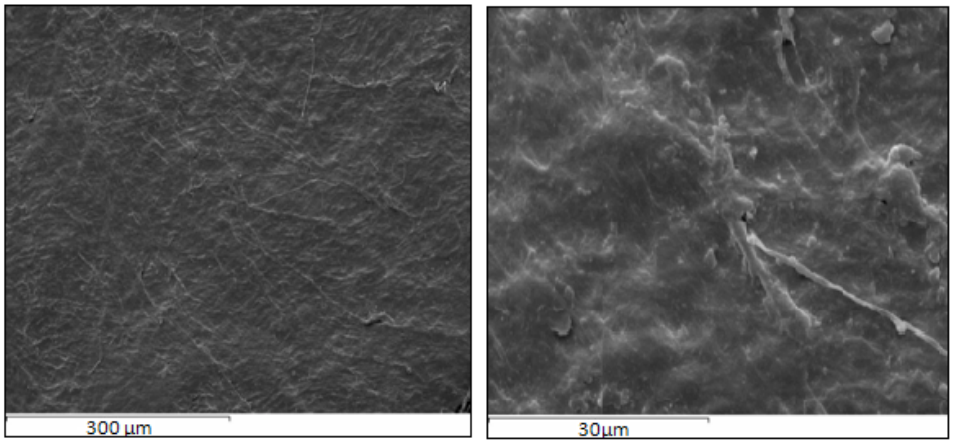

Figure 5.24. SEM images of SIS at different magnifications.

The surface roughness results for both membranes are shown in Figure 5.25. The values obtained for the membranes were 1.51 µm for pericardium and 2.20±0.01 µm for SIS. As expected, the surface roughness values for both membranes were higher than the surface roughness values obtained for P(3HO) films (0.17 µm) (section 5.2.1.3).

(A)

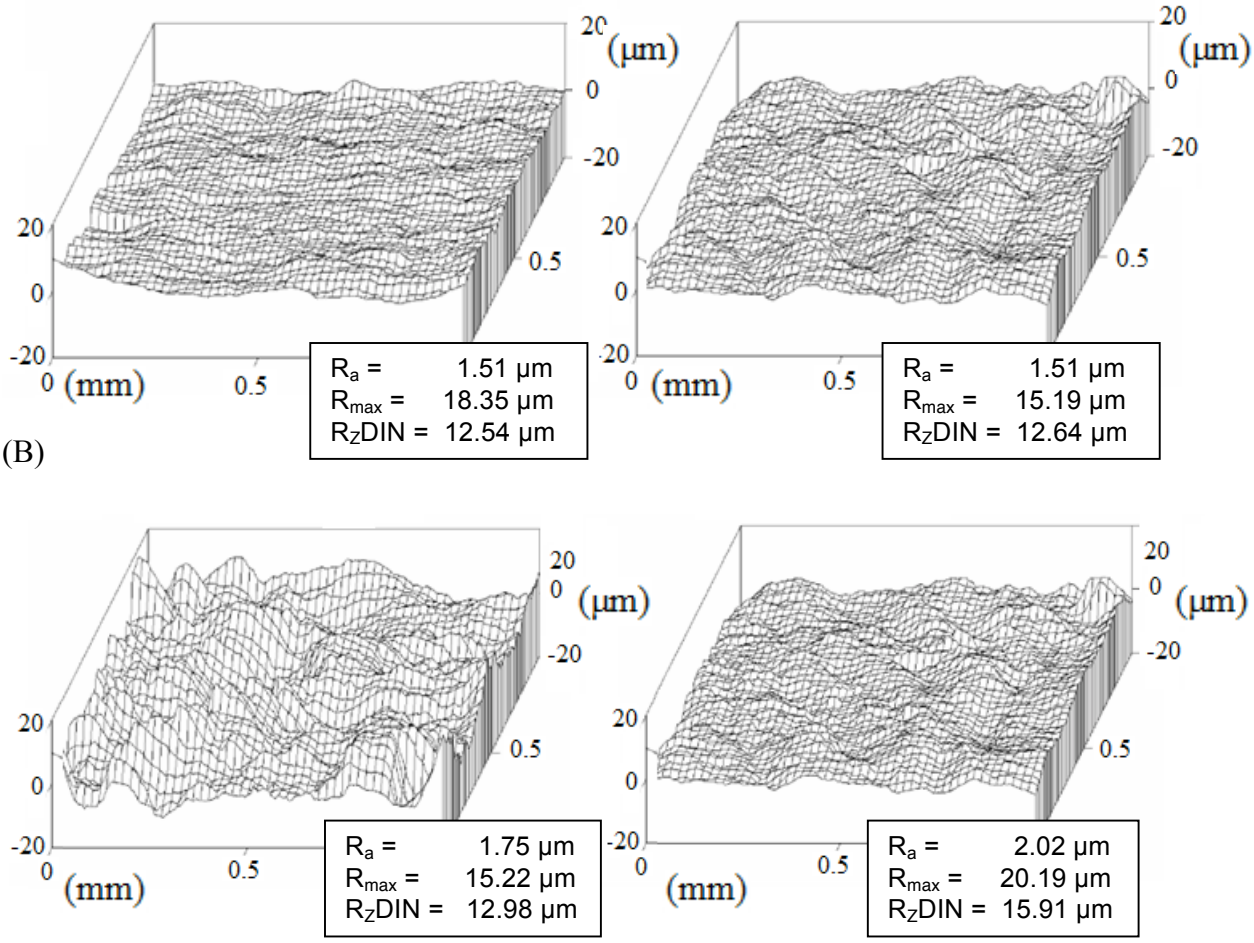

Figure 5.25. Surface roughness analysis of (A) pericardium and (B) SIS. R_a describes the average surface roughness, R_{max}, the maximum roughness depth, R_ZDIN, the average peak to valley height minus R_{tm} and R_{tm} is the average distance between the highest peak and lowest valley in each sample.

It is well known that as soon as a foreign body is implanted in the body, proteins are adsorbed onto the surface of the implant. As a result, it is expected that cells interact with the biomaterial surface rather than directly with the material itself. Hence, the initial protein adsorption onto a biomaterial surface is a key factor that will determine how the body will

react to an implanted material (Anderson *et al.,* 1990, Tang *et al.,* 1995). The protein adsorption on both biological membranes and the P(3HO) film were measured as described in section 2.2.10.6 and results are represented in Figure 5.26. For this, films were incubated in foetal bovine serum and the total adsorbed protein was quantified. Results showed that protein adsorption on P(3HO) films is considerably lower than the SIS and the pericardium.

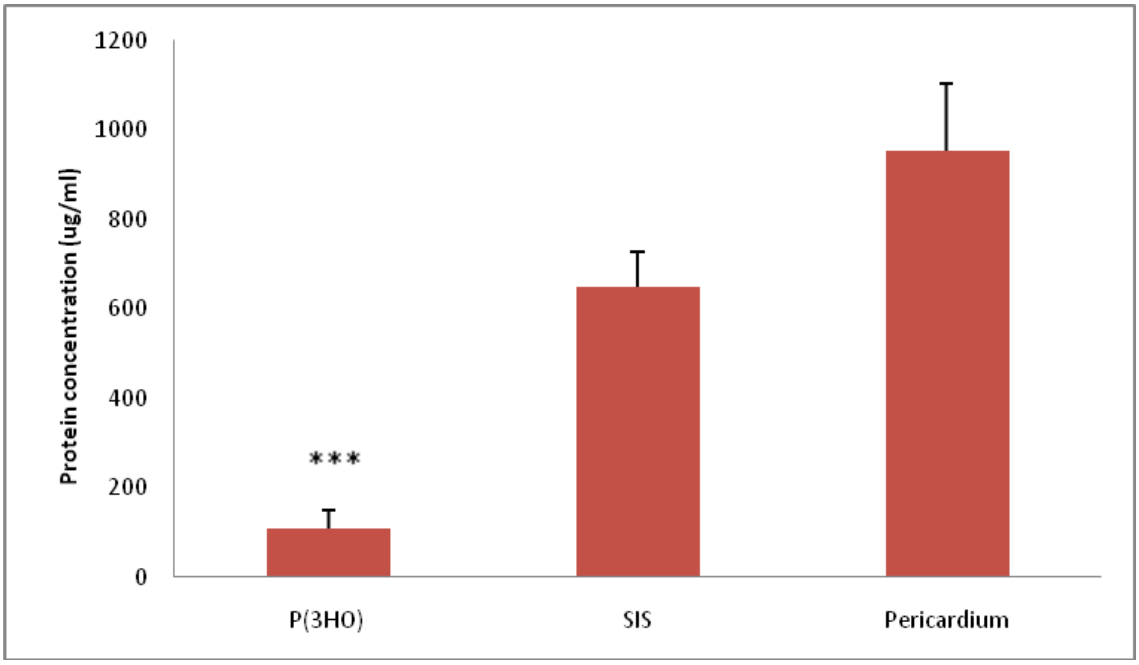

Figure 5.26. The concentration of proteins adsorbed on the surface of the P(3HO) films vs. SIS and pericardium (n=3; error bars=±SD). The data were compared using ANOVA and the differences were considered significant when ***$p < 0.001$.

In order to confirm the integrity of the proteins adsorbed on the surface of the structures and to verify the origin of these proteins, adsorbed proteins were run on a SDS-PAGE gel. Figure 5.27 shows the gels. As albumin is the main protein present in the serum the presence of the band at 66 KDa in all the samples confirms the integrity of this protein. In the case of the pericardium and SIS, results show that not only albumin but also other proteins were eluted (Figure 5.27 (B) and (C)). The fact that some bands appear in the negative control, in which the membranes were not treated with FBS, indicates that proteins that were originally present on the surface of the pericardium and SIS were not completely removed. In the case of SIS (Figure 5.27 (C)), the membrane showed a high concentration of protein that eluted from the

membrane and a low concentration of albumin. Some of these proteins did not appear either in the negative control in which PBS was used instead of FBS or the positive control where FBS was loaded, hence, it was not possible to confirm the origin of these proteins. However, it is possible that these proteins were present in the serum and due to the fact that the concentration of albumin in the serum in significantly higher than other proteins they are not visible in the positive control. Hence, we can suggest that SIS has higher affinity for other proteins as compared to albumin.

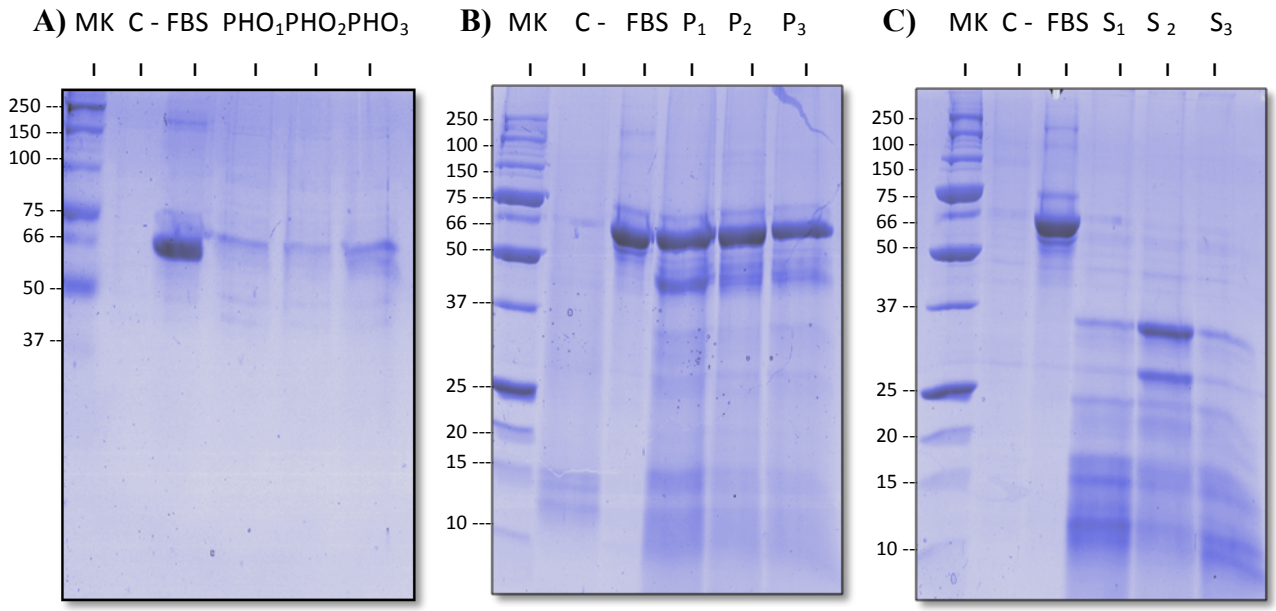

Figure 5.27. SDS-PAGE showing the integrity of the proteins adsorbed on the surface of A) P(3HO) films B) Pericardium and C) SIS. MK: Bio-rad® reference protein ladder; C-: negative control that contains the proteins eluted from the membranes without FBS treatment; FBS: whole serum; PHO_1, PHO_2 and PHO_3: proteins eluted from the P(3HO) film after FBS treatment; P_1,P_2 and P_3: proteins eluted from pericardium after FBS treatment; S_1, S_2 and S_3: proteins eluted from SIS after FBS treatment.

Table 5.1 summarizes the results obtained from the various analyses carried out on P(3HO), pericardium and SIS.

Table 5.1. A summary of the results obtained from the characterization of the P(3HO) film, SIS and pericardium

	P(3HO)	Pericardium	SIS
Young'smodulus (MPa)	3.7±0.3	0.4 ±0.1	329.9±2.2
Tensile strength (MPa)	3.4±0.2	6.3	10.5
Elongation at break (%)	299±29	114.5	10
Melting temperature (ºC)	43.8±4.1	60	60
Water contact angle	101.1±0.8	41.6±9.6	96.2±6.6
Thickness (mm)	0.18	0.58	0.16
Surface roughness (µm)	0.17	1.51	2.20±0.01
Protein adsorption (µg/mL)	108.61±40.30	648.06±80.30	954.17±150.70

Although the biomaterial's surface properties have been extensively described to have an effect on cell adhesion and proliferation, no general principles that allow the prediction of cell behaviour have been established and this has to be specifically determined in each particular case. In the following experiment the effect of the polymer and the two biological membranes on cell attachment and proliferation was assessed. To this end, myoblast cells (C2C12) were seeded on the P(3HO) films, pericardium and SIS, as described in section 2.2.11.3.3. The cell adhesion and proliferation were measured after 24 hr of cell seeding with the MTT colorimetric assay (section 2.2.11.3.4). The results obtained were normalized against the cell proliferation observed on tissue culture plates. The results showed no significant difference in the % cell proliferation observed on P(3HO) and SIS, at 24 hr (Figure 5.28). A 14 % higher cell proliferation was observed on the pericardium in comparison to P(3HO) or SIS.

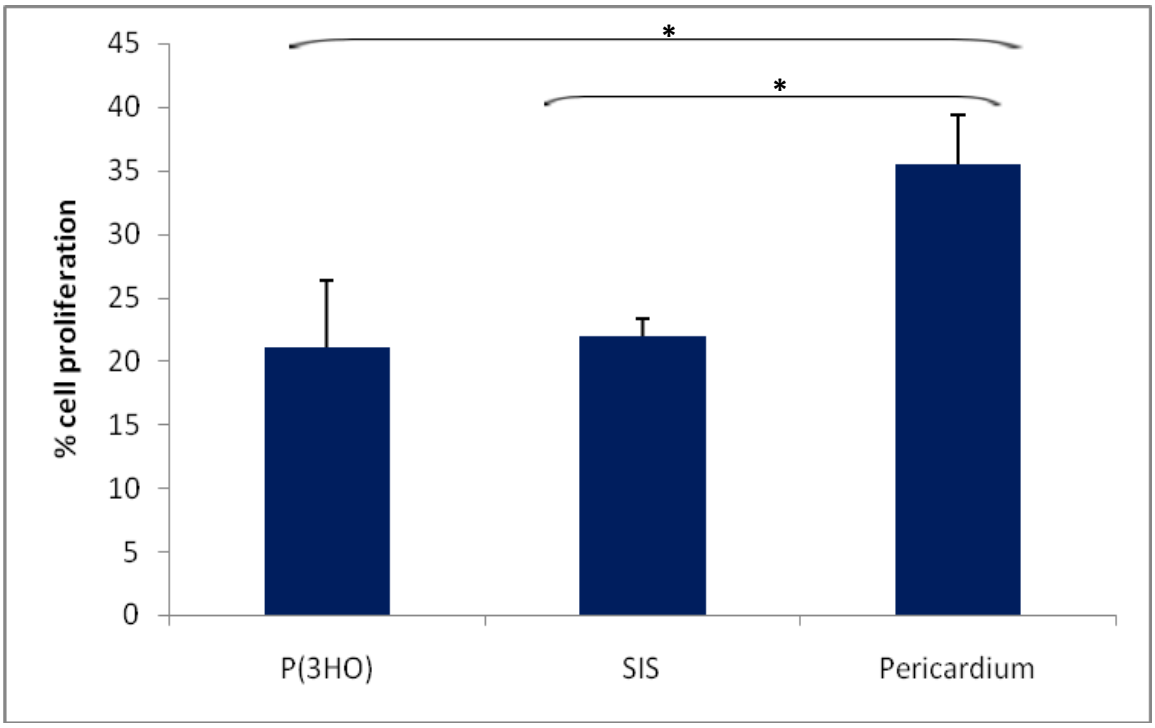

Figure 5.28. % Cell proliferation of C2C12 cell line at 24 hr on P(3HO), SIS and pericardium (n=4; error bars=±SD). The data were compared using ANOVA and the differences were considered significant when $*p < 0.05$.

SEM was carried out to visualize myoblast cells grown on the different materials. Sample preparation for the SEM analysis was performed as described in section 2.2.10.4. SEM images are shown in Figure 5.29. Although the % cell proliferation is compared between a P(3HO) neat structure and two 3D structures, similar proliferation was observed between P(3HO) and SIS and comparable values were obtained with the pericardium.

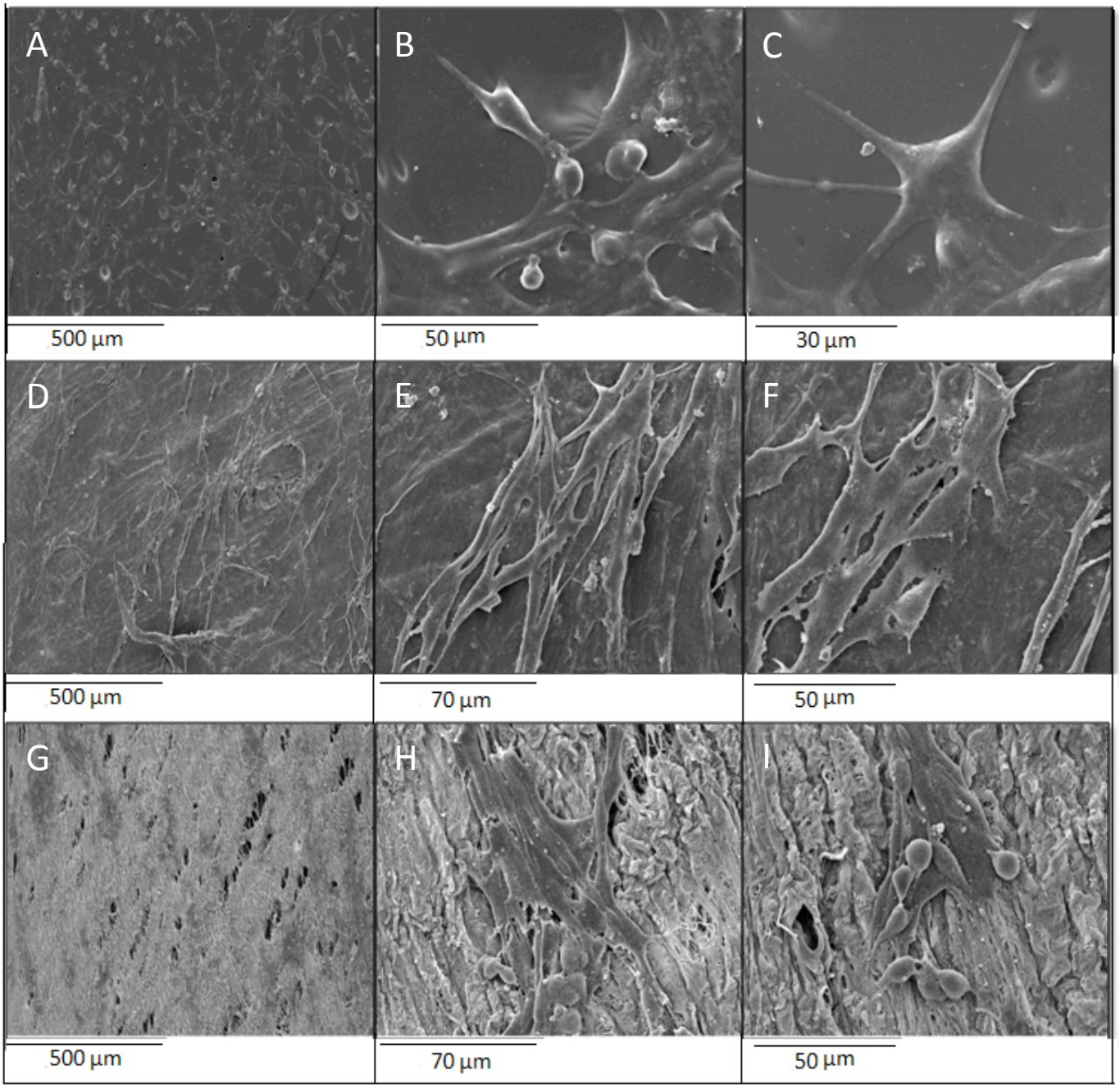

Figure 5.29. SEM images of C2C12 cells after 24 hr at different magnifications growing on A), B) and C) P(3HO) neat film; D), E) and F) SIS membrane and G), H), I) pericardium.

5.3. DISCUSSION

Medium chain length PHAs, with a typical monomer chain length from 6-16 carbon atoms, are polymers produced in Gram-negative bacteria, mainly *Pseudomonas sp*. Mcl-PHAs are of great interest because according to the number of carbons in the side chain, the physical properties of these biodegradable polymers can be varied, allowing the production of tailor made materials. Previous reports have shown that mcl-PHAs are flexible elastomeric polymers, with low crystallinity, low glass transition temperature, low tensile strength, and high elongation to break (Zinn *et al.,* 2001). In this chapter we studied poly(3-hydroxyoctanoate), a mcl-PHA, as a potential material for cardiac tissue engineering. P(3HO) was known to be produced as an homopolymer by *P. medocina,* as described by Rai *et al.,* (2011a).

5.3.1. P(3HO) properties

P. mendocina was grown in 2 L bioreactors, in MSM media, with sodium octanoate as the sole carbon source and PHAs were extracted and characterized. Structural characterization of the polymer was carried out by FTIR, GC-MS and NMR and results showed that, as expected, the produced polymer was the P(3HO) homopolymer.

The mechanical properties of the material will play an essential role in supporting the injured organ during regeneration. The P(3HO) mechanical properties were measured using dynamic mechanical analysis. As myocardial stiffness is considered to be an essential myocardial property, especially during the diastole, P(3HO) stiffness was quantified by examining the relationship between stress and strain (Watanabe *et al*., 2006). According to our results the Young's modulus of the P(3HO) neat film was 3.7±0.3 MPa. This value shows that the P(3HO) stiffness is approximately one order of magnitude higher as compared to that of myocardial structures (human myocardium stiffness 0.02-0.5MPa). Further experiments will include production of P(3HO) structures that will decrease the material's Young's modulus. The ability to resist breaking under tensile stress is one of the most important properties of materials used in structural applications. The tensile strength obtained for P(3HO) was 3.4±0.2 MPa. Although this value is higher than myocardial structures (human myocardium tensile strength 3-15 KPa), a higher tensile strength might have a positive effect as after a myocardial infarction, the abrupt loss of myocardium triggers a ventricular remodeling that

includes dilatation, hypertrophy, and the formation of a collagen scar that increases the load of the infarcted region. Furthermore, it has been described that negative ventricular remodeling continues for weeks or moths until the distending forces the cardiac tissue are counterbalanced by the tensile strength of the collagen scar, hence, a higher tensile strength could have a positive effect after a myocardial infarction (Sutton *et al.,* 2000). The percentage elongation at break of P(3HO) recorded at the moment of rupture of the specimen, expressed as a percentage of the original length was 299±29 %. This value is similar to the upper limit of myocardial structures (human myocardial elongation at break is between 100-300 %).

Thermal analyses of P(3HO) showed two peaks corresponding to the glass transition temperature and melting temperature observed at -32.9±3.8 ºC and 43.7±4.1 ºC during the first heat scan, respectively. A glass transition temperature below room temperature and the low melting temperature, which reflects the low crystallinity of the polymer imparts to the material an elastomeric behavior. No melting temperature peaks were observed during the second heat scan as P(3HO) polymer chains were unable to rearrange again into ordered structures during the cooling run after the melting process.

The surface of the biomaterials plays a significant role in determining the outcome of the biological system and biomaterial interaction (Flemming *et al*., 1999). Biomaterials interact with the biological environment at their surface, making the characterization of the surface crucial for understanding subsequent biological effects. In order to study the surface properties of the P(3HO) polymer, films were created by the solvent casting technology. The hydrophobicity of a biomaterial surface is directly related to cell adhesion. The cell adhesion to a surface occurs by adhesion receptors present in the cell that binds to proteins adsorbed on the surface and the conformation of these proteins depends on the surface wettability (Lee *et al.,* 2003). It has been described that the water contact angle of hydrophobic surfaces is higher or equal to 90º (Li, 2011). The P(3HO) water contact angle was 101.1 ± 0.8º. This value showed that the P(3HO) film surface is hydrophobic, however, the value is not much higher than the upper limit of 90°, known for hydrophilic surfaces. In general, hydrophilic surfaces display better affinity for cells but lower affinity for many proteins as compared to hydrophobic surfaces (Lampin *et al*., 1997).

Finally, SEM analysis and surface roughness studies revealed that the P(3HO) neat films present a smooth surface. With regard to roughness of the surface affecting the growth of different kinds of cells, most researchers have shown that increased surface roughness has a

positive effect on cell adhesion (Richert *et al.,* 2008). Further experiments in this thesis will include surface functionalization of the P(3HO) film in order to promote cell adhesion and growth.

5.3.2. Use of P(3HO) in cardiac tissue engineering

The interaction of cardiomyocytes with the extracellular matrix is essential for the proper functioning of cardiomyocytes since the extracellular matrix provides an adhesive surface for cells and a structural organization to the tissue (Gupta *et al.,* 2006). In the second part of this chapter, the effect of P(3HO) on freshly isolated cardiomyocytes was assessed. In a preliminary study, cardiomyocytes were seeded on P(3HO) polymer films and the number of live vs. dead cells was measured at different time points. Results were compared to the control in which plastic tissue culture was used. Results showed a slightly higher number of live cells on P(3HO) than in the control (tissue culture plastic) at different time points. These results suggest that P(3HO) is not toxic and a good cell adhesive surface for the cardiomyocytes.

The proper contraction of individual cardiomyocytes is essential for the normal functioning of the heart. Intracellular calcium is the main factor that regulates cardiomyocyte contraction. First, an action potential leads to the opening of L-Type calcium channel present in the membrane of the cells. Second, the calcium entering the cells triggers the release of calcium from the sarcoplasmatic reticulum, leading to a marked increase of cytosolic calcium concentration. High concentrations of intracellular calcium initiate the interaction of contractile filaments and subsequent contraction. Relaxation occurs by the removal of calcium from the cytosol by calcium transporters. It has been described that Gap junctions coordinate the contraction of individual cardiomyocytes and this force is transduced to the extracellular matrix, which coordinates the overall contraction of the heart (Harvey *et al.,* 2011). Engler *et al.,* (2008) have shown that the culturing of embryonic cardiomyocytes on a series of substrates of different elasticity has a significant effect in the transmission of contractile work and that cells in a rigid matrix are deficient in the assembly of contractile proteins and their beating frequency slows down over time. As a result, the extracellular matrix to which cardiomyocytes attach is a key factor for a highly regulated system such as the heart. In order to analyze the effect of P(3HO) on isolated cardiomyocyte contraction, fresh cardiomyocytes were seeded on P(3HO) coated cover slips and the effect of a range of

frequencies on the cardiomyocyte contraction was examined. Results show that no significant differences were observed between the polymer and the control (glass cover slips) in terms of 'time to peak 90%', 'time to baseline 50%' and the amplitude of contraction (% shortening). As expected, increasing stimulation frequencies, leads to a progressive decrease in the amplitude of contraction in myocytes due to a shorter time for cytosolic calcium replenishment. Decreased function of individual cardiomyocyte contraction is known to lead to the deterioration of cardiac performance. Our results showed that the polymer is not reducing the effect of frequency on cardiomyocytes. Differences were observed with 'time to peak 90%' when the frequency of stimulation was increased from every 5 to 0.5 seconds in both polymer and control. When the frequency of stimulation was increased from every 5 to 2, 1 and 0.5 seconds, a significant diminution in 'time to baseline 50%' was observed in the control but not on the polymer. Additionally, when the frequency of the electrical impulse was increased from 5 to 0.5 seconds, the cardiomyocyte contraction decreased significantly in the control but not on the polymer. The decrease in time to relaxation might lead to a decrease in the contraction amplitude for the control. There is a usual negative effect at high frequencies due to a reduction in the time for calcium replenishment, which leads to a diminution in the contraction amplitude performance. However, this negative effect on the contraction performance with increment in electrical impulse frequency was not observed in the case of P(3HO).

As described before, calcium is a central regulator of cardiac contractibility. We have studied the effect of increasing calcium concentrations on cardiomyocyte contraction. It has been reported that an intracellular calcium increment leads to an increment in the force of contraction that results in a higher contraction amplitude until a saturation point at which no further increment in contraction occurs (Bers 2000). Our results show that no significant differences were observed between the polymer and the control in terms of 'time to peak 90%', 'time to baseline 50%' and amplitude of contraction (% shortening). As expected, an increment in cardiomyocyte contraction was observed when the concentration of calcium was increased from 1mM to 2mM on both the polymer sample and the control, reaching a point of maximum contraction. Additionally, a slight increment was observed in 'time to baseline 50%' when the concentration of calcium was increased from 2 to 3 and 4 mM in the control but not on the polymer. These results showed that the polymer is not reducing the effect of calcium.

In agreement with Engler *et al.,* (2008), who observed a reduced contraction ability of cardiomyocytes in rigid surfaces, our results showed a reduction in the contraction amplitude at high frequencies of electrical impulses in the rigid surface of the control in contrast to the constant contraction amplitude observed on the surface of the P(3HO) elastomeric polymer. Our results showed that P(3HO) did not have a deleterious effect on the contraction of adult cardiomyocytes and hence P(3HO) is a potential material that can be effectively used in myocardial tissue engineering.

5.3.3. P(3HO), SIS and pericardium

Over the past years, different materials have been proposed to support and regenerate the myocardial infarcted tissue as adult cardiomyocytes lack the capacity for self-repair or regeneration. Among these materials are porcine small intestinal submucosa (SIS) and bovine pericardium. SIS is an extracellular matrix rich in collagen, glycosaminoglycans and fibronectin (Perla *et al*., 2006). This membrane has been used as a biomaterial for soft tissue engineering in different tissues including the artery, abdominal body wall, skin and the urinary tract (Badylak *et al.,* 1989, Campodonico *et al.,* 2004, Kim *et al*., 2005 and Zhang *et al*., 2003). On the other hand, bovine pericardium is an extracellular membrane mainly composed of collagen and elastin. Bovine pericardium is commonly used in the repair of vascular tissue, cardiac tissue, the urinary tract and in thoracic surgery (Li *et al*., 2011, Provencher *et al*., 2003, Us *et al*., 2004). In order to understand and compare the properties of SIS and the pericardium with P(3HO), in the first part of the chapter we have focused on the characterization of these two biological membranes available in the market. As discussed previously, mechanical properties play a key role in supporting the organ during the regeneration process. Mechanical properties of SIS and the pericardium were determined by dynamic mechanical analysis. Figure 5.19 and 5.20 show the mechanical profiles obtained for each membrane. The initial slope of the plot corresponds to the Young's modulus and the obtained values were 0.4 ±0.1 MPa and 329.9±2.2 MPa for pericardium and SIS, respectively. These results showed that stiffness of these two materials, used as cardiac patches by different groups, differs in three orders of magnitude (Pires *et al.,* 1999, Rosen *et al*., 2005). It is important to mention that an unusual mechanical profile was obtained in the case of pericardium. The reason of this observation could be related to the dehydration of the membrane at room temperature during the measurement. Section 5.2.1.2 shows that the

Young's modulus of P(3HO) was 3.7±0.3 MPa and hence, the P(3HO) stiffness is closer to pericardium. In order to achieve a contraction in unison with the heart, it is important that the biomaterial has similar mechanical properties to the heart tissue. As described previously, the Young's modulus of the human myocardium is 0.02-0.5 MPa. Consequently, we can conclude that only the bovine pericardium stiffness is in the range of myocardial structures. In case of the pericardium, the tensile strength was 6.33 MPa and elongation at break was 114.5%. For SIS the obtained tensile strength was 10.50 MPa and elongation at break 10%. The tensile strength and elongation at break of myocardial structures have been found to be 3-15 KPa, and 100-300%, respectively. The tensile strength of P(3HO) was 3.4±0.2 MPa and 299±29 %, respectively. Therefore, these results confirmed that the P(3HO) and pericardium elongation at break values and the P(3HO) tensile strength value showed values closest to myocardial structures. Hence, our results suggest that P(3HO) mechanical properties are very similar to that of the pericardium, a material that is currently used in cardiac surgery. This confirms that P(3HO) has the potential to be used equally successfully in cardiac tissue engineering.

The thermograms of the pericardium and SIS showed denaturation at 70 ºC, corresponding to collagen denaturation. Collagen is a major component of both membranes. The melting temperature for P(3HO) was measured to be 43.8±4.1 ºC, hence, both membranes can be predicted to have better processability/stability at higher temperatures as compared to P(3HO).

Surface studies including wettability, surface roughness and protein adsorption for pericardium and SIS were also carried out. The contact angle obtained for the pericardium was 41.6±9.6 º and for SIS was 96.2±6.6 º. As described previously, the water contact angles smaller or equal to 90º are characteristic of hydrophilic surfaces (Li, 2011). In this case, the pericardium was found to have a hydrophilic surface, whereas SIS was found to have a hydrophobic surface. The P(3HO) film's wettability properties were similar to SIS, indicating that the P(3HO) surface was hydrophobic in nature. The surface roughness values for the pericardium and SIS were 1.51 µm and 2.20±0.01 µm, respectively. Finally, protein adsorption/elution studies showed significantly higher proteins concentration on the SIS and pericardium surface as compared to neat P(3HO) films. However, SDS-PAGE results suggest that some of the eluted proteins from both the membranes were present on the membranes before the FBS treatment. It is important to point out that although adsorbed proteins on the surface have a positive effect in cell adhesion, the presence of proteins on the membranes is

much less desirable because it can elicit adverse host responses such as blood coagulation and complement activation (Hlady *et al*., 1996).

Due to the continuous contractile activity of myocytes, cardiac tissue has high oxygen and nutrient's demand and hence, a high level of vascularization is essential. It has been found that absence of vasculature in tissues thicker than 300 µm can be a limiting factor in the selection of a material for cardiac tissue engineering (Bronzino 2006). The thickness of the P(3HO) sample, pericardium and SIS were 0.18 mm, 0.58 mm and 0.16 mm, respectively. These results show that the thickness of the pericardium is higher than desired values.

The cell proliferation on P(3HO), SIS and the pericardium was studied using the C2C12 myoblast cell line. Results showed that at 24 hr, the % cell proliferation on both P(3HO) and the pericardium were similar. Higher % cell proliferation was observed for the pericardium at 24 hr as compared to SIS and P(3HO). As P(3HO) was processed in to a neat film, lower cell proliferation on its surface was expected, hence surface modifications of P(3HO) were carried out in future experiments. However, contrary to expectation, P(3HO) as a neat film showed similar cell proliferation values as SIS and values comparable to that of the pericardium. In conclusion, our results showed that P(3HO) is a promising material for the fabrication of engineered grafts for cardiac tissue engineering applications.

CHAPTER 6

Production of P(3HO) based cardiac patches

6. 1. INTRODUCTION

Myocardial tissue engineering is based on the regeneration of cardiac tissue by the implantation of cells, capable of forming cardiomyocytes and grown on a biocompatible and biodegradable scaffold, which eventually will be implanted onto the injured site of the heart. The combination of living cells seeded onto a biomaterial has been proposed as an alternative option to replace the scarred non-contractile fibrous tissue caused post-infarction (Jawad *et al.,* 2008).

Williams *et al.,* (1999) defined six key requirements for a biomaterial to succeed in cardiac tissue engineering: (1) biocompatible, (2) support cell adhesion and growth, (3) guide and organize the cells, (4) allows cell ingrowth and passage of nutrients and waste products (5) biodegradable and (6) mechanical properties to support the organ during regeneration.

Engineering biomaterials to promote cell adhesion and direct cellular behavior is crucial for the development of materials capable of restoring tissue function. Several reports have proven that cells are sensitive to the physical and chemical environment which determines cell specific migration, proliferation, differentiation and production of proteins which in turn influences tissue organization and regeneration (Jell *et al.,* 2009). This chapter is devoted to the production of cardiac patches using P(3HO). Our first approach was the design of permeable porous structures with an appropriate surface structure for cell attachment that permits the ingress of cells and guides their growth, leading to tissue regeneration in three dimensions. Eventually, the polymer matrix would be degraded leaving behind new tissue. The diameter of the cardiomyocytes dictated the minimum pore size (Yang *et al.,* 2001). The size of the fabricated porous structures were comparable to cardiomyocytes (250-300 μm) in order to allow cell permeation. Additionally, the mechanical properties were adjusted to match myocardial structures.

Several reports have shown that the appropriate modification of the biomaterial's surface can have a high impact on the biocompatibility, cell adhesion and cell interactions (Williams *et al*., 2011). As collagen is the main constituent of the extracellular matrix and exhibits a distinct fibrous architecture, in order to mimic such fibrous structure, the neat P(3HO) and porous film surfaces were modified using P(3HO) fibres, which were produced using electrospinning. In this technique, a syringe fitted with a nozzle is filled with polymer solution and an electric field is applied to the nozzle. As the electric field increases, a charge builds on the polymer solution. When the force due to the charge in the polymer solution exceeds the surface tension of the solution, a charged jet of polymer solution is released

(Doshi *et al.,* 1995). P(3HO) fibres were deposited on neat and porous P(3HO) films. Curtis *et al.,* (1999) have shown that cell adhesion, morphology and orientation can be highly affected by the size and shape of the topographical features on a polymer surface (Curtis *et al.,* 1999). In order to find the optimal fibre size, myoblast cells were seeded on a range of fibres with different diameters. Optimal fibre size was selected according to the highest cell affinity and proliferation observed. Finally, P(3HO) neat and porous surfaces were modified with the optimal fibre size and the resulting cardiac patch prototypes were characterized. *In vitro* cell culture work was carried out to assess the final cardiac patches.

6.2. RESULTS

6.2.1. P(3HO) porous patches

Controlled porosity in biomaterials is a key factor when they are used as a physical support for cell adhesion and growth (Lebourg *et al*., 2008). In this study, porous P(3HO) films were created by the particle leaching method according to section 2.2.9.1 and the effect of porosity on the mechanical properties and on cell adhesion and proliferation were studied. For this, 0.5% sucrose with controlled particle size ranging from 250 to 300 µm was used as porogen. Mechanical properties of the resulting porous films were measured using dynamic mechanical analysis, according to section 2.2.10.1. Figure 6.1 shows the mechanical profile of the porous films. It is expected that mechanical strength decrease with increasing porosity. In this case, the obtained Young's modulus was 0.41±0.03 MPa. The Young's modulus of neat P(3HO) film was measured to be 3.7±0.3 MPa (section 5.2.1.2). Hence, the stiffness of the material decreases by one order of magnitude. The obtained tensile strength and elongation at break were 0.7±0.1 MPa and 447±5 %, respectively. The tensile strength of the neat P(3HO) film was 3.4±0.2 MPa and the elongation at break was 299±29 % (section 5.2.1.2). Hence, the incorporation of porosity in the film resulted in a decrease in its tensile strength and an increase in the elongation at break, as compared to the neat film.

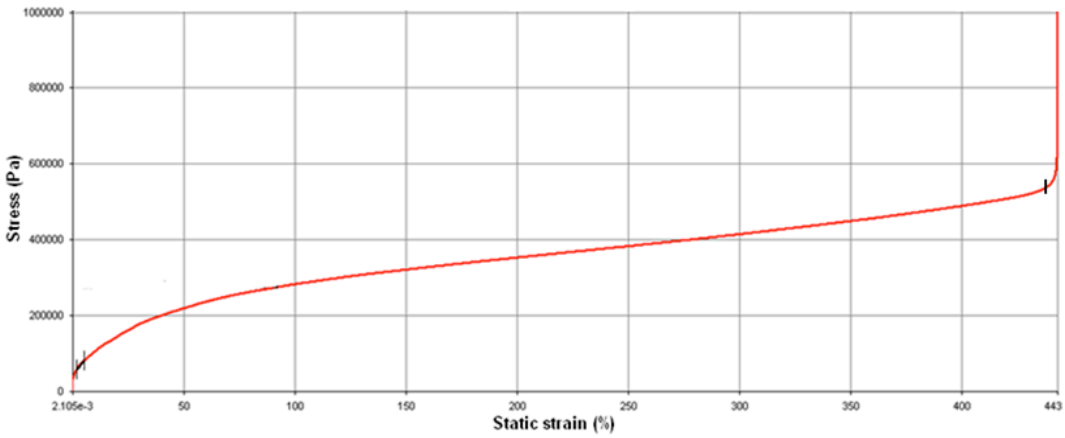

Figure 6.1. Static strain vs. stress profile of the P(3HO) porous films. The initial slope and the maximum elongation are indicated with a black line.

The surface wettability of the P(3HO) porous films was studied with a contact angle measuring device as described in section 2.2.10.3. The obtained water contact angle was 104.9 ± 6.0 º. No differences were observed in terms of the surface wettability as compared to the neat film which also had a contact angle of 101.1±0.8 º. The surface roughness of the film was measured using the white light interferometry technique, as described in section 2.2.10.5. The results obtained showed that the surface roughness of the P(3HO) porous films was 0.9±0.2 µm (Figure 6.2). The average surface roughness of the neat film was 0.17 µm and, hence, the incorporation of porous structures increases the surface roughness by approximately five times. Figure 6.3 shows the SEM images of the porous structures obtained, showing pore sizes ranging from 250 to 300µm.

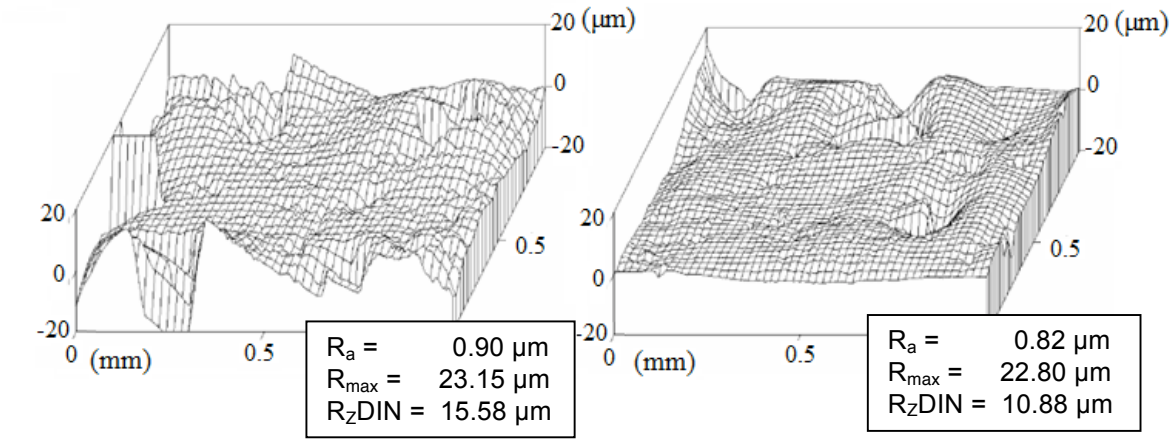

Figure 6.2. Surface roughness analysis of two representative samples of P(3HO) porous films created by the particle leaching method. R_a describes the average surface roughness, R_{max} the maximum roughness depth, R_ZDIN the average peak to valley height minus R_{tm} and R_{tm} is the average distance between the highest peak and lowest valley in each sample.

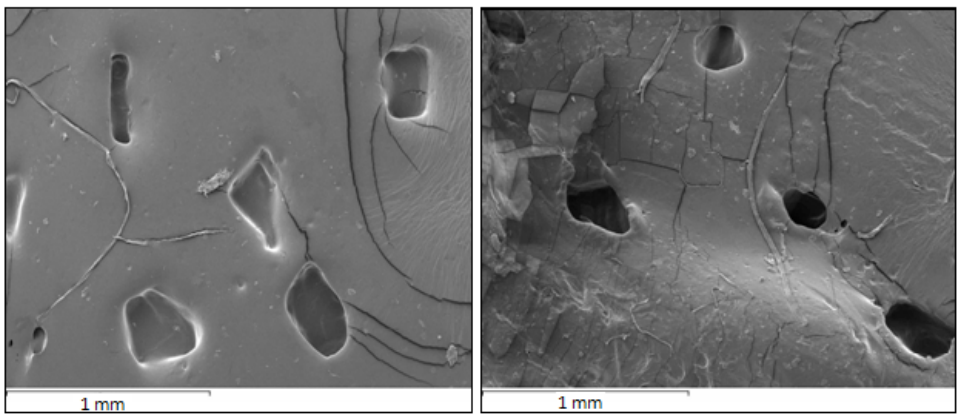

Continues on the following page

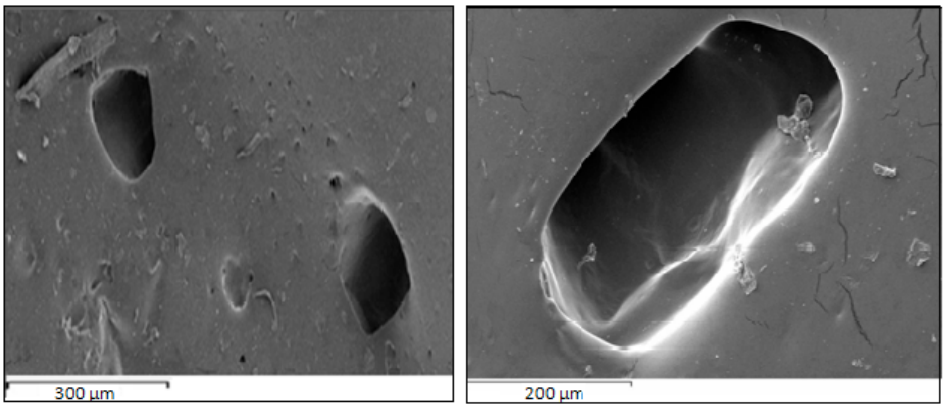

Figure 6.3. SEM images of the P(3HO) porous films showing the structure of the pores at different magnifications.

The protein adsorption of the P(3HO) porous films was measured as described in section 2.2.10.6. The obtained values were compared with neat P(3HO) films. No significant differences were observed in terms of the protein adsorption properties with the incorporation of porous structures (Figure 6.4).

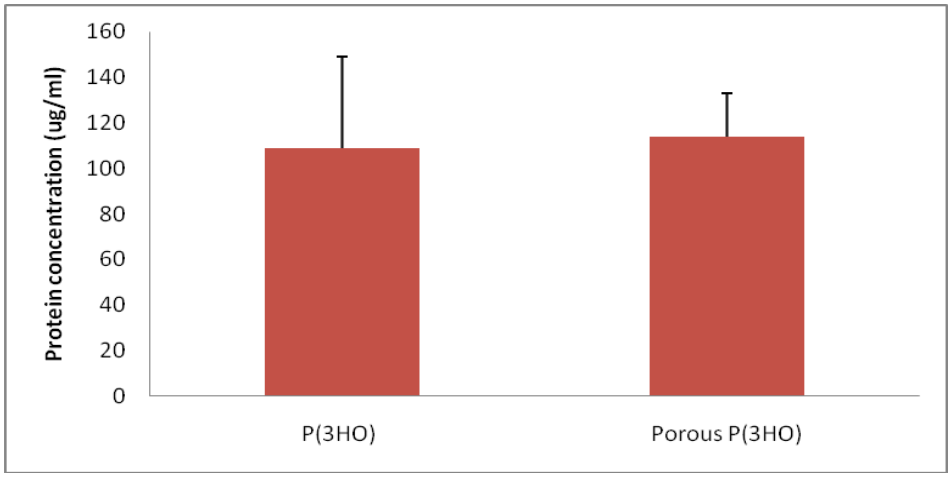

Figure 6.4. Concentration of proteins adsorbed on the neat P(3HO) film vs. P(3HO) porous film (n=3; error bars=±SD). The data was compared using the *t*-test.

In order to study the effect of porous structures on cell adhesion and proliferation, C2C12 cells were seeded on the P(3HO) porous films and the % cell proliferation was measured at 24 hr after seeding. Figure 6.5 compares the % cell proliferation observed on the surface of

neat P(3HO) and porous films, where the proliferation observed on tissue culture plates was considered to be 100%. The results showed that the % cell proliferation increased 2.5 fold when porous structures were incorporated on the P(3HO) films.

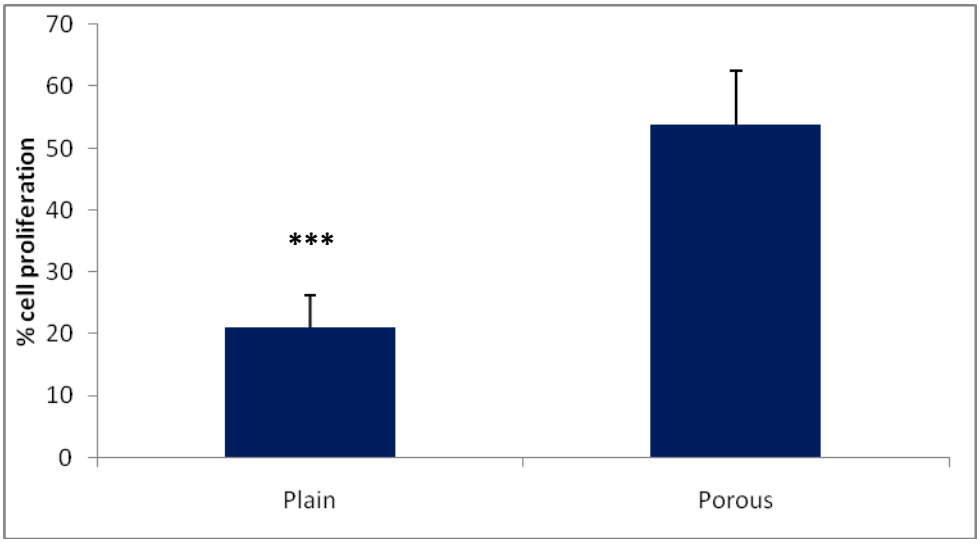

Figure 6.5. The % cell proliferation of C2C12 cell line at 24 hr on neat P(3HO) films and on porous films normalized with respect to tissue culture plastic (n=4; error bars=±SD). The data were compared using the *t*-test and the differences were considered significant when ***$p < 0.001$.

SEM analysis was carried out in order to visualize the C2C12 myoblast cell line on the P(3HO) porous films. Samples were prepared as described in section 2.2.11.4. Figure 6.6 shows typical SEM images observed for samples after 24 hr of cell growth. It was observed that at 24 hr, cells grew inside the pores and almost covered the pore structures.

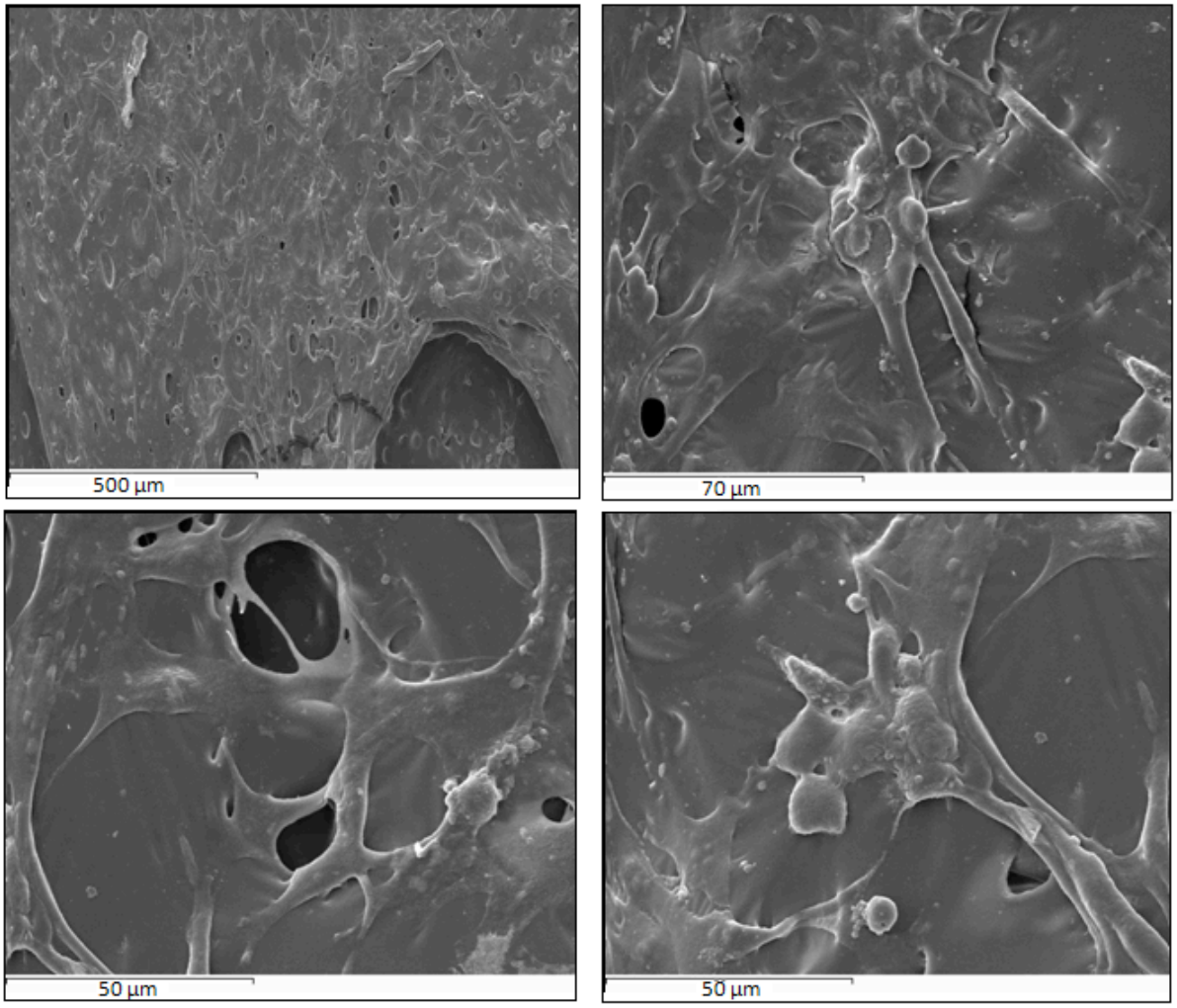

Figure 6.6. SEM images of C2C12 cells at 24 hr on porous P(3HO) films at different magnifications.

6.2.2. P(3HO) fibres

In order to mimic the fibrillar structure of the extracellular matrix which provides essential guidance for cell organization, survival and function, P(3HO) fibres were created by electrospinning, as described in section 2.2.9.2. Electrospinning is a process based on the production of fibres by the application of a high voltage source to a polymer solution in a suitable solvent. For the optimization of the electrospinning conditions, a range of P(3HO) solutions were created in acetone (0.2 wt%, 0.5 wt%, 0.6 wt%, 0.7 wt%, 1 wt% and 1.2 wt%). Additionally, two sizes of inner diameter nozzles (330µm and 660µm) were tested at a range of flow rates (from 30 µl/min to 250 µl/min). A stable jet and homogeneous fibres were obtained when the 330 µm needle and 30 µl/min flow rate were used and the electric potential was adjusted (Figure 6.7). Higher electric potentials were required with lower polymer

concentrations. The electric potential used for the 1.2 wt%, 1 wt%, 0.7 wt%, 0.6 wt%, 0.5 wt% and 0.2 wt% polymer solution were 8.9 KV, 10.9 KV, 11.4 KV, 11.6 KV 13.4 KV and 13.8 KV, respectively. A distance of 15 cm between the needle and collector was used in all conditions tested.

Figure. 6.7. The stable jet obtained with a 330 μm needle at a flow rate of 30 μl/min was employed for electrospinning. The arrow indicates the single stable jet obtained.

The size of the fibres obtained in each condition was measured by optical microscopy and the results are shown in Table 6.1. It was observed that the fibre diameters decreased with decreasing P(3HO) concentration and particles rather than fibres were obtained with the lowest concentration. In, the case of 0.5 wt% P(3HO) solution, a transition between fibre formation and particle formation occurred, hence, both fibres and particles were obtained. Figure 6.8 shows optical images of the material obtained with different polymer concentration solutions.

Table 6.1. Fibre and particle diameters obtained by electrospinning of different solutions of P(3HO) in acetone. Values are shown ± standard deviation.

P(3HO) concentration (wt%)	Fibre diameter (nm)	Particle diameter (nm)
1.2	750 ± 130	-
1	700 ± 100	-
0.7	630 ± 100	-
0.6	370 ± 90	-
0.5	340 ± 100	660 ± 60
0.2	-	580 ± 120

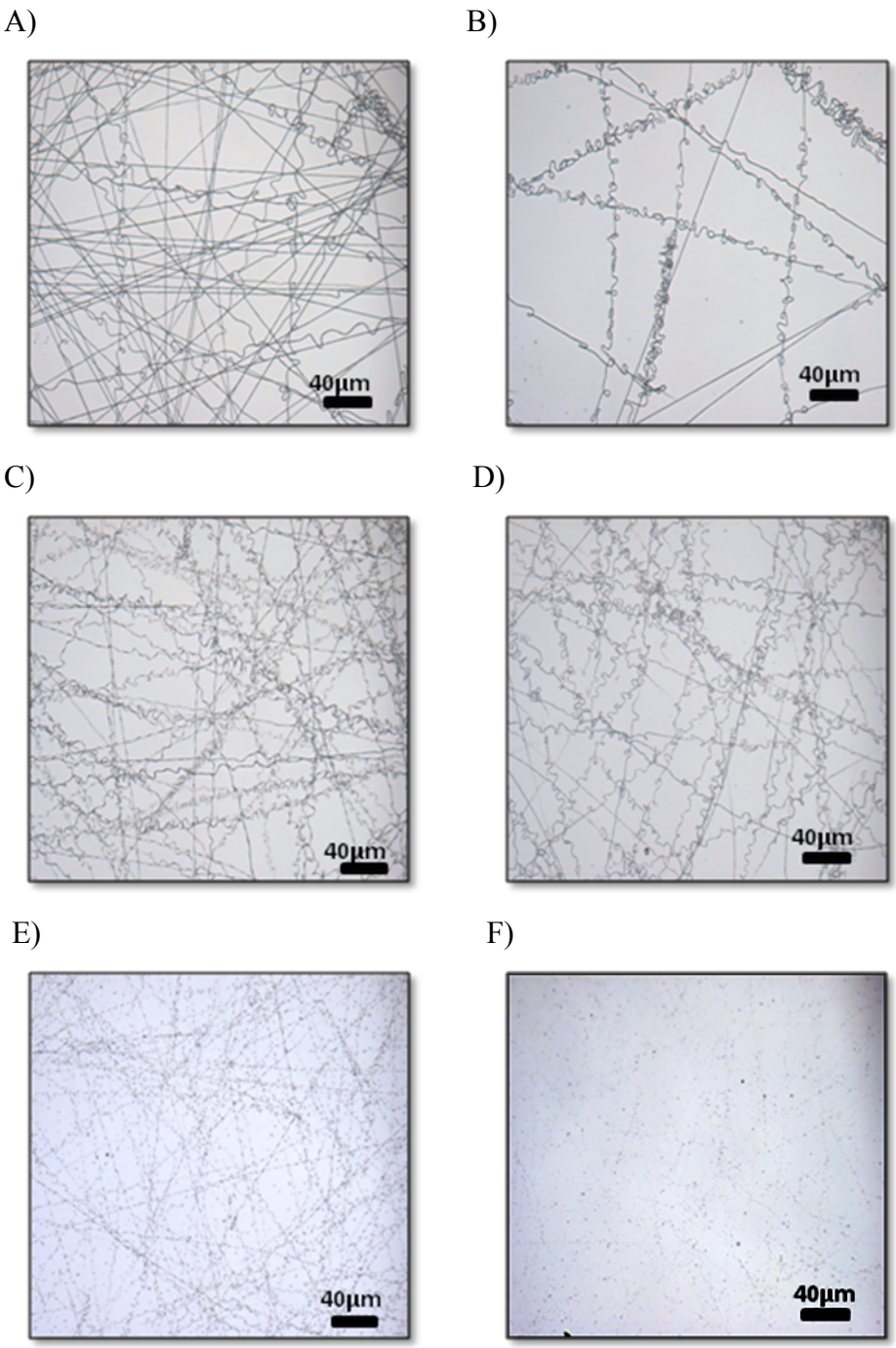

Figure 6.8. Optical microscopy images of P(3HO) electrospun fibres/particles obtained with varying concentrations of P(3HO) solutions in acetone, after 10 seconds of collection: A) 1.2 wt%, B) 1 wt%, C) 0.7 wt%, D) 0.6 wt%, E) 0.5wt% and F) 0.2wt%.

In order to determine the most suitable fibre or particle size to be used for the design of cardiac patches, fibres or particles were collected from the 1.2 wt%, 1 wt%, 0.7 wt%, 0.6 wt%, 0.5 wt% and 0.2 wt% polymer solution on glass slides for 10 minutes in order to ensure

that the full surface of the slides were covered. Contact angle measurements were performed on the glass slides coated with different P(3HO) fibre diameters, in order to determine differences in surface properties that would influence cell adhesion and proliferation. No differences were observed in terms of water contact angle between the 750 nm fibres, 700 nm fibres, 630nm fibres, and 340 nm fibres + particles (Figure 6.9). Smaller water contact angles were obtained with 580 nm particles than with the other fibres or particle diameters.

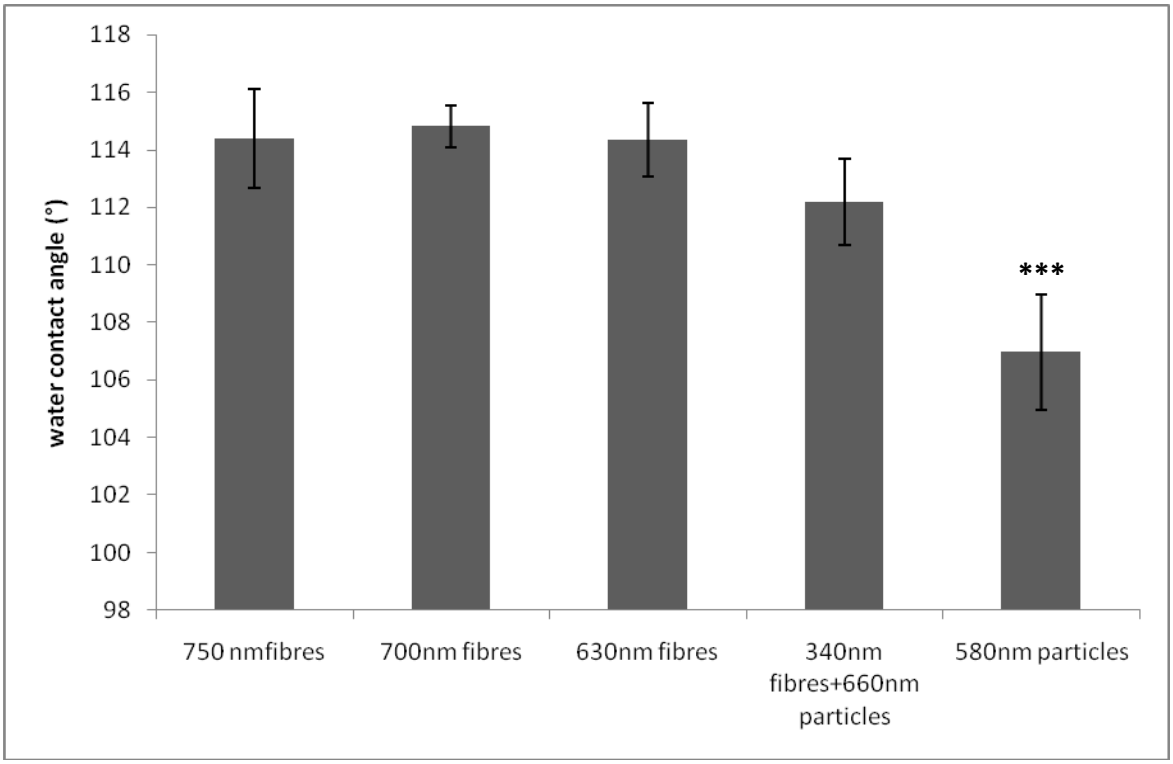

Figure 6.9. Surface wettability properties of the different fibres or particles of different diameters, obtained by electrospinning (n=3; error bars=±SD).The data was compared using ANOVA and the differences were considered significant when ***$p < 0.001$.

In the following experiments cell proliferation on the P(3HO) fibres was assessed with the C2C12 myoblast cell line. Cells were seeded on the glass slides coated with different sizes of P(3HO) fibres or particles. Cell adhesion and proliferation were determined after 24 hr using the MTT colorimetric assay, as described in section 2.2.11.3.4. Figure 6.10 shows the results obtained. Our results showed that an increment in fibre diameter resulted in a higher % cell proliferation, achieving the highest value of 196.8± 16.0 with 750 nm fibres. Also, cells showed preference for fibrous structures as compared to particle structures.

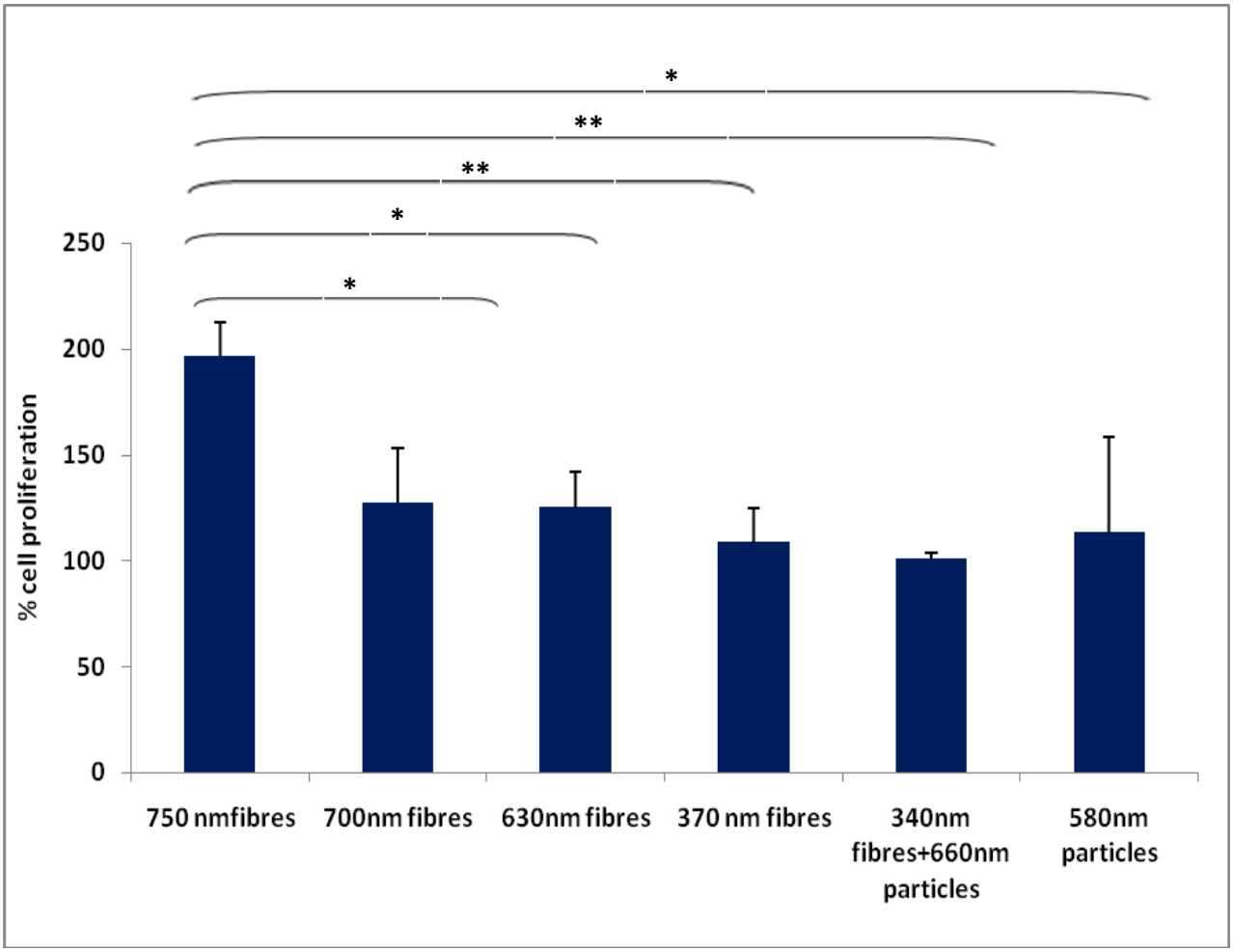

Figure 6.10. The % cell proliferation of C2C12 cell line normalized against cell growth on tissue culture plastic (n=4; error bars=±SD). The data were compared using ANOVA and the differences were considered significant when *p<0.05 and **p<0.01.

Figure 6.11 shows the C2C12 myoblast cell line growing on glass slides coated with 750 nm electrospun P(3HO) fibres (Figure 6.20 (A), (C) and (E)) vs. slides coated with 370 nm electrospun P(3HO) fibres (Figure 6.20 (B), (D) and (F)) collected for ten seconds. In the case of cells growing on 750 nm fibres it was possible to identify cells attaching through their focal adhesions to the fibres.

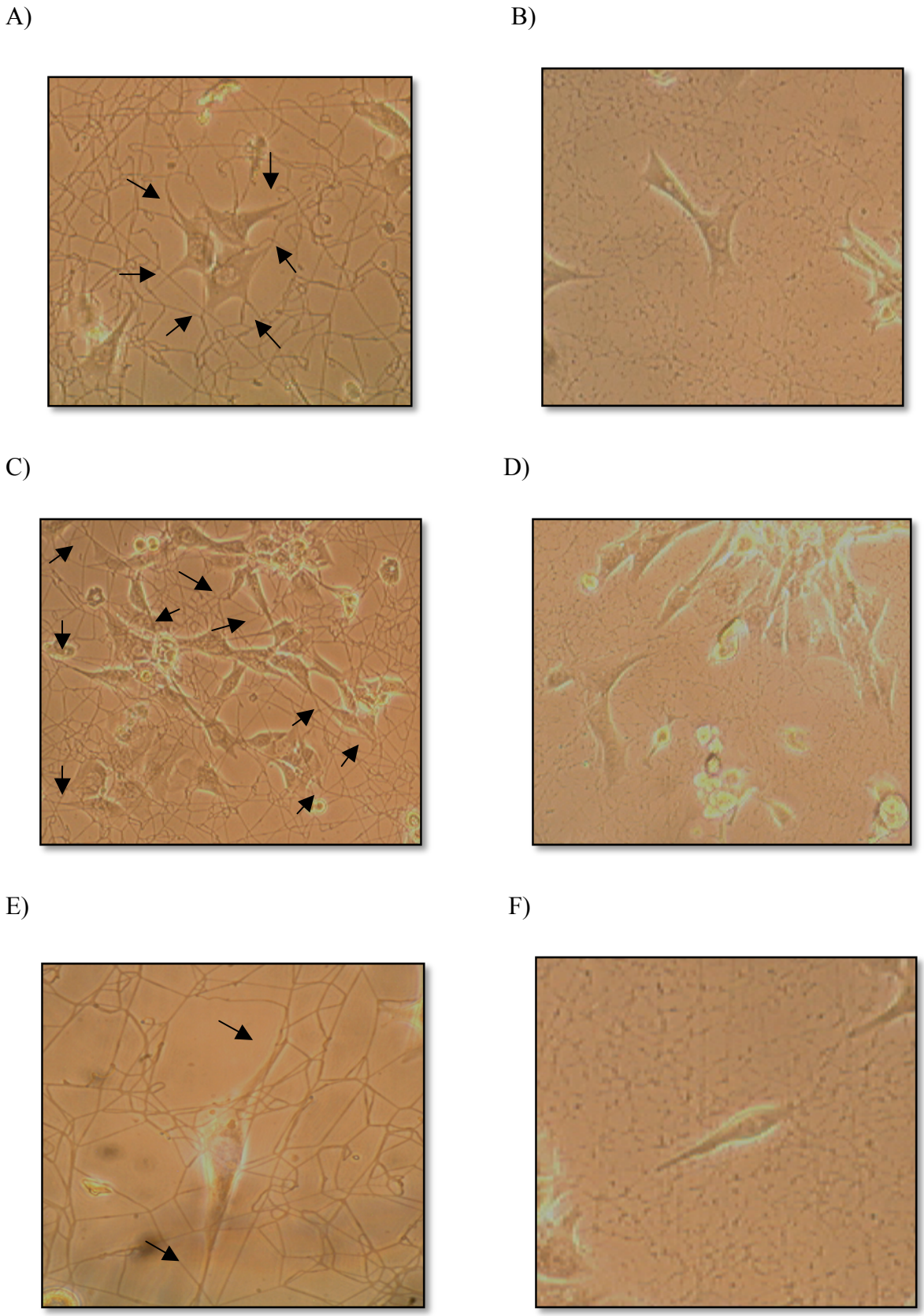

Figure 6.11. Optical microscopy images of C2C12 myoblast cell line grown on glass slides coated with: (A), (C) and (E) 750 nm electrospun P(3HO) fibres vs. (B), (D) and (F) 370 nm

electrospun P(3HO) fibres collected for ten seconds. A), B), C), D) 100x and E), F) 400x magnification. The cell's focal adhesions attaching to the fibres are indicated with black arrows.

Several studies have shown that fibrous matrices, which allow cell infiltration into their porous structure, are attractive substrates as tissue engineering scaffolds (Lee *et al*., 2011, Kurpinski *et al*., 2012). Pores in an electrospun fibrous structure are formed by differently oriented fibres and the size and shape of those pores will be directly related to the fibre concentration. In order to find the optimal concentration of fibres that will allow cell infiltration, in the next experiment, the collection times for the 750 nm fibres on glass slides were varied and the fibre concentration was evaluated by optical microscopy. Figure 6.12 shows optical microscopy images of the 750 nm fibres at (A) 1 second, (B) 10 seconds, (C) 30 seconds, (D) 60 seconds and (E) 90 seconds collection times. The selected collection time was 30 seconds (Figure 5.12 C), in which the fibres covered the entire surface, leaving some gaps for the cells to infiltrate.

A) B)

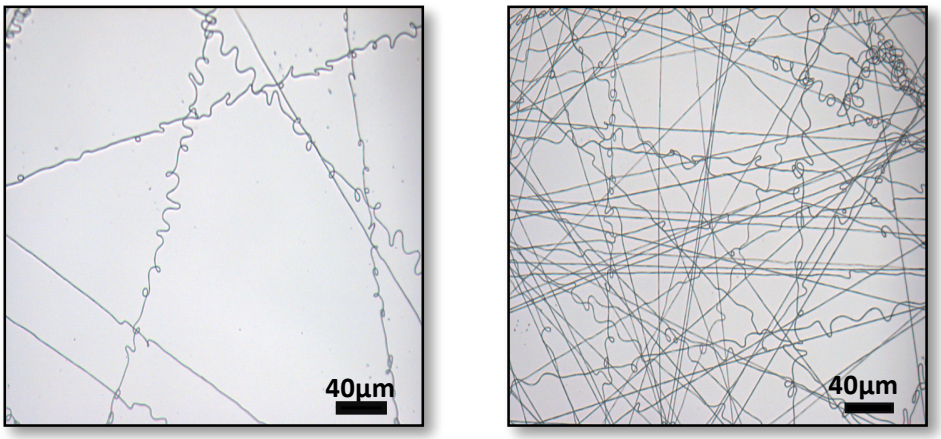

Continues on the following page

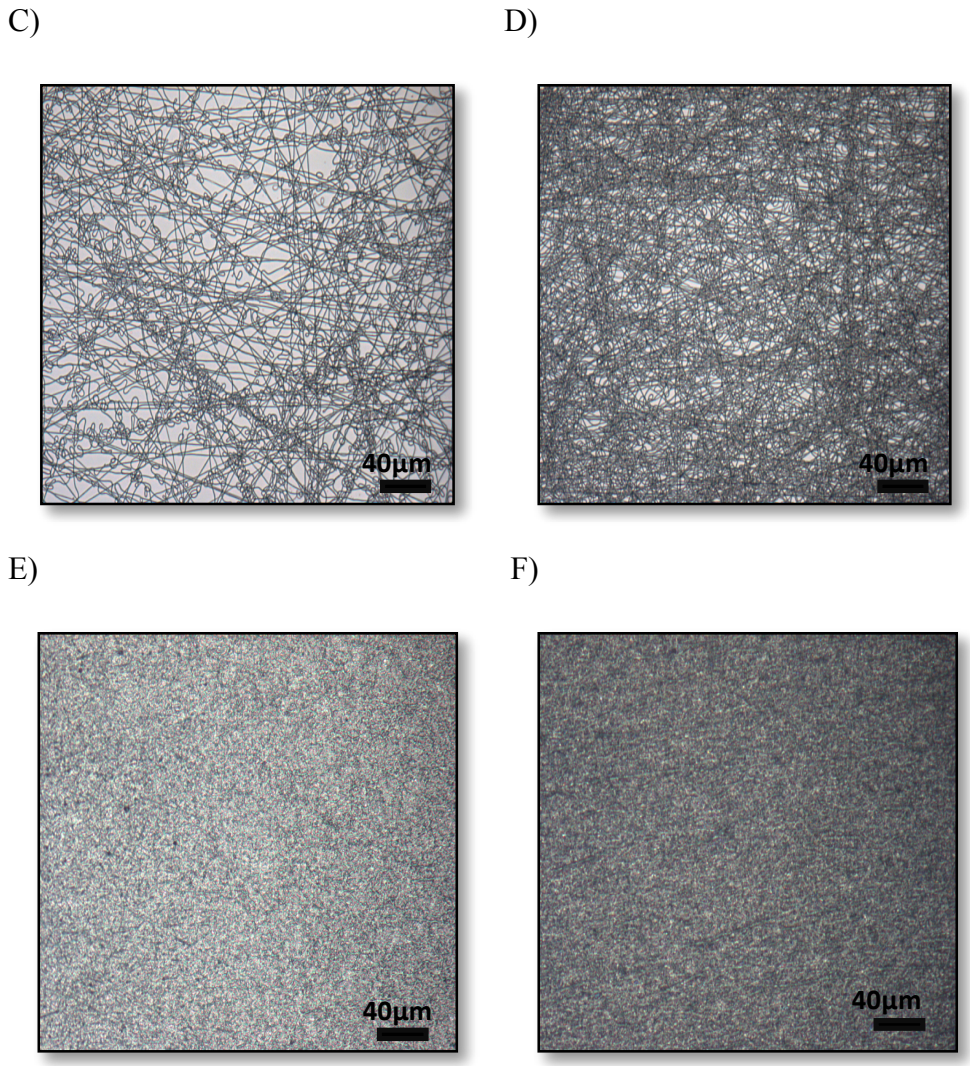

Figure 6.12. Optical microscopy images of the 750 nm P(3HO) electrospun fibres at (A) 1 second, (B) 10 seconds, (C) 30 seconds, (D) 60 seconds and (E) 90 seconds collection times.

6.2.3. P(3HO) cardiac patches

In this section the fabrication of cardiac patches is described. 750 nm fibres were collected for 30 seconds on neat and porous 5 wt% P(3HO) films. The surface of the resulting film was analyzed in terms of the wettability, surface roughness and protein adsorption. The visualization of the fibres by SEM was not possible due to the high temperature sensitivity of the P(3HO) fibrous structures which melted under the SEM focused beam of high-energy electrons. In order to confirm that fibres were collected on the P(3HO) film surface, the patches were observed under the optical microscope (Figure 6.13).

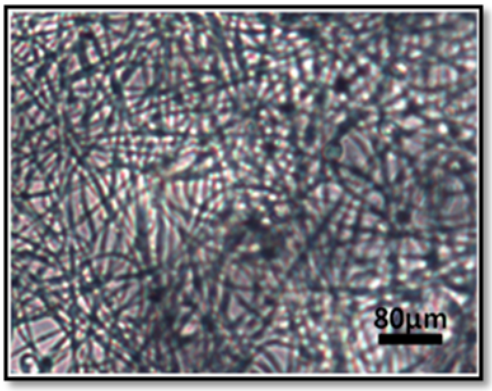

Figure 6.13. Optical microscopy image of the 750 nm P(3HO) electrospun fibres at 30 seconds collection time on the 5 wt% P(3HO) film.

The surface wettability analysis was carried out as described in section 2.2.10.3. The water contact angles measured were 110.2± 3.7 for neat P(3HO) films containing 750 nm fibres and 99.8 ± 1.9 for porous films containing 750 nm fibres. The water contact angle measured for the neat P(3HO) film was 101.1±0.8 (section 5.2.1.3) and for porous P(3HO) film was 104.9 ± 6.0 (section 6.2.1). Surprisingly, an increment in the surface hydrophobicity was observed when neat films were functionalized with fibres and a decrease in the surface hydrophobicity was observed when porous films were functionalized with fibres.

The surface roughness of the cardiac patches was measured according to section 2.2.10.5. The obtained values were 0.90±0.01 µm for neat films with 750 nm fibres and 1.1±0.1 µm for porous films with 750 nm fibres. The surface roughness of the neat P(3HO) film was 0.17 µm and for the porous film was 0.9±0.2 µm (section 5.2.1.3 and section 6.2.1, respectively). As expected, an increment is the surface roughness was observed when films were functionalized with fibrous structures, achieving the maximum roughness when porous and fibrous structures were combined.

(A)

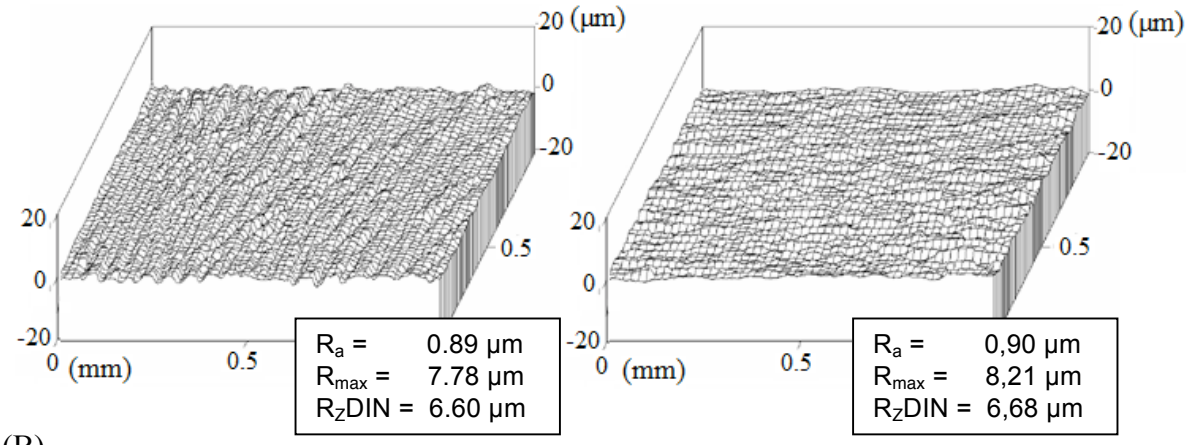

(B)

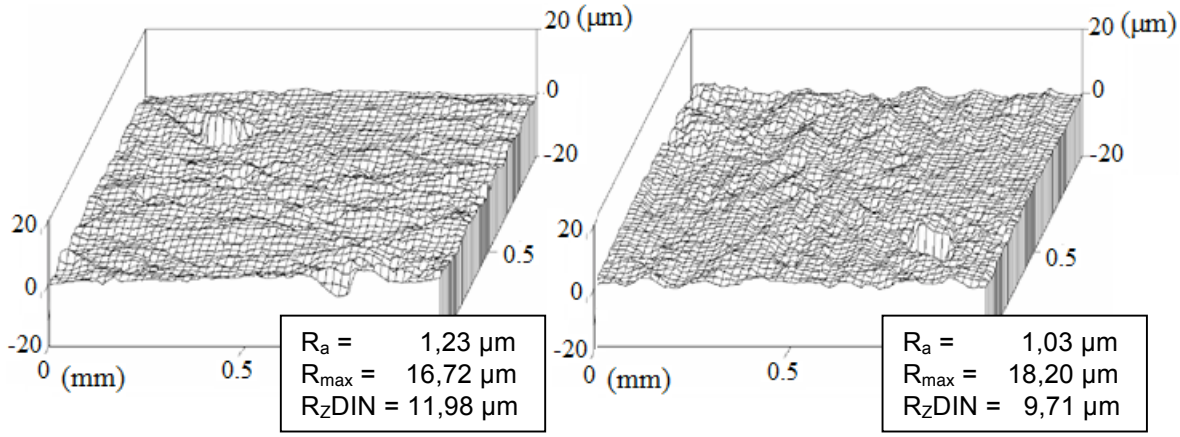

Figure 6.14. Surface roughness analysis of two representative samples of A) P(3HO) neat film modified with 750nm fibres and B) P(3HO) porous films modified with 750nm fibres. R_a describes the average surface roughness, R_{max} the maximum roughness depth, R_ZDIN the average peak to valley height minus R_{tm} and R_{tm} is the average distance between the highest peak and lowest valley in each sample.

The protein adsorption capacity of the patches was assessed according to section 2.2.10.6. Results were compared with the neat P(3HO) and porous films (Figure 6.15). No significant differences were observed in terms of the protein adsorption capacity between the P(3HO) neat and porous films and the P(3HO) neat and porous films coated with fibres.

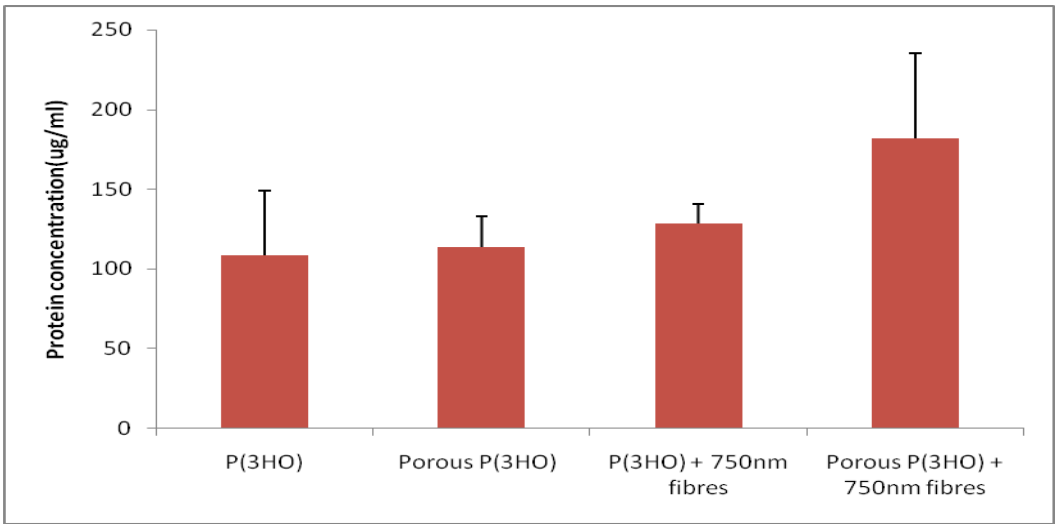

Figure 6.15. Concentration of proteins adsorbed on the surface of neat P(3HO) films, porous P(3HO) films, neat P(3HO) films + 750 nm fibres and porous P(3HO) films + 750 nm fibres (n=3; error bars=±SD). The data were compared using ANOVA.

As the structure of the P(3HO) fibres was intended for cardiac tissue engineering, its suitability was evaluated *in vitro* using C2C12, a myoblast cell line. Cells were seeded on the cardiac patches as described in section 2.2.11.3.3 and the % cell proliferation was assessed at 24 hr with the MTT colorimetric assay according to section 2.2.11.3.4. Cell proliferation results on the patches were compared with the values obtained for neat P(3HO) and porous films (Figure 6.16). Our results showed that a significant increment in the % cell proliferation was obtained when fibre structures were incorporated on the surface of the neat P(3HO) films and porous films. Similar values for cell proliferation were observed with the porous films and neat films modified with fibres, suggesting that both structures contribute in a similar way to cell proliferation. Finally, P(3HO) porous films containing the P(3HO) fibrous structures showed the highest cell proliferation rate and hence this was the best matrix for cell adhesion and proliferation.

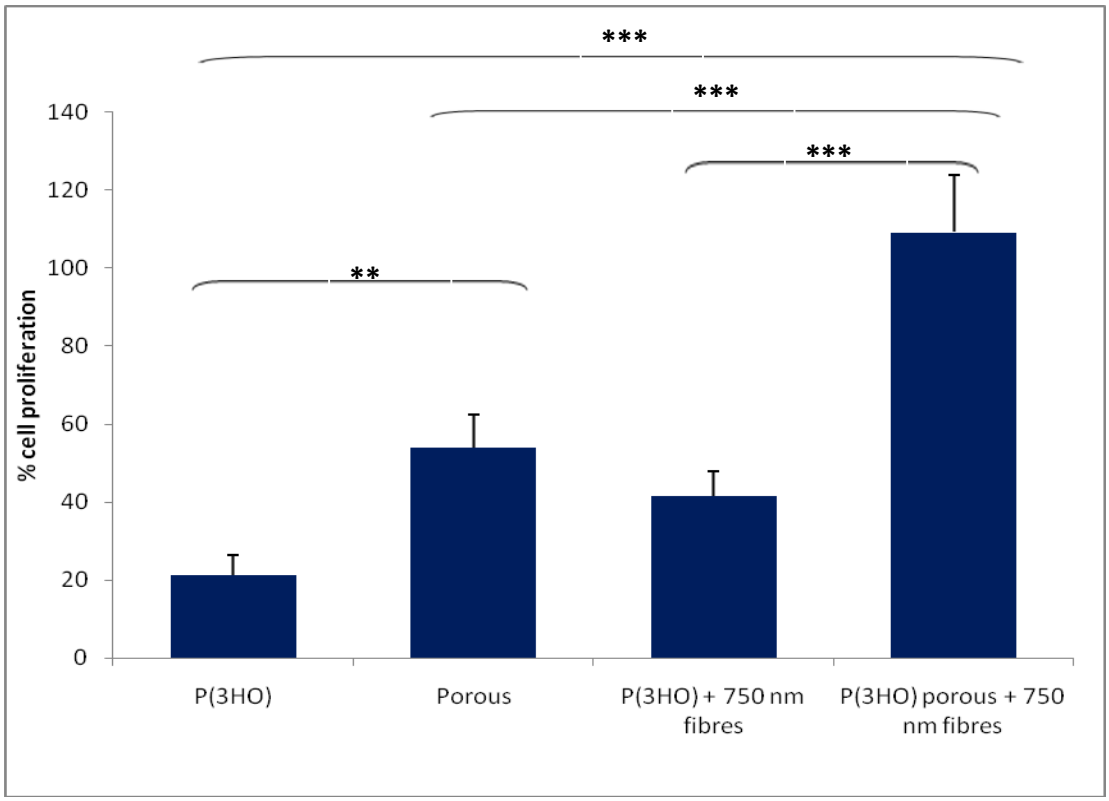

Figure 6.16. The % cell proliferation of C2C12 cell line on neat P(3HO) films containing porous structures, fibrous structures and both fibrous and porous structures. Results were normalized against cell growth results on tissue culture plastic, used as a control (n=4; error bars=±SD). The data were compared using ANOVA and the differences were considered significant when ***p*<0.01 and ****p*<0.001.

SEM analysis was carried out to visualize the C2C12 myoblast cell line on the neat and porous P(3HO) films modified with fibres. Samples were prepared as described in section 2.2.11.4. Figure 6.17 shows the SEM images obtained at 24 hrs. These results show that at 24 hr the surface of the cardiac patches is covered with cells and new cells growing on top of the first cell layer can be observed.

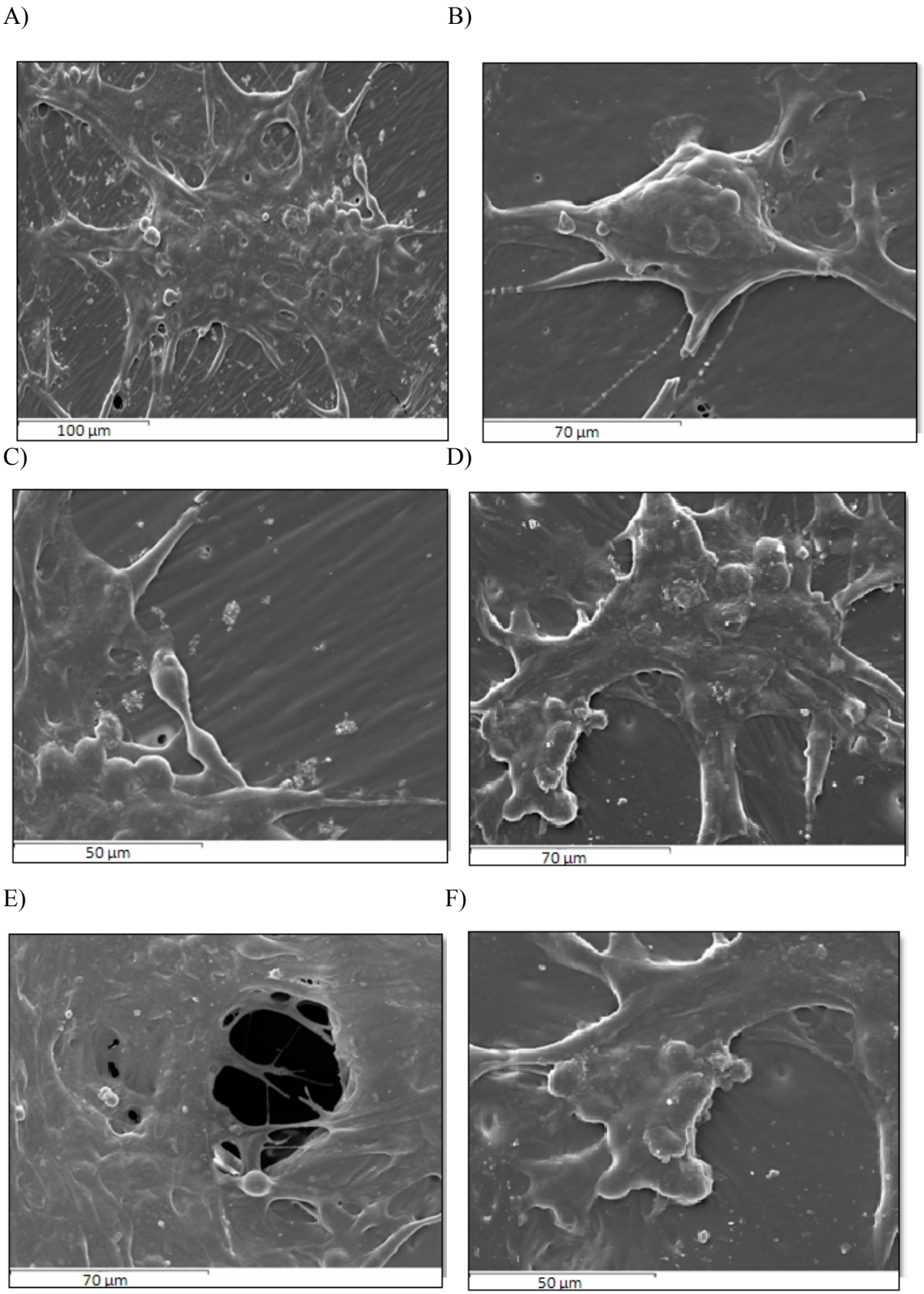

Figure 6.17. SEM images of C2C12 cells at 24 hr on A), B) and C) neat P(3HO) and C), D) and E) porous films modified with 750 nm fibres.

6.3. DISCUSSION

6.3.1. P(3HO) porous patches

In order to provide more space for incorporation of cells and to allow the formation of a three dimensional structure, pores were incorporated in to the cardiac patches. As P(3HO) is a biodegradable material, it is anticipated that the biomaterial structure will reabsorb leaving behind new tissue. P(3HO) based porous films were fabricated by the solvent cast particle leaching method. The average diameter of the porous structures were 250-300 µm, which is the size of human myocytes. It is important to mention that although porous structures provide more surface for cell residence, the number of porous structures that can be created are limited by the desired mechanical properties of the biomaterial. Materials with high porosities displayed diminished mechanical properties (Goldstein *et al.,* 1995). As one of the main requirements for a biomaterial in cardiac tissue engineering is to support the high mechanical demands of the organ during regeneration, the porogen concentration, which would determine the porosity in the patch, was chosen to allow some cell ingrowth without substantial deterioration of the mechanical properties. For this, P(3HO) porous films were created with 0.5 wt% sucrose and the mechanical properties of the constructs were assessed. The Young's modulus value of the porous film was 0.41±0.03 MPa. The Young's modulus of the P(3HO) neat film was 3.7±0.3 MPa. These results show that with a 0.5 % porogen, the stiffness of the material decreases by one order of magnitude. The Young's modulus of the human myocardium is 0.02-0.5 MPa, hence, the stiffness of the P(3HO) porous film matches this range very well. As the lower value of myocardial stiffness is 0.02 MPa, it is possible to further increase the number of porous structures, decreasing the stiffness of the construct. However, after a myocardial infarction, the abrupt loss of myocardium triggers a ventricular remodeling which includes dilatation, hence increasing the load on the infarcted region. Hence we hypothesized that among the range of cardiac patches, the one with a higher stiffness is convenient for myocardial support (Sutton *et al.,* 2000). The tensile strength and elongation at break measured for the porous material was 0.7±0.2 MPa and 447±5 %, respectively. The tensile strength of the P(3HO) neat film was 3.4±0.2 MPa and the elongation at break 299±29 %. With the incorporation of porous structures, the tensile strength of the cardiac patch was closer and elongation at break was a bit higher to that of myocardial structures. As, expected, an increment in the surface roughness was obtained with the incorporation of porous structures. Finally, although no differences were observed in terms of surface wettability and protein adsorption between the neat and porous P(3HO)

films, the % cell proliferation increased 2.5 times as compared to the neat film, when porosity was incorporated.

6.3.2. P(3HO) fibres

The extracellular matrix provides not only structural support to the cells but also regulatory cues for cells assembling into tissues, for growth and communication. As a result, one of the main goals in tissue engineering is to develop a tailored *in vitro* environment that mimics the intricate and organized meshwork of native extracellular matrix. As the extracellular matrix is mainly composed of collagen fibrils, the structure and topography of the fibres were recreated by electrospinning. Electrospinning is a versatile technique which allows the fabrication of nano and micro scale fibres or particles which mimic the extracellular matrix architecture. Different P(3HO) concentrations ranging from 0.2 wt% to 1.2 wt% were used to create electrospun fibres. The results obtained showed an increment in the fibre diameter from 340 nm to 750 nm when the polymer concentration was increased from 0.6 wt% to 1.2 wt% (Table 6.1). These results were in agreement with Boland *et al.,* (2001) who showed a direct relation between polymer concentration and electrospun fibre diameter. When the P(3HO) concentration was 0.5 wt%, both fibres and particles were obtained. Only particles where obtained with 0.2 wt% polymer solution.

In order to find out the most suitable matrix for cells to grow, glass slides were coated with the different fibre sizes obtained. The surface wettability analyses of the samples showed no differences between 750 nm fibres, 700 nm fibres, 630 nm fibres, and 340 nm fibres + particles (Figure 6.9). Smaller water contact angles were obtained with the 580 nm particles than with other fibres or particle diameters, which indicated a more hydrophilic surface. C2C12 myoblast cells were seeded on the electrospun coated slides. The results obtained showed that the fibre diameter has a direct effect on cell adhesion and proliferation, with an increment in cell density with fibre size. In contrast to our results, Chen *et al*., (2007) observed an increment in fibroblast adhesion as a function of decreasing electrospun polycaprolactone fibre diameter from 1051 to 428 nm. Optical microscopy images revealed that the cell's focal adhesions attach to the 750 nm fibres. It has been demonstrated that differences in fibre diameter result in highly significant differences in focal adhesion formation and cell proliferation (Hsia *et al.,* 2011).

It is important to mention that fibre diameter also has a crucial role in controlling the pore diameter of the networks. It has been proven that increasing fibre diameter results in an increase in mean pore radius and hence cellular ingrowth (Eichhorn *et al.,* 2005). Previous findings have shown that nanofibre structures impede cell migration into the scaffolds as they act as a sieve, keeping cells on the surface of the scaffold (Balguid *et al.,* 2009). In order to allow cell migration into the interior of the electrospun fibres and porous structures, different collection times were assessed. The selected collection time was 30 seconds (Figure 6.12 C), the one in which the fibres have covered the full area leaving gaps for the cells to infiltrate. Note that the although some pores are smaller than myocardial cells, they should not impede cell migration as the fibres are lying loosely upon each other and cells can perform amoeboid movements to migrate through the pores by pushing adjacent fibres (Li *et al*., 2002).

6.3.3. P(3HO) cardiac patches

P(3HO) cardiac prototypes were fabricated by modifying the P(3HO) neat and porous films with 750 nm fibres. The surface of the construct was characterized by measuring the water contact angle, surface roughness and protein adsorption. It has been described that the wettability depends on the type of material as well as the surface treatment of the material (Lu *et al*., 1998). Our experiments showed an increment in the surface hydrophobicity when neat cardiac patches were functionalized with fibres. The reason is assumed to be an increase in the roughness of the surface. However, in contrast to our expectations, a decrease in the surface hydrophobicity was observed when porous cardiac patches were functionalized with fibres. The surface roughness of the cardiac patches was 0.90±0.01 µm for neat films with 750 nm fibres and 1.13±0.14 µm for porous films with 750 nm fibres. The surface roughness of the neat P(3HO) film was 0.17 µm and hence with the incorporation of fibrous and porous structures, as expected, it was possible to increase the surface roughness by 6.5 fold. Although it could be expected an increment in the protein adsorption due to the structure of the patches, especially when porous structures were combined with fibres, no significant differences were observed between the different cardiac patches in terms of protein adsorption.

Several reports show the influence of surface wettability, surface roughness and protein adsorption in the cell-biomaterial interaction, however, no general principles that can help in the prediction of cellular behavior by the combination of these parameters are known.

Therefore, cell adhesion and proliferation were assessed. Myoblast (C2Cl2) cell proliferation was analyzed and compared on neat P(3HO) patches, porous patches, neat P(3HO) cardiac patches with 750 nm diameter fibres and porous cardiac patches with 750 nm diameter fibres on their surface. The proliferation observed on these patches were 21.11±1.85 %, 53.83±3.05 %, 41.60±2.40 % and 109.20±1.50 %, respectively, when proliferation observed in tissue culture plates was considered to be 100 %. Results showed that both porous and fibrous structures increased the % cell proliferation due to their higher surface area-to-volume ratio as well as their topographical features that can enhance cellular adhesion and proliferation. A higher cell proliferation was observed when porous structures were incorporated than with fibrous structures. P(3HO) porous films modified with 750 nm fibres resulted in the best matrix for cells to proliferate .

Thus results from this study suggests that the P(3HO) porous cardiac patches functionalized with 750 nm fibres are promising materials to support the infarcted myocardium, due to their mechanical properties and to deliver cells in order to allow efficient tissue regeneration due to their good cell adhesion properties.

CHAPTER 7

Functionalization of PHAs with active molecules

7.1. INTRODUCTION

Cardiac tissue engineering aims to create constructs that can re-establish the structure and function of the infarcted myocardium. The basic strategy of tissue engineering includes the combination of living cells and a biocompatible material that mimics the structure of the extracellular matrix leading to the proliferation and differentiation of the seeded cells (Jawad *et al*., 2008). In addition to the engineered matrix, the cardiac cell microenvironment can be improved by the addition of adhesion, growth, migration or differentiation signals. In this chapter we have focused on the incorporation of protein based active factors capable of inducing vascularisation, modulating cell adhesion, favouring cell migration and differentiation, in the PHA based cardiac patches.

The arginine-glycine-aspartic acid RGD tripeptide sequence is a cell attachment motif recognized by several adhesion receptors (Ruoslahti *et al.,* 1996). Due to the widespread distribution of the RGD peptide, its use in a range of organisms and its high biological effect on cell adhesion, cell behaviour and cell survival, the RGD sequence is one of the most effective active molecule used in tissue engineering (Hersel *et al.*, 2003). In the first part of this chapter, RGD motifs were immobilized on the P(3HO) film surfaces. The immobilization was carried out in two stages. First, the P(3HO) polymer was aminated and films were cast using solvent casting. Then, surface immobilization of the RGD peptide was carried out on the aminated solvent cast films. The presence of RGD motifs on the P(3HO) film surface was confirmed by FTIR, water contact angle studies and SEM.

As cardiac tissue requires high oxygen levels due to the continuous contractile activity of the myocytes, the lack of vasculature in the engineered cardiac patches is the main cause of failure after implantation (Bronzino 2006, Cohen *et al*., 2012). In order to promote angiogenesis and vascularisation, in this work, vascular endothelial growth factor (VEGF) was incorporated into the P(3HO) films (Neufeld *et al*., 1999).

P(3HO) cardiac patches containing the immobilized RGD motifs or VEGF were characterized in terms of the mechanical, thermal and wettability properties. Cell proliferation studies were carried out using C2C12 myoblast cells on modified cardiac patches to determine the effect of RGD and VEGF effects on the biocompatibility of the P(3HO) based cardiac patch.

Finally, as VEGF has a short biological half-life and high tumorigenic potential, a sustained and controlled release is desirable (Faranesh *et al.,* 2004). VEFG can be incorporated into the constructs or engineered and supplemented in microspheres separately for a controlled release. Biocompatible and biodegradable P(3HB) microspheres have shown a high loading efficiency and a controlled release with a high potential to be used in biomedical applications (Francis *et al.,* 2011). In order to create a controlled release system, P(3HB) microspheres containing VEGF were produced from the polymer obtained from the recombinant *B. subtilis pha*C1-pHCMC04 described in Chapter 3.TheVEGF release from P(3HO) cardiac patches and P(3HB) microspheres was measured and compared over a period of a month.

7.2. RESULTS

7.2.1. RGD immobilization

The cell-polymer and cell-cell interactions play a key role in controlling cell adhesion, proliferation, migration and differentiation. Several reports show the role of the RGD peptide in controlling these interactions (Hersel *et al*., 2003, Rezania *et al*., 2008, Yoon *et al*., 2004). In order to improve the properties of the P(3HO) cardiac patches, RGD peptides were immobilized onto the surface of the patch. The RGD peptide immobilization protocol used in this project was adapted from Yoon *et al*., 2003, where RGD motifs were immobilized on PLGA (section 2.2.9.4). Firstly, the carboxylic acid terminal group of P(3HO) was aminated by reacting the polymer with hexaethyleneglycol-diamine. FTIR was carried out to confirm that the amination had occurred as described in Section 2.2.9.4.3. The FTIR spectrum obtained from the modified P(3HO) patch was compared with the neat P(3HO) patch (Figure 7.1). Results show the presence of a band at 3400 cm^{-1}, which corresponds to the N-H bond. Additionally, a band was observed at 1000 cm^{-1} confirming the presence of a C-N bond. These absorbance peaks were missing in the neat patch. This result confirmed that the P(3HO) patch had been successfully aminated.

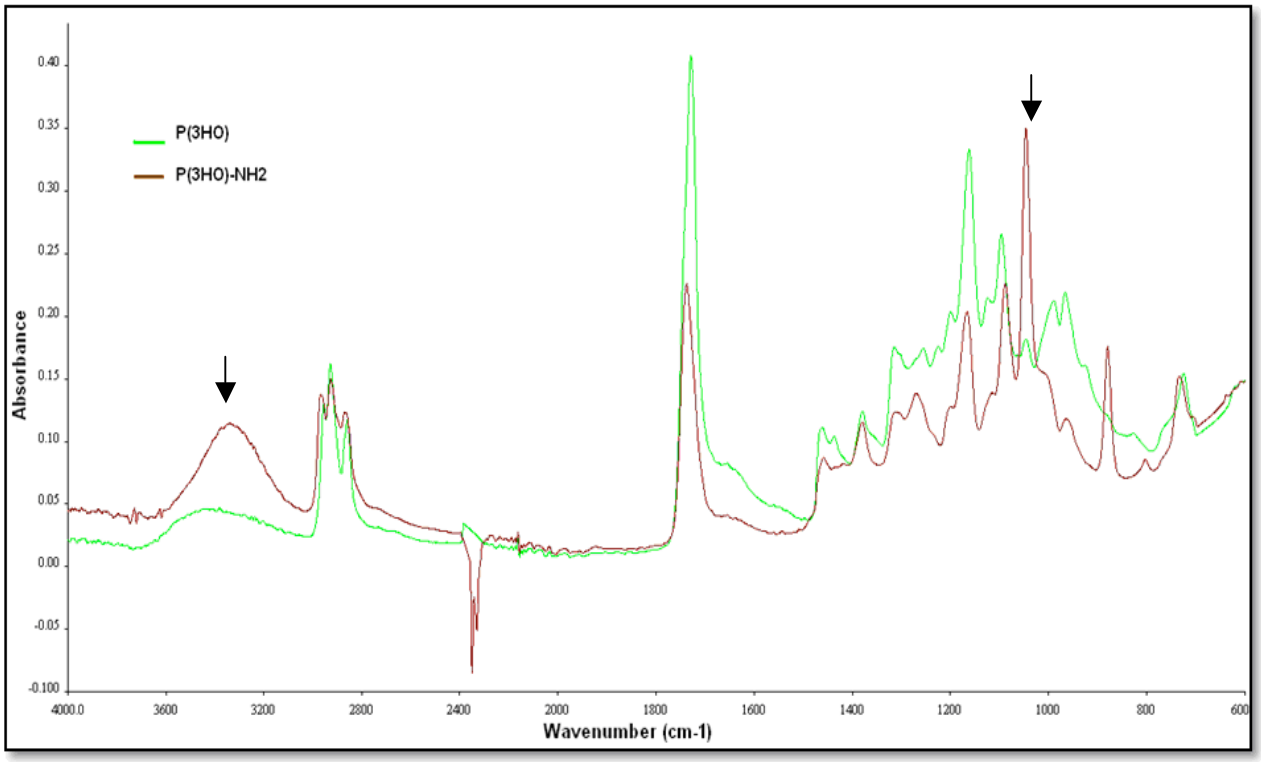

Figure 7.1. FTIR spectra of as synthesized P(3HO) polymer vs. aminated P(3HO) (P(3HO)-NH_2). The arrows at 3400cm^{-1} and 1000 cm^{-1} indicate the N-H and C-N bonds, respectively.

The aminated P(3HO) polymer was blended with P(3HO) 50:50 and films were fabricated by the solvent casting technique. The resultant patches were modified with RGD tripetides on one side of the structure. In order to verify the presence of RGD motifs covalently linked to the membrane, FTIR was carried out according to section 2.2.9.4.3. The FTIR spectra obtained from the RGD immobilized P(3HO) film was compared with the as synthesized P(3HO) film (Figure 7.2). Results showed the presence of a strong band at 1287 cm^{-1} corresponding to the C-N bonds present on the RGD-P(3HO) polymer. Also, other bands were observed at 825 cm^{-1}, 1047 cm^{-1} and 1226 cm^{-1} due to the bend of the N-H bond and the stretch of C-O and C-O-C bonds from the PEG group linked to the structure, respectively. Note that, as expected, the band observed at 3400 cm^{-1}corresponding to the $–NH_2$ functional group in Figure 7.1 was not observed in this case. This is due to the fact that this terminal amine group would have reacted with the RGD sequence and hence the new terminal group is the carboxylic group from the RGD peptide.

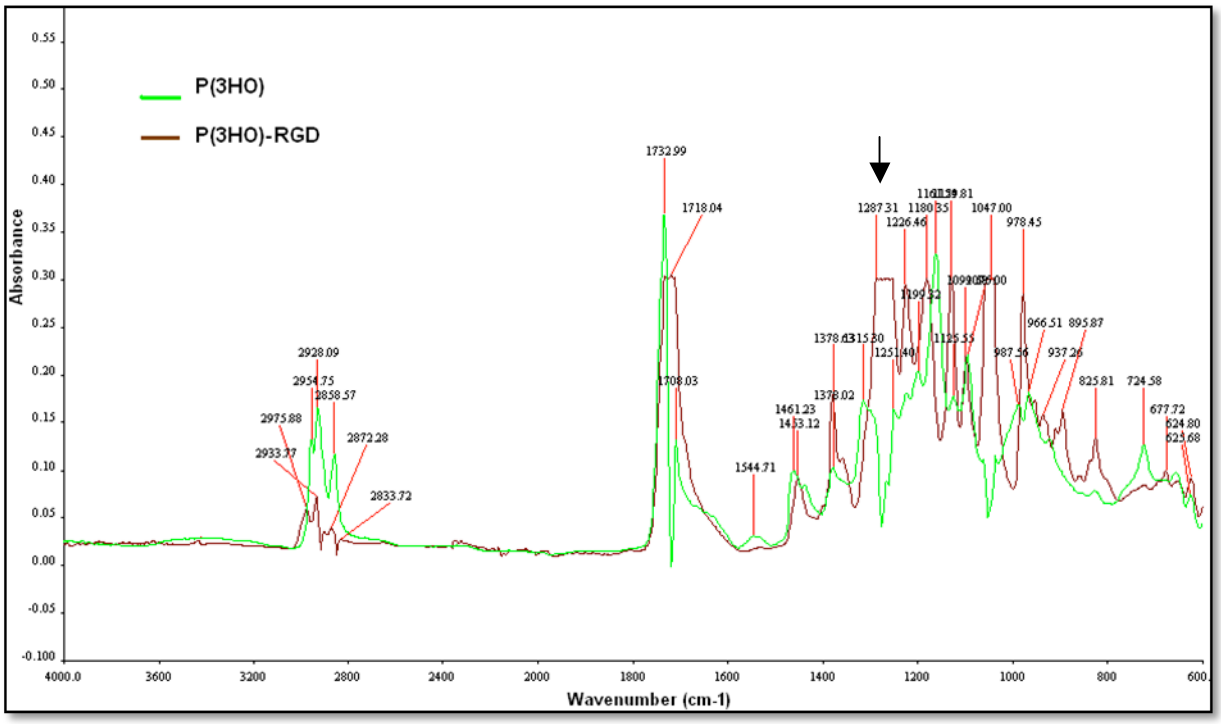

Figure 7.2. FTIR spectra of P(3HO) polymer vs. P(3HO)-RGD. The arrow at 1200 cm^{-1} indicates the C-N bond.

Several reports have shown the relation between RGD immobilization and surface wettability. It was observed that the incorporation of RGD structures on the surface of the

polymer has a direct effect in decreasing the hydrophobicity of the structure. In order to confirm the presence of RGD motifs linked to P(3HO) cardiac patches the surface wettability of the cardiac patches was analysed according to section 2.2.9.4.3 The water contact angle obtained for the P(3HO)-RGD film was 93.44±0.09°. P(3HO) water contact angle was 101.12±0.82º (section 5.2.1.3). Our results show a significant decrease in the water contact angle which indirectly confirms the presence of the RGD immobilized peptide (Figure 7.3).

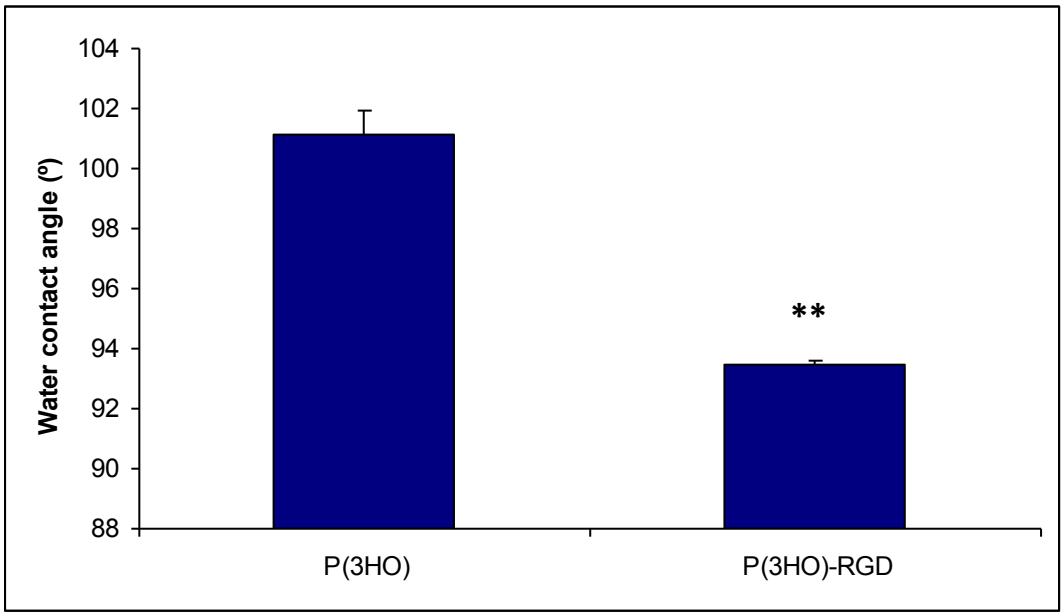

Figure 7.3. Surface wettability properties of P(3HO) vs. P(3HO)-RGD cardiac patches (n=3; error bars=±SD).The data were compared using t-test and the differences were considered significant when $^{**}p < 0.01$.

As described previously, mechanical properties of the cardiac patch play an essential role in the patch function supporting the heart during regeneration. In order to study the possible influence of the P(3HO) modification on the patch mechanical properties, Dynamic mechanical analysis was carried out on P(3HO)-RGD cardiac patches according to section 2.2.10.1. The Young's modulus of the RGD modified film was 3.9 MPa. Section 5.2.1.2 shows that P(3HO) Young's modulus was 3.7±0.3 MPa, hence no differences were observed in terms of the material stiffness after the RGD modification. The tensile strength for P(3HO)-RGD was 0.66 MPa and elongation at break 426.53%. The tensile strength and elongation at break for P(3HO) was 3.4±0.2MPa and 299±29 %, respectively. These results show a decrease by 19% in tensile strength and an increase by 42% in elongation at break after the RGD modification. In order to visualize the surface of the modified cardiac patches,

SEM was carried out as described in section 2.2.10.4. Figure 7.4 shows the SEM images of P(3HO)-RGD cardiac patches. These pictures revealed that the incorporation of RGD peptides structures changed the surface morphology by introducing a rough topography to the surface.

A)

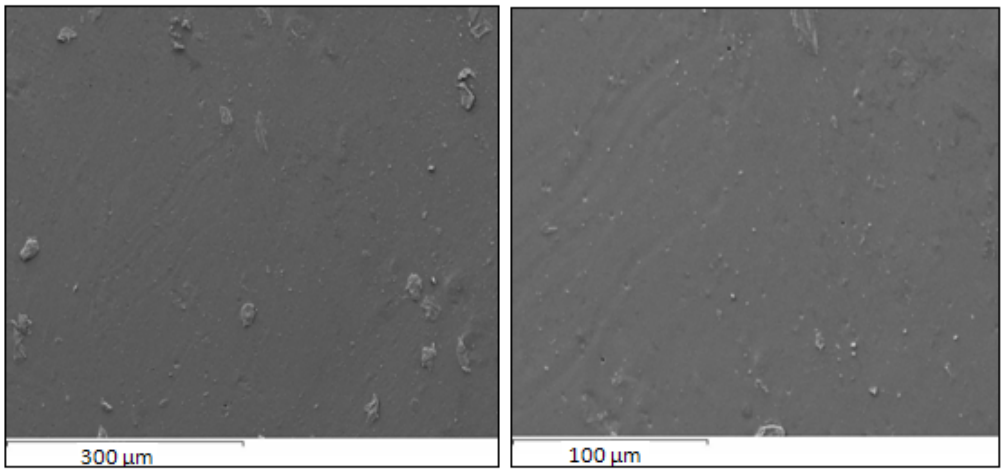

B)

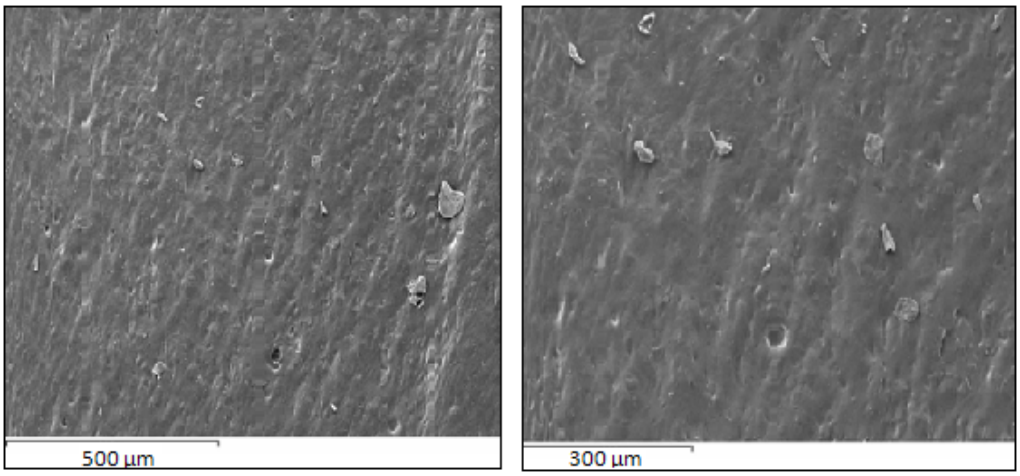

Figure 7.4. SEM images of A) neat and B) RGD immobilized P(3HO) film at different magnifications showing the rough surface of the RGD modified cardiac patches compared to neat films.

7.2.2. VEGF incorporation in P(3HO) films

As vascularisation and angiogenesis are key factors in cardiac tissue engineering, VEGF was incorporated into the P(3HO) films. The mechanical properties of the resulting cardiac patches were measured as described in section 2.2.10.1. The Young's modulus obtained for the VEGF modified film was 6.82 MPa, the tensile strength was 0.56 MPa and the elongation at break was 449.32%. The tensile strength and elongation at break for P(3HO) was 3.4±0.2 MPa and 299±29 %, respectively. These results show a decrease in tensile strength by 17% and an increase by 50% in elongation at break after the VEGF incorporation. The surface of the VEGF modified cardiac patches was analysed by water contact angle and SEM. The water contact angle of P(3HO) cardiac patches containing VEGF factor incorporated was 102.49 ± 1.40°. P(3HO) water contact angle was 101.1±0.8 ° (section 5.2.1.3). These results show no differences in the surface wettability with the VEGF incorporation. The surface of the cardiac patches was visualized by SEM (Figure 7.5). SEM images show qualitatively a slight increment in the surface roughness compared to P(3HO) plain films.

A)

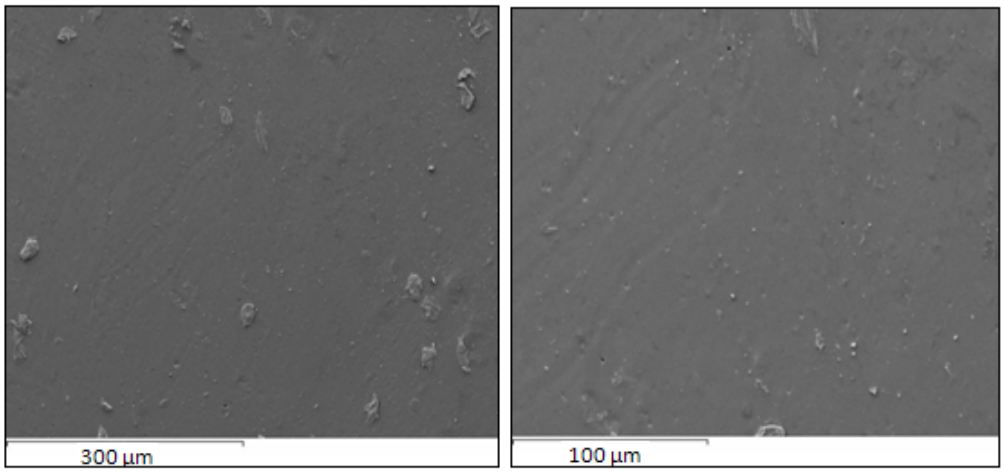

Continues on the following page

B)

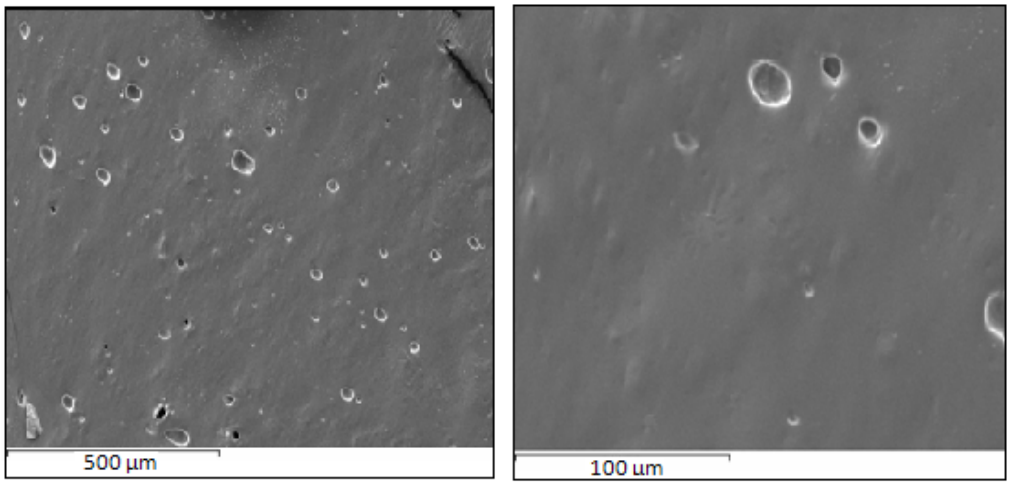

Figure 7.5.SEM images of A) P(3HO) neat film and B) P(3HO) containing VEGF at different magnifications showing the surface of the films.

7.2.3. Cell proliferation

In this part of the study, the effect of P(3HO)-RGD immobilized cardiac patches and P(3HO)-VEGF on cell proliferation as compared to the neat polymer patch was studied. To this end, C2C12 myoblast cells were seeded on P(3HO) modified cardiac patches according to section 2.2.12.3.3 and cell proliferation was measured by the MTT colorimetric assay, as described in section 2.2.11.3.4. Figure 7.6 shows the % cell proliferation on P(3HO), P(3HO)-VEGF, P(3HO)-RGD and P(3HO)-VEGF+RGD cardiac patches when proliferation observed on tissue culture plastic was considered to be 100%. The % cell proliferation on P(3HO) films was 21.11±5.29 %. A significant increase in cell proliferation was observed when VEGF and RGD were incorporated into the P(3HO) cardiac patches. However, a higher cell proliferation was achieved with VEGF. A synergistic effect was observed when both VEGF and RGD were incorporated together, showing a highly significant effect on cell proliferation.

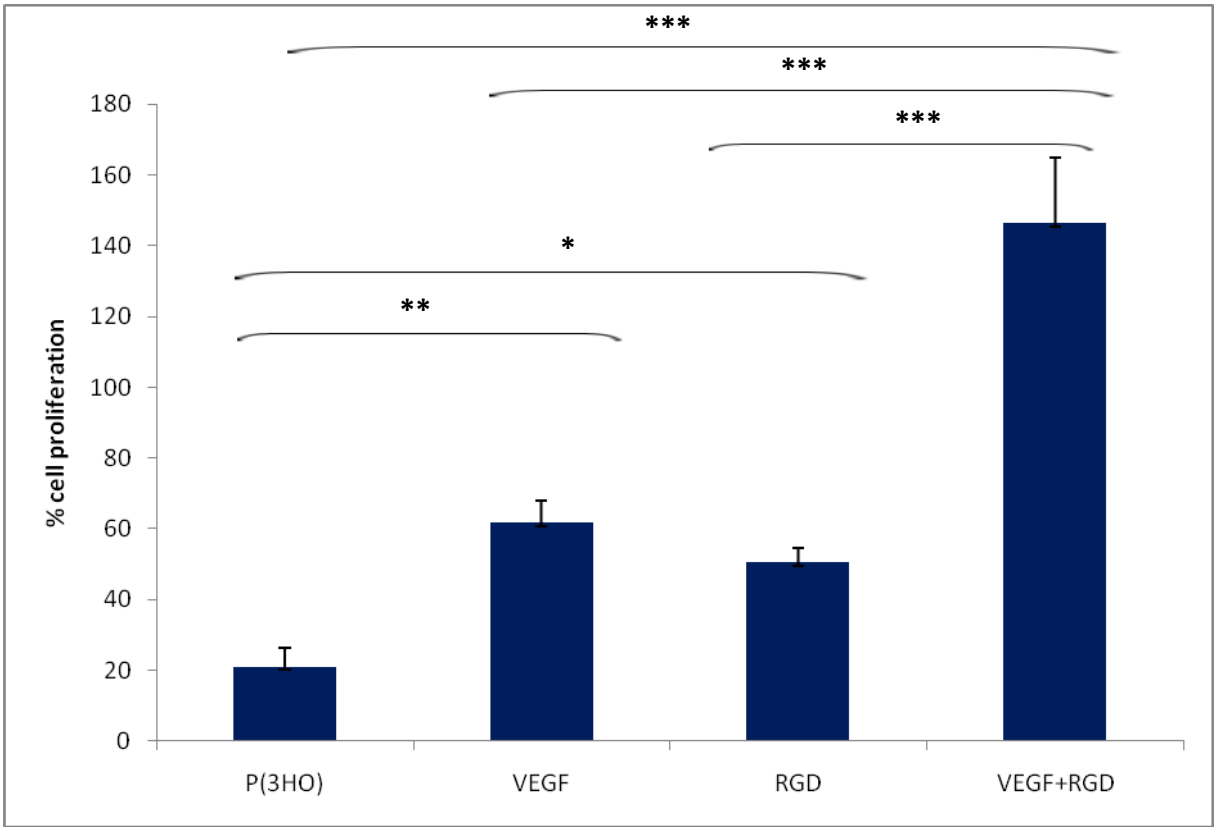

Figure 7.6. The % cell proliferation of C2C12 cell line at 24 hr on P(3HO), VEGF, RGD and VEGF+RGD modified P(3HO) patches (n=4; error bars=±SD).The data were compared using ANOVA and the differences were considered significant when *p<0.05,**p<0.01 and ***p<0.001.

7.2.4. VEGF encapsulation in P(3HB) microspheres

VEGF was encapsulated in P(3HB) microspheres anticipating that this approach could lead to localised and controlled delivery. P(3HB) microspheres were fabricated according to section 2.2.12.1. Fabricated microspheres containing VEGF were visualized with SEM. Figure 7.7 shows the obtained images. SEM images reveal the spherical shape with a smooth surface morphology.The average size of the P(3HB) fabricated microspheres was 127.69±16.41 µm. As microsphere porosity plays an important role in determining the encapsulation efficiency and release kinetics, the porosity of the microspheres were determined using equation 2.4 described in section 2.2.12.2 (Cai *et al*., 2013). The porosity of the microspheres was calculated to be 85±13 %.

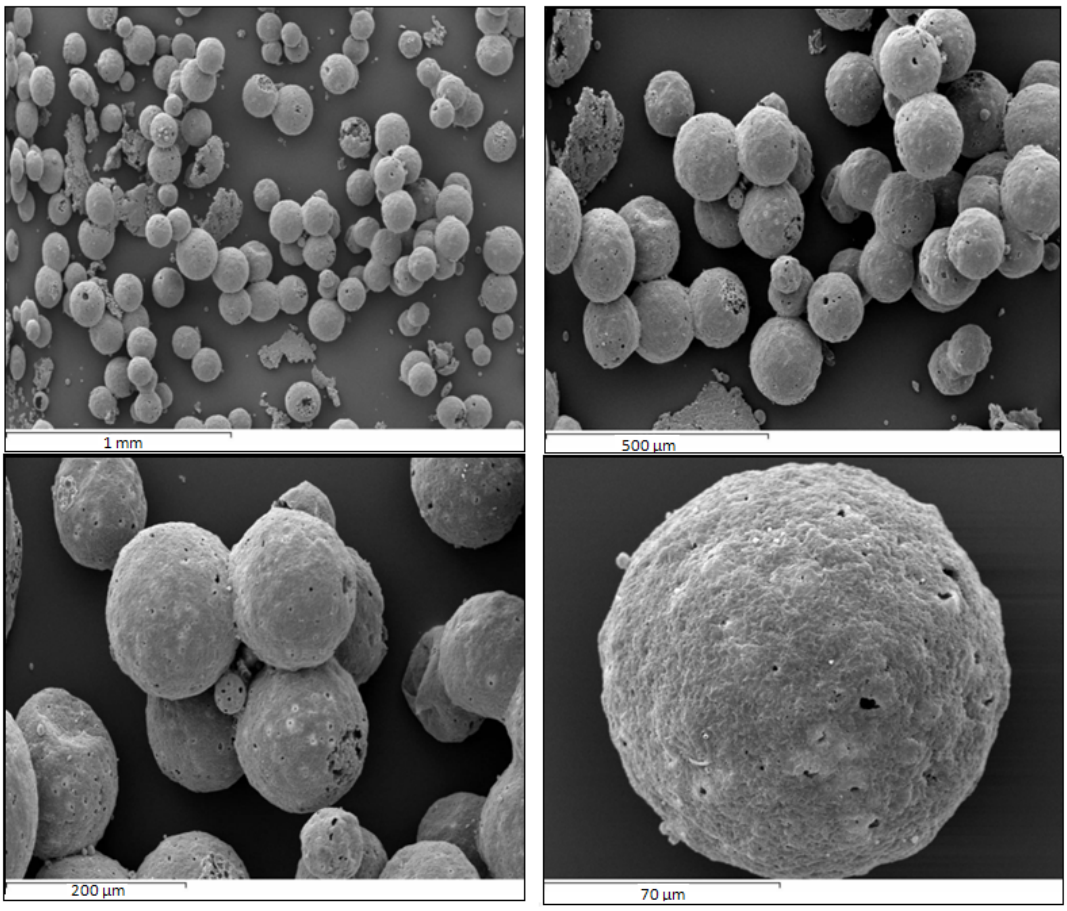

Figure 7.7.SEM images of P(3HB) microspheres, containing VEGF, at different magnifications showing the spherical and smooth surface of the microspheres.

In order to confirm drug encapsulation and possible drug-polymer interactions, FTIR and DSC (described in section 2.2.12.4) were carried out. Unloaded microspheres were used as a negative control. The FTIR spectrum for VEGF loaded and unloaded microspheres are shown in Figure 7.8. The appearance of a band at 2978 cm^{-1} corresponding to the benzene ring of the tyrosine and phenylalanine aminoacids present in VEGF protein, indicate the presence of VEGF. No other differences were observed between the spectra of VEGF loaded and unloaded microspheres which indicated that either no covalent interaction had occurred between P(3HO) and VEGF or the amount of VEGF incorporated was too low to be observed using FTIR.

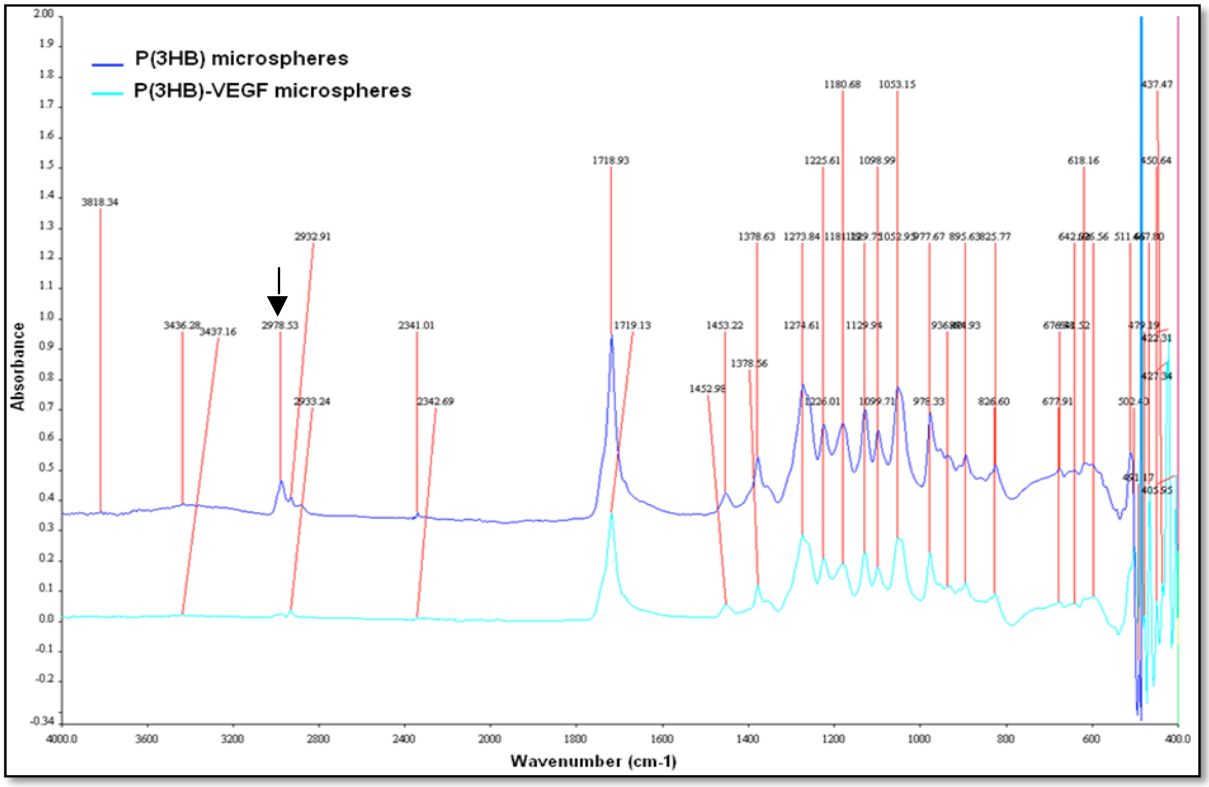

Figure 7.8. FTIR spectra of P(3HB) unloaded microspheres vs. VEGF loaded P(3HB) microspheres. The arrow at 2978 cm^{-1} indicates the aromatic groups present in the VEGF protein.

The DSC thermograms for unloaded and VEGF loaded micrspheres are shown in Figure 7.9 (A) and (B), respectively. The thermal properties of P(3HB) crude polymer obtained from the recombinant *B. subtilis pha*C1-pHCMC04 described in Chapter 3 were determined. The T_m and T_c values were 169.81ºC and 119.51ºC, respectively. For the unloaded microspheres the T_m was 167.07 ºC and T_c was 62.90 ºC. Finally, for VEGF loaded microspheres the T_m was 157.74 ºC and T_c was 92.33 ºC. These results showed a shift in the T_m towards lower temperature with crude P(3HB) > unloaded microspheres > VEGF loaded microspheres. On the other hand, a decrease in T_c was also observed when comparing crude polymer with unloaded and loaded microspheres. Note that VEGF does not appear as a separate peak and this might be due to the low amount of protein compared to the polymer. However, a change in the T_m and T_c values between the loaded and unloaded microspheres indicates the presence of VEGF in the VEGF loaded microspheres. Also, in the next section VEGF release was quantitatively measured using ELISA from the VEGF loaded microspheres confirming the successful encapsulation of VEGF.

A)

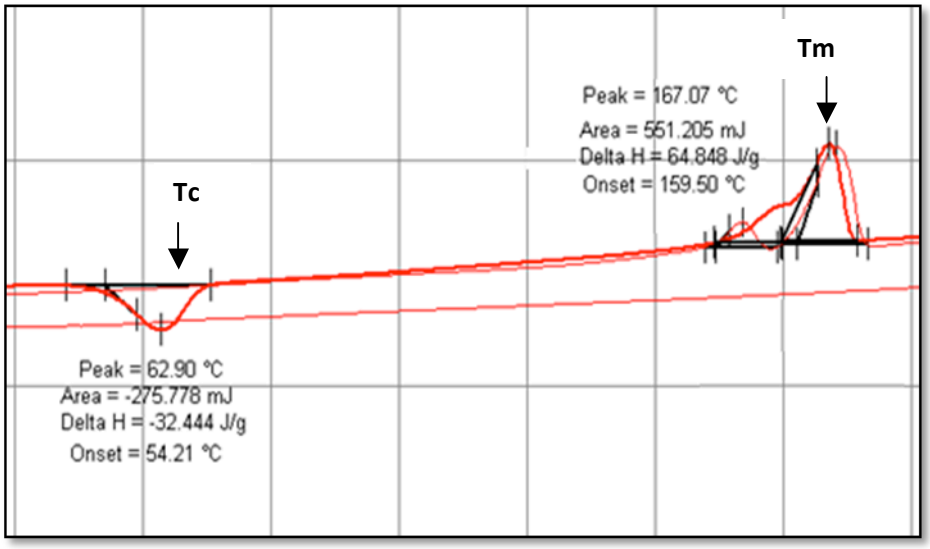

B)

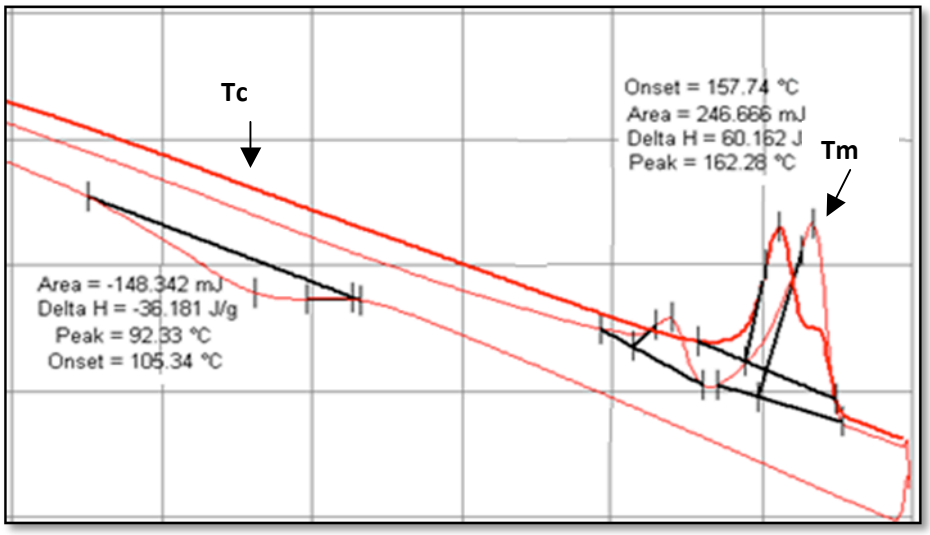

Figure 7.9. Thermal profile of (A) unloaded P(3HB) microspheres and (B) VEGF loaded P(3HB) microspheres. The arrows in the pictures indicate the Tm and Tc obtained.

7.2.5. VEGF release

The cumulative *in vitro* release of VEGF from P(3HB) microspheres and P(3HO) cardiac patches was studied over 30 days, as described in section 2.2.12.5. The amount of VEGF released in the medium was measured using the Invitrogen® VEGF human ELISA kit. The cumulative VEGF release was normalized against the total experimental amount of drug

loaded within the microsphere. The encapsulation efficiency was calculated using equation 2.5 described in section 2.2.12.3.1. The obtained value was EE%= 34.98 %. The release profile is shown in Figure 7.10. Our results showed a biphasic VEGF release for both P(3HB) microspheres and P(3HO) cardiac patches with an initial burst release followed by a period of sustained release. Significant differences were observed at days 1 and 3 between P(3HB) microspheres and P(3HO) patches. The VEGF released from the microspheres was 10.78±1.79 % and 21.71±1.95 % on day 1 and 3 respectively, whereas from the cardiac patches was 21.92±1.58 % and 30.02±1.78 % on day 1 and day 3 respectively. Note that in addition, both in the cardiac patches and the microspheres, the VEGF release kinetics changed at day 7, showing a slower release rate.

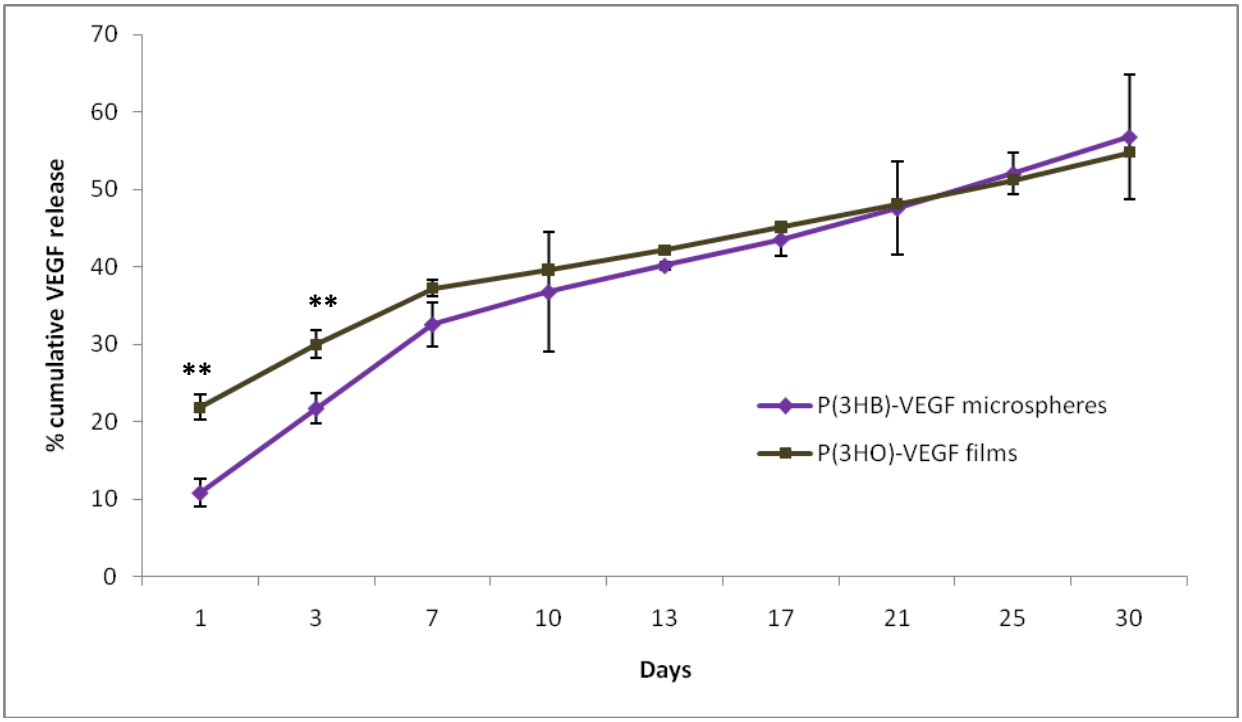

Figure 7.10. Release profile of VEGF from P(3HB) microspheres and P(3HO) cardiac patches (n = 3; error bars=±SD).

7.3. DISCUSSION

7.3.1. RGD immobilization

The fabrication of biodegradable constructs in tissue engineering is essential to provide a matrix for cell proliferation, migration and differentiation and to act as a support for the organ during regeneration. In addition to the biomaterial matrix, the control of cardiac cell environment can be enhanced by the design of biomaterials that provide adhesion, growth, migration or differentiation signals. In this chapter, the cardiac patch was further functionalised via the incorporation of active factors. It has been observed that proteins that contain the Arg-Gly-Asp (RGD) sequence are recognized by several different integrins in their adhesion protein ligands (Ruoslahti *et al*., 1996). In order to allow efficient host cell recruitment and adhesion, in the first part of the chapter RGD motifs were immobilized on the films. For the RGD immobilization a series of chemical reactions were carried out to incorporate active amino terminal structures on the carboxyl terminal end of the P(3HO) molecule, followed by the reaction of the terminal amine with the RGD sequence. The incorporation of the amino terminal group into the P(3HO) molecule was carried out through the addition of hexaethyleneglycol-diamine to the P(3HO) carboxylic acid end. The incorporation of the hexaethyleneglycol-diamine group to the P(3HO) was confirmed by FTIR. The appearance of a band at 3400 cm^{-1} which corresponded to the N-H bond and the appearance of a band at 1000 cm^{-1} showing the presence of a C-N bond suggested the presence of the hexaethyleneglycol-diamine in the P(3HO) film. In a second step, the covalent linkage of the RGD peptide to the hexaethyleneglycol-diamine present on the P(3HO) film was studied by FTIR. Results showed the presence of a strong band at 1200 cm^{-1} corresponding to the C-N bonds that should be present in the RGD-P(3HO) polymer due to the linkage of the hexaethyleneglycol-diamine with P(3HO) and with the RGD peptide. In addition, the disappearance of the band corresponding to the NH_2 primary amine group further confirmed the formation of the RGD-hexaethyleneglycol-diamine-P(3HO) linkage.

With the incorporation of RGD structures in the P(3HO) cardiac patches, an increment in the hydrophilicity of the surface was expected (Lin *et al*., 1992, Lin *et al.,* 1994). As polar molecules interact better with water than non-polar molecules, an increment in the molecular hydrophilicity is usually detected when RGD motifs are immobilized (Lin *et al*., 1992, Lin *et al*., 1994). The water contact angle of the P(3HO)-RGD immobilized cardiac patches was

93.44±0.09º. P(3HO) water contact angle was 101.1±0.8 º (section 5.2.1.3). These results thus showed a significant decrease in the water contact angle. Hence, the expected increase in the surface hydrophilicity after the modification with RGD peptides reconfirmed the incorporation of the RGD peptide onto the P(3HO) film.

In order to study any possible effect of the RGD immobilized peptides on the mechanical properties of the P(3HO) cardiac patches, dynamic mechanical analysis under static conditions was carried out. No differences were observed in terms of the polymer stiffness after the RGD incorporation. However, a decrease in the tensile strength was observed with the RGD immobilization. As the linkage of the RGD motifs to the surface of the P(3HO) cardiac patches were carried out through hexaethyleneglycol-diamine molecules incorporated to the polymer, differences in the mechanical properties can be attributed to the presence of these molecules which perhaps embedded themselves between the chains of the polymer, spacing them apart. In agreement with our results, previous reports have shown a decrease in the tensile strength and an increment in the elongation at break when polyethylene-glycol was incorporated into cellulose acetate films as a plasticizer (Yuan *et al*., 2001). Finally, SEM images show an increment in the surface roughness after the RGD modification.

7.3.2. VEGF incorporation

As vascularisation is crucial in cardiac constructs, VEGF was incorporated in order to assist cell growth and tissue vascularisation. Mechanical properties of the P(3HO)-VEGF cardiac patches were determined and compared with P(3HO) films. Similar stiffness was obtained after the VEGF incorporation. However, a decrease in the tensile strength and an increment in the elongation at break were observed with VEGF. It has been observed that the addition of different molecules on a polymer reduce the molecular weight of the material and a decrease in the molecular weight is directly related with a decrease in tensile strength (Barron 2013, Odian 1991). The elongation at break may be influenced by water used as VEGF solvent, which may have decreased the interaction of the polymer chains when the polymer was mixed with the VEGF solution, making them more stretched due to interactions of water with the hydrogen bonds of the polymer (Wang *et al.,* 2005). Although an increment in the surface hydrophilicity can be expected with the incorporation of VEGF molecules, due to an increment in the surface polarity, no significant differences were observed in terms of the surface wettability after the VEGF incorporation. The reason of this observation can be related to the amount of VEGF incorporated, which was too low to have an effect on the

surface wettability. SEM images show a slight increment in the surface roughness in P(3HO) VEGF cardiac patches. Surface roughness studies should be carried out for a quantitave analysis.

7.3.3. *In vitro* cell proliferation in P(3HO) cardiac patches containing VEGF and RGD peptide

C2C12 myoblast cells were seeded on P(3HO) cardiac patches containing VEGF, P(3HO) cardiac patches containing RGD and P(3HO) cardiac patches containing both VEGF and RGD. Cell proliferation was evaluated at 24 hr with the MTT colorimetric assay. Results showed a significant increment in the cell proliferation when VEGF or RGD were incorporated in comparison to P(3HO) films. In terms of RGD, these results suggested that as previously reported in literature, the increased cell-polymer interactions play a pivotal role in simulating cell proliferation (Neff *et al.,* 1999). Yoon *et al.,* (2004) showed a significant increment in cell attachment when bone marrow stem cells isolated from rat were seeded on PLGA films immobilized with RGD motifs. On the other hand, VEGF has also been shown to have a positive effect in cell proliferation. These results are in agreement with previous reports that show the presence of VEGF receptors, which were thought to be present exclusively in endothelial cells, in a number of different cell types (Couper *et al*., 1997, Pancholi *et al*., 2000, Shen *et al*., 1993). Sipahigil *et al.,* (2012) showed a significant increment in L-929 cell line proliferation with VEGF incorporationinpoly(lactic-co-glycolic acid) microspheresand a direct relation between VEGF concentration and % cell proliferation. Additionally, our results showed a slightly higher increment in cell proliferation with VEGF than with RGD incorporation. However, from these results it is not possible to conclude if the higher effect on cell proliferation with VEGF is due to the difference in the actual effects of this factor on the cells or due to the different amounts of VEGF and RGD used in this study as the VEGF amount incorporated in each film was 2μg and in the case of the RGD, each film was reacted with a 1.5 nm/ml RGD solution. Finally, when both VEGF and RGD were incorporated, a synergetic effect was observed, with an increment in cell proliferation by 7 times with respect to P(3HO) films. These results suggested that there is no interference of VEGF with RGD proteins and, hence, both can be incorporated together to achieve better conditions that mimic the extracellular matrix structure in the tissue encouraging cell attachment and proliferation.

7.3.4. VEGF encapsulation in P(3HB) microspheres

Several advantages have been described with the development of controlled release systems including temporal and spatial presentation of the active factor in the target tissue, protection of the active factor from physiological degradation or elimination and patient compliance (Siegel and Rathbone, 2012). In order to achieve a controlled release of VEGF, VEGF was encapsulated in P(3HB) microspheres. SEM images confirmed the spherical shape of the constructs with a smooth surface morphology and with an average diameter of 127.69±16.41 μm. The importance of porous microspheres is widely reported in tissue engineering. A highly porous structure with interconnected pores is crucial to achieve sufficient drug absorption and drug release kinetics, large specific surface area, and low density (Cai *et al*., 2013). In this work, the porosity of the microspheres was found to be 85±13 %, showing a highly porous structure. It is widely known that differences in drug release between different constructs were not only attributed to the matrix porosity, but also to the polymer composition, the solubility of the drug in the media and amount of drug loaded (Gould *et al.,* 1987, Dash *et al.,* 1992). As a result, the optimal porosity should be determined in each case by drug release studies. FTIR and DSC analysis were carried out to confirm the presence of the VEGF in the microspheres and to study possible VEGF–polymer interactions. The FTIR spectra showed the appearance of only one band at 2978 cm^{-1} that was not present in the unloaded microspheres. This band showed the presence of the aromatic group of tyrosine and phenylalanine present in VEGF, confirming the presence of VEGF in the microspheres. Additionally, FTIR spectral studies showed no other differences between VEGF loaded and unloaded microspheres suggesting no significant covalent interactions between the drug and the polymer or the relative amount of VEGF being too low to be detected by FTIR. DSC studies showed a reduction of 10ºC in the melting temperature for VEGF loaded microspheres with respect to unloaded microspheres similar to the observations previously made by Bidone *et al.*, (2009) with the incorporation of ibuprofen in P(3HB):mPEG-PLA blend microspheres. Our results indicate that the crystalline structure of the polymer was affected in the presence of the VEGF. No separate peaks were observed for the active factor, which might be due to the low concentration of the VEGF in the sample with respect to the polymer.

7.3.5. VEGF release

The drug release profiles of VEGF were measure during VEGF loaded P(3HO) cardiac patches and P(3HB) microspheres for a period of 30 days. The results obtained showed a biphasic VEGF release profile for both P(3HB) microspheres and P(3HO) film, with an initial burst release followed by controlled release. However, the results showed that the P(3HB) microsphere drug release, during the initial phase, was half of that obtained using the P(3HO) films. These results indicated that a better initial controlled release is obtained with P(3HB) microspheres. Note that due to the fact that the structure of the constructs and the nature of the polymer used are different, the differences in the release profile must be attributed to both these factors. However, due to the more crystalline structure of P(3HB), lower degradations rates leading to lower drug release rates are expected, as compared to P(3HO). Hence, the more controlled release in microspheres cannot be attributed only to the structure of the constructs due to the different nature of the polymer. Although differences in the % cumulative release were observed in the P(3HB) microspheres and P(3HO) cardiac patches, at day 1 and 3, similar VEGF release rates were obtained from day seven until day 30. On day 30 only 50 % of the drug was released in both microspheres and cardiac patches indicating a sustained drug release during longer periods than 30 days as is suggested by the slope pendant, an advantage for long term release. Sipahigil *et al.,* (2012) have worked on VEGF encapsulation in PLGA microspheres. A similar release profile was obtained in P(3HB) microspheres with an initial burst release of 10 %, following by a controlled release. However, for PLGA microspheres at the end of 30 days, the cumulative release achieved was around 75 %. In this study, P(3HB) microspheres showed a slower release rate than PLGA microspheres which can be attributed to differences in the VEGF-polymer interaction and slower degradation times of PHAs as compared to PLGA that allow drug release for longer periods of time.

A sustained release of VEGF over a 30 day period is crucial for because of a short biological half-life of VEGF and its high tumorigenic potential. This was successfully achieved with both P(3HB) microspheres and P(3HO) cardiac patches with a more controlled initial burst release in microspheres (Faranesh *et al.,* 2004). In conclusion, functionalised patches containing RGD and VEGF proteins can create a perfect microenvironment that would induce vascularization and improve cell-matrix and cell-cell interactions to promote the assembly of a functional heart tissue and enhance the therapeutic effectiveness of cardiac patches.

CHAPTER 8

Conclusions and future work

8.1. CONCLUSIONS

In the first part of this study we investigated the *pha*C1 gene expression from *P. mendocina* in *B. subtilis 1604*. The *B. subtilis 1604-pha*C1 recombinant strain showed PHA accumulation in Ramsay media, when sucrose was used as a sole carbon source. *B. subtilis* wild type and *B. subtilis* containing the pHCMC04 vector with no *pha*C1 insert were used as controls. Results showed that PHA accumulation in *B. subtilis* wild type and *B. subtilis* containing the vector with no insert was lower than 3% DCW. In contrast, PHA accumulation in *B. subtilis* containing the *pha*C1 gene from *P. mendocina*, was more than 32 %DCW. These results confirmed the role of the *pha*C1 gene in PHA accumulation in the recombinant *B. subtilis*. The chemical characterization of the produced polymer was carried out showing the presence of the P(3HB) homopolymer in both the controls and the recombinant strain. In order to understand the substrate preference of the *pha*C1 encoded PHA synthase from *P. mendocina*, when sucrose was used as the carbon source, wild type *P. mendocina* was grown in MSM media with sucrose as the carbon source. In contrast to results obtained with other *Pseudomonas* strains, where mcl-copolymers were accumulated, *P. mendocina* showed the presence of the scl-mcl-PHA copolymer, P(3HB-co-HO). Although it is not possible to observe the sole effect of the *pha*C1 gene due to the presence of other genes related with PHA metabolism, this result showed the capability of the *pha*C1 encoded PHA synthase from *P. mendocina* to utilize coenzyme A thioesters of scl- and mcl-3-hydroxyalkanoates when sucrose was used as the carbon source. As previously described, the particular pathway used for PHA production was found to depend on the particular metabolic pathways that are operating in a particular microorganism and the carbon source provided. Additionally, the synthesis of mcl-3-hydroxyacyl-CoA units can occur mainly by two different pathways, one involving with the fatty acid degradation pathway from fatty acids and other involved with the fatty acid biosynthetic pathway from carbohydrates (Kim *et al.,* 2007, Doi *et al*., 1990, Poirier *et al*., 1995, Steinbüchel *et al*., 1991). When the recombinant *B. subtilis* strain was growth on sucrose, mcl-PHA production was expected to occur via the fatty acid biosynthetic pathway. However, as no mcl-PHAs were obtained with sucrose as the carbon source, the recombinant *B. subtilis* was grown in a range of fatty acids to test the capability of the strain to utilize mcl-3-hydroxyacyl-CoA monomers for mcl-PHA production using the fatty acid degradation pathway. In this case PHA production was only observed when pentanoic, hexanoic and heptanoic acids were used and the polymer produced was poly(3-

hydroxybutanoate-co-3-hydroxyvalerate), P(3HB-co-3HV), copolymer in all the three cases. As previously reported by Valappil *et al.*, (2007) from the Gram-positive genera, only *Corynebacterium*, *Nocardia* and *Rhodococcus* can naturally synthesize this commercially important co-polymer P(3HB-co-3HV) from simple carbon sources such as glucose (Haywood *et al*., 1991, Alvarez *et al*., 2000). In this case, incorporation of the *pha*C1 gene from *P. mendocina* to *B. subtilis* allowed the strain to synthesize LPS-free P(3HB-co-3HV) copolymer a useful process. However, no mcl-PHA production was observed. Multiple sequence alignment showed certain amino acid differences in the core region of the *pha*C1 encoded protein sequence from *P. mendocina*, which were otherwise conserved in other mcl-PHA producers such as the *P. aeruginosa*, *P. putida* and *P. oleovorans*. These differences may explain the different outcomes observed. Our results, however, showed the capability of a Gram positive GRAS organism, *B. subtilis*, to express a gene from a Gram negative bacterium, i.e. *Pseudomonas mendocina,* and the low specificity of the *pha*C1encoded PHA synthase from *P. mendocina*, which can utilize both mcl- and scl-3-hydroaxyl CoA units for PHA production.

As no P(3HO) was obtained from the recombinant strain, for this project, P(3HO) was produced using wild type *P. mendocina* and rigorously purified by sequential washing with acetone, ethanol, and methanol. Rai *et al*., (2011a) showed that an effective LPS removal was observed after strict purification steps, achieving 0.35 EU/mL, which complies with the endotoxin requirements of the FDA for biomaterials to be used for biomedical applications (Kato *et al*., 1996). P(3HO) production by *P. mendocina* was optimized in 2 L bioreactors. Four conditions with different carbon nitrogen ratios, and pH were tested. The highest PHA yields were obtained when pH 7.15, carbon/nitrogen 20:1 and stirrer speed of 200 rpm was used. Scaling-up studies were carried out for P(3HO) production in 20 L and 72 L bioreactors, based on the constant oxygen transfer method. The highest PHA yield (% DCW) was 26.84±0.35 for the 2 L bioreactor, 23.17±1.47 for the 20 L bioreactor and 13.80±2.82 for the 72 L bioreactor. Comparable results obtained from both 2L and 20L bioreactors suggested that it is possible to scale-up PHA production from 2 L to 20 L bioreactors based on a constant oxygen transfer. Considerably lower values of PHA yield was obtained with the 72 L bioreactor, suggesting that other parameters needed to be considered at this scale, such as specific power input or superficial air velocity, which cannot be maintained when k_La is maintained.

The purified P(3HO) was studied as a potential material for cardiac tissue engineering applications. In a first experiment, fresh ventricular cardiomyocytes from adult rats were seeded on P(3HO) films and the cell viability was compared with that on tissue culture plastic. Results showed a slightly higher viability on the polymer than in the control and confirmed the non-toxic nature and good cardiomyocyte adhesive property of the P(3HO) surface. In the following experiment, the effect of P(3HO) on cardiomyocyte contraction was studied using a range of frequencies of electrical impulses and calcium concentrations. The results obtained showed that the polymer did not reduce the effect of frequency or calcium on cardiomyocyte contraction when compared to the control. Moreover, the negative effect on the contraction performance with increment in electrical impulse frequency usually observed, was not observed with P(3HO). Results from these experiments confirmed that P(3HO) was a potential material to be used as an extracellular matrix in cardiac tissue engineering applications.

It is widely accepted that the most promising materials that will allow efficient beating of the heart and proper matrix for new cardiac tissue regeneration will be the materials that most resemble the native myocardium. For this reason P(3HO) engineered constructs that attempt to mimic cardiac tissue were produced. In a first approach, 5%wt P(3HO) films were fabricated by solvent casting. The films were studied in terms of mechanical, thermal and surface studies. Due to the contractile function of the heart, one of the pivotal factors that will dictate the success of a material in tissue engineering applications is the mechanical properties of the engineered construct. As previously described, the mechanical properties of myocardium are as follows: Young's modulus 0.02-0.5 MPa, tensile strength 3-15 KPa, and elongation at break between 100-300 % (Nagueh *et al*., 2004 and Watanabe *et al*., 2006). The stiffness of the P(3HO) film was 3.7±0.3 MPa, tensile strength 3.4±0.2 MPa and elongation at break 299±3 %. In order to reduce the stiffness and tensile strength, to provide more structural space for cell infiltration and to allow the formation of a three dimensional structure by permitting cell ingrowth, P(3HO) porous films were created by solvent cast particle leaching using 0.5% sucrose particles ranging from 250-300 μm diameter as the porogen. The stiffness of the porous film achieved with 0.5 % sucrose particles was 0.41±0.03 MPa, tensile strength 0.7±0.2 MPa and elongation at break was 447±5 %. In this case, the desirable stiffness was achieved, the tensile strength was closer to myocardial structures and elongation at break was a bit higher than plain P(3HO) films, when porous structures were incorporated. Although the tensile strength was still higher than myocardial

structures, this may have a positive effect as it would prevent negative myocardial remodelling. The comparison of the mechanical properties of the P(3HO) film with most studied materials which is summarised in Table 1.1 (Chapter 1) indicates that (P3HO) porous film is the most promising candidate from the mechanical compatibility point of view. As collagen fibrils are the main constituent of the extracellular matrix and since we aimed to achieve an extracellular matrix like topography, electrospinning was used to produce P(3HO) fibres which were then used to functionalize P(3HO) plain and porous films. Different fibre sizes were created by electrospinning and optimal fibre size was selected according to cell proliferation studies. Significantly higher cell proliferation values were obtained with 750 nm fibre diameter. Final constructs were assessed *in vitro* with C2C12 myoblast cell line. The results obtained showed that cell adhesion and proliferation was improved when porous or fibrous structures were incorporated on the surface of the P(3HO) films and was highly improved when both fibrous and porous structures were incorporated simultaneously.

Concluding remarks

This study has shown the possibility of production of LPS-free PHAs by expressing the PHA synthase gene from a Gram-negative into a Gram-positive strain. In addition, results suggest the possibility of mcl-PHAs production in *Bacillus subtilis* using genes from *P. mendocina.* This study showed, for the first time, that *Bacillus subtilis* is as a potential candidate for producing PHAs. P(3HO) production based on constant oxygen transference was successfully scaled-up from 2 L to 20 L bioreactors for the first time. P(3HO) fibres were produced by electrospinning and used to surface functionalise the P(3HO) patches. Also, RGD tripeptide was immobilized on (3HO) patches. The final cardiac patches developed in this project exhibited enhanced cell adhesion and proliferation *in vitro,* and desirable mechanical properties, suggesting that P(3HO) is a promising material for future cardiac tissue engineering applications.

8.2. FUTURE WORK

Based on the results obtained in this project the following investigations will provide a better understanding of the future potential of applying P(3HO) in cardiac tissue engineering:

- The fact that *B. subtilis* containing the *pha*C1 gene from *P. mendocina* was unable to synthesize mcl-PHAs can be attributed to the predominance of the scl-PHA metabolic pathway operating in the organism or the lack of the enzymes from the mcl-PHA metabolic pathway, including hydroxyacyl-ACP-CoA transferase which links the R-3-Hydroxyacyl-ACP precursor from the fatty acid *de novo* biosynthesis metabolic pathway to the PHA synthase for the mcl-PHA production. Although BLAST analyses suggested the presence of a hypothetical protein, which is predicted to be a hydrolase/acyltransferase, this protein has not been studied in detail, hence, further studies should be carried out to confirm its presence and activity. Additionally, metabolic engineering techniques with the obstruction of the scl-PHAs metabolic pathway to facilitate the mcl-PHA biosynthesis should be carried out.
- As one of the main factors that limits the use of mcl-PHAs in different applications is the limited capacity to produce high yields of mcl-PHAs and relatively low P(3HO) yields were obtained in this work using *P. mendocina,* future studies should be carried out to find optimal fermentation conditions based on a full factorial study with pH, C/N and rpm as varying parameters.
- As similar yields results were not obtained when P(3HO) production was scaled-up from 20 L to 72 L bioreactors based on a constant oxygen transfer coefficient, further experimentation is required to achieve a comparable operating condition in both these scales based on a range of other conditions including volumetric power input and superficial air velocity.
- Confirmation of VEGF functional activity after incorporation on the P(3HB) patches should be carried out by ligand-receptor assay for VEGF (Leopol'd *et al.,* 2012).
- Determination of the optimal amounts of RGD peptide and VEGF to be incorporated on the surface of the patch, should be carried out based on cell proliferation studies combined with active factor release studies. To assess cell proliferation and active factor release, MTT or neutral red and ELISA assays should be carried out, respectively. Immobilization of optimal amounts of the RGD peptide and incorporation of optimal amounts of VEGF should be carried out in the final cardiac patches.

- The capacity of the engineered P(3HO) patch as an extracellular matrix to allow cardiomyocyte differentiation should be assessed *in vitro*. For this, cells capable of forming cardiomyocytes should be seeded and differentiated *in vitro* with signal molecules such as ascorbic acid or retinoic acid on the P(3HO) cardiac patches containing RGD peptides and VEGF (Ling-Ling *et al*., 2006, Woubus *et al*., 1998). For this, viability tests such as the MTT or neutral red or observation in light microscopy in order to assess live cells, combined with gene expression profiling of cardiac specific RNA and proteins to determine cell differentiation, should be carried out. Functional activity of the engineered graft including continuous, rhythmic, and synchronized contractions can be tested in spontaneously beating artificial myocardial tissues by electrocardiography (Kofidis *et al.,* 2002a).
- *In vivo* experiments on infarcted animals will be crucial to define the potential of the engineered P(3HO) based cardiac patch. Myocardial infarction can be induced i.e. by ligation of the left anterior descending coronary artery (Laake *et al.,* 2007). In this case, P(3HO) engineered cardiac constructs created by seeded and differentiated pluri- or multipotent cells should be implanted in the infracted region of the heart and the following parameters should be assessed at different periods of time:
  1. Degradation studies of the final constructs should be carried out in order to assess the capability of cells to synthesize new extracellular matrix before complete degradation of the material. For this, histological analysis combined with collagen I, IV, laminin and fibronectin expression patterns and SEM can provide useful information in terms of material degradation and new extracellular matrix formation.
  2. Adequate integration and coupling of implanted and host cells should be assessed by cell junction expression molecules, including connexin 43 and cadherin.
  3. Biocompatibility of the final constructs should be assessed by the expression of inflammatory mediators and material encapsulation. Acute or chronic inflammation and possible ultimate rejection of the biomaterial should be determined by studying cell infiltration and bioactive molecule expression. For instance, occurrence of acute inflammation could be determined by neutrophil infiltration and production of histamine, nitric oxide, bradykinin, C3A, C3B, C5A, PAF, IL-1 and IL-8 among others. Chronic inflammation can be assessed by lymphocyte and macrophage infiltration and TNF-α and INF-γ expression. Material encapsulation should be evaluated by determining the presence and origin of fibrotic tissue surrounding

P(3HO) grafts. Although secretion of fibrotic tissue could lead to separation of host and implanted cells, this would not necessarily exclude functional coupling completely, since electrophysiological signalling can be conducted through relatively thick layers of fibrotic tissue (Gaudesius *et al.,* 2003). However, inappropriate or excessive secretion of fibrotic tissue can increase the occurrences of arrhythmias (Breithardt *et al*., 1989).

4. Structural and biochemical properties in common with the native cardiac tissue can be assessed by histological analysis.
5. The ability of the newly formed tissue to contribute to long-term contractile function should be assessed using long-term experiments.

REFERENCES

Abe H, Doi Y (1999). Structural effects on enzymatic degradabilities for poly[(R)-3-hydroxybutyric acid] and its copolymers. *Int. J. Biol. Macromol.* 25(1-3): 185-92.

Adams H, Irving G, Koeslag H, Lochner D, Sandell R and Wilkinson C (1987). Beta-adrenergic blockade restores glucose's antiketogenic activity after exercise in carbohydrate-depleted athletes. *J. Physiol. Lond*. 386, 439–454.

Akaraonye E, Keshavraz T, Roy I (2010). Production of polyhydroxyalkanoates: the future green materials of choice. *J. Chem. Technol. Biotechnol.* 85: 732-743.

Akaraonye E, Moreno C, Knowles J, Keshavarz T, Ipsita Roy I (2012). Poly(3-hydroxybutyrate) production by *Bacillus cereus* SPV using sugarcane molasses as the main carbon source. *Biothecnol. J*. 7(2): 293-303.

Alvarez H, Kalscheuer R, Steinbuchel A (2000). Accumulation and mobilization of storage lipids by *Rhodococcus opacus* PD630 and *Rhodococcus ruber* NCIMB 40126. *Appl. Microbiol. Biotechnol.* 54: 218–223.

Amara A and Rehm H A. (2003). Replacement of the catalytic nucleophile cysteine-296 by serine in class II polyhydroxyalkanoate synthase from *Pseudomonas aeruginosa* mediated synthesis of new polyester: identification of catalytic residues. *Biochemical J.* 374(2): 413–421.

Amaral P, Freire M, Rocha-Leao M, Marrucho I, Coutinho J, Coelho M (2008). Optimization of oxygen mass transfer in a multiphase bioreactor with perfluorodecalin as a second liquid phase. *Biotechnol. Bioeng*. 99(3): 588–598.

Anderson J, Bonfield T, Ziats N (1990). Protein adsorption and cellular adhesion and activation on biomedical polymers. *Int. J. Artif. Organs.* 13(6): 375-82.

Antoons G, Mubagwa K, Nevelsteen I, Sipido K (2002). Mechanisms underlying the frequency dependence ofcontraction and [Ca2+]i transients in mouse ventricular myocytes. *J. of Physiology.* 543(3): 889–898.

Ashby R, Solaiman D, Foglia T, Liu C (2001). Glucose/lipid mixed substrates as a means of controlling the properties of medium chain length poly(hydroxyalkanoates). *Biomacromolecules.* 2(1): 211-6.

Atala A, Lanza R (2001). Methods of tissue engineering. San Diego. Academic Pr.

Babic A, Berkmen M, Lee C, Grossman A (2011). Efficient Gene Transfer in Bacterial Cell Chains. *mBio.* 2(2): 00027-11.

Badylak S, Lantz G, Coffey A, Geddes L (1989). Small intestinal submucosa as a large diameter vascular graft in the dog. *J. Surg. Res*. 47: 74–80.

Badylak S, Obermiller J, Geddes L, Matheny R (2002). Extracellular Matrix for Myocardial Repair. *The Heart Surgery Forum*. 6(2): 20-6.

Balguid A, Mol A, van Marion M, Bank R, Bouten C, Baaijens F (2009). Tailoring fiber diameter in electrospun poly(epsilon-caprolactone) scaffolds for optimal cellular infiltration in cardiovascular tissue engineering. *Tissue Eng. Part A.* 15(2): 437-44.

Barron A (2013). Molecular Weight of Polymers. *Physical Methods in Chemistry and Nano Science.*Oxford University Pr.

Bellino M, Golbert S, De Marzi M , Soler-Illia G and Desimone M (2013). Controlled adhesion and proliferation of a human osteoblastic cell line by tuning the nanoporosity of titania and silica coatings. *Biomater.* 1: 186-189.

Bers D (2000). Calcium Fluxes Involved in Control of Cardiac Myocyte Contraction. *Circ Res.* 87: 275-281.

Bidone J, Melo A, Bazzo G, Carmignan F, Soldi M, Pires A, Lemos-Senna E (2009). Preparation and characterization of ibuprofen-loaded microspheres consisting of poly(3-hydroxybutyrate) and methoxy poly (ethylene glycol)-*b*-poly (D, L-lactide) blends or poly(3-hydroxybutyrate) and gelatin composites for controlled drug release. *Materials Science and Engineering: C.* 29(2): 588–593.

Bishay R (2011). The 'Mighty Mouse' Model in Experimental Cardiac Transplantation. *Hypothesis.* 9(1): e5.

Biswas S, Hughes G, Scarborough J, Domkowski P, Diodato L, Smith M, Landolfo C, Lowe J, Annex B, Landolfo K(2004). Intramyocardial and intracoronary basic fibroblast growth factor in porcine hibernating myocardium: A comparative study. *J. Thorac. Cardiovasc. Surg.* 127: 34-43.

Boland E, Wnek G, Simpson D, Pawlowski K, Bowlin G (2001). Tailoring tissue engineering scaffolds using electrostatic processing techniques: a study of poly(glycolic acid) electrospinning. *J Macromol. Sci. Pure Appl. Chem.* 38(12): 1231–43.

Breithardt G, Borggrefe M, Martinez-Rubio A, Budde T (1989). Pathophysiological mechanisms of ventricular tachyarrhythmias. *Eur. Heart J*. 10: 9–18.

Bronzino J (2006). Tissue engineering and artificial organs. Taylor and Francis group. CRC Pr.

Byrom D (1992). Production of poly-beta-hydroxybutyrate-poly-beta-hydroxyvaleratecopolymers. *FEMS Microbiol Rev.* 103: 247–250.

Byrom D (1994). Polyhydroxyalkanoates. Plastic from microbes: microbial synthesis of polymers and polymer precursors. *Hanser Munich*. 5-33.

Cai Y, Chen Y, Zhenguo X, Yuan L (2013). Porous microsphere and its applications. *Int. J. of Nanomedicine.* 8: 1111–1120.

Campodonico F, Benelli R, Michelazzi A, Ognio E, Toncini C, Maffezzini M (2004). Bladder cell culture on small intestinal submucosa as bioscaffold: experimental study on engineered urothelial grafts. *Eur. Urol*. 46: 531–7.

Chang H, Perrie I, Coombes A (2006). Delivery of the antibiotic gentamicin sulphate from precipitation cast matrices of polycaprolactone. *J. Control. Rel.* 110: 414-421.

Chen G (2010). Plastics Completely Synthesized by Bacteria: Polyhydroxyalkanoates. *Microbiology Monographs*. 14: 17-37.

Chen G, Page W (1997). Production of poly-β-hydroxybutyrate by *Azotobacter vinelandiiin* a two-stage fermentation process. *Biotechnology Technology*. 11: 347-350.

Chen G, Wu Q (2005). The application of polyhydroxyalkanoates as tissue engineering materials. *Biomaterials.* 26: 6565–6578.

Chen G, Zhang G, Park S, Lee S (2001). Industrial production of poly(hydroxybutyrate-co-hydroxyhexanoate). *Appl. Microbiol. Biotechnol.* 57: 50–55.

Chen Q, Harding S, Ali N, Jawad H, Boccaccini A (2008). Cardiac tissue engineering. *Tissue Engineering Using Ceramics and Polymers.* Woodhead. CRC Pr.

Chen Q, Ishii H, Thouas G, Lyon A, Wright J, Blaker J, Chrzanowski W, Boccaccini A, Ali N, Knowles J, Harding S (2010). An elastomeric patch derived from poly(glycerol sebacate) for delivery of embryonic stem cells to heart. Biomaterials. 31:3885-3893.

Chen M, Patra P, Warner S, Bhowmick S (2007). Role of fiber diameter in adhesion and proliferation of NIH 3T3 fibroblast on electrospun polycaprolactone scaffolds. *Tissue Eng.* 13(3): 579-87.

Chopra K, Mummery P, Derby B, Gough J (2012). Gel-cast glass-ceramic tissue scaffolds of controlled architecture produced via stereolithography of moulds. *Biofabrication*. 4(4): 045002.

Chung H, Park T (2007). Surface engineered and drug releasing pre-fabricated scaffolds for tissue engineering. *Advanced Drug Delivery Reviews.* 59(4-5): 249-262.

Cohen S, Ruvinov E, Amitay-Shafrut S, Sapir Y (2012). Cardiac Tissue Engineering: Principles, Materials, and Applications. *Synthesis Lectures on Tissue Engineering*. Academic Pr.

Conti D, Pezzin S, Coelho L (2006). Mechanical and Morphological Propertiesof Poly(3-hydroxybutyrate)/Poly(3-hydroxybutyrate-co-3-hydroxyvalerate) Blends. *Macromol. Symp.* 245–246: 491–500.

Couper L, Bryant S, Eldrup-Jorgensen J, Bredenberg C, Lindner V (1997). Vascular endothelial growth factor increases the mitogenic response to fibroblast growth factor-2 in vascular smooth muscle cells *in vivo* via expression of fms-like tyrosine kinase-1. *Circ. Res.* 81: 932–939.

Curtis A, Wilkinson C (1999). New depths in cell behaviour: reactions of cells nanotopography. *Biochem. Soc. Symp.* 65: 15-26.

D'Alessandro D, Michler R (2010). Current and future status of stem cell therapy in heart failure. *Curr. Treat Options Cardiovasc. Med.* 12(6) 614–627.

Dash AK, Suryanarayanan R (1992). An implantable dosage form for the treatment of bone infections. *Pharm. Res.* 9: 993-1002.

Dhariwala B, Hunt E, Boland T (2004). Rapid prototyping of tissue-engineering constructs, using photopolymerizable hydrogels and stereolithography. *Tissue Eng*. 10(9-10): 1316-22.

De Smet M, Eggink G, Witholt B, Kingma J, Wynberg H (1983). Characterization of intracellular inclusions formed by *Pseudomonas oleovorans* during growth on octane. *J. Bacteriol*. 154: 870-878.

Diniz S, Taciro M, Gomez J, Pradella J (2004). High cell-density cultivation of *Pseudomonas putida* IPT 046 and medium-chain-length polyhydroxyalkanoate production from sugarcane carbohydrates. *Appl. Biochem. Biotechnol.* 119: 51–70.

Doi Y, Abe C (1990). Biosynthesis and characterization of a new bacterial copolyesterof 3-hydroxyalkanoates and 3-hydroxy-ω-chloroalkanoates. *Macromolecules.* 23: 3705-3707.

Doshi J, Reneker D (1995). Electrospinning process and applications of electrospun fibers. *J. of electrostatics*. 35 (2-3): 151-160.

Duan B, Wu L, Li X, Yuan X, Li X, Zhang Y, Yao K (2007). Degradation of electrospun PLGA-chitosan/PVA membranes and their cytocompatibility *in vitro*. *J. Biomater. Sci. Polym.* 18(1): 95-115.

Dubos R (1946). Effect of Long Chain Fatty Acids on Bacterial Growth. *Exp. Biol. Med.* 63: 156.

Drury J, Dennis R, Mooney D (2004). The tensile properties of alginate hydrogels. *Biomaterials.* 25(16): 3187–3199.

Duvernoy O, Malm T, Ramström J, Bowald S (2007). A Biodegradable Patch used as a Pericardial Substitute after Cardiac Surgery: 6- and 24-Month Evaluation with CT. *Thorac. cardiovasc. Surg*. 43(5): 271-274.

Eichhorm S, Sampson W (2005). Statistical geometry of pores and statistics of porous nanofibrous assemblies. *R. Soc. Interface*. 2: 309–318.

El-Hadi A, Schnabel R, Straube E, Müller G, Henning S (2002). Correlation between degree of crystallinity, morphology, glass temperature, mechanical properties and biodegradation of poly (3-hydroxyalkanoate) PHAs and their blends. *Polymer Testing.* 21: 665-674.

Engler A, Carag-Krieger C, Johnson C, Raab M, Tang H, Speicher D, Sanger J, Sanger J and Discher D (2008). Embryonic cardiomyocytes beat best on a matrix with heart-like elasticity: scar-like rigidity inhibits beating. *J. Cell Sci*. 121: 3794–3802.

Epstein S, Kornowski R, Fuchs S, Dvorak H (2001). Angiogenesis therapy: Amidst the hype, the neglected potential for serious side effects. *Circulation.* 104: 115–119.

Eschenhagen T, Zimmermann W (2005). Engineering Myocardial Tissue. *Circ Res.* 97: 1220-1231.

Eshraghi S, Das S (2010). Mechanical and microstructural properties of polycaprolactone scaffolds with one-dimensional, two-dimensional, and three-dimensional orthogonally oriented porous architectures produced by selective laser sintering. *Acta Biomater.* 6(7): 2467-76.

Faranesh A, Nastley M, Perez de la Cruz C, Haller M, Laquerriere P, Leong K, McVeigh E (2004). *In Vitro* release of Vascular Endothelial Growth Factor From Gadolinium-Doped Biodegradable Microspheres. *Magnetic Resonance in Medicine.* 51: 1265–1271.

Fernandes S, Pharm D, Naumova A, Zhu W, Laflamme M, Gold J and Murry C (2010). Human embryonic stem cell-derived cardiomyocytes engraft but do not alter cardiac remodeling after chronic infarction in rats. *J. Mol. Cell Cardiol.* 49(6): 941–949.

Flaibani M, Elvassore N (2012). Gas anti-solvent precipitation assisted salt leaching for generation of micro- and nano-porous wall in bio-polymeric 3D scaffolds. *Materials Science and Engineering: C.* 32(6): 1632-1639.

Flemming R, Murphy C, Abrams G, Goodman S, Nealey P (1999). Effects of synthetic micro and nano-structures surfaces on cell behaviour. *Biomaterials*. 20, 573-588.

Francis L, Meng D, Knowles J, Keshavarz T, Boccaccini A, Roy I (2011). Controlled Delivery of Gentamicin Using Poly(3-hydroxybutyrate) Microspheres. *Int. J. Mol. Sci. 12*(7): 4294-4314.

Gagnon K, Fuller R, Lenz R, Farris R (1992). A thermoplastic elastomer produced by the bacterium Pseudomonas oleovorans. *Rubber World.* 207, 32 -38.

Galaction A, Cascaval D, Oniscu C, Tumea M (2004). Enhancement of oxygen mass transfer in stirred bioreactorsusing oxygen-vectors. Simulated fermentation broths. *Bioprocess Biosyst. Eng*. 26: 231–238.

Galvez-Monton C, Prat-Vidal C, Roura S, Soler-Botija C and Bayes-Genis A (2013). Cardiac Tissue Engineering and the Bioartificial Heart. *Rev. Esp. Cardiol*. (13)00035-3.

Garcia-Ochoa F, Gomez E (2009). Bioreactor scale-up and oxygen transfer rate in microbial processes: an overview. *Biotechnol Adv*. 27(2): 153-76.

Garlotta D*(* 2001). Literature review of poly(lactic acid). *J Polym Environ 9*(2): *63*–84.

Gaudesius G, Miragoli M, Thomas SP, Rohr S (2003) Coupling of cardiac electrical activity over extended distances by fibroblastsof cardiac origin. *Circ Res.* 93: 421–428.

Giraud M, Armbruster C, Carrel T, Tevaearai H (2007). Current state of the art in myocardial tissue engineering. *Tissue Eng. 13: 1825-1836.*

Goldstein A, Zhu G, Morris G, Meszlenyi R, Mikos A (1995). Effect of osteoblastic culture conditions on the structure of poly(DL-lactic-co-glycolic acid) foam scaffolds. *Tissue Eng*. 5: 421-433.

Gonzalez-GranilloM, GrichineA, Guzun R, Usson Y, Tepp K, Chkulayev V, Schevchuk I, Karu-Varikimaa M, Kuznetsov A, Grimm M, Saks V, Kaambre T (2012). Studies of the role of tubulin beta II isotype in regulation of mitochondrial respiration in intracellular energetic units in cardiac cells. *J. Mol. Cell Cardiol*. 52: 2, 437-447.

Goujon M, McWilliam H, Li W, Valentin F, Squizzato S, Paern J, Lopez R (2010). A new bioinformatics analysis tools framework at EMBL-EBI. *Nucleic acids research* 38: 695-9.

Gould PL, Holland SJ and Tighe BJ (1987). Polymers for biodegradable medical devices IV Hydroxybutyrate- hydroxyvalerate copolymers as non-disintegrating matrices for controlled release oral dosage forms. *Int. J. Pharm.* 38: 231-237.

Gupta V, Grande-Allen K (2006). Effects of static and cyclic loading in regulating extracellular matrix synthesis by cardiovascular cells. *Cardiovascular Research*. 72, 375–383.

Hangii U (1990). Pilot scale production of PHB with *Alcaligenes latus. Novel Biodegradable Microbial Polymers.* 186: 65-70.

Harvey P and Leinwand L (2011). Cellular mechanisms of cardiomyopathy. *The J. Of cell biol*. 194: 3 355-365.

Haywood G, Anderson A, Dawes E (1989). A survey of the accumulation of novel polyhydroxyalkanoates by bacteria. *Biotechnol. Lett.* 11: 471-476.

Haywood G, Anderson A, Williams R, Dawes E, Ewing D (1991). Accumulation of a poly(hydroxyalkanoate) copolymer containing primarily 3-hydroxyvalerate from simple carbohydrate substrates by *Rhodococcus sp*. NCIMB 40126. *Int. J. Biol. Macromol*. 13: 83–88.

Hein S, Paletta J and Steinbüchel A (2002). Cloning, characterization and comparison of the *Pseudomonasmendocina* polyhydroxyalkanoate synthases PhaC1 and PhaC2. *Appl. Microbiol. Biotechnol.* 58: 229–236.

Hersel U, Dahmen C, Kessler H (2003). RGD modified polymers: biomaterials for stimulated cell adhesion and beyond. *Biomaterials.* 24: 4385–4415.

Hlady V and Buijs J (1996). Protein adsorption on solid surfaces. *Curr. Opin. Biotechnol*. 7(1): 72–77.

Hocking P, Marchessault R (1994). Biopolyesters, Chemistry and Technology of Biodegradable Polymers*. London: Chapman and Hall*. Academic Pr.

Hoogerwerf J, Vos A, Bresser P, Zee J, Pater J, Boer A, Tanck M, Lundell D, Jenh C, Draing C, Aulock Sand Poll T (2008). Lung Inflammation Induced by Lipoteichoic Acid or Lipopolysaccharide in Humans. *Am. J. Respir. Crit. Care.* 178: 34–41.

Hrabak O (1992). Industrial production of poly-beta-hyrdoxybutyrate. *FEMS Microbiol Rev.* 103: 251–255.

Hsia H, Nair M, Mintz R, Corbett S (2011). The fibre diameter of synthetic bioresorbable extracellular matrix influences human fibroblast morphology and fibronectin matrix assembly. *Plast. Reconstr. Surg. 127(6): 2312–2320.*

Hubbell L. Bioactive biomaterials (1999). *Curr. Opin. Biotechnol*. 10: 123-9.

Huijberts G, Eggink H, Waard P, Huisman G, Witholt B (1992). *Pseudomonas putida KT2442* Cultivated on Glucose Accumulates Poly(3-Hydroxyalkanoates) Consisting of Saturated and Unsaturated Monomers. *App. and env. Microbiology*. 536-544.

Ikada Y (2006). Challenges in tissue engineering. *J. R. Soc. Interface*. 3: 589–601.

Ikada Y (2011). Tissue Engineering: Fundamentals and Applications. *Interface science and technology.* Academic Pr.

Jakowlew S (2006). Transforming growth factor-beta in cancer and metastasis. *Cancer Metastasis.* 25(3): 435-57.

Jawad H, Lyon A, Harding S, Ali N and Boccaccini A (2008). Myocardial tissue engineering. *British Med. Bulletin*. 87: 31–47.

Jell G, Minelli C, Stevens M (2009). Biomaterial-Related Approaches: Surface Structuring. Fundamentals of Tissue Engineering and Regenerative Medicine. Springer. 469-484.

Jendrossek D and Handrick R (2002). Microbial degradation of polyhydroxyalkanoates. *Annu. Rev. Microbiol.* 56: 403-32.

Ju L, Chase G (1992). Improved scale-up strategies of bioreactors. *Bioprocess Eng*. 8: 49-53.

Jung K, Hazenberg W, Prieto M, Witholt B (2001). Two-Stage Continuous ProcessDevelopment for the Production of Medium-Chain-Length Poly(3-Hydroxyalkanoates). *Biotechnol. Bioeng*. 72(1): 19-24.

Jurasek L and Marchessault R (2004). Polyhydroxyalkanoate (PHA) granule formation in *Ralstonia*. *Appl. Microbiol. Biotechnol.* 64: 611–617.

Kabilan S, Ayyasamy M, Jayavel S, Paramasamy G (2012). *Pseudomonas sp*. as a Source of Medium Chain Length Polyhydroxyalkanoates for Controlled Drug Delivery: Perspective. *Int. J. of Microbiology.* 317828.

Kadner A, Zund G, Maurus C, Breymann C, Yakarisik S, Kadner G (2004). Human umbilical cord cells for cardiovascular tissue engineering: A comparative study. *Eur. J. Cardio. thorac. Surg*. 25: 635–641

Kamelger F, Marksteiner R, Margreiter E, Klima G, Wechselberger G, Hering S (2004). A comparative study of three different biomaterials in the engineering of skeletal muscle using a rat animal model. *Biomaterials*. 25: 1649–1655.

Kasemsap C, Wantawin C (2007). Batch production of polyhydroxyalkanoate by low-polyphosphate-content activated sludge at varying pH. *Bioresource Technology*. 98: 1020-1027.

Kato M, Fukui T, Bull D (1996). Biosynthesis of polyester blends by *Pseudomonas sp*. 61-3 from alkanoic acids. *Chem. Soc. Jpn.* 69: 515–520.

Kazunori T, Takeharu T, Ken'ichiro M, Sumiko N, Seiichi T, and Yoshiharu D (2001). Investigation of metabolic pathways for biopolyester production. *Ecomolecular Science Research.* 42: 71-74.

Keith A, Robinson, Jinshen L, Megumi M, Alka R, Jianhua C, Nicolas A, Chronos M, Robert G. Matheny M and Stephen F (2005). Extracellular Matrix Scaffold for Cardiac Repair. *Cell Transplantation and Tissue Engineering*. 112-135-143.

Kelley L, Sternberg M (2009). Protein structure prediction on the web: a case study using the Phyre server. *Nature Protocols.* 4, 363 – 371.

Keshavarz T. and Roy I (2010). Polyhydroxyalkanoates: bioplastics with a green agenda. *Current Opinion in Microbiology.* 13: 321–326.

Khan A, Ahmed Z, Edirisinghe M, Wong F, Rehman I (2008). Preparation and characterization of a novel bioactive restorative composite based on covalently coupled polyurethane–nanohydroxyapatite fibres. *Acta Biomaterialia*. 4 1275–1287.

Khil M, Cha D, Kim H, Kim I, Bhattarai N (2003). Electrospun nanofibrous polyurethane membrane as wound dressing. *J. Biomed. Mater. Res*. 67B(2): 675–9.

Kim D, Kim H, Chung M, Rhee Y (2007). Biosynthesis, Modification, and Biodegradation of Bacterial Medium-Chain-Length Polyhydroxyalkanoates. *The J. of Microb*. 45: 2; 87-97.

Kim G, Lee I, Yoon S, Shin Y, Park Y (1997). Enhanced yield and a high production of medium-chain-length poly(3-hydroxyalkanoates) in a two-step fed-batch cultivation of *Pseudomonas putida* by combined use of glucose and octanoate. *Enzyme Microb. Technol*. 20: 500–505.

Kim M, Hong K, Shin H, Kim S, Kim S, Lee M (2005). Preparation of porcine small intestinal submucosa sponge and their application as a wound dressing in full-thickness skin defect of rat. *Int. J. Biol. Macromol.* 36: 54–60.

Knollmann B, Roden D (2008). A genetic framework for improving arrhythmia therapy. *Nature*. 451: 929-936.

Kofidis T, Akhyari P, Boublik J, Theodorou P, Martin U, Ruhparwar A, Fischer S, Eschenhagen T, Kubis H, Kraft T, Leyh R, Haverich A (2002a). *In vitro* engineering of heart muscle: Artificial myocardial tissue. *J. Thorac. Cardiovasc. Surg.* 124: 63-9.

Kofidis T, Akhyari P, Wachsmann B, Boublik J, Mueller-Stahl K, Leyh R, Fischer S, Haverich A (2002b). A novel bioartificial myocardial tissue and its prospective use in cardiac surgery. *Eur. J. Cardiothorac. Surg*. 22(2): 238-43.

Konstam M, Kramer D, Patel A, Maron M, Udelson J (2011). Left Ventricular Remodeling in Heart Failure. *JACC Cardiovasc. Imaging*. 4(1): 98-108.

Krumholz H, Baker D, Ashton C, Dunbar S, Friesinger G, Havranek E, Hlatky M, Konstam M, Ordin D, Pina I, Pitt B, Spertusj (2000). Evaluating Quality of Care for Patients with Heart Failure. *Circulation*. 101: 122-140.

Krupnick A, Kreisel D, Szeto W, Popma S, Rosengard B (2001). A murine model of left ventricular tissue engineering. *J. Heart Lung Transplant.* 20: 197–198.

Laake L, Passier R, Monshouwer-Kloots J, Nederhoff M, Oostwaard D, LJ F, Echteld C, Doevendans P, Mummery C (2007). Monitoring of cell therapy and assessment of cardiac function using magnetic resonance imaging in a mouse model of myocardial infarction. *Nat. Protoc.* 2: 2551–2567.

Lageveen R, Huisman W, Preusting H, Ketelaar P, Eggink G, Witholt B (1988). Formation of polyesters by Pseudomonas oleovorans—effect of sustrates on formation and composition of poly-(R)-3-hydroxyalkanoates and poly-(R)-3-hydroxyalkenoates. *Appl. Environ. Microbiol*. 54, 2924–2932.

Laizzo P (2009). Handbook of Cardiac Anatomy, Physiology, and Devices. *Springer.*

Lampin R, Warocquier-Cle´rout, Legris C, Degrange M, Sigot-Luizard F (1997). Correlation between substratum roughness and wettability, cell adhesion, and cell migration. *J. Biomed Mater. Res.* 36(1): 99-108.

Langer R, Vacanti J (1993). Tissue engineering. *Science.* 260: 920-926.

Lanza R, Langer R, Vacanti J (2011). Principles of Tissue Engineering. Academic Pr.

Leatrese H, Byung-Soo K, Money D. (1998). Open pore biodegradable matrices formed with gas foaming. *J. of Biomed. Materials Research.* 42(3): 396-402.

Lebourg M, Sabater Serra R, Más Estellés J, Hernández Sánchez F, Gómez Ribelles JL, Suay Antón J (2008). Biodegradable polycaprolactone scaffold with controlled porosity obtained by modified particle-leaching technique. *J. Mater. Sci. Mater. Med.* 19(5): 2047-53.

Lee J, Jeong S, Bae M, Yang H, Heo D, Kim C, Alsberg E, Kwon K (2011). Highly Porous Electrospun Nanofibers Enhanced by Ultrasonication for Improved Cellular Infiltration. *Tissue Eng Part A.* 17: 21-22.

Lee S, Choi J (2000). Production of Microbial Polyester by Fermentation of Recombinant Microorganisms. *Advances in Biochemical Engineering/Biotechnology*. 71: 183-207.

Lee Y, Park S, Lee W, Ko J, Kim H (2003). MG63 osteoblastic cell adhesion to the hydrophobic surfaceprecoated with recombinant osteopontin fragments. *Biomaterials*. 24: 1059–1066.

Lemoigne M (1926). Products of dehydration and of polymerization of Phydroxybutyricacid. *Bull. Soc. Chem. Biol.* 8: 770-782.

Lenz R, Kim Y, Fuller R (1992). Production of through cometabolism. *FEMS Microbiol. Rev*. 103: 207-214.

Leopol'd A, Baklaushev V, Korchagina A, Shein S, Grinenko N, Pavlov K,Ryabukhin I, Chekhonin V (2012). Ligand-receptor assay for evaluation of functional activity of human recombinant VEGF and VEGFR-1 extracellular fragment. *Bull. Exp. Biol. Med.* 152(6):707-11.

Leor J, Aboulafia-Etzion S, Dar A, Shapiro L, Barbash I, Battler A, Granot Y and Cohen S (2000). Bioengineered cardiac grafts: A new approach to repair the infarcted myocardium? *Circulation*. 102(19-3): 11156-61.

Leor J, Amsalem Y, Cohen S (2005). Cells, Scaffolds and molecules for myocardial tissue engineering. *Pharmacol. Ther*. 105(2): 151-163.

Levenberg S, Huang N, Lavik E, Rogers A, Itskovitz-Eldor J, Langer R (2003). Differentiation of human embryonic stem cells on three-dimensional polymer scaffolds. *Proc. Natl. Acad. Sci*. 100: 12741 – 12746.

Li D (2011). Encyclopedia of Microfluidics and Nanofluidics. *Springer*.

Li R, Jia Z, Weisel R, Mickle D, Choi A and Yau T (1999). Survival and function of bioengineered cardiac grafts. *Circulation.* 100(19)1163–1169.

Li S, Dong C, Wang S, Ye H and Chen G (2011). Microbial Production of Polyhydroxyalkanoate Block Copolymer by Recombinant *Pseudomonas putida. Applied Microbiol. Biotechnol.* 90: 659-669.

Li W, Laurencin C, Caterson E, Tuan R, Ko F (2002). Electrospun nanofibrous structure: A novel scaffold for tissue engineering. *J. Biomed. Mater. Res.* 15;60(4): 613-21.

Li X, Guo Y, Ziegler K, Model L, Eghbalieh S, Brenes R, Kim S, C and Dardik S (2011). Current usage and future directions for the bovine pericardial patch. *Ann. Vasc. Surg*. 25(4): 561–568.

Liebergesell M, Steinbüchel A (1992). Cloning and nucleotide sequences of genes relevant for biosynthesis of poly(3-hydroxybutyric acid) in *Chromatium vinosum* strain D. *Eur J Biochem.* 209(1): 135-50.

Liebergesell M, Rahalkar S, Steinbüchel A (2000). Analysis of the Thiocapsa pfennigii polyhydroxyalkanoate synthase: subcloning, molecular characterization and generation of hybrid synthases with the corresponding Chromatium vinosum enzyme. *Appl Microbiol Biotechnol*. 54(2): 186-94

Lin H, Garciaecheverria C, Asakura S, Sun W, Mosher D, Cooper S (1992). Endothelial-cell adhesion on polyurethanes containing covalently attached RGD-peptides. *Biomaterials.* 13: 905–14.

Lin H, Sun W, Mosher D, Garciaecheverria C, Schaufelberger K, Lelkes P, Cooper S (1994). Synthesis, surface, and cell adhesion properties of polyurethanes containing covalently grafted RGD-peptides. *J. Biomed. Mater. Res*. 28: 329–42.

Ling-Ling E, Zhao Y, Guo X, Wang C, Jiang H, Li J, Duan C, Song Y (2006). Enrichment of Cardiomyocytes Derived From Mouse Embryonic Stem Cells. *The J. of Heart and Lung Transpl*. 25(6): 664-674.

Liu Q, Chen G (2008). *In vitro* biocompatibility and degradation of terpolyester 3HB-co-4HB-co-3HHx, consisting of 3-hydroxybutyrate, 4-hydroxybutyrate and 3-hydroxyhexanoate. *J. Biomater. Sci. Polymer.* 19(11): 1521–1533.

Liu Q, Luo G, Zhou X, Chen G (2011). Biosynthesis of poly(3-hydroxydecanoate) and 3-hydroxydodecanoate dominating polyhydroxyalkanoates by b-oxidation pathway inhibited *Pseudomonas putida. Metabolic Engineering.* 13: 11–17.

Lu L, Wang Y, Mao X, Xiao Z and Huang N (2012). The effects of PHBV electrospunfibers with different diameters and orientations on growth behavior of bone-marrow-derived mesenchymal stem cells. *Biomed. Mater.* 7(1): 015002.

Lu X , and Chung D (1998). A comparative study of the wettability of steel, carbon, and polyethylene fibres by water. *Cement and Concrete Research*. 28(6): 783–786.

Lu Y, Chen S (2004). Micro and nano-fabrication of biodegradable polymers for drug delivery. *Advanced Drug Delivery Reviews.* 56(11): 1621-1633.

Ma L, Zhang H, Liu Q, Chen J, Zhang J, Chen G (2009). Production of Two Monomer Structures Containing Medium-Chain- Length Polyhydroxyalkanoates by β-Oxidation-Impaired Mutant of *Pseudomonas putida* KT2442. *Bioresource Technol.* 100(20): 4891-4894.

Mader S (1999). Inquiry into life Mader. 8th edition. New York. Cambridge University Pr.

Madigan M, Martinko J, Parker J (2000). Brock biology of microorganisms. Prentice-Hall. Academic Pr.

Malm T, Bowald S, Bylock A, Busch C, Saldeen T (1994). Enlargement of the right ventricular outflow tract and the pulmonary artery with a new biodegradable patch in trans-annular position. *Eur. Surg. Res*. 298 - 308.

Malm T, Bowald S, Bylock A, Saldeen T, Busch C 1(992). Regeneration of pericardial tissue on absorbable polymer patches implanted into the pericardial sac. An immunohistochemical, ultrasound and biochemical study in sheep. *Scand J. Thorac. Cardiovasc. Surg*. 26(1): 15-21.

Marques M, Cabral J and Fernandes P (2010). Bioprocess scale-up: quest for the parameters to be used as criterion to move from microreactors to lab-scale. *J. Chem. Technol. Biotechnol.* 85: 1184–1198.

Matsubayashi K, Fedak P, Mickle D, Weisel R, Ozawa T, Li R (2003). Improved left ventricular aneurysm repair with bioengineered vascular smooth muscle grafts. *Circulation* 108(1): 11219 – 11225.

Matsuzaka K, Yoshunari M, Kokubu E, Shimono M, Inoue T (2004). Behavior of osteoblastic-like cells on fibronectin of BMP-2 immobilized surface. *Biomedical Research.* 25 (6) 263-268.

Mikos A, Bao Y, Cima L, Ingber D, Vacanti J, Langer R (1993). Preparation of poly(glycolic acid) bonded fiber structures for cell attachment and transplantation. *J. Biomed. Mater. Res*. 27: 183-189.

Min B, Lee G, Kim S, Nam Y, Lee T, Park W (2004). Electrospinning of silk fibroin nanofibers and its effect on the adhesion and spreading of normal human keratinocytes and fibroblasts *in vitro*. *Biomaterials*. 25(7-8): 1289–97.

Mitalipov S and Wolf D (2009). Totipotency, Pluripotency and Nuclear Reprogramming. *Adv. Biochem. Eng. Biotechnol.* 114: 185–199.

Morosco J (2002). Conquering heart disease: a call to action. *Prev. Cardiol*. 5: 31– 6

Nagueh S, Shah G, Wu Y, Torre-Amione G, King N, Lahmers S (2004). Altered titin expression, myocardial stiffness and left ventricular function in patients with dilated cardiomyopathy. *Circulation*. 110: 155-162.

Neal R, Jean A, Park H, Wu P, Hsiao J, Engelmayr G, Langer R, and Freed L (2012). Three-Dimensional Elastomeric Scaffolds Designed with Cardiac-Mimetic Structural and Techanical Features. *Tissue Engineering Part A*. 19(5-6): 793-807.

Neff J, Tresco P, Caldwell K (1999). Surface modification for controlled studies of cell-ligand interactions. *Biomaterials.* 20(23-24): 2377-93.

Nelson T, Kaufman E, Kline J, Sokoloff L (1981). The extraneural distribution of hydroxybutyrate. *J. Neurochem*. 37: 1345-1348.

Neufeld G, Cohen T, Gengrinovitch S, Poltorak Z (1999). Vascular endothelial growth factor (VEGF) and its receptors. *The FASEB J.. 13(1) 9-22.*

Nguyen H, Nguyen Q, Ferreira R, Ferreira L, Tran L, Schumann W (2005). Construction of plasmid-based expression vectors for Bacillus subtilis exhibiting full structural stability. *Plasmid.* 54(3): 241-8.

Nomura C, Tanaka T, Gan Z, Kuwabara K, Abe H, Takase K, Taguchi K, Doi Y (2004). Effective enhancement of short-chain-length-medium-chain-length polyhydroxyalkanoate copolymer production by coexpression of genetically engineered 3-ketoacyl-acyl-carrier-protein synthase III (fabH) and polyhydroxyalkanoate synthesis genes. *Biomacromolecules.* 5(4): 1457-1464.

Nunes S, Song H, Chiang C, Radisic M (2011). Stem Cell-Based Cardiac Tissue Engineering. *J. of Cardiovasc. Trans. Res*. 4: 592–602.

Odian G (1991). Principles of polymerization, 3rd edn. Wiley. Academic Pr.

Ojumu T, Yu J and Solomon B (2004). Production of Polyhydroxyalkanoates, a bacterial biodegradable polymer. *African J. of Biotechnology* 3: 1, 18-24.
Omar S, Rayes A, Eqaab A, Voß I, Steinbüchel A (2001). Optimization of cell growth and poly(3-hydroxybutyrate) accumulation on date syrup by a *Bacillus megaterium* strain. *Biotechnology Letters.* 23(14): 1119-1123.

Ota T, Sawa Y, Iwai S, Kitajima T, Ueda Y, Coppin C, Matsuda H, Okita Y (2005). Fibronectin-hepatocyte growth factor enhances reendothelialization in tissue-engineered heart valve. *Ann. Thorac. Surg.* 80(5): 1794-801.

Page W, Knosp O (1989). Hyperproduction of polyhydroxybutyrate during exponential growth of *Azotobacter vinelandii* UWD. *App. and Env. Microbiol.* 55(6): 1334-1339.

Palmeri R, Pappalardo F, Fragala M, Tomasello M, Damigella A, Catara A (2012). Polyhydroxyalkanoates (PHAs) Production through Conversion of Glycerol by Selected Strains of *Pseudomonas Mediterranea* and *Pseudomonas Corrugata. Chem. eng. Trans.* 27, 121-126.

Pamula E, Kokoszka J, Cholewa-Kowalska K, Laczka M, Kantor L, Niedzwiedzki L, Reilly G, Filipowska J, Madej W, Kolodziejczyk M, Tylko G, Osyczka A (2011). Degradation, Bioactivity, and Osteogenic Potential of Composites Made of PLGA and Two Different Sol–Gel Bioactive Glasses. *Ann. Biomed. Eng.* 39(8): 2114–2129.

Pancholi S, Earle K (2000). Pattern of angiogenic cytokine release from human vascular smooth muscle cells programmed by amino acid deprivation. *Cytokine.* 12: 1322–1325.

Park J, Huh T, Lee Y (1997). Characteristics of Cell Growth and Poly-β-Hydroxybutyrate Biosynthesis of *Alcaligenes eutrophus* Transformants Harbouring Cloned *phaCAB* genes. *Enzyme Microb. Technol.* 21: 85-90.

Park M, Aiyar A, Park J, Reichmanis E, Srinivasarao M (2011). Solvent evaporation induced liquid crystalline phase in poly(3-hexylthiophene). *J. Biomed. Mat. Res*. 133(19): 7244-7247.

Pena C, Castillo T, Nunez C, Segura D (2011). Bioprocess design: fermentation strategies for improving the production of alginate and poly-β-hydroxybutyrate (PHB) by *Azotobacter vinelandii. Bioengineering.*

Perets A, Baruch Y, Weisbuch F, Shoshany G, Neufeld G, Cohen S (2003). Enhancing the vascularization of three-dimensional porous alginate scaffolds by incorporating controlled release basic fibroblast growth factor microspheres. *J. Biomed. Mater. Res. A.* 65(4): 489-97.

Perla V, Webster T (2006). Nano-hydroxyapatite–thermally denatured small intestine sub-mucosa composites for entheses applications. *Int. J. Nanomedicine*. 1(3): 351–359.

Perry E, Roth J (2003). Cardiovascular tissue engineering: constructing living tissue cardiac valves and blood vessels using bone marrow, umbilical cord blood, and peripheral blood cells. *J. Cardiovasc. Nurs*. 18: 30.

Philip S, Keshavarz T, and Roy I (2007). Polyhydroxyalkanoates: biodegradable polymers with a range of applications. *J. of chemical technol. and biotechnol.* 82: 233-247.

Pinz I, Zhu M, Mende U, Ingwall J (2011). An Improved Isolation Procedure for Adult Mouse Cardiomyocytes. *Cell Biochem. Biophys.* 61(1): 93–101.

Pires A, Saporito W, Cardoso S, Ramaciotti O (1999). Bovine pericardium used as a cardiovascular patch. *Heart Surg. Forum.* 2(1): 60-9.
Poirier Y, Nawrath C, Somerville C (1995). Production of polyhydroxyalkanoates, a family of Biodegradable plastics and elastomers in bacterial and plant. *Biotechnol.* 13: 142-150.

Pok S, Jacot J (2011). Biomaterials Advances in Patches for Congenital Heart Defect Repair. *J. Cardiovasc. Transl. Res*. 4: 646-654.

Povolo S, Toffano P, Basaglia M, Casella S (2010). Polyhydroxyalkanoates Production by Engineered *Cupriavidusnecator* from Waste Material Containing Lactose. *Bioresource Technol*. 101(20): 7902-7907.

Prabhakaran M , Venugopal J, Kai D , Ramakrishna S (2011). Biomimetic material strategies for cardiac tissue engineering. *Materials Science and Engineering.* 31: 503–513.

Preusting H, Kingma J, Witholt B (1991). Physiology and polyester formation of *Pseudomonas oleovoran*sin continuous two-liquid-phase cultures. *Enzyme Microbiol. Technol.* 13: 770–780.

Prieto M (2006). From Oil to Bioplastics, a Dream Come True?. *Bacteriol.* 189 (2): 289-290.
Provencher S, Deslauriers J (2003). Late complication of bovine pericardium patches used for lung volume reduction surgery. *Eur. J. Cardiothorac. Surg*. 23(6): 1059–1061.

Puthli M, Rathod V, Pandit A (2005). Gas-liquid mass transfer studies with triple impeller system on a laboratory scale bioreactor. *Biochem. Eng. J*. 23(1): 25–30.

Quinteros R, Goodwin S, Lenz R, Park W (1999). Extracellular degradation of medium chain length poly(β-hydroxyalkanoates) by *Comamonas* sp. *Int. J. Biol. Macromol.* 25(1-3): 135-143.

Rai R, Boccaccini A, Knowles J, Mordon N and Salihd V Locke I, Moshrefi-Torbat M, Keshavarz Tajalli, Roy I(2011a). The homopolymer poly(3-hydroxyoctanoate) as a matrix material for soft tissue engineering. *J. of App. Polymer Science*. 122 (6): 3606-3617.

Rai R, Keshavarz T, Roether J, Boccaccini A, Roy I (2011b). Medium chain length polyhydroxyalkanoates, promising new biomedical materials for the future. *Materials Science and Eng.* 72: 29–47.

Rai R, Yunos D, Boccaccini A, Knowles J, Barker I, Howdle S, Tredwell G, Keshavarz T, and Roy I (2010). Poly-3-hydroxyoctanoate P(3HO), a Medium Chain Length Polyhydroxyalkanoate Homopolymer from *Pseudomonas mendocina*. 13;12(6): 2126-2136.

Ramsay B, Lomaliza K, Chavarie C, Dubé B, Bataille P, and Ramsay J (1990). Production of poly-(beta-hydroxybutyric-co-beta-hydroxyvaleric) acids. *App. and Envir. microbiology*. 56: 7, 2029-2098.

Rebollar E, Frischauf I, Olbrich M, Peterbauer T, Hering S, Preiner J, Hinterdorfer P, Romanin C, Heitz J (2008). Proliferation of aligned mammalian cells on laser-nanostructured polystyrene. *Biomaterials*. 29(12): 1796-806.

Rehm B (2003). Polyester synthases: natural catalysts for plastics. *Biochem. J*. 376: 15–33.

Rehm B, Steinbüchel A (2002). PHA synthases the key enzymes of PHA synthesis in "Biopolymers". Verlag *Wiley*. Polyesters I, 3a: 173-215.

Rehm B (2009). Microbial production of biopolymers and polymer precursors: applications and perspectives. Academic Pr.

Renzi P (1995). A comparative study of biological activities of lipoteichoic acid and lipopolysaccharide. *Innate immunity*. 2, 6 431-441.

Rezania A, Healy K (2008). Biomimetic Peptide Surfaces That Regulate Adhesion, Spreading, Cytoskeletal Organization, and Mineralization of the Matrix Deposited by Osteoblast-like Cells. *Biotechnology Progress*. 15(1): 19-32.

Richardson T, Peters M, Ennett A, Mooney D (2001). Polymeric system for dual growth factor delivery. *Nature biotechnology.* 19: 1029 – 1034.

Richert L, Vetrone F, Yi J, Zalzal S, Wuest J, RoseiF, and Nanci A (2008). Surface Nanopatterning to Control Cell Growth. *Adv. biomaterials.* 20: 8, 1488-1492.

Roeder B, Kokini K, Sturgis J, Robinson J, Voytik-Harbin S (2002). Tensile mechanical properties of three-dimensional type I collagen extracellular matrices with varied microstructure. *J. Biomech. Eng*. 124(2): 214-22.

Rosas O, Rojas J, Dellamary F, Arellano J, Reynoso O (2007). Production and characterization of polyhydroxyalkanoates in *Pseudomonas aeruginosa* ATCC 9027 from glucose, an unrelated carbon source. *Canadian J. of Micr*. 53(7): 840-851

Rosen M, Roselli E, Faber C, Ratliff N, Ponsky J, Smedira N (2005). Small intestinal submucosa intracardiac patch: an experimental study. *Surg Innov.* 12(3): 227-31.

Ruiz J, López N, Fernández R and Méndez B (2001). Polyhydroxyalkanoate Degradation Is Associated with Nucleotide Accumulation and Enhances Stress Resistance and Survival of *Pseudomonas oleovorans* in Natural Water Microcosms. *Appl. Environ. Microbiol.* 67(1): 225–230.

Ruoslahti E (1996). RGD and othe recognitions sequences for integrins. *Annual Review of Cell and Developmental Biology.* 12: 697-715.

Ryu J, Kim I, Cho S, Cho M, Hwang K, Piao H (2005). Implantation of bone marrow mononuclear cells using injectable fibrin matrix enhances neovascularization in infarcted myocardium. *Biomaterials.* 26, 319–326.

Saad B, Neuenschwander P, Uhlschmid G and Suter U (1999). New versatile, elastomeric, degradable polymeric materials for medicine. *Int. J. Biol. Macromol.* 25: 293–301.

Schirmer A, Jendrossek D, Schlegel G (1993). Degradation of poly(3-hydroxyoctanoic acid) [P(3HO)] by bacteria—purification and properties of a P(3HO) depolymerase from *Pseudomonas fluorescens* Gk13. *Appl. Environ. Microbiol*. 59, 1220–1227.

Schmidt F (2005). Optimization and scale up of industrial fermentation processes. *Appl. Microbiol. Biotechnol*. 68: 425–435.

Sevastianov V, Perova N, Dovzhik I, Titushkin I, Nemets E, Belomestnya Z, Shishatskaya E and Volvoa T (2001). Biomedical properties of polyhydroxyalkanoates-biodegradable bacterial polymers. *Advanced materials*. 5: 47-55.

Sevastianov V, Perova N, Shishatskaya E, Kalacheva G Volova T (2003). Production of purified polyhydroxyalkanoates (PHAs) for applications in contact with blood. *J. Biomater. Sci. Polym*. 14(10): 1029-42.

Shachar M, Tsur-Gang O, Dvir T, Leor J, Cohen S (2011). The effect of immobilized RGD peptide in alginate scaffolds on cardiac tissue engineering. *Acta Biomater*. 7(1): 152-62.

Shen H, Clauss M, Ryan J, Schmidt A, Tijburg P, Borden L, Connolly D, Stern D, Kao J (1993). Characterization of vascular permeability factor/vascular endotelial growth factor receptors on mononuclear phagocytes. *Blood*. 81: 2767–2773.

Shin M, Ishii O, Sueda T, Vacanti J (2004). Contractile cardiac grafts using a novel nanofibrous mesh. *Biomaterials*. 25: 3717–3723.

Shinoka T, Matsumura G, Hibino N, Naito Y, Watanabe M, Konuma T, Sakamoto T, Nagatsu M, Kurosawa H (2005). Midterm clinical result of tissue engineered vascular autografts seeded with autologous bone marrow cells. *J. Thorac. Cardiovasc. Surg*. 129(6): 1330-8.

Shishatskaya E, Volova T, and Gitelson A (2002). *In vivo* Toxicological Evaluation of Polyhydroxyalkanoates. *Doklady Biological Sciences.* 383(4): 565-567.

Shum-Tim D, Stock U, Hrkach J, Shinoka T, Lien J, Moses M, Stamp A, Taylor G, Moran A, Landis W, Langer R, Vacanti J, Mayer J (1999). Tissue engineering of autologous aorta using a new biodegradable polymer. *Ann. Thorac. Surg*. 2298 – 2305.

Siegel R, Rathbone M (2012). Overview of Controlled Release Mechanisms. *Advances in Delivery Science and Technology. Springer.*

Singh M, Patel S and Kalia V (2009). *Bacillus subtilis* as potential producer for polyhydroxyalkanoates. *Microbial cell factories*. 8: 38.

Singh S, Wu V, Dunn J (2012). Delivery of VEGF using collagen‐coated polycaprolactone scaffolds stimulates angiogenesis. *J. of Biomedical Materials Research Part A.* 100A (3).

Sipahigil O, Alarçin E, Türko lu M, Dortunç B, Karagöz H, Ülkür E, Vural M, Çapan Y (2012). Characterization, cell proliferation and cytotoxicity evaluation of vascular endotelial growth factor loaded poly(lactic-co-glycolic acid) microspheres. *Nobel Med. 8(1): 77-82.*

Smaill B, McGiffin D, Legrice I, Young A, Hunter P, Galbraith A (2000). The effect of synthetic patch repair of coarctation on regional deformation of the aortic wall. *J. Thorac. Cardiovasc. Surg*. 120(6): 1053-63.

Smith I, Liu X, Smith L, and Ma P (2009). Nano-structured polymer scaffolds for tissue engineering and regenerative medicine. *Wiley Interdiscip. Rev. Nanomed. Nanobiotechnol*. 1(2): 226–236.

Sorensen H, Mortensen K (2005). Advanced genetic strategies for recombinant protein expression in *Escherichia coli. J. of Biotechnology.* 115(2): 113-128.

Steinbüchel A (1991). Polyhydroxyalkanoic acids. *Biomaterials: novel materials from biological sources*. Stockton, New York. CRC Pr.

Steinbüchel A, Hustede E, Liebergesell M, Pieper U, Timm A, Valentin H (1992). Molecular basis for biosynthesis and accumulation of polyhydroxyalkanoic acid in bacteria. *FEMS Microbiol. Rev*. 103: 217-230.

Steinbijchel A, Schlegel H (1991). Physiology and molecular genetics of poly(p-hydroxy-alkanoic acid) synthesis in *Alcaligenes eutrophus*. *Molec. Microbiology*. 5(3): 535-542.

Stock U, Sakamoto T, Hatsuoka S, Martin D, Nagashima M, Moran A, Moses M, Khalil P, Schoen F, Vacanti J, Mayer J (2000). Patch augmentation of the pulmonary artery with bioabsorbable polymers and autologous cell seeding. *J. Thorac. Cardiovasc. Surg.* 1158 - 1168.

Sultana N, Wang M (2012). PHBV/PLLA-based composite scaffolds fabricated using an emulsion freezing/freeze-drying technique for bone tissue engineering: surface modification and in vitro biological evaluation. *Biofabrication*. 4: 1.

Sun Z, Ramsay J, Guay M, Ramsay B (2007). Carbon-limited fed-batch production of medium-chain-length polyhydroxyalkanoates from nonanoic acid by *Pseudomonas putida* KT2440. *Appl. Microbiol. Biotechnol.* 74(1): 69-77.

Sun Z, Ramsay J, Guay M, Ramsay B (2007). Fermentation process development for the production of medium-chain-length poly-3-hydroxyalkanoates. *Appl. Microbiol. Biotechnol.* 75: 475-485.

Sutton M and Sharpe N (2000). Left Ventricular Remodeling After Myocardial Infarction : Pathophysiology and Therapy. *Circulation.* 101: 2981-2988.

Suwannasing W, Moonamart S, Kaewkannetra P (2011). Yields of Polyhydroxyalkanoates (PHAs) during Batch Fermentation of Sugar Cane Juice by *Alcaligenes latus* and *Alcaligenes eutrophus*. *J. of Life Sciences*. 5: 960-966.

Tan M, Zhi W, Wei R, Huang Y, Zhou K, Tan B, Deng L, Luo J, Li X, Xie H, Yang Z (2009). Repair of infarcted myocardium using mesenchymal stem cell seeded small intestinal submucosa in rabbits. *Biomaterials.* 30: 3234–3240.

Tang L, Eaton J (1995). Inflammatory responses to biomaterials. *Am. J. Clin. Pathol*. 103(4): 466-71.

Taylor G (1969). Electrically driven jets. *Proc. R. Soc. Lond.* 313: 1515 453-475.

Thull R. Surface functionalization of materials to initiate autobiocompatibilization *in vivo* (2001). MaterialwissWerkst. 32: 949-52.

Tottey S, Johnson S, Crapo P, Reing J, Zhang L, Jiang H (2011). The effect of source animal age upon extracellular matrix scaffold properties. *Biomaterials*. 32(1), 128–136.

Tracqui P, Ohayon J, Boudou T (2008). Theoretical analysis of the adaptive contractile behaviour of a single cardiomyocyte cultured on elastic substrates with varying stiffness. *J. of Theoretical Biology.* 255: 92–105.

Tu C, Cai Q, Yang J, Wan Y, Bei J and Wang S (2003). The Fabrication and Characterization of Poly(lactic acid) Scaffolds for Tissue Engineering by Improved Solid–Liquid Phase Separation. *Polym. Adv. Technol*. 14, 565–573.

Us M, Sungun M, Pocan S Cebeci B, Ogus T, Ucak A, Guler A (2004). A retrospective comparison of bovine pericardium and polytetrafluoroethylene patch for closure of ventricular septal defects. *J. Int. Med. Res.* 32(2): 218–221.

Valappil S, Boccaccini A, Bucke C, Roy I (2007). Polyhydroxyalkanoates in Gram-positive bacteria: insights from the genera Bacillus and Streptomyces. *Antonie Van Leeuwenhoek*. 91, 1-17.

Valappil S, Misra S, Boccaccini A, Roy I (2006). Biomedical applications of polyhydroxyalkanoates, an overview of animal testing and *in vivo* responses. *Expert review of Med. Devices.* 3(6): 853-868.

Verlinden R, Hill D, Kenward M, Wiliams C, Radecka I (2007). Bacterial synthesis of biodegradable polyhydroxyalkanoates. *J. of Applied Microbiology*. 102: 1437- 1449.

Volova T (2004). Polyhydroxyalkanoates-plastic materials of the 21st century: production, properties, applications. *Published by Nova Publishers*.

Volvoa T, Gladyshev M, Trusova M, Zhila N (2006). Degradation of polyhydroxyalkanoates and the composition of microbial destructors under natural conditions. *Microbiology*. 75(5): 135-143.

Wahab H. A, Ahmad Khairudin N. B, Samian M. R, and Najimudin, N (2006). Sequence analysis and structure prediction of type II *Pseudomonas* sp. USM 4–55 PHA synthase and an insight into its catalytic mechanism. *BMC Structural Biology.* 6, 23.

Wang J, Wu W (2005). Swelling behaviors, tensile properties and thermodynamic studies of water sorption of 2-hydroxyethyl methacrylate/epoxy methacrylate copolymeric hydrogels. *European Polymer J.*. 41: 1143–1151.

Wang Y, Ruan L, Lo WH, Chua H, Yu HF (2006). Construction of recombinant *Bacillus subtilis* for production of polyhydroxyalkanoates. *Appl. Biochem. Biotechnol.* 129-132: 1015-22.

Watanabe S, Shite J, Takaoka H, Shinke T, Imuro Y, Ozawa T, Otake H, Matsumoto D, Ogasawara D, Paredes O and Yokoyama M (2006). Myocardial stiffness is an important determinant of the plasma brain natriuretic peptide concentration in patients with both diastolic and systolic heart failure. *European Heart J.* 27, 832–838.

Waterhouse A, Procter J, Martin D, Clamp M, Barton G (2009). Jalview version 2: A Multiple Sequence Alignment and Analysis Workbench. *Bioinformatics* 25(9): 1189-1191.

Webb A, Yang J, Ameer G (2004). Biodegradable polyester elastomers in tissue engineering. *Expert Opin. Biol. Ther.* 4(6): 801-12.

Weng Y, Wang X, Wang Y (2011). Biodegradation behaviour of PHAs with different chemical structures under controlled composting conditions. *Polymer testing* 30: 372-380.

Whang K, Thomas C, Healy K, Nuber G (1995). A novel method to fabricate bioabsorbable scaffolds. *Polymer*. 36(4): 837-842.

Wiggam I, O'Kane M, Harper R, Atkinson B, Hadden R, Trimble R and Bell M (1997). Treatment of diabetic ketoacidosis using normalization of blood 3-hydroxybutyrate concentration as the endpoint of emergency management. *Diabetes Care.* 20, 1347–1352.

Williams R (2011). Surface Modification of Biomaterials: Methods, Analysis and Applications. *Woodhead Publishing Series in Biomaterials. 2011-415.*

Williams S, Martin D (1996). Applications of PHAs in medicine and pharmacy. *Medicine.* 4: 1– 38.

Williams S, Martin D, Horowitz D, Peoples O (1999). PHA applications: addressing the price performance issue. I. Tissue engineering. *Int. J. Biol. Macromol.* 25: 111–121.

Witholt B, and Kessler B (1999). Perspectives of medium chain length poly(hydroxyalkanoates), a versatile set of bacterial bioplastics. *Current Opinion in Biotechnol*. 10: 279-285.

Wobus A, Guan K (1998). Embryonic Stem Cell-Derived Cardiac Differentiation: Modulation of Differentiation and "Loss-of-Function" Analysis *In Vitro. Trends in cardiovascular medicine.* 8(2): 67-74.

Wu L, Zhang H, Zhang J, Ding J (2005). Fabrication of three-dimensional porous scaffolds of complicated shape for tissue engineering. I. Compression molding based on flexible-rigid combined mold. *Tissue Eng.* 11(7-8): 1105-14.

Xing Y, Anlin L, Wang L, Yan X, Zhao WCao F (2012). Engineered myocardial tissues constructed *in vivo* using cardiomyocyte-like cells derived from bone marrow mesenchymal stem cells in rats. *J. of Biomed. Science*. 19: 6.

Yamamoto M, Takahashi Y, Tabata Y (2003). Controlled release by biodegradable hydrogels enhances bone formation of bone morphogenetic protein. *Biomaterials.* 24: 4375–4383.

Yang S, Leong K, Du Z, Chua C (2001). The Design of Scaffolds for Use in Tissue Engineering. Part I. Traditional Factors. *Tissue engineering.* 7(6): 679-89.

Yao J, Zhang G, Wu Q, Chen G and Zhang R (1999). Production of polyhydroxyalkanoates by *Pseudomonas nitroreducens. Antonie van Leeuwenhoek. 75: 345–349.*

Ye K, Black L (2011). Strategies for Tissue Engineering Cardiac Constructs to Affect Functional Repair Following Myocardial Infarction. *J. of Cardiovasc. Trans. Res*. 4: 575–591.

Yipp B, Andonegui G, Howlett C, Robbins S, Hartung T, Ho M, Kubes P (2002). Profound differences in Leukocyte-Endothelial Cell Responses to Lipopolysaccharide VersusLipoteichoic Acid. *The J. of Immunology.* 168: 4650–4658.

Yoon J, Song S, Lee D, Park T (2003). Immobilization of cell adhesive RGD peptide onto the surface of highly porous biodegradable polymer scaffolds fabricated by gas foaming/salt leaching method. *Biomaterials*. 25: 5613-5620.

Yoon S, Mofrad M (2011). Cell adhesion and detachment on gold surfaces modified with a thiol-functionalized RGD peptide. *Biomaterials*. 32: 7286-7296.

Yu J, Stahl H (2008). Microbial utilization and biopolyester synthesis of bagasse hydrolysates. *Bioresour Technol*. 99(17): 8042-8.

Yuan J, Shang P, Wu S (2001). Effects of Polyethylene Glycol on Morphology, Thermomechanical Properties, and Water Vapor Permeability of Cellulose Acetate–Free Films. *Pharmaceutical Technology*. 25(10): 62-74.

Zein I, Hutmacher D, Tan K, Teoh S (2002). Fused deposition modeling of novel scaffolds architectures for issue engineering applications*. Biomaterials.* 23: 1169-1185.

Zhang F, Zhang J, Lin S, Oswald T, Sones W, Cai Z (2003). Small intestinal submucosa in abdominal wall repair after TRAM flap harvesting in a rat model. *Plast. Reconstr. Surg.* 112: 565–70.

Zhao K, Deng Y, Chen CJ, Chen G-Q (2003). Polyhydroxyalkanoates (PHA) scaffolds with good mechanical properties and biocompatibility. *Biomaterials.* 24: 1041-1048.

Zheng Z, Chen T, Zhao M, Wang Z, Zhao X (2012). Engineering *Escherichia coli* for succinate production from hemicellulose via consolidated bioprocessing. *Microbial Cell Factories*. 11: 37.

Zinn M, Hanry R (2005). Tailored material properties of polyhydroxyalkanoates through biosynthesis and chemical modification. *Adv. Eng. mater*. 7: 408-441.

Zinn, M, Witholt B, and Egli T (2001). Occurrence, synthesis andmedical application of bacterial polyhydroxyalkanoate. *Adv. Drug Del. Rev.* 53, 5-21.

Zong X, Bien H, Chung C, Yin L, Fang D, Hsiao S, Chu B, Entcheva E (2005). Electrospun fine-textured scaffolds for heart tissue constructs. *Biomaterials.* 26: 5330–5338.

Zweers J, Barák I, Becher D, Driessen A, Hecker M, Kontinen V, Saller M, Vavrová L and Dijl J (2008). Towards the development of *Bacillus subtilis* as a cell factory for membrane proteins and protein complexes. *Microbial Cell Factories*. 7: 10.